UNIVERSITA' DI SIENA

DOTTORATO DI RICERCA IN MEDICINA MOLECOLARE

CICLO XXXV

COORDINATORE Prof. Vincenzo Sorrentino

TITOLO DELLA TESI

At the roots of genetic cardiomyopathies: from 2D to 3D models based on human iPSC-derived cardiomyocytes

SETTORE SCIENTIFICO-DISCIPLINARE BIO/09

DOTTORANDO

Marianna Langione

TUTOR

Cecilia Ferrantini

ANNO ACCADEMICO
2021/2022

Table of contents

Chapter 2

MATERIALS AND METHODS

Chapter 3

Calcium handling maturation and adaptation to increased substrate stiffness in human iPSC-derived cardiomyocytes: The impact of full-length dystrophin deficiency

Chapter 4

Slower calcium handling balances faster crossbridge cycling in human MYBPC3 HCM

Chapter 5

Engineered Heart Tissues for studying twitch tension and inotropic pharmacological interventions

Chapter 6

Summary

Human pluripotent stem cell-derived cardiomyocytes (hiPSC-CMs) represent a powerful model for studying the mechanisms underlying inherited cardiomyopathies. Since hiPSCs preserve the entire individual genetic profile, they can help to identify the most appropriate pharmacological interventions to correct specific functional alterations. HiPSC-CMs have been used to study various pathological mechanisms underlying inherited genetic heart disease, particularly as a model to study dilated (DCM) and hypertrophic cardiomyopathies (HCM). However, the most consistent limitation of hiPSC-CMs as a model of cardiomyopathies is their immature cellular features after differentiation; therefore, new methods to promote their maturation have been investigated in the recent years. This work describes approaches to mature hiPSC-CMs, such as biomaterial-based micropatterned substrates (2D-system) and engineered cardiac tissues (EHTs, 3D-system); both can promote cell alignment and elongation, and overall enhancing cardiac cell maturation. In the first part of this work, we demonstrated that micropatterned surfaces have a strong impact on the cardiomyocytes regulation of calcium homeostasis and cellular electrophysiology. We developed different (polyethylene- and diethyleneglycol-based) substrates with different stiffness that were applied to Duchenne Muscular Dystrophy (DMD) hiPSC models. These results provided understanding on the lack of full-length dystrophin in cardiomyocytes and the possible role of cardiac cells with the extracellular environment interaction. A simultaneous measurement of the time-course of action potentials and calcium transients revealed that abnormal calcium handling in DMD-hiPSC-CMs is mostly related to defects in SR calcium accumulation (likely due to RyR leakage) and reduced ability to remove intracellular calcium during diastole. These mechanisms were exacerbated on stiffer substrates. Furthermore, hiPSC-CMs maturation can be enhanced by cardiac tissue engineering approaches by organizing the cells in a 3D environment that more closely resembles the physiological cardiac tissue. In the second part of this work, hiPSC-CMs were used to EHTs, which can be used for in vitro disease modeling and potentially developing precise therapies based on genotype-driven pathogenesis. EHTs were used for contractile force recordings and a direct comparison with cardiac samples from patients. In particular, we focused on the c.772G>A variant, present in the *MYBPC3* gene, that causes hypertrophic cardiomyopathy (HCM). To better understand the pathogenetic mechanisms driven by this variant frequent in the florentine patient cohort, myectomy samples were collected from HCM patients carrying this mutation, and PBMCs were obtained from the same patients to be reprogrammed into hiPSCs. We observed that the c.772G>A mutation impairs sarcomere energetics and cross bridge cycling leading to a reduction of cMyBP-C expression in myectomy samples and c.772G>A -hiPSC-CMs. In addition, myocardial samples showed prolonged APs and Ca-T duration and preserved twitch duration. The same electrophysiological changes were observed in patient hiPSC-CMs and -EHTs, suggesting an early adaptive response to primary sarcomeric changes. In the last part of the thesis, EHTs were used as a model to test the long-term effect of Mavacamten, a novel first-in-class allosteric myosin inhibitor developed to reduce contractility and improve myocardial energy in HCM patients. After chronic treatment with Mavacamten ($0.3\mu M$ and $0.75\mu M$) for 20 days, the HCM-EHTs showed reduced contractile force development under isometric conditions in drug-treated EHTs compared with untreated EHTs, with mild reduction of the twitch duration. Overall, this work provides an overview on the advantage and limitations of using both 2D and 3D approaches for modeling genetic cardiomyopathies and drug testing using hiPSC models.

Chapter 1

INTRODUCTION

1.1 Human induced pluripotent stem cells and engineered heart tissues for in vitro disease modeling

1.1.1 Human induced pluripotent stem cells

Advances in *in vitro* culture technology have led to the development of myocardial models to test drug efficacy and toxicity (Navarrete et al. 2013)*,* for disease modeling *(Alessandra Moretti et al. 2010)* and for mechanistic studies of cardiac development (Paige et al. 2012)*.* Several studies have been conducted to assess the suitability of a variety of cell sources, including embryonic stem cells (ESCs) (Clements and Thomas 2014) and induced pluripotent stem cells (iPSCs) (Mathur et al. 2015)*,* which can be differentiated into cardiac cells that recapitulate the phenotype of native ones. Pluripotent stem cells can differentiate into any of the three germ layers: endoderm, mesoderm, or ectoderm, but not into extraembryonic tissues. Because they can propagate indefinitely, they represent a unique source of cells that could be used to replace those lost to damage or disease. The best-known pluripotent stem cells are embryonic stem cells (ESC), which are derived from the inner cell mass of mammalian blastocysts and can grow indefinitely, while maintaining pluripotency and the ability to differentiate into different cell types (Evans and Kaufman 1981). However, there are ethical concerns associated with the use of human (Alessandra Moretti et al. 2010) embryos in research and one way around these problems is the generation of pluripotent cells directly from the patient's own somatic cells. Induced pluripotent stem cells (iPSCs) can differentiate into multiple different lineages, are easy to expand, and their use reduces ethical problems.

The generation of iPSCs from somatic cells began with the work of Dr. Shinya Yamanaka's research group (Takahashi and Yamanaka 2006). They hypothesized that genes important for embryonic stem cell (ESC) function could induce an embryonic state in adult cells. They chose twenty-four genes previously identified as important for ESCs and used retroviruses to transport these genes into mouse fibroblasts. After administration of all factors, ESC-like colonies emerged that could propagate indefinitely. Through these experiments, the researchers identified four specific factors, OCT4, SOX2, KLF4 and c-MYC, which were necessary and sufficient to generate ESC-like colonies. Reprogramming of somatic cells into iPSCs can be performed using cells from different tissue sources. In 2007, Takahashi and Yamanaka successfully performed the first reprogramming of human dermal-derived fibroblasts using the 4 discovered factors. They obtained human iPSCs like human embryonic stem cells (ESC) in morphology, proliferation, gene expression, epigenetic status of pluripotent cell-specific genes and telomerase activity (Takahashi et al. 2007). Several characteristics of fibroblasts support their use for iPSC generation, such as high availability from skin biopsies or other organs, but their use is also limited by time and reprogramming efficiency. The percentage of reprogrammed fibroblasts is usually very low and in addition, skin biopsy remains an invasive approach, which is a major disadvantage in using fibroblasts as a source (Raab et al. 2014)*.* After Yamanaka's finding, many studies have reported the reprogramming factors and methods applied to other human somatic cells, such as keratinocytes, which have been described to show 100-fold higher reprogramming efficiency than fibroblasts (Raab et al. 2014), extra-embryonic tissues from umbilical cord and placenta (Cai et al.

2010), urine-derived cells (Xue et al. 2013); (T. Zhou et al. 2012) and mononuclear cells from peripheral blood, which represent an easy and non-invasive-handling source (Loh et al. 2009). Several methods have been developed to improve the efficiency of iPSC generation, including viral and lentiviral integration, non-integrating viral vectors, and protein- and small-molecule-based reprogramming. The use of iPSCs lines in basic and clinical research has raised concerns about the identity of these cells compared with ESCs. On the one hand, it has been argued that iPSCs and ESCs have characteristics in common, such as a high proliferation rate, the ability to self-renewal and to differentiate *in vitro* into cell types of the three germ layers and to faithfully preserve the donor genotype. On the other hand, hundreds of genes, as well as DNA methylation patterns, are differentially expressed between iPSCs and ESCs (Chin et al. 2009; Newman and Cooper 2010). Therefore, despite the reported differences between iPSCs and ESCs, cardiomyocytes produced from these cell sources are not known to exhibit differences once differentiated; for this reason, iPSCs remain an advantageous model for *in vitro* disease modeling and for the screening of therapeutic compounds and remain attractive candidates for application in basic and clinical research.

1.1.2 Cardiomyogenesis

The process of hiPSC-derived cardiomyocyte generation recapitulates embryonic development, so it is important to understand how the cardiac lineage is established in the early embryo.

Cardiomyogenesis begins with the generation of the mesoderm germ layer differentiation with NODAL signaling in the proximal epiblast which maintains BMP4 expression in the extraembryonic ectoderm. Expression of WNT and NODAL antagonists shifts to the anterior visceral endoderm, limiting their signaling to the posterior epiblast. A subset of cells located in the mesoderm gives rise to two main cardiogenic populations, named first and second cardiac fields (FHF and SHF). FHF cells generate the primitive heart tube, contributing to the formation of the left ventricle and the nodal conduction system, while SHF cells contribute to the formation of the right ventricle, part of the atria and the outflow tract. (Rana, Christoffels, and Moorman 2013); (Rochais, Mesbah, and Kelly 2009); (Zaffran et al. 2004). Furthermore, another mesodermal cell population in the so-called pro-epicardium gives rise to epicardial cells (Lavine and Ornitz 2008). In the 7th week of human gestation, the developing heart shows fully septated chambers connected to the pulmonary trunk and aorta.

The differentiation of hiPSCs into cardiomyocytes is induced by specific growth factors involved in heart development (Vidarsson, Hyllner, and Sartipy 2010). To modulate differentiation in vitro, the same signaling pathways as previously mentioned come into play, such as BMP, NODAL, FGF, and Wnt (Filipczyk et al. 2007). Over time, numerous advances have been made in methodologies for directing cardiac differentiation, trying to increase the final percentage of CMs. For example, Laflamme and collaborators's group observed that by using a serum-free medium supplemented with BMP4 and Activin A the differentiation efficiency in cardiomyocytes was better in the monolayer system (Laflamme et al. 2007). Furthermore, Zhang and collaborators reported that it has been observed that the extracellular matrix (ECM) influences differentiation and that the combination of ECM and growth factor signaling in a protocol that uses a double Matrigel layer allows CMs to be generated with high purity (J. Zhang et al. 2012).
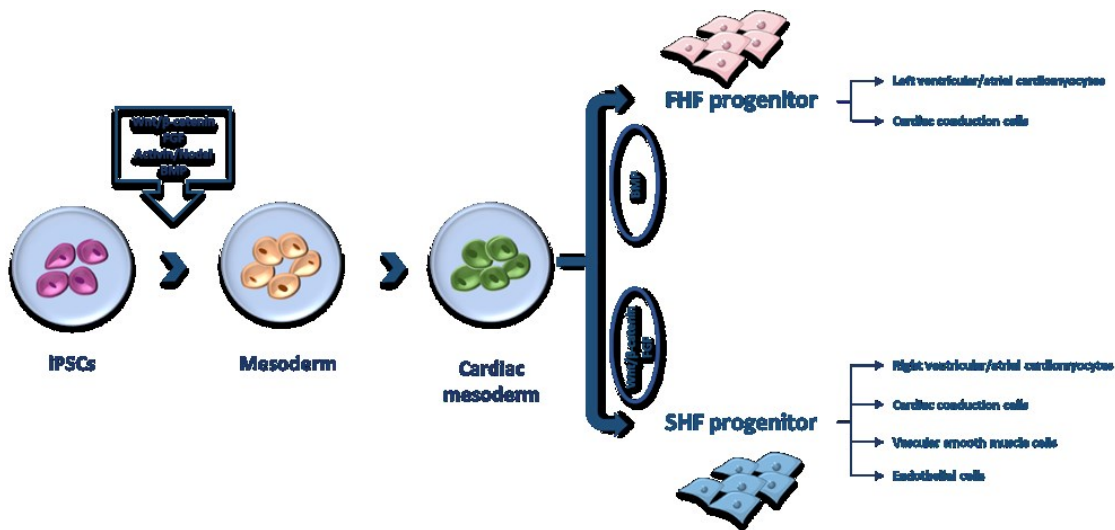
Figure 1.1. *Schematic representation of the initial steps of cardiac lineage commitment. Indication of signaling pathways that influence each differentiation stage and the specific cellular markers expressed during lineage differentiation. FHF, first heart field. SHF, second heart field. Modified by (Leitolis et al. 2019)*

1.1.3 Modeling cardiomyopathies using hiPSC-derived cardiomyocytes (hiPSC-CMs)

hiPSCs obtained from somatic cells have the genetic background of the subject from which they are derived and can be generated from patients with specific diseases to be used as an *in vitro* disease model, for drug screening and in the future are expected to offer new opportunities for regenerative and personalized medicine and for developing tailored therapies for subgroups of patients (Collins and Varmus 2015). hiPSCs can be differentiated into various cell types, including cardiomyocytes, which are an excellent resource for modeling inherited cardiomyopathies, opening new perspectives in the study of early disease defects before the onset of clinical manifestations.
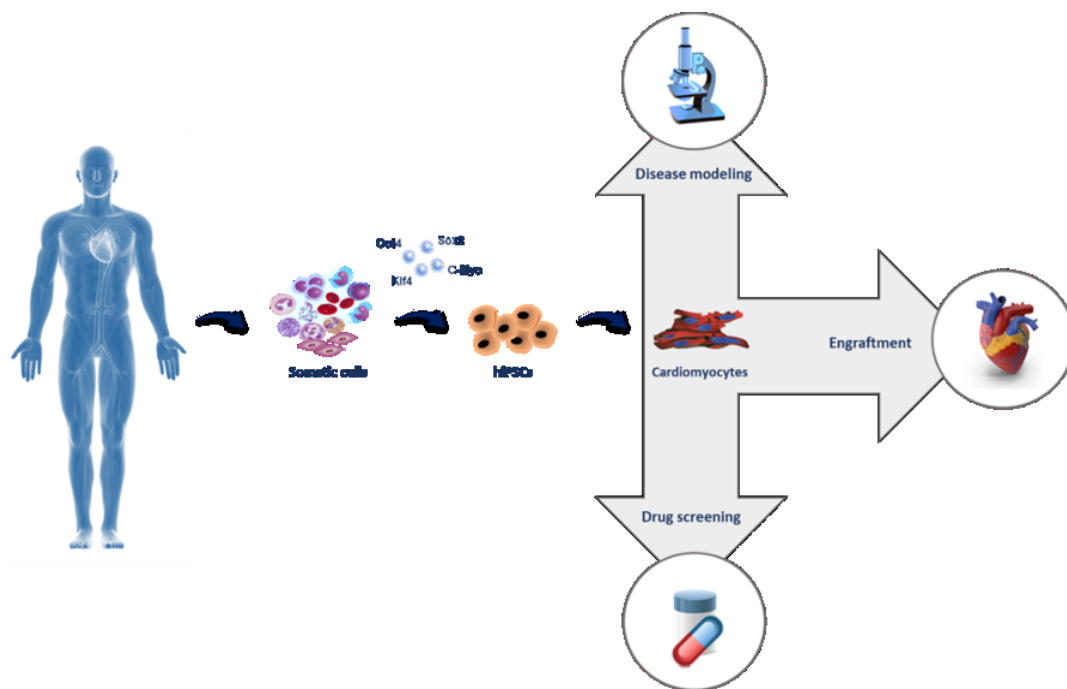
Figure 1.2. Demonstration of somatic cells as a cell source, hiPSC derivation and differentiation into cardiomyocytes. Applications in disease modeling, heart grafting, drug discovery. Modified by (Burridge et al. 2012)

More accurate studies can be carried out by combining the hiPSC model with new genome editing techniques such as CRISPR-Cas9 (Clustered Regularly Interspaced Short Palindromic Repeats), which allows relatively efficient and simple generation of isogenic cell lines that differ only in the DNA sequence of interest. The CRISPR system consists of two components: a small strand of RNA, programmed to search for a specific DNA sequence, and the endonuclease Cas9, an enzyme that can cut a double strand of DNA. Once inside a cell, the CRISPR search device recognizes and binds to the target DNA, and the Cas9 enzyme cuts both DNA strands. In this way, new sections of DNA in the cutting region can be inserted into the cell (Doudna and Charpentier 2014). The CRISPR/Cas9 system has been shown to be an effective technique for creating KO or knockin genes in human cells and particularly in iPSCs (Cong et al. 2013; Horii et al. 2013)(Merkle et al. 2015)(Cong et al. 2013; Horii et al. 2013). In fact, because phenotypic differences between patient-derived iPSC-CMs and controls may be the result of different epigenetic backgrounds, rather than disease-specific variants, it is possible to generate isogenic cell lines by CRISPR-Cas9, which differ only in the mutation to be studied. In this way, it is possible to directly compare hiPSC-CMs carrying disease-associated mutations with corresponding wild-type isogenic controls to determine the exact effect of the mutation on the disease (Wu et al. 2019). This system has already begun to be applied to the study of several heart diseases, such as (Yamamoto et al. 2017) created a specific iPSC clone carrying a heterozygous CALM2 mutation that causes long QT syndrome and used the CRISPR-Cas9 system to perform allele-specific ablation in LQT15-hiPSCs, observing the same electrophysiological abnormalities found in the patient's mutated hiPSC-CMs. Another study was performed on the R302Q mutation in the PRKAG2 gene that causes HCM and hiPSC-CMs carrying this mutation showed electrophysiological abnormalities. In contrast, in

hiPSC-CMs in which the mutation was corrected with CRISPR-Cas9, it was seen that electrophysiological abnormalities were absent compared with mutated cells (Ben Jehuda, Shemer, and Binah 2018). So, this technique can be used to insert new genes, to treat genetic diseases, and to create models for studying human diseases.

Strategy	Advantages	Disadvantages
Patient specific cell lines	● Direct comparison with the same patient tissue ● Pharmacological/pre-clinical studies	● At least 3 patients and clones + healthy controls ● Interindividual variability ● Related or unrelated healthy controls?
CRISPR-Cas9 cell line	● Single cell line comparison ● Mutation-specific phenotype	● Not related to the original patient ● Off target genome editing

Various research works have presented the development of iPSC-based models to study inherited diseases such as channelopathies and cardiomyopathies. Using this *in vitro* model, pathological mechanisms present in human samples can be analyzed to search for potential therapeutic targets. Cardiomyocytes obtained from hiPSCs are used to study inherited cardiomyopathies associated with alterations in sarcomeric proteins (HCM, DCM), mitochondrial proteins (Friedreich's ataxia, Barth syndrome, carnitine palmitoyltransferase II deficiency), desmosomal proteins (arrhythmogenic right ventricular cardiomyopathy, ARVC), dystrophin deficiency (DMD cardiomyopathy) and other rare genetic syndromes (Burridge et al. 2015).

In previous studies, hiPSC-cardiomyocytes from patients with hypertrophic cardiomyopathy (HCM) have been used as an *in vitro* disease-model. Hypertrophic cardiomyopathy is the most common inherited heart disease and studies for the pharmacological treatment are still ongoing. It is also characterized by hypertrophy and disarray at the cellular level and myocardial stiffness due to interstitial fibrosis, causing impaired left ventricular filling and diastolic dysfunction. In 2013, Lan's research group produced an HCM hiPSC-CM line and studied its electromechanical properties. Using patch clamp methods, they demonstrated an increased propensity for delayed after depolarizations in HCM cardiomyocytes compared to controls and observed abnormal Ca^{2+} handling (Lan et al. 2013). Further studies were conducted on a hiPSC-CMs carrying the MYH7-R442G mutation, which caused an AP prolongation and up-regulation of Na^+ and Ca^{2+} currents, the same alterations observed in human cardiomyocytes obtained from HCM patients (Han et al. 2014); (Coppini et al. 2013). Hypertrophic cardiomyopathy is also often caused by mutations in MYBPC3, a gene encoding myosin-binding protein C. Many studies have been conducted on mutations in this protein using hiPSC-CMs as an in vitro model. (Seeger et al. 2019) used isogenic human hiPSC-CMs generated from HCM

patients carrying MYBPC3 PTC mutations (p.R943x; p.R1073P_Fsx4) to study the molecular mechanisms underlying the pathogenesis of HCM associated with this mutation. They observed aberrant calcium handling properties with prolonged decay kinetics and elevated diastolic calcium levels in the absence of structural abnormalities in HCM iPSC-CMs compared with isogenic controls. Furthermore, at the molecular level, they observed that the HCM hiPSC-CMs had the nonsense-mediated decay (NMD) pathway active and several genes involved in major cardiac signaling pathways dysregulated. They also showed that inhibition of the NMD pathway in HCM iPSC-CMs can improve the HCM phenotype at both functional and molecular levels. Thus, they demonstrated that the NMD pathway associated with MYBPC3 PTC mutations may play a role in the pathogenesis of HCM. In addition, it is known that frameshift mutations in cardiac protein C can cause haploinsufficiency, altered phosphorylation of contractile proteins, and reduced ability to generate maximal force in cardiomyocytes (van Dijk et al. 2009). In fact, another study was concerned with assessing the impact of cMyBP-C deficiency on the contractile force generation of hPSC-CMs, and it was observed that hiPSCs cardiomyocytes derived from patients carrying a nonsense mutation in MYBPC3 had <50% of normal cMyBP-C levels and were found to exert significantly less force at the single cell level. These findings were in line with what was observed in adult patient-derived cardiomyocytes, in which a 30%-40% decrease in maximal Ca^{2+}-activated force development was observed. Potential causes of the altered force generation in hPSC-CMs could include a defect in sarcomerogenesis, with reduced myofibril density, disrupted crossbridge cycling, or increased calcium sensitivity of the sarcomere, leading to diastolic dysfunction (Birket et al. 2015). Interesting is also the study conducted on hiPSC-CMs to analyze myeloperoxidase (MPO) levels in cardiomyocytes derived from HCM patients with sarcomeric mutations in MYBPC3 and MYH7 genes. It was observed that in hiPSC-CMs derived from HCM patients, MPO levels were higher than in controls, causing an increase in 3-chlorotyrosine-modified cardiac myosin binding protein-C levels, an attenuation of MYBPC3 phosphorylation, an alteration in calcium signaling and a reduction in cardiomyocyte relaxation. The data obtained prompted the researchers to test on HCM hiPSC-CMs an MPO inhibitor (AZD5904) and observed a restoration of MYBPC3 phosphorylation and a reduction in defects in calcium signaling and relaxation. Because MPO levels are found to be increased in the hearts of patients with left ventricular hypertrophy, these results highlight that the MPO protein may be a novel therapeutic target for improving HCM-associated myocardial relaxation (Ramachandra et al. 2022).

A hiPSC-CM model has also been created for the study of dilated cardiomyopathy (DCM). The first to develop this model with a mutation in the TNNT2 gene were researchers from Sun's group (Sun et al. 2012); subsequently hiPSC-derived cardiomyocytes were also generated from patients with mutations in LMNA (lamin A/C), which cause the onset of DCM, characterized by early onset of atrial fibrillation and conduction system disease, and subsequent progression to sudden cardiac death and heart failure. hiPSC-CMs were then used to recapitulate the disease phenotype, pathophysiology, and drug screening *in vitro* (Siu et al. 2012).

hiPSC-cardiomyocyte models have also been created to study Duchenne Muscular Dystrophy (DMD), which is associated with a vast array of mutations causing a knockout of the dystrophin protein. The absence of this protein makes muscle cells more susceptible to mechanical stress and rupture, leading to muscle scarring and degeneration. Guan et al., in 2014, developed a DMD model from urine-derived

iPSCs and observed that these cells exhibited increased sensitivity to hypotonic stress compared to controls and altered contractile mechanics (Guan et al. 2014). Other studies with DMD hiPSC-CMs showed that the absence of full-length dystrophin is sufficient to decrease force production and to slow kinetics, resulting in impaired contractility (Bremner et al. 2022). Furthermore, it was also observed that DMD hiPSC-CMs showed no improvement in Ca^{2+} release during maturation in contrast to control cells, which displayed a gradual increase in Ca-T amplitude with advanced maturation (Josè Manuel Pioner et al. 2022). The presence of smaller Ca-Ts may indicate an alteration in cardiomyocytes with dystrophin deficiency and this may be associated with a reduction in the force generation in DMD cells (Chang et al. 2021). Additionally, DMD hiPSC-CMs also showed high resting Ca^{2+} levels, causing mitochondrial damage and cell apoptosis. Based on these results, a membrane sealant, Poloxamer 188, was tested on hiPSC-CMs, as previous studies showed that, in CMs isolated from mdx mice, P188 maintained membrane integrity. It was seen that treatment of hiPSC-CMs DMDs with P188 reduced apoptosis by suppressing CASP3 activation, but unfortunately, due to concerns about its toxicity, P188 may not be suitable for long-term use in humans (Lin et al. 2015; Yasuda et al. 2005; Moloughney and Weisleder 2012).

All these studies conducted on hiPSC-CM demonstrate how this model can recapitulate the complex genetic background of disease entities, providing an indispensable platform for the development of techniques for modeling the physiological environment, reducing the use of animal models, to better understand human heart disease and for a more refined therapeutic approach.

Cardiac disease	Gene	Protein	Mutation	Cardiomyocyte subtype	Ref.
HCM	*MYH7*	Myosin heavy chain β	R663H		(Lan et al., 2012)
DCM	*LMNA*	Lamin A	R225X	V- and A-like	(Siu et al., 2012)
	TNNT2	Troponin T type 2	R173W	V-, A-, and N-like	(Sun et al., 2012)
LQT1	*KCNQ1*	Kv7.1/I(Ks)	R190Q	V-, A-, and N-like	(Moretti et al., 2010)
LQT2	*KCNH2*	hERG/I(Kr)	R176W A561T A561V A614V	V- and A-like V-, A-, and N-like V- and A-like V-, A-, and N-like	(Lahti et al., 2012; Matsa et al., 2011; Mehta et al., 2014; Itzhaki et al., 2011)
LQT3	*SCN5A*	Nav1.5 /I(Na)	F1473C V1763M V240M, R535Q	V- and A-like V-, A-, and N-like V-, A-, and N-like	(Terrenoire et al., 2013; Ma et al., 2013; Fatima et al., 2013)
LQT8	*CACNA1C*	CaV1.2/I(Ca)	G1216A	V-, A-, and N-like	(Yazawa et al., 2011)
CPVT	*RYR2*	Ryanodine receptor 2/I(Ca)	F2483I P2328S S406L M4109R E2311D	V-, A-, and N-like Mostly V-like V-, A-, and N-like V-, A-, and N-like V-, A-, and N-like	(Fatima et al., 2011; Kujala et al., 2012; Jung et al., 2012; Itzhaki et al., 2012; Di Pasquale et al., 2013)
ARVC	*PKP2*	Plakophilin-2	L614P	V-, A-, and N-like	(Ma et al., 2013)

Table 1. *Examples of inherited heart diseases modeled using hiPSC-CMs.* HCM: Hypertrophic cardiomyopathy; DCM: Dilated cardiomyopathy; LQT: Long-QT; CPTV: Catecholaminergic polymorphic ventricular tachycardia; ARVC: Arrhythmogenic right ventricular cardiomyopathy

Gene	Protein	Function	Population frequency (%)	Mutations	Phenotypes of hiPSC-CMs with HCM mutations
MYH7	β-Myosin heavy chain	ATPase activity and force generation	~ 15	Het p.Arg663His	Elevated $[Ca^{2+}]_i$, decreased Ca^{2+} release, increased DAD. (Lan et al., 2013)
				Het p.Arg442Gly	Decreased Ca^{2+} store, APD prolongation (60%), I_{Ca} and I_{Na} up. (Han et al., 2014)
				Het p.Glu848Gly	Increased Ca2+ sensitivity, impaired fractional shortening (Pioner et al., 2016; Yang et al., 2018)
				Het/Hom c.C9123T	Increased DAD, increased ATP production, MYH7/MYH6 ratio up. (Mosqueira et al., 2018)
				Het p.Arg403Gln	Maximal contraction velocity + 79%–121%, elevated mitochondrial content, increased ROS, and elevated ratio of ADP/ATP. (Cohn et al., 2019)
				Het p.Arg663His	Increased diastolic [Ca2+]i and Ca2 + sensitivity. (Wu et al., 2019)
MYBPC3	Myosin-binding protein C	Regulator of myocardial contraction and relaxation	~ 20	Het Gly999-Gln1004del	cMyBPC−20% (Tanaka et al., 2014)
				Het c.2373dupG	cMyBPC haploinsufficiency (Birket et al., 2015)
				Het c.1358-1359insC	cMyBPC haploinsufficiency (Prondzynski et al., 2017)

				Het Δ25/ p.Asp389Val	Ca^{2+} transient irregularities. (Viswanathan et al., 2018)
				Het p.Arg943x; Het p.Arg1073Pro	Increased diastolic $[Ca^{2+}]_i$, slower Ca^{2+} decay, decreased contraction and relaxation velocity. (Seeger et al., 2019)
				Het p.Val321Met; Het p.Val219Leu;	Increased diastolic $[Ca^{2+}]_i$ and Ca2 + sensitivity, slower Ca^{2+} decay, reduced NCX function. (Wu et al., 2019)
TPM1	α-tropomyosin	Places the troponin complex on cardiac actin	~ 2	Het p.Asp175Asn	Prolonged APD, increased arrhythmias. (Ojala et al., 2016)
TNNT2	Cardiac troponin T	Regulator of actin–myosin interaction	~ 2	Het c.236 T > A	Increased Ca^{2+} sensitivity, decreased peak Ca^{2+} transients, APD50 prolongation. (Wang et al., 2017)
				Het p.Ile79Asn	Decreased sarcomere length, increased Ca^{2+} sensitivity, decreased peak Ca^{2+} transients. (Wang et al., 2018)
TNNI3	Cardiac troponin I	Inhibitor of actin–myosin interaction	~ 2		
ACTC1	Cardiac α-actin	Major constituent of contractile apparatus	<1	Het p.Glu99Lys	Increased arrhythmias, increased DAD. (Smith et al., 2018)
MYL2	Regulatory myosin light chain	Affects actin–myosin dissociation and regulates contraction	~ 1	Het p.Arg58Gln	Diastolic $[Ca^{2+}]_i$ – 23%, peak Ca^{2+} transients – 45 %, I_{Ca} – 45%, increased arrhythmias. (Zhou et al., 2019)
MYL3	Essential myosin light chain	Binds to myosin heavy chain and stabilizes myosin conformation	<1	Het c.170C > G	Increased diastolic $[Ca^{2+}]_i$, DAD, contraction and relaxation. (Ma et al., 2018)

Table 2. *List of genes causing HCM and studies reporting phenotypes of human iPSC-CM lines with HCM mutations. Modified from (J. Li, Feng, and Wei 2022)*

17

1.1.4 Comparison of hiPSC-, human fetal- and adult ventricular- cardiomyocytes structure and function

The cardiomyocytes obtained from hiPSCs described possess a defined cardiac phenotype, but they exhibit immature structural and functional properties; the resulting cardiac population is heterogeneous and consists of atrial, ventricular, and nodal cells. hiPSC-CMs exhibit characteristics much more like those of human fetal cardiomyocytes, in fact have disorganized sarcomeres, reduced contraction forces and reduced action potentials compared with adult cardiomyocytes. The characteristics of adult, fetal and hiPSC-derived cardiomyocytes are described below to assess maturation status.

Morphology

Cell size and shape are important parameters as they affect pulse propagation, maximum depolarization rate of action potential, total contractile force, and E-C coupling (Spach et al. 2004)As is described in **Table 3**, the surface area of hiPSC-CMs is like that of fetal cardiomyocytes and is much smaller than that of adult cardiomyocytes. In addition, adult cardiomyocytes are elongated, longitudinally aligned, and have mitochondria, polarized intercalated disc complexes and T-tubules, which allow rapid propagation of AP into the cell and play an important role in regulating cellular calcium concentration (Vreeker et al. 2014). Also, multinucleation is a sign of maturation, has a great impact on the elevation of gene expression and cell growth and varies among species. For instance, about 30% of adult cardiomyocytes are binucleated, unlike fetal- and hiPSC-cardiomyocytes are almost exclusively mononucleated (H. Kim 1992); (Olivetti 1996). Moreover, the latter mentioned are smaller than adult cardiomyocytes and have a round or polygonal shape, a more chaotic organization and T-tubules are few or absent (Louch, Sheehan, and Wolska 2011); (Itzhaki, Rapoport, et al. 2011); (Mummery et al. 2003); (Snir et al. 2003).

Metabolism

The energy demand of the heart is very high and energy production pathways are therefore extremely important for working cardiomyocytes. During heart development, mitochondria manifest structural and functional changes; in adult cardiomyocytes, mitochondria are regularly distributed and occupy 20% to 40% of cell volume, and their main source of energy is β-oxidation of fatty acids. In hiPSC-CMs, mitochondria are small, less numerous, and located in the perinuclear region, and unlike adult cardiomyocytes, the preferred metabolic substrates of hPSC-CMs are glucose and lactate, as in the fetal heart. (Gherghiceanu et al. 2011); (C. Kim et al. 2013); (Schaper et al. 1980); (Lopaschuk and Jaswal 2010).

Sarcomere

The sarcomere is the functional unit of the striated muscle and is composed of longitudinally repeated subunits of myofibrils that serve as the contractile apparatus of the cardiomyocytes. The sarcomere structure of adult cardiomyocytes is highly organized and the different functional units such as the Z-discs, which mark sarcomere borders, and the A-, I-, H- and M-bands are visible (Gregorio and Antin

2000; Boateng and Goldspink 2008). In fetal cardiomyocytes, the sarcomeric structure develops gradually during gestation and the Z-discs and I-bands are formed first. Ultrastructural analysis revealed that hiPSC-CMs present a myofibrils disarray and an immature sarcomeric structure, in which only the Z-discs and I-bands are visible (Snir et al. 2003). In addition, sarcomeric length, which represents the distance between two Z-discs, is another indicator of cell maturation. In adult cardiomyocytes, the sarcomeric length is approximately 2.2μm, whereas in hiPSC- and fetal cardiomyocytes, the length is shorter and is approximately 1.6-1.8μm (Bird 2003); (Lundy et al. 2013); (H. Kim 1992).

The presence of an immature structure in hiPSC-CMs is also reflected in their reduced contractile force. The active force generated by these cardiomyocytes is in the range of 0.1 to 4 mN/mm^2, depending on the conditions under which is measured, and is significantly lower than that of adults CMs, which is around 10–50 mN/mm^2 *(Schaaf et al. 2011); (Holubarsch 1998).* In support of this observation, Pioner's research group measured the contractile force of single myofibrils isolated from hiPSC cardiomyocytes, and it was observed that myofibrils from these cardiomyocytes (80 days p.d.) have a force-generating capacity much more like that of human fetal ventricular myofibrils (74 days gestational) than adult human ventricular myofibrils (Josè Manuel Pioner et al. 2016); (Piroddi et al. 2007); (Racca et al. 2016). This may also be due to the different expression of myofibrillar proteins, which modulates the contractile function of cardiomyocytes and are also expressed differently between mature and immature cardiomyocytes, as many isoforms change during maturation. For example, the beta-myosin heavy chain (β-MHC), encoded by *MYH7*, is highly expressed in adult ventricular cardiomyocytes compared to the α-MHC isoform, encoded by *MYH6*, and in fetal cardiomyocytes, it has been observed that α-MHC is initially expressed, but during gestation the switch to the β-MHC isoform occurs (Reiser et al. 2001) . In contrast to fetal and adult cardiomyocytes, in hiPSC-CMs more α-MHC is present, but at later stages of cell maturation they also begin to partially express β-MHC (Ivashchenko et al. 2013)*; (X. Q. Xu et al. 2009).* Troponin I also undergoes an isoform switch during cardiac development: in fetal heart, slow skeletal troponin I (ssTnI) is the most expressed isoform before a complete switch to the adult cardiac troponin I (cTnI) (Bhavsar et al. 1991). Therefore, the ssTnI isoform controls immature sarcomere, in fact it's present in hiPSC-CMs and appears to have greater Ca^{2+}- sensitivity for tension production than cTnI (Hunkeler, Kullman, and Murphy 1991)*.* Another sarcomeric protein with numerous spliced isoforms is titin, which plays a key role in maintaining sarcomere elasticity and integrity. In adult cardiomyocytes, the most abundant isoform is N2B, which is a shorter and stiffer form than N2BA, the most highly expressed isoform in fetal and adult cardiomyocytes. These variations regulate the passive tension of cardiomyocytes during maturation (Lahmers et al. 2004); (Neagoe et al. 2002).
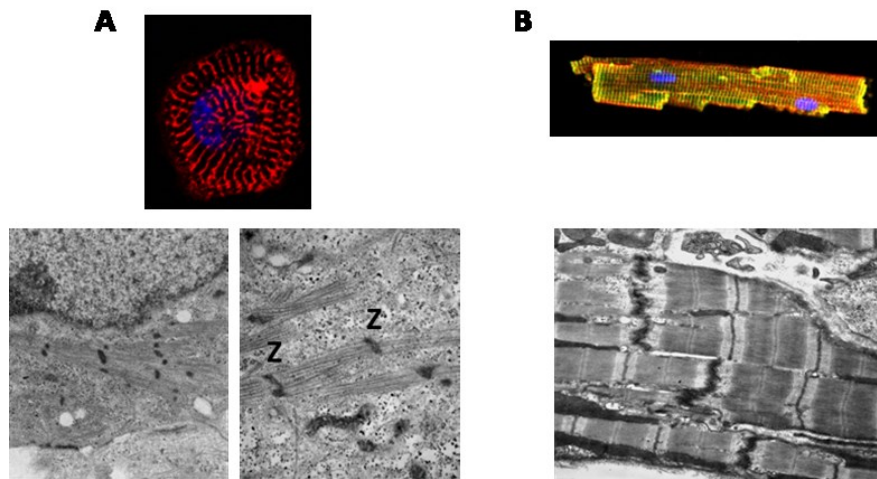
Figure 1.3. Ultrastructural images of hiPSC- and adult cardiomyocytes. A) Disoriented myofibrils and immature sarcomeric structure in hiPSC-Ms; B) Sarcomere structure and a large intercalated disk in adult cardiomyocytes.
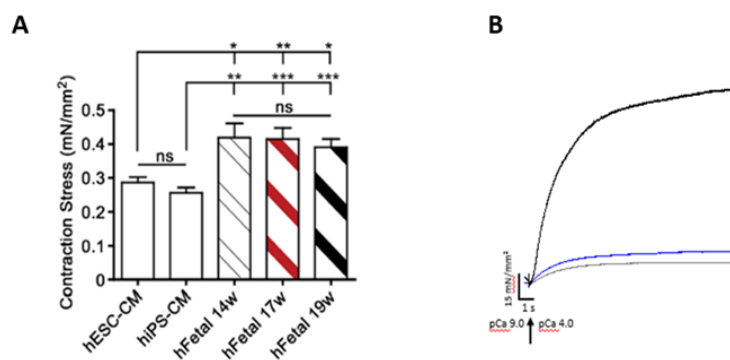
Figure 1.4. Functional analogies between hiPSC- and fetal-CMs. A) Comparison of contraction and B) representative traces of tension generation of hiPSC-CM (blue), human ventricular fetal (gray) and adult (black) myofibrils maximally activated. (Pioner, 2016)

Electrophysiological properties

The cardiac action potential (AP) is the electrical stimulation created by a sequence of ionic flows through specialized channels in the membrane of cardiomyocytes. AP features are unique for each subtype of cardiomyocytes (atrial, ventricular, pacemaker, Purkinje). Many factors can contribute to the variation of atrial-, nodal- and ventricular-like APs, including culture conditions of the differentiated cardiomyocytes and recording procedures. The electrophysiological phenotype of hiPSC-CMs is distinct from that of adult CMs, mainly due to different expression of key ion channels. Indeed, the spontaneous contractile activity of hiPSC-CMs is due to a high expression of HCN4 channels that mediate the pacemaker current (I_f); this current is very low in adult ventricular cardiomyocytes, which only beat when stimulated (Sartiani et al. 2007);(Verkerk et al. 2007). hiPSC-CMs are also characterized by significantly depolarized resting membrane potential (RMP), which ranges from −50 mV to −60 mV and is more positive than the adult RMP (−85 mV), partly also due to low/absent I_{K1} hyperpolarizing current (Amin, Tan, and Wilde 2010; J. Ma et al. 2011). Recently,

Moretti's research group (2010) demonstrated that the other main repolarizing currents, I_{Kr} and I_{Ks} are present in hiPSC-CMs at similar levels to adult cardiomyocytes; in addition, the hiPSC-CMs present a lower levels of the sodium channel Nav1.5 and the L-type calcium channel, leading to slower upstroke velocity and to a lack or a shorter plateau phase (Liu, Laksman, and Backx 2016); Sartiani et al.,2007). Lastly, the electrical conduction velocity in hiPSC-CMs is slower (10 cm/s) than in adult human left ventricle (60 cm/s), partly due to the different gap-junctions density and composition and probably also due to the cell size, which is positively correlated with conduction velocity (Scuderi and Butcher 2017); (Taggart et al. 2000); (P. Lee et al. 2012).
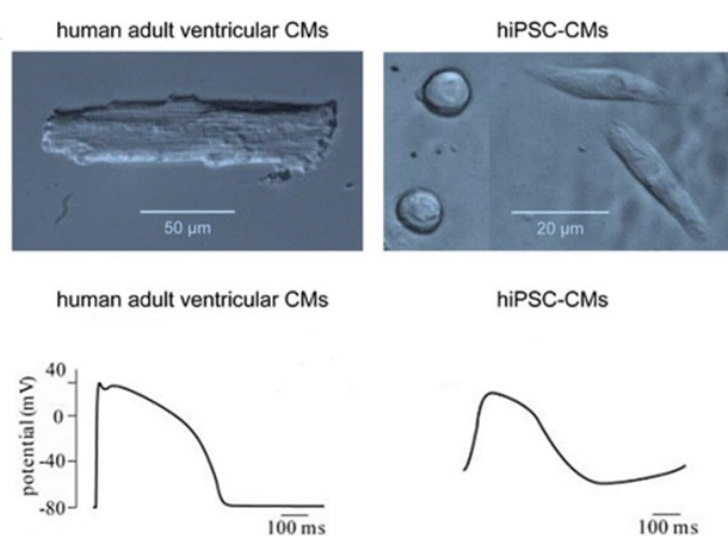
Figure 1.5. Morphological differences between human adult ventricular CMs and hiPSC-CMs and examples of action potential in human adult ventricular CMs and hiPSC-CMs. (Figure modified from (Meijer van Putten et al. 2015) (Veerman et al. 2015).

Calcium Handling

The cardiomyocyte has a sophisticated regulatory system known as excitation-contraction coupling. Ca^{2+} is the second essential messenger in cardiac electrical activity and is the direct activator of myofilaments, which promote contraction. During an action potential, Ca^{2+} enters the cell through voltage-dependent Ca^{2+} channels as inward Ca^{2+} current (I_{Ca}) and stimulates the release of Ca^{2+} from the ryanodine receptors (RyRs) of the sarcoplasmic reticulum (SR), raising intracytoplasmic Ca^{2+} levels. The rising Ca^{2+} binds to troponin C in the myofilaments and this led to mechanical contraction. This is followed by the relaxation phase, in which the Ca^{2+} cytosolic level must fall, whereby the Ca^{2+} dissociates from the troponins and is repumped partly into the SR by the sarcoplasmic reticulum Ca^{2+} ATPase (SERCA) and partly extruded from the cell via the sodium/calcium exchanger (NCX). This Ca^{2+} transient modulates cardiac contraction and takes place in a time order of 600-800 ms in human heart muscle (Bers 2002).
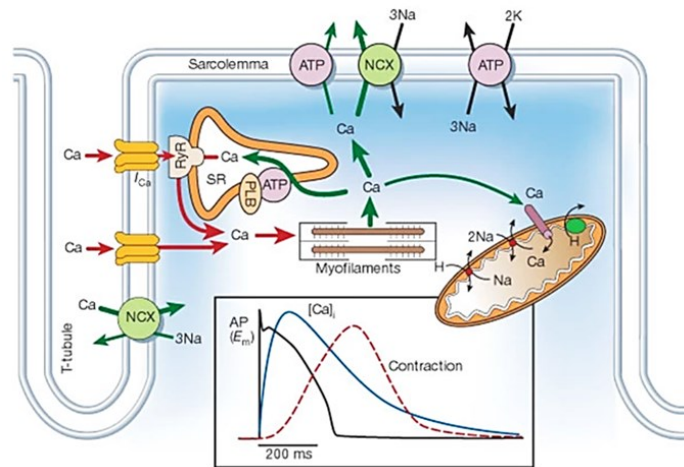
Figure 1.6. *Representation of Ca²⁺ transport in myocytes (Bers, 2002)*

Ca^{2+} release and extrusion are efficient in adult cardiomyocytes (Beuckelmann, Näbauer, and Erdmann 1992)*, whereas fetal- and hiPSC- cardiomyocytes show a more immature phenotype regarding calcium handling. This is due to a lack of T-tubules, invaginations in the membrane where L-type Ca^{2+} channels are concentrated near RyR channels, an underdeveloped SR and reduced expression of proteins that regulate calcium handling, such as SERCA, calsequestrin (calcium-buffering protein), ryanodine receptor type 2 (RyR2) and phospholamban (PLN). Therefore, the kinetics in immature cardiomyocytes are slower and the amplitudes reduced compared to adult cardiomyocytes (Synnergren et al. 2012); (Itzhaki, Rapoport, et al. 2011)*;(Dolnikov et al. 2006)*.
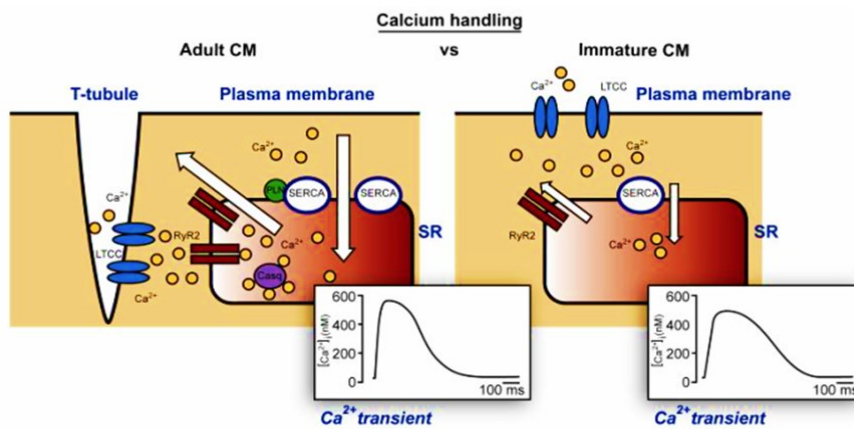
Figure 1.7. *Illustrative scheme representing Ca²⁺ influx and extrusion in adult and immature cardiomyocytes. (Veerman et al., 2015)*

		hiPSC-CMs	hFetal-CMs	hAdult-CMs	Ref.
Morphology	**Shape**	Flat, round or polygonal	Round or polygonal	Rod-shaped and elongated	(Snir et al., 2003, Mummery et al., 2003)
	Alignment	Chaotic	Chaotic	Longitudinal	(Yang et al., 2014, Peters et al., 1993)
	Surface area	1000-1300µm²	1216±45µm²	12.315±2.103µm²	(Ribeiro et al., 2015; Li et al.,1996)
	T tubules	No	Perinatal formation	Yes	(Snir et al., 2003, Lundy et al., 2013, Ferrantini et al., 2013)
Nuclei		Mononucleate	Mono/Bi-nucleated	bi- or poly-nuclear	(Snir et al., 2003, Kim et al., 1992)
Mitochondria		Low number	Few in number in the earlier period of fetal development	20–40% of cell volume	(Kim et al., 1992, Shaper et al., 1980)
Metabolism		Glycolysis	Glycolysis	Fatty acids	(Yang et al., 2014)
Sarcomere	**Organisation**	Disarrayed	Organised	Highly organised	(Yang et al., 2014, Kim et al., 1992)
	Banding pattern	Mainly Z-discs and I-bands	Mainly Z-discs and I-bands	Z-discs, I-, H-, A- and M-bands	(Gregorio et al., 2000, Boateng et al., 2008, Snir et al., 2003)
	Lenght	1.6 µm	1.8µm	2.2 µm	(Lundy et al., 2013; Yang et al., 2014)
	MHC	(αMHC)>(βMHC)	(βMHC)>(αMHC)	(βMHC)>(αMHC)	(Yang et al., 2014, Reiser et al., 2001)
	TnI	ssTnI	ssTnI > cTnI	cTnI	(Yang et al., 2014)
	Titin	N2BA	N2BA	N2B	(Yang et al., 2014)
Electrophysiology	**Beating rate (Bpm)**	Atrial-like: 107 Ventricular-like: 51.3	Spontaneous	Paced	(Doss et al., 2012)
	Resting membrane potential (RMP)	−20 to −60 mV	-40 to -50 mV	− 80 to − 90 mV	(Lundy et al., 2013; van den Heuvel et al., 2014, Drouin et al.,1995)
	APD 90 (msec)	Atrial-like: 232.9 Ventricular-like: 324.8	~300-400ms	~350ms	(Doss et al., 2012, Coppini et al., 2013, Crescioli et al., 2007)
	I_f	-4.1, -3.0 pA/pF	n.d	-1.18 pA/pF	(Ma et al., 2011, Zhang et al. 2015, Hoppe et al., 1998)

	I_{CaL}	-6.6 pA/pF	n.d	-10.2 pA/pF	(Ma et al., 2011, Veerman et al., 2016, Zhang et al., 2013, Magyar et al., 2000)
	I_{K1}	From -0.8 to -5.1 pA/pF	From 9 to 13 pA/pF	From -3.6 to 32.1 pA/pF	(Ma et al., 2011, Lee et al., 2016, Doss et al. 2012, Meijer et al., 2015, Crescioli et al., 2007)
Cell contractility	Shortening	Few response to electric stimuli	n.d	Fully responsive to electric stimuli	
	Time to peak (msec)	300-500ms	n.d.	200ms	(Brixius et al., 2007)
	Tension	0.1 to 0.5 mN/mm^2 0.08–4 mN/mm^2 (3D constructs)	0.4 mN/mm^2	10–50 mN/mm^2 (muscle strips)	(Schaaf et al., 2011; Mulieri et al., 1992)
Calcium Handling	Transient amplitude	~0.25 F/F$_0$	n.d.	~300nmol/l	(Lundy et al., 2013, Coppini et al., 2013)
	Transient Decay (50%)	~220-440ms	n.d.	200ms	(Lundy et al., 2013)
	Sarcoplasmic Reticulum	Partially developed	Partially developed	Ca^{2+}induced Ca^{2+} release (CICR) via SR	(Yang et al., 2014, Li et al., 2013)
Myofibrils	Tension	18.6 mN/mm^2 (80 days p.d.)	23.1 mN/mm^2 (74 days gestational)	90-110 mN/mm^2	(Pioner et al., 2016, Racca et al., 2016, Piroddi et al., 2007, Belus et al., 2010)
	Kinetics of activation and relaxation	k_{ACT} 0.51 s^{-1} $k_{REL\ slow}$ 0.30 s^{-1} (80 days p.d.)	k_{ACT} 0.43 s^{-1}; $k_{REL\ slow}$ 0.22 s^{-1} (74 days gestational)	k_{ACT} 0.73-0.84 s^{-1}; $k_{REL\ slow}$ 0.3 s^{-1}	(Pioner et al., 2016, Racca et al., 2016, Piroddi et al., 2007, Belus et al., 2010)

Table 3. Comparison of current knowledge in structure and function of hiPSC-, human fetal- and adult ventricular- CMs from the literature

1.1.5 Limitations and strategies for hiPSC-CMs maturation

Although hiPSC-CMs possess a definite cardiac or cardiomyopathic phenotype that makes them a promising model for a wide range of applications, it is necessary to consider and address some inherent limitations that these cells present. In general, hiPSC-derived cardiomyocytes exhibit immature structural and functional properties and this remains an obstacle for using this model to study new therapies and evaluate the efficacy and/or toxicity of new drugs. In recent years, several techniques have been developed to improve cell maturity, including cells growing patterning scaffolds, exposure to electrical stimuli, application of mechanical stress, co-culture with other cell types and culture of hiPSC-CMs in a three-dimensional tissue configuration. Much progress has been made in inducing the maturation of hiPSC-CMs, improving their structure and function, and demonstrating that

they cannot be permanently relegated to an immature state (Lundy et al., 2013). The various methods adopted over the years to improve cell maturation are described below.

Long-term culture

One of the approaches to improving cell maturation is long-term culturing, classifying post-differentiation days into early (15-30 p.d.) and later stages (>60 days p.d.) of maturation. In many research works, the reported data show that hiPSC-CMs mature over time both morphologically and functionally. Lundy et al. (2013), observed morphological differences between early- (20–40 days) and late-stage CMs (80–120 days), including an increase in cell size and anisotropy, greater myofibril density and alignment and an increase in the fraction of multinucleated CMs.
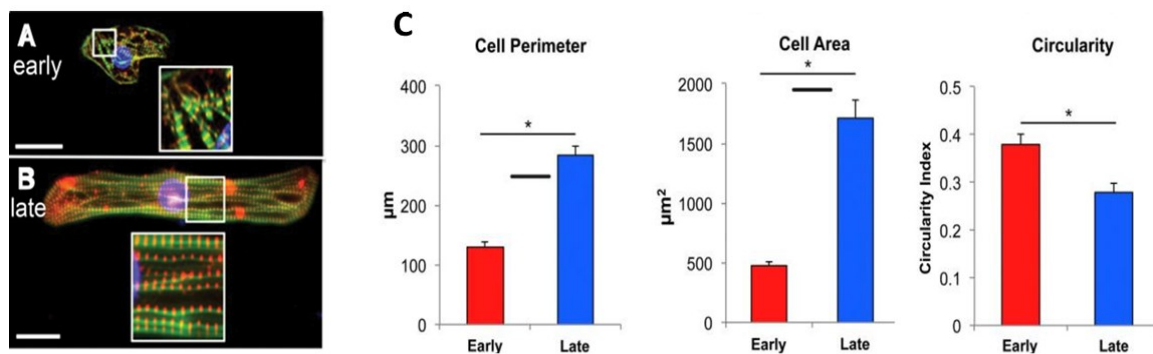
*Figure 1.8. Effects of long-term culture on hiPSC-CMs maturation. **A)** and **B)**, Representative hiPSC-CMs immunostained for α-actinin (red) and filamentous actin (phalloidin, green). Nuclei (blue). **C)** cell perimeter and cell area were increased with a decrease in cell circularity. (Lundy et al. 2013)*

Very interesting is also the ultrastructural analysis performed by Kamakura's group (Kamakura et al. 2013) on hiPSC-CMs during 1 year of culture after cardiac differentiation and it was observed that through long-term culture up to 180 days, the myofibrils formed parallel arrays with the presence of mature Z, A, H, and I band, but not M bands. Surprisingly, M-bands were detected after 360 days of maturation, but the expression levels of M-band-specific genes in hiPSC-CMs remained lower than in the adult heart (**Fig. 9**).
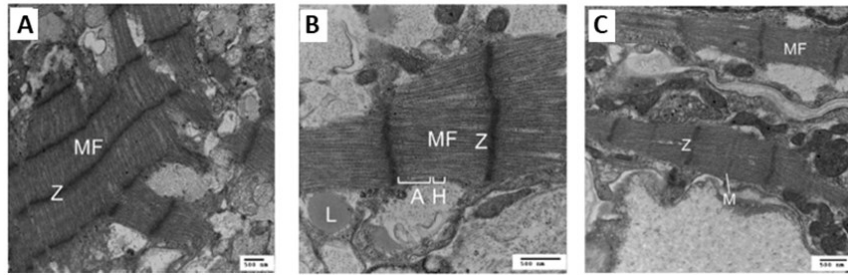
*Figure 1.9. Transmission electron microscopy images of hiPSC-CMs at 60 **(A)**, 180 **(B)** and 360 days **(C)** after cardiac differentiation (Kamakura et al., 2013)*

In addition, at the sarcomeric level, the expression of cardiac myosin was analyzed, which is considered a marker to assess hiPSC-CMs maturation during long-term culture. There are two isoforms of cardiac myosin light chain 2 (MLC2), MLC2a and MLC2v; the latter is considered a marker of cardiac myocyte maturity (Kubalak et al. 1994). It was observed that hiPSC-CMs at early stages expressed the MLC2a isoform, whereas after long-term culture they also expressed the MLC2v isoform, with a reduction in MLC2a. After long-term culture, it was also seen that hiPSC-CMs expressed cTnI in addition to ssTnI, but the ratio of cTnI:ssTnI stabilized at ∼2:98, confirming that hiPSC-CMs in late stages of maturation, despite showing more mature characteristics than early stages, continue to be more similar to fetal cardiomyocytes than adult cardiomyocytes (Bedada et al. 2014; Bedada, Wheelwright, and Metzger 2016).

Through electrophysiological study, Sartiani et al. (2007) analyzed the current density and kinetics of different ion channels during cardiomyocyte maturation. The results showed an increased density of I_{k1} and I_{t0} and slower activation kinetics of I_f current. Finally, it was observed that late-stage cardiomyocytes were characterized by increased calcium release and reuptake rates (Lundy et al., 2013). In addition, spontaneous beating rate after 2 months of culture was reported to decrease in some culture conditions (Hazeltine et al. 2012).

In line with this, Pioner et al. (2019) evaluated the regulatory mechanisms of cardiac contraction in hiPSC-CMs at different time points of maturation (60, 75, and 90 days post differentiation) by simultaneous recordings of AP and calcium transients using a dual optical method. The duration of APs was recorded from individual hiPSC-CMs using the patch-clamp technique (earlier-stages) and Fluovolt approach (later-stages) at any progressive time point. They observed that at the later stages of maturation, hiPSC-CMs showed prolonged APs and increased calcium transient amplitude and at day 90 p.d. (**Fig. 1.10**), the average AP duration and calcium transients (CaT) duration in hiPSC-CMs were more similar to the AP profile and CaT kinetics of ventricular hAdult-CMs. The AP prolongation observed in hiPSC-CMs may be associated with a greater contribution of I_{CaL} during the plateau phase, which prevails over the increase of repolarizing outward potassium currents (I_{Kr} and I_{to1}), as previously described (Lundy et al., 2013). The results also showed a more negative resting membrane potential recorded after day 60 probably due to an increase in ionic currents contributing to the diastolic potential, such as I_{k1}. The increase in I_{k1}, also observed by Sartiani et al. (2007), may explain the decrease in spontaneous beating rate at 60 days p.d. and the subsequent greater response to external electrical stimulation. Other possible contributors to the acquisition of this physiological behavior

during hiPSC-CM maturation are the decrease of funny current (If) and the increase of the delayed rectifier potassium currents (I_{Ks} + I_{Kr}) (Bosman et al. 2013). Many ion currents (e.g., I_{to1}) undergo developmental changes, similar to those occurring during the fetal cardiac development (Sartiani et al. 2007). For this reason, the AP profile of early hiPSC-CMs maintains some of the features of fetal cardiomyocytes.
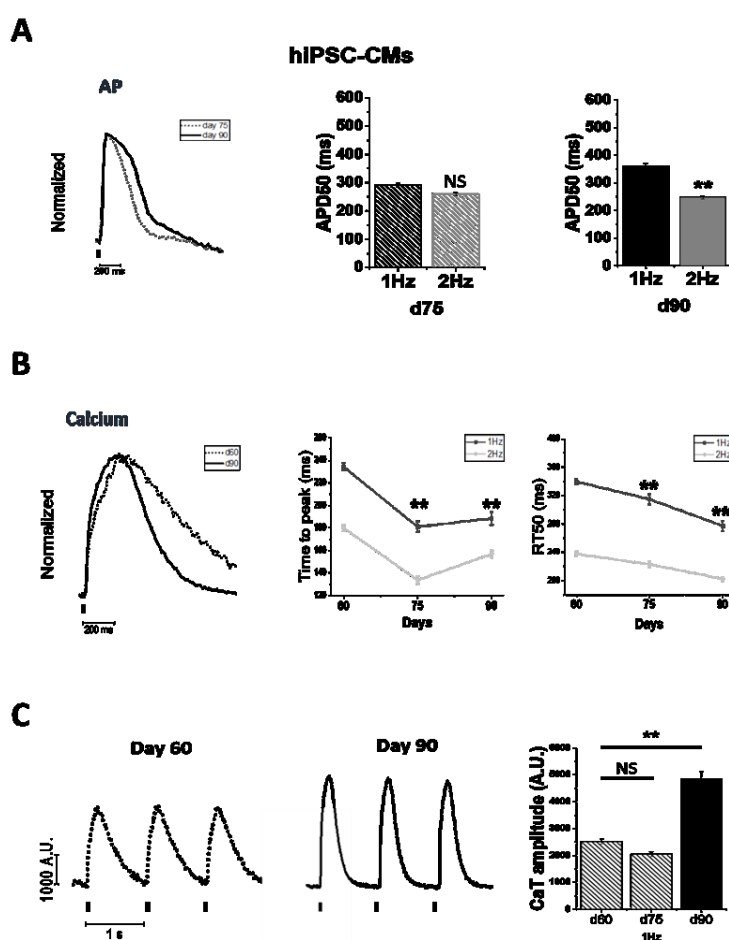
Figure 1.10. A) Superimposed action potential (AP) traces of day 75 vs day 90 recorded both at 1 and 2 Hz. C) superimposed normalized traces of calcium transients recorded by Cal630 at day 60, 75,90 : average CaT rise (time to peak TTP, ms) and CaT decay (difference of 50% of CaT decay and TTP, RT50, ms) are reported, during pacing at 1 and 2 Hz and representative CaT profiles at day 60 and 90 and average CaT amplitude at day 60,75 and 90. From (Josè Manuel Pioner et al. 2019).

In addition, an acceleration of CaT duration and adaptation of CaT kinetics and amplitude to frequency changes in later stages was observed, probably attributable to the increase in SERCA/PLB function associated with sarcoplasmic reticulum development. The presence of a more mature SERCA function is also supported by observation of the caffeine transient decay rate (τ) in hiPSC-CMs. A post rest potentiation protocol was applied to evaluate the maturation of cardiomyocyte inotropic reserve and they saw that CaT amplitude after the rest pause displayed a modest potentiation over the amplitude before the pause at day 60. However, the amplitude of post-rest CaTs almost doubled at day 90, suggesting increased SR loading capacity during maturation (day 60 vs. 90). To verify the contribution of SR calcium content, they evaluated caffeine-induced calcium transients after a pacing train of 2 Hz. The amplitude of caffeine-induced CaT at d60 was doubled compared to corresponding steady state

calcium transients at 2 Hz pacing. These results indicated a significant contribution of calcium release from the SR to the amplitude of calcium transients starting from day 60 p.d. **(Fig. 1.11)**.
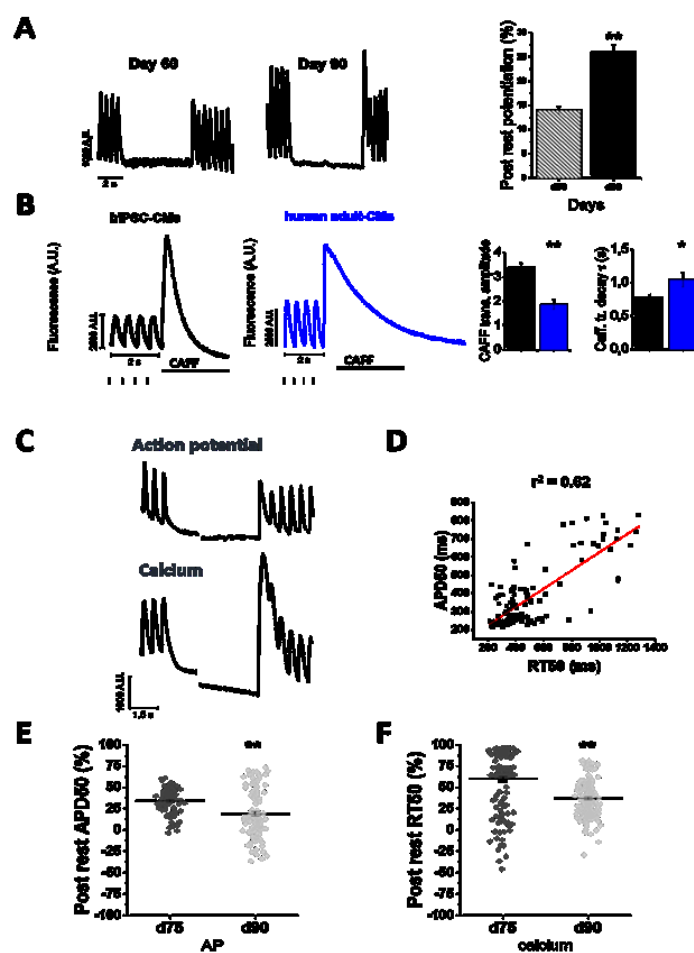
Figure 1.11. Sarcoplasmic reticulum (SR) contribution in calcium handling maturation was tested by a post rest potentiation protocol and caffeine-induced CaTs elicited in hiPSC-CMs at multiple maturation time-points. (A) The post-rest potentiation of CaT amplitude was estimated after a resting pause of 5 s, inserted in a regular train of stimulation at 2 Hz. Post rest potentiation is estimated at day 60 and day 90. (B) Caffeine-induced CaTs (quick exposure to 10 μM caffeine) after a series of 2 Hz paced CaTs. Average of caffeine transient amplitude was normalized by the amplitude of steady-state calcium transients at 2 Hz prior to caffeine exposure (N = 2; n = 83). Caffeine transient CaT amplitude (CaTA CAFF/CaTA 2Hz ratio) and decay (τ, s−1) of hiPSC-CMs were calculated and compared with caffeine-CaT recorded in hAdult-CMs (N = 5; n = 14). (C) Simultaneously recorded APs and CaTs during the pause protocol. (D) APs and CaTs from the same cells were compared to show Pearson's correlation (r2) between post rest AP duration (APD50, ms) and post rest CaT decay (RT50, ms, p < 0.05). (E) Variations of post rest APD50 and (F) post rest RT50 were measured both at day 75 (AP: N = 2, n = 119; CaT: N = 5, n = 251) and day 90 (AP: N = 2, n = 119; CaT: N = 3, n = 165). (Pioner et al., 2019)

In addition, they also observed a positive lusitropic effect under β-adrenergic stimulation, which involves an amplified contribution of SERCA. They tested the effect of isoproterenol (ISO), which binds β-adrenergic receptors (βARs) type 1 and 2 in cardiac cells and activates the cAMP-PKA phosphorylation pathway, and forskolin (FSK), which stimulates adenylate cyclase, increasing cAMP levels to activate PKA.

Figure 1.12. *Positive β-adrenergic response of later stage hiPSC-CMs. Day 90 hiPSC-CMs were exposed to isoproterenol (ISO, 1 μM) and forskolin (FSK, 1 μM). **(A)** Represent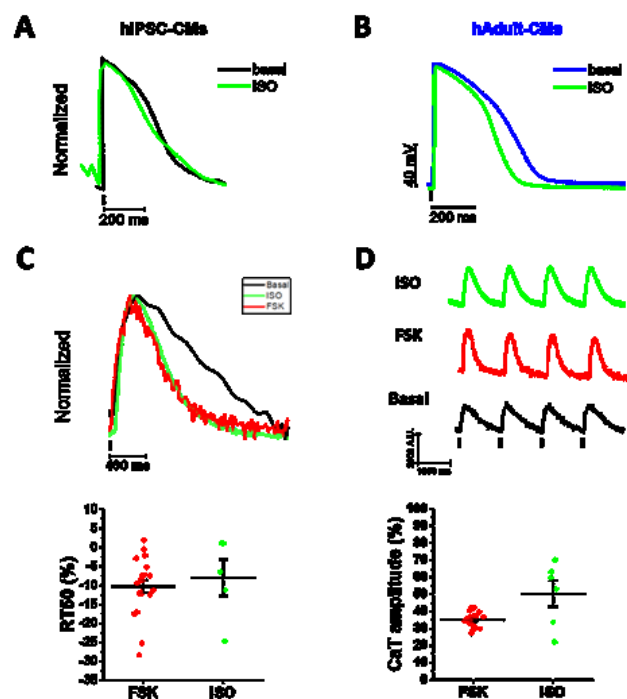ative traces of hiPSC-CM AP recorded before and under ISO stimulation. APD50 reduction under ISO was 12 ± 4%, p > 0.05. **(B)** Representative traces of ISO effect on the APD50 of human adult cardiomyocytes (15 ± 3%, p < 0.05)(hAdult-CMs: N = 5 patients, n = 12 cells). **(C,D)** Relative positive inotropic and lusitropic effects of both ISO and FSK (%) in later stages hiPSC-CMs (ISO: N = 2, n = 7; FSK: N = 2, n = 21).(Pioner et al., 2019)*

Pioner and coworkers exposed hiPSC-CMs at day 90 to ISO or FSK and observed that ISO reduced APD50 in hiPSC-CMs stimulated at 1Hz, as in adult CMs. In addition, RT50 of CaT was faster under both ISO and FSK exposure (positive lusitropic effect) in hiPSC-CMs and in both cases CaT amplitude was also increased, indicating a positive inotropic response (**Fig. 1.12**) (Pioner et al., 2019).

Substrate stiffness

To improve the cultured performance of hiPSC-CMs, many researchers are exploiting the ability of these cells to respond to stimuli from their surrounding microenvironment; these signals can influence cell fate, proliferation, and differentiation. Knowing that these stem cells sense the external environment, it is thought that exposure to physiological stimuli and the use of nano-structured biomimetic surfaces may help to enhance cell adhesion, proliferation, and migration, as well as cardiomyogenic differentiation and structural development. It has been observed that biomimetic surfaces are valuable in promoting the structural and functional maturation of immature cardiomyocytes in culture. (D.-H. Kim et al. 2010), constructed a nanofabricated anisotropic substrate with ridges and grooves ranging from 150 to 800 nm to faithfully reproduce a nanoscale structure of the myocardial extracellular matrix and observed that cardiomyocytes were able to align along the direction of the topographical structure and that there were differences in cell geometry, conduction velocity and Cx43 expression between aligned and non-aligned cells in culture. Thus, morphological anisotropy of culture surfaces leads to a more rapid elongation of cardiomyocytes, and their stiffness may also influence cell shape, which is crucial for modulating cell survival, and maturation. In addition,

compared with the softer substrate, cardiomyocytes cultured on stiffer substrates are able to generate higher tension, which may be related to higher matrix resistance and the formation of many focal adhesions (**Fig. 1.14**) (Park et al. 2012; Querceto et al. 2022). (Josè Manuel Pioner et al. 2019), demonstrated that micropatterned surfaces with linear grooves and ridges have a strong impact on the regulation of calcium homeostasis and cellular electrophysiology; hiPSC-CMs showed a prolonged action potential, probably associated with an increased contribution of I_{CaL} during the plateau phase, which overrides the increase in repolarising outward potassium currents (I_{Kr} and I_{to1}). Cells cultured on these surfaces for long time thus more closely reflect the functional properties of native human cardiomyocytes; understanding the effects of substrates on cell maturation is extremely important for in vitro modeling of e.g cardiomyopathies, which may be related to changes in extracellular stiffness (myocardial fibrose accumulation) that severely affect cardiomyocyte function.
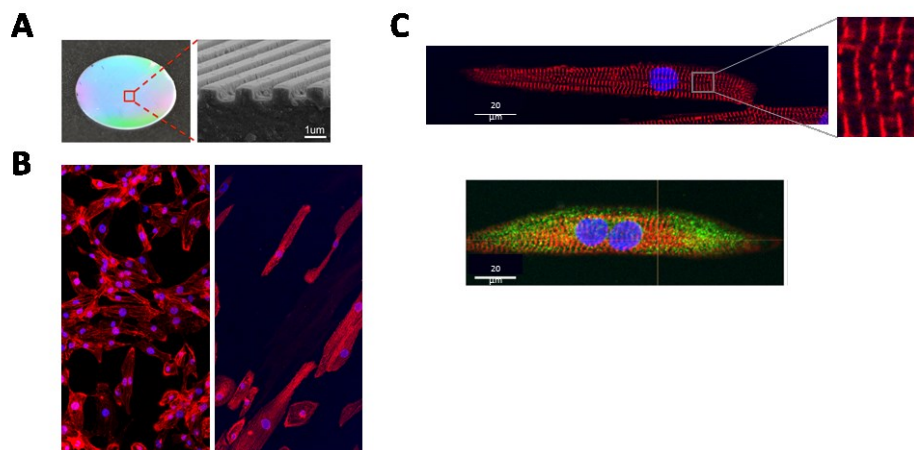
Figure 1.13. A) Photograph of a large-area of nanopatterned surfaces on a glass coverslip and B) effect of biomimetic surfaces on anisotropic cell growth. Representation of unaligned cells on flat surfaces (left) and aligned cells grown on nanopatterned surfaces (right). C) Confocal images of later-stage hiPSC-CMs grown on nanopatterned surfaces show a mature morphology with rod-shaped, aligned myofibrils, clearly defined Z bands and transverse-axial tubular system (TATS). Cells were stained for Z bands (α-actinin, red), nuclei (DAPI, blue) and caveolin-3 (green). (Pioner et al., 2016)

	Relaxed	Contracted	Contracted
		Softer matrix	Stiffer matrix
Matrix deformation			
Membrane deformation			
Matrix resistence	No	Low	High
Mechano-transduction	No	Low tension	High tension
Nuclear signalling	No	Low YAP/TAZ	Active YAP/TAZ
Cell morphology		Round shape	Elongated shape
Sarcomere organization		Low myofibril alignment	High myofibril alignment
Calcium transient amplitude	No	Smaller	Higher
Active tension	No	Lower	Higher

Figure 1.14. Comparison between softer and stiffer matrix in relaxed and contracted state. From Querceto et al., 2022.

Electrical stimulation and mechanical strain

Mechanical and electrical stimulation is also a widely used method to promote hiPSC-CM maturation in vitro by promoting contractile protein expression and structural organization. The mechanisms underlying the increase in maturation by electrical stimulation may be due to the mechanical stretching generated by the stimulation leading to remodeling of cardiomyocytes, with enhancement and polarization of gap junctions, which promote electrical conduction (Banyasz et al. 2008). Several studies have shown that electrical stimulation of hiPSC-CMs promoted increased I_{k1} current, with reduced RMP, improved Ca^{2+} handling, increased sarcomeric organization and increased contractile force (Lieu et al. 2013)*; (Chan et al. 2013).* Normally 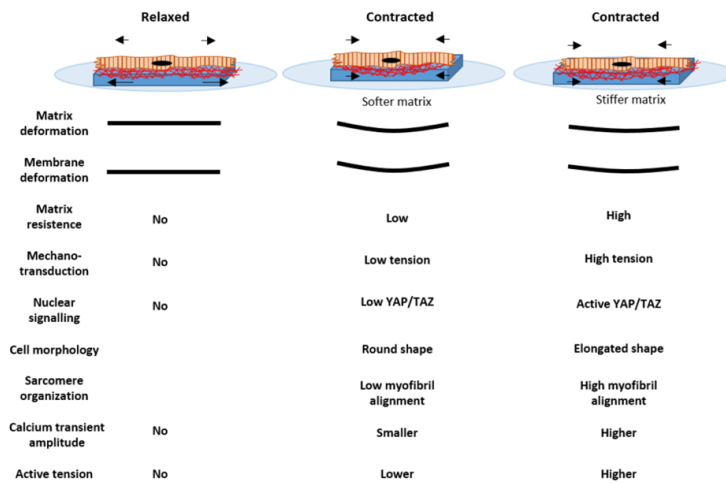the heart is subjected to continuous mechanical stress, which favors cell alignment in the direction of applied traction, so this method has also been extensively used on hiPSC-CMs to induce maturation (Shyu 2009)*.* Studies by (Tulloch et al. 2011) have shown that stretching promotes cell elongation, a higher degree of sarcomeric organization, increased gap junction density and up-regulation of RYR2 and SERCA2, which improves Ca^{2+} management in cardiomyocytes. Other studies have also shown that a gradual increase in stretch leads to an improvement in cell organization, but also to an increase in active and passive forces (Kensah et al. 2013)*.*

Co-Culture

In vivo, cardiomyocytes normally interact with other cell types such as fibroblasts, endothelial and smooth muscle cells, which contribute to the production of ECM and the release of paracrine factors that support cardiomyocyte development. Therefore, direct cell-cell contact influences the maturation of CMs and for this reason, in a series of studies hiPSC-CMs were cultured with mesenchymal stem cells (MSCs) and endothelial cells (ECs), resulting in improved cell maturation (Iorga et al. 2017). Cardiomyocytes were also co-cultured with cardiac fibroblasts, and it was observed that cardiomyocytes showed more mature characteristics and had a conduction velocity comparable

to that of an adult human heart (Thavandiran et al. 2013). In addition, the co-culture of cardiomyocytes with non-cardiac cells makes it possible to understand changes in performance in disease states and ischaemic tissues. (Campostrini et al. 2021) developed a protocol using the three main cell types found in the heart, such as cardiomyocytes, cardiac fibroblasts, and cardiac endothelial cells, and combined them to form three-dimensional cardiac microtissues. They observed that in this conformation, the ultrastructural characteristics of hiPSC-CMs improved, and after isolation of CMs from tissues, they observed an action potential similar to that of adult CMs. Co-culture of cardiomyocytes and cardiac fibroblasts may also allow us to study how the mechanical interaction between these cell types may impair cardiac conduction during cardiac injury (Thompson et al. 2011).

1.1.6 2D vs 3D Cell Culture

For many years, two-dimensional cell cultures have been used as an in vitro model for research studies to understand cellular responses in the presence of biophysical and biochemical stimuli. Although this approach has significantly advanced our understanding of cell behavior, the 2D model remains a system that deviates significantly from the in vivo response. To overcome this limitation and to better mimic in vivo conditions, new 3D cell culture platforms have been created, which currently have many applications in cancer research, on stem cells, in drug discovery and research related to other types of diseases. 2D cell culture is based on cell adhesion on flat surfaces and to control cell shape in 2D cell culture, micro-patterned substrates, such as microwells and micropillars were created or sandwich culture method was adopted to provide ECM imitation (X. Xu et al. 2014) (Fu et al. 2010). The introduction of 3D cell culture approaches has opened new possibilities for the study of biochemical and biomechanical signals, (Burdick and Vunjak-Novakovic 2009); (Huh, Hamilton, and Ingber 2011) as this model summarizes cell-cell and cell-matrix interactions in vivo. Recently, research is making use of 3D cardiac models consisting for example of hiPSC-CMs with the addition of other cell types and with or without the presence of extracellular matrix protein scaffolds. These tissue constructs are available in many shapes and sizes, from scaffold-free spheroids to 3D cardiac models based on scaffolds with longitudinal elongation that can be used to quantitatively calculate the force generated by the tissues. These constructs can be very useful for in vitro disease modeling and drug screening and for this reason, many research groups have developed different platforms that take many forms that vary widely in geometry and scale. Normally, smaller ones such as spheroids and microtissues facilitate cardiotoxicity screening, whereas larger platforms, including cardiac sheets, strips, rings, and chambers allow force measurement and resemble more closely to native heart tissue. The different platforms used in the research studies are described below in **Table 5**.

	2D CELL CULTURE	3D CELL CULTURE
Description	· CMs grown in plates or wells in culture · Cells shape is flat and elongated · Thin layers or sheet constructs · Cells in the culture receive the same amount of nutrients and growth factors from the medium	· Cells grow into 3D aggregates/spheroids · Natural cell shape
Advantages	· Ease of preparation · Better for long-term cultures · Amenable to high- throughputs · Measures of impulse propagation and arrhythmias · Matured by media, patterning extracellular matrix manipulation	· Auxotonic contraction, stretching · Good electrical coupling · Able to easily generate · Measures of force, AP · Natural alignment of cells/sarcomeres · Cells are well differentiated · 3D cell culturing reduces the differences between in vitro and in vivo drug screening
Disadvantages	· Immature CMs phenotype · Cell junctions are less common · Insufficient influence of non-CMs and the 3D environment · Unable to recapitulate some heart disease phenotypes · Drugs are not well metabolized and can easily induce apoptosis	· Real adult CM phenotypes have not been recapitulated · Nutrients does not have to be equally divided amongst all cells · The core cells often remain inactive since they receive less oxygen and growth factors · Requiring large cell numbers and preparation with devices · Risk of breaking · Unequal distribution of cells

Sarcomere	Sarcomere length 1.65/1.81μm (early/late phase) Myofibrils poorly organized	Sarcomere length 2.2 μm Clear Z-lines, I-bands, and A-bands, no M-line
Contractility and cell size	CMs size; 480/1716 μm^2 (early/late phase)	CMs size: 1,500 μm2 Contractility: ~3 mN/mm2

Table 4. Comparison of 2D and 3D cell culture. Modified from (Jensen and Teng 2020) (Tani and Tohyama 2022)
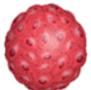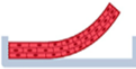
Cardiac spheroids	Spheroids are a scaffold-free aggregates of cells and the small size of these platforms requires a low number of cells. These culture systems allow a cell-cell connection and an analysis of cell viability, but do not allow any direct measurement of force. Spheroids are more suitable for testing pharmacological compounds and for analysing contractility and arrhythmogenicity by measuring their deflection. *(Beauchamp et al., 2015)*
Cardiac cell sheets	Cardiac sheets consist of one or more layers of cells and are particularly useful for detecting arrhythmogenicity. Microgrooves can be added to these platforms to provide cell alignment. Due to their large surface area, they can be used for optical mapping and can be electrically stimulated, allowing analysis of Ca^{2+} transients. However, they cannot be used for direct force measurements. *(Shum et al., 2017)*
Microtissues	Microtissues are platforms made up of a few cells, sometimes in a hidrogel scaffold, and unlike spheroids they provide uniaxial cell alignment, facilitating a more rigorous measurement of contractile function. It was observed that these platforms give much more accurate drug responses than 2D culture. *(Thavandiran et al., 2020)*
Cardiac strips	Cardiac strips consist of cells embedded in a hydrogel that is cast into a mold where it solidifies between two pillars; the resulting tissue then begins to beat spontaneously. These platforms allow to measure contractile forces more efficiently by tracking the deflection of the elastomeric supports and can be used to test drugs, as they allow the force and contraction kinetics to be analysed, providing information on the inotropic and arrhythmogenic effects of the compounds under examination. *(Eschenhagen et al., 1997; Hansen et al., 2010; Bielawski et al., 2016)*
Cardiac rings	Cardiac rings are cast in circular molds and then transferred to isometric supports. Due to the large surface area they allow optical mapping and can be electrically stimulated and used for contractile force analysis. *(Tiburcy et al., 2014; Goldfracht et al., 2020)*
Cardiac chambers	Cardiac chambers are platforms that resemble the native ventricle on a smaller scale. They are generated using cells embedded in hydrogel around a balloon catheter or using nanofibrous scaffolds that mimic the concentric and anisotropic orientation of the native myocardium. Cells contracting in this conformation can generate pressure, so these scaffolds are very useful for analysing ejection fraction, cardiac output and pressure-volume loops. They can also be used for drug screening and with the addition of electrical stimulation, cell maturation can be enhanced. *(MacQueen et al., 2018; Keung et al., 2019; Williams et al., 2020)*

Table 5. Description of scaffold-free and scaffolded human engineered heart tissue models

1.1.7 Induced pluripotent stem cell-derived Engineered Heart Tissues (EHTs)

The use of an in vitro cardiac model can be useful for further studies of mechanical and electrophysiological function under physiological and pathological conditions and can be an efficient platform for screening new pharmaceutical molecules. Conventional two-dimensional (2D) cell cultures have long been the most widely used cell culture system, but in some circumstances this model is unable to control the development of important cellular characteristics, failing to faithfully reproduce the cell developmental processes observed in the in vivo physiological environment. In addition, 2D systems are unable to generate contractile force, one of the most important parameters related to cardiac function; these limitations can be overcome by using, for example, a 3-dimensional model. In fact, tissue engineering represents a new approach that can accurately replicate the myocardial niche and reproduce the physiological function of the heart better than 2-dimensional cell cultures. Engineered cardiac tissues represent a promising method for *in vitro* research on cardiac function and tissue replacement therapy. These platforms were first realized using neonatal or embryonic rat and chicken cardiomyocytes (Eschenhagen et al. 1997)(Zimmermann et al. 2000) and are currently used to enhance the maturation of hiPSC-CMs. Their generation consists of embedding the cardiomyocytes in a fibrin hydrogel scaffold, which compacts to form a tissue between two pillars. Through this method, anchoring applies continuous mechanical stress on the growing cardiac tissues and induces cell orientation parallel to the lines of force. The use of fibrinogen for tissue engineering applications also may be advantageous because it is easily purified from different species and is able to covalently bind growth factors. During tissue formation, fibrinogen is converted to fibrin by thrombin, and the resulting gel must be soaked in aprotinin-supplemented medium to prevent proteolytic degradation. In addition, the rapid solidification of fibrin promotes a more homogeneous and reproducible distribution of cells in the gel. EHTs are a good model for studying contractile force, which can be calculated by optical tracking of the flexible post deflection (Schaaf et al. 2011)(Ruan et al. 2016)*,* and to monitor the effects of drugs on all major parameters of heart function, such as force, relaxation kinetics and pacemaker activity. (Mannhardt et al. 2016) observed that EHTs respond positively to physiological and pharmacological regulators of inotropy, modulators of ion channel currents, and proarrhythmic compounds. Their studies show that EHTs exhibit a high degree of similarity with native human cardiac tissue. Other studies showed that the maturation of cardiomyocytes in EHTs can be enhanced by electrical and mechanical stimulation, leading to a better organization of the cellular ultrastructure and an increase in electrophysiological activities. (Ronaldson-Bouchard et al. 2018) showed that cardiac tissues generated with early-stage hiPSC-CMs, when subjected to increasing stimulation, exhibited gene expression profiles like those of an adult, with a remarkably organized ultrastructure, a physiological sarcomeric length and a positive force-frequency relationship. Another study showed that constant electrical stimulation in an isometric format promotes β-myosin heavy chain expression levels like those in adult myocardium, thus indicating cardiomyocyte maturation (Ng et al. 2021).
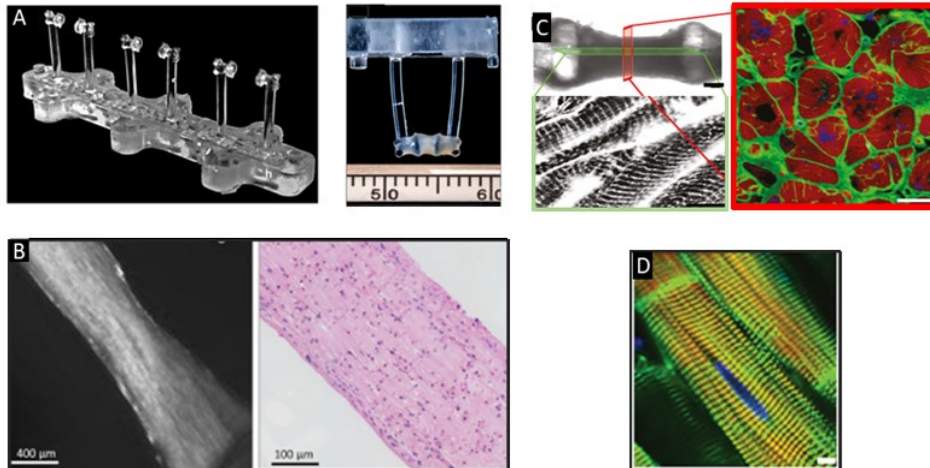
Figure 1.15. A) Photograph of silicon posts and tissue attached to pillars. B) Representative image of an EHT (left) and a longitudinal section on the right C) Cross-sections to evaluate T-tubules (Green, WGA; red, cTnT; blue, nuclei; scale bar, 10 µm) and D) Immunofluorescence of whole tissues showing the enhanced cardiac ultrastructure (α-actinin, green; cTnT, red; nuclei, blue; Scale bar, 5 µm) (Mannhardt et al., 2016; Ronaldson-Bouchard et al., 2018)
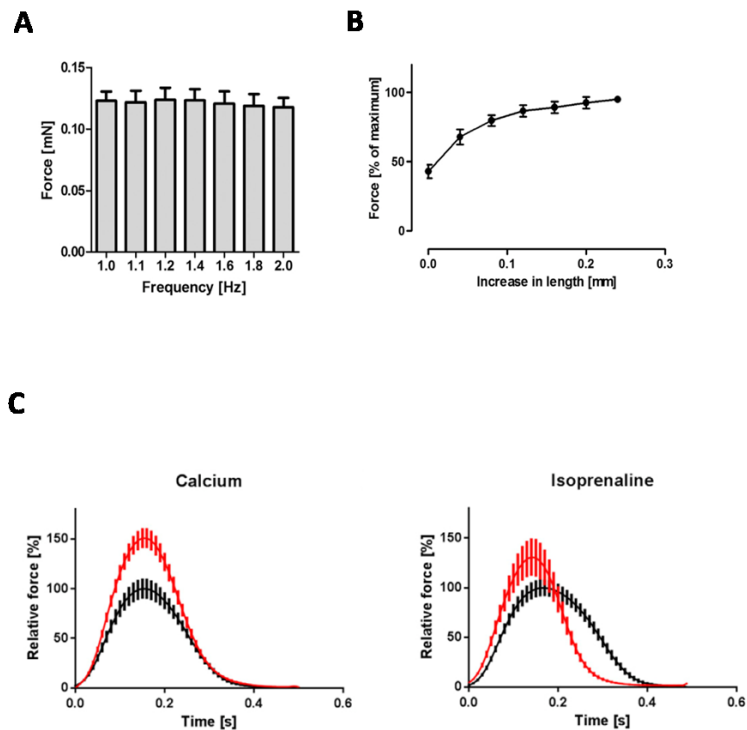
Figure 1.16. A) Representation of the force contraction -frequency relationship in EHT and B) Frank-Starling mechanism: increase in force in relation to increase in stretch; C) Examples of contractile force changes in response to inotropic stimuli. (Mannhardt et al., 2016)

New technologies are also being used in recent years to generate engineered tissues, using 3D printing and laser cutting of biomaterials, so that highly controlled tissues can be obtained (Gao et al. 2017; Borovjagin et al. 2017).

36

As described so far, the advantages of this platform lie in the fact that it allows the generation of human models of advanced maturity, in a short time, enabling the study of healthy and diseased cardiac tissue. However, the level achieved is not yet fully at the level of an adult, in fact, the force values generated are lower than those expected for adult cardiomyocytes. In addition, this model requires many cells, which is a disadvantage for its utilization in high-throughput screening. Nevertheless, this in vitro model is widely used to model cardiomyopathies, as it is suitable for measuring contraction force changes associated with these conditions. Such cardiac tissues generated from hiPSCs can in fact serve as platforms for patient-specific disease studies. So far, specific EHTs were developed to study various diseases, such as channelopathies, dilated cardiomyopathy (Streckfuss-Bömeke et al. 2017); *(John T. Hinson et al. 2015)*, hypertrophic cardiomyopathy, and familial cardiomyopathy (K.-C. Yang et al. 2018)(J. Travis Hinson et al. 2016; Prondzynski et al. 2019). All these studies show that human EHTs are a powerful tool to better understand cardiomyocyte biology and a good model for studying diseases, for preclinical drug testing and to generate personalized therapies.

1.2 Dilated cardiomyopathy

Dilated cardiomyopathy is a disease that affects the myocardium and impairs the heart's ability to pump blood effectively. DCM is characterized by left ventricular (LV) systolic dysfunction and LV enlargement, in the absence of abnormal loading conditions such as hypertension or coronary artery disease (Anastasakis and Basso 2018). This type of cardiomyopathy is predominant in the pediatric population, with a higher incidence in the first year of life (Lipshultz et al. 2003). Very frequent mutations affect genes coding for sarcomeric proteins: titin, myosin, actin, troponin, and tropomyosin, causing alterations in calcium homeostasis, muscle contraction, and ion channel function. Mutations in titin, a giant protein that works as a nano-spring, are present in 25% of cases of end-stage disease (Roberts et al. 2015; Herman et al. 2012) and in 20-25% of familial cases of DCM. Variants in the Lamin A/C (LMNA) gene are present in up to 6% of DCM cases (Parks et al. 2008) and are characterized by an aggressive phenotype with conduction abnormalities and malignant ventricular arrhythmias. Other mutations involve genes coding for cytoskeletal proteins such as filamines, dystrophin, and desmin. Pathogenic variants in these genes can lead to muscular dystrophies that are most often associated with DCM. The presence of mutations or polymorphisms in modifier genes, as well as several environmental factors, may be responsible for the clinical heterogeneity of DCM (Bondue et al. 2018). In addition, the clinical phenotype and disease outcome may depend on several factors such as age, hormones, innate immune system status, the presence of chronic inflammatory diseases or hypertension, inherited mitochondrial alterations, or exposure to particular environmental factors, such as cardiotoxic substances or drugs. DCM, like arrhythmogenic cardiomyopathy and channelopathies have in common the electrical instability that leads to an increased risk of sudden cardiac death (Gigli et al. 2019).

Gene	Prevalence	Clinical phenotype	#hiPSC studies (REF.)	Functional output
Titin (*TTN*)	19-25% of familial forms 11-18% of sporadic forms	Usually milder forms of DCM, with LV reverse remodeling described after OMT. Can be associated with tibial muscle dystrophy and HCM [7]. Truncating variants are related to alterations in mitochondrial function, increased interstitial fibrosis and reduced hypertrophy, along with increased ventricular arrhythmias at long-term follow-up, with a similar survival and overall cardiac function with respect to idiopathic DCM (Verdonschot et al. 2018).	5 (Chopra et al. 2018) (Zaunbrecher et al. 2019)	Contractile deficit
Lamin A/C (*LMNA*)	5-6% of genetic DCM	Malignant DCM characterized by young onset, high penetrance, dysrhythmias (sinus node dysfunction, AF, atrioventricular node dysfunction, VT, VF, SCD), LV dysfunction and HF with reduced survival and frequent need for HT. Cardiac conduction system disease usually precedes the development of LV dilation and dysfunction (Hasselberg et al. 2018).	5 (Bertero et al. 2019) (Wyles et al. 2016)	LMNA haploinsufficieny; conduction defects; contractile defects
β-Myosin heavy chain (*MYH7*)	3%–4% of DCM	Sarcomeric rare variant carriers show a more rapid progression toward death or HT compared to non-carriers, particularly after 50 years of age (Merlo et al. 2013).	?	
Cardiac troponin T (*TNNT2*)	3% of DCM	Clinical and prognostic profiles depend on type of mutation: carriers of Arg92Gln mutation have a worse prognosis than those with other mutations in *TNNT2* or other sarcomeric genes (Ripoll-Vera et al. 2016).	6 (Broughton et al. 2016; Wu et al. 2015)	Contractile defects

Type V voltage-gated cardiac Na channel (*SCN5A*)	2%–3% of DCM	Arrhythmias (commonly AF) and myocyte dysfunction leading to progressive deterioration of LV systolic function (Bondue et al. 2018). Overlapping phenotypes: LQT, Brugada.	1 (Moreau et al. 2018)	Electrophysiological defects; Arrhythmias
RNA-binding protein 20 (*RBM20*)	1-5% of DCM	Malignant arrhythmic phenotype with high frequency of AF and progressive HF.	3 (Streckfuss-Bömeke et al. 2017; Wyles et al. 2016)	Calcium handling abnormalities; contractile defects
Desmoplakin (*DSP*)	2% of DCM	Associated with Carvajal syndrome (autosomal recessive genetic disorder characterized by woolly hair, striate palmoplantar keratoderma and DCM). Additional phenotypic signs: dental abnormalities and leukonychia. LV dilatation is usually asymptomatic at an early age. DCM progresses rapidly, leading to HF or SCD in adolescence (Yermakovich et al. 2018; Ng et al. 2019).	1 (Ng et al. 2019)	ACM
Dystrophin (*DMD*, Xp21.1 locus 16)	<2% of genetic DCM	Associated with Duchenne and Becker muscular dystrophy. Severe cardiac involvement in Duchenne (milder and later onset in Becker muscular dystrophy) with supraventricular arrhythmias, atrio-ventricular blocks and right bundle branch block, progressive LV dysfunction and HF (Mestroni et al. 2014).	20 (J. Manuel Pioner et al. 2020) (A. Moretti et al. 2020)	Calcium handling abnormalities; contractile defects
α-Tropomyosin (*TPM1*)	1%–2% of DCM	Overlapping phenotypes: LVNC, HCM (McNally and Mestroni 2017)	1	Sarcomere defects

			(Takasaki et al. 2018)	
Desmin (*DES*)	1-2% of DCM (Taylor et al. 2007)	Malignant phenotype associated with desminopathies and myofibrillar myopathy. Can cause a spectrum of phenotypes from skeletal myopathy, mixed skeletal–cardiac disease ("desmin-related myopathy"), and cardiomyopathy (DCM as well as HCM or RCM). DCM is typically preceded by skeletal myopathy and can be associated with conduction defects (Mestroni et al. 2014).	1 (Tse et al. 2013)	
Filamin C (*FLNC*)	1% of DCM	Cardiomyopathy is associated with myofibrillar myopathy and LVNC; high rate of ventricular arrhythmias and SCD (particularly in truncating variants) (Ader et al. 2019).	?	
Metavinculin (*VCL*)	1% of DCM	Can cause either DCM or HCM phenotype (Vasile et al. 2006)	?	
Phospholamban (PLN)	Rare (except for Netherlands where prevalence reaches 15% of DCM due to R14del mutation with founder effect) (van der Zwaag et al. 2012)	Early onset DCM with lethal ventricular arrhythmias. Low QRS complex potentials and decreased R wave amplitude, negative T waves in left precordial leads (Hof et al. 2019). PLN R14del mutation associated with high risk for malignant arrhythmias and end-stage HF from late adolescence, can cause either a DCM phenotype or ARVC (Mestroni et al. 2014). A milder phenotype is also reported (DeWitt et al. 2006).	4 (Ceholski et al. 2018) (Stroik et al. 2020)	Electrophysiological defects
α-/β-/δ-Sarcoglycan	Rare	Recessive mutations in δ-sarcoglycan linked to limb girdle muscular dystrophy 2F, dominant mutations in δ-	?	Ca handling abnormalities;

(SGCA, SGCB, SGCD)		sarcoglycan linked to DCM (Campbell et al. 2016).		Contractile defects
α-cardiac actin (*ACTC1*)	Rare	Familial atrial septal defect combined with a late-onset DCM (Frank et al. 2019). Can be associated with HCM and LVNC	?	
Cardiac troponin I (*TNNI3*)	Rare	Overlapping phenotype: HCM (McNally and Mestroni 2017)	1 (Chang et al. 2018)	Telomere shortening
Cardiac troponin C (*TNNC1*)	Rare	Overlapping phenotypes: LVNC, HCM. (McNally and Mestroni 2017)	?	
Troponin I–interacting kinase (*TNNI3K*)	Rare	Conduction defect, AF (McNally and Mestroni 2017)	?	
α-actinin 2 (ACTN2)	Rare	Overlapping phenotype: LVNC (McNally and Mestroni 2017)	?	
BCL2-associated athanogene 3 (*BAG3*)	Rare	Associated with myofibrillar myopathy (McNally and Mestroni 2017).	1 (Judge et al. 2017)	
α-B-crystallin (*CRYAB*)	Rare	Associated with protein aggregation myopathy (McNally and Mestroni 2017).	1 (Mitzelfelt et al. 2016)	Disrupted myofibril; Contractile deficit

Titin-cap/telethonin (*TCAP*)	Rare	Associated with limb-girdle muscular dystrophy (McNally and Mestroni 2017).	?	Protein Aggregates; cellular stress
Muscle LIM protein (*CSRP3*)	Rare	Overlapping phenotype: HCM (McNally and Mestroni 2017).	1 (X. Li et al. 2019)	
Cardiac ankyrin repeat protein (*ANKRD1*)	Rare	Associated with congenital heart disease (McNally and Mestroni 2017).	?	Calcium handling abnormalities
Cypher/ZASP (*LDB3*)	Rare	Overlapping phenotype: LVNC (McNally and Mestroni 2017).	?	
Nebulette (*NEBL*)	Rare	Overlapping phenotypes: LVNC, HCM (McNally and Mestroni 2017).	?	
Emerin (*EMD*)	Rare	Associated with Emery–Dreifuss muscular dystrophy (McNally and Mestroni 2017).	1 (Shimojima et al. 2017)	
Sulfonylurea receptor 2A, component of ATP-sensitive potassium channel (*ABCC9*)	Rare	Associated with AF, Osteochondrodysplasia. (McNally and Mestroni 2017)	?	Calcium handling abnormalities

Potassium channel (*KCNQ1*)	Rare	Associated with AF, LQT1, short QT1, Jervell and Lange-Nielsen syndrome. (McNally and Mestroni 2017)	?	
HSP40 homolog, C19 (*DNAJC19*)	Rare	Associated with 3-methylglutaconic aciduria, type V. (McNally and Mestroni 2017)	1	
Tafazzin (*TAZ/G4.5*)	Rare	Associated with LVNC, Barth syndrome, endocardial fibroelastosis 2. (McNally and Mestroni 2017)	1 (G. Wang et al. 2014)	Mitochondrial defects

Table 6. Principal pathogenic gene mutations described in genetic DCM along with their clinical and cellular phenotype (Pioner et al., 2020)

1.2.1 Dystrophin gene mutations associated with DCM

Mutations in the dystrophin gene (DMD) are associated with the development of dystrophinopathies, such as Duchenne or Becker muscular dystrophies (DMD/BMD), and account for <2% of dilated cardiomyopathy (DCM) cases. The DMD gene, located on the X chromosome at the Xp21.2 locus is the largest known gene in the human genome (Mandel 1989) and was also the first to be associated with DCM (Towbin et al. 1993). Despite its low prevalence (<3/10,000), dystrophin-associated cardiomyopathy is the form of DCM that has been modeled in vitro more extensively using induced pluripotent stem cell-derived cardiomyocytes (hiPSC-CMs) from patients. Duchenne muscular dystrophy (DMD) is the most severe form of the disease and its onset occurs during childhood, presenting initially with musculoskeletal involvement and later with the development of myocardial dysfunction (Verhaart and Aartsma-Rus 2019).
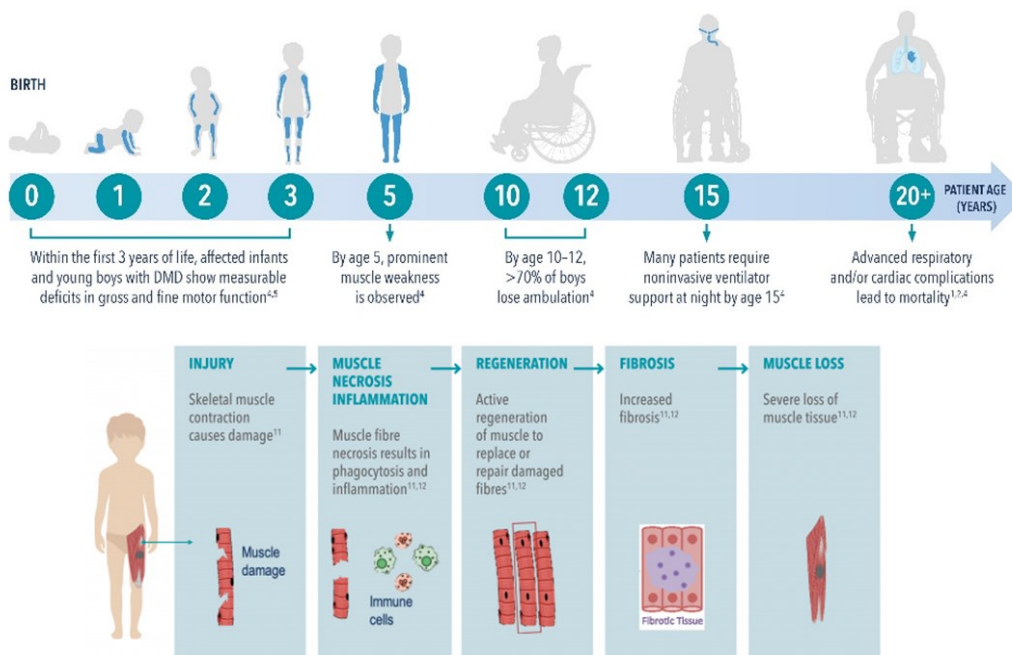
Figure 1.17. Representative image of the progressive course of DMD that begins in childhood and leads to muscle deterioration and continued decline in physical function. From www.neurologylive.com/view/the-duchenne-muscular-dystrophy-dmd-continuum-the-case-for-early-intervention-and-long-term-treatment

DMD can occur at any age, but it often presents around 14 to 15 years of age and is very common in patients older than 18 years (Nigro et al. 1990). It remains asymptomatic for many years despite the progression of cardiac dysfunction, because energy expenditure and oxygen consumption are severely reduced by muscle weakness.

DMD-associated cardiomyopathy is characterized by a consistently severe phenotype, with a progression of contractile impairment related to increased LV size and myocardial stiffness, with the extension of myocardial fibrosis (Frankel and Rosser 1976). Repetitive mechanical stress leads to apoptosis, fibrotic replacement, and scarring that proceeds from the epicardium to the endocardium and spreads progressively toward the apex, eventually leading to DCM (Yilmaz et al. 2008). Dilated cardiomyopathy in dystrophic individuals is becoming an increasingly important cause of morbidity and mortality due to HF and ventricular arrhythmias leading to sudden death (McNally 2007).

Figure 1.18. Progression of DCM related to Duchenne Muscular Dystrophy. Modified from (Adorisio et al. 2020)

Drug therapies for the DMD treatment are still in progress. Several advances have led to the development of gene therapi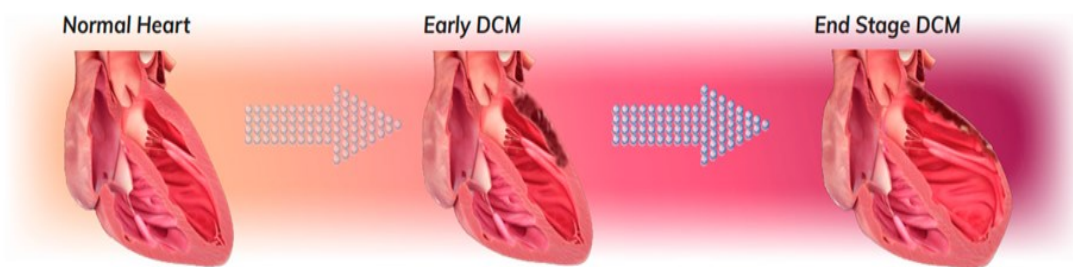es and other therapeutic approaches, but unfortunately some compounds with promising results in early phases of clinical trials have not met efficacy endpoints in later phases. For now, glucocorticoids remain the only treatment that has been shown to slow disease progression, despite the adverse effects associated with their long-term use (Markati et al. 2022).

1.2.2 Dystrophin structure overview

Dystrophin is a 427-kDa cytoskeletal protein expressed by the DMD gene and is a member of the β-spectrin/α-actinin protein family (Koenig and Kunkel 1990). Complete dystrophin is composed of 4 structural domains. The amino (N)-terminal domain is homologous to α-actinin and binds, among other proteins, F-actin; the central rod domain, on the other hand, contains 24-25 spectrin-like repeats. The third is a cysteine-rich domain, while the last carboxyl (C)-terminal domain associates with several other proteins to form an important protein complex called the dystrophin-glycoprotein complex (DGC) (Hoffman, Brown, and Kunkel 1987)(J. M. Ervasti and Campbell 1993). Dystrophin is localized on the cytoplasmic face of the plasma membrane of the muscle cell, providing membrane stability and transduction of mechanical force from the extracellular matrix during muscle contraction/elongation. Full-length dystrophin has been identified at both the cardiac and skeletal levels, whereas it shows reduced expression in unmyelinated axons and dendrites.
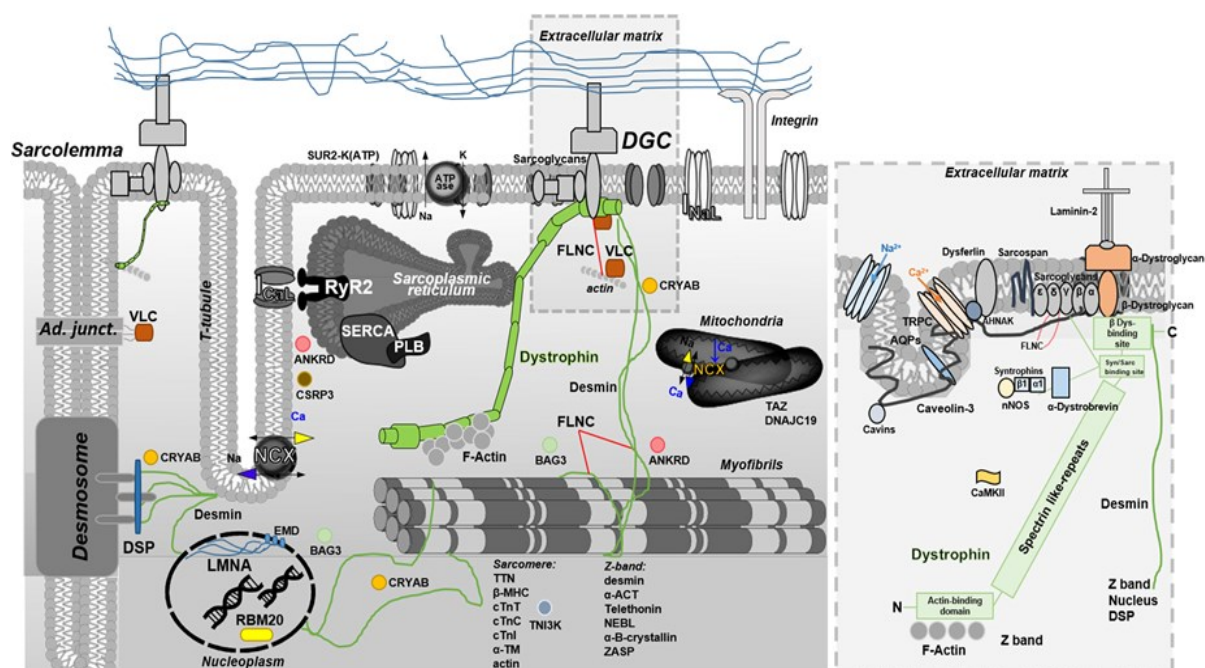
Figure 1.19. Overview of full-length dystrophin in the context of other DCM-related proteins. The blow-up box is a focus on full-length dystrophin structure and interactions. DGC is closely associated with acetylcholine receptor, skeletal and cardiac isoforms of voltage-gated sodium channels (Nav1.4 and Nav1.5), L-type Ca²⁺ channel, aquaporin, and cation channels activated by stretch or transient receptor potential (TRP) (Shirokova and Niggli 2013). In cardiac tissue, dystrophin is also associated with: Cavin-1 and Caveolin-3, Ahnak1, CryAB, and Cipher. Furthermore, dystrophin may also be the target of phosphorylation by calmodulin-dependent kinase II (CaMKII)(Madhavan and Jarrett 1994). Modified from (Josè Manuel Pioner et al. 2020)

DGC is involved in several signaling pathways that regulate various myocyte functions, including Ca^{2+} homeostasis and excitation-contraction coupling, mitochondrial function, motor protein interaction, and gene expression. Mutations in the DMD gene generate a truncated protein, which cannot anchor to the glycoprotein complex. The reduced presence of protein causes increased cellular vulnerability to the mechanical stress associated with muscle contraction and altered calcium homeostasis, as demonstrated by studies in DMD animal models (Merrick et al. 2009)(Dumont et al. 2015)

1.3 Hypertrophic cardiomyopathy

1.3.1 Spectrum of genetic mutations in hypertrophic cardiomyopathy

Hypertrophic cardiomyopathy (HCM) has been recognized as the most common inherited heart disease affecting 1:500 adults worldwide (B. J. Maron et al. 2014) with an estimated prevalence of 1:200 (Semsarian et al. 2015). The patient's symptoms can be minimal or inexorably progressive resulting in heart failure and/or sudden cardiac death (B. J. Maron 1999). HCM is inherited in an autosomal dominant manner with a highly variable degree of penetrance among different individuals (B. J. Maron 2002; Kokado et al. 2000) and is typically regional and asymmetric, characterized by abnormal thickening of the ventricular wall. The degree of hypertrophy can be mild (13-15 mm) or extreme (> or = 30 mm) (Nistri et al. 2006)(Iacopo Olivotto et al. 2003). Most patients have the classic form of HCM with asymmetric septal hypertrophy and diastolic dysfunction, which is an early hallmark of the disease and can be caused by mutation-mediated changes in cardiomyocytes and can also be attributed to fibrosis, which may represent a substrate for arrhythmia and cardiac arrest (Watkins 2000). HCM has been defined primarily as a sarcomere disease (B. J. Maron, Maron, and Semsarian 2012), as more than 1500 mutations in 11 genes encoding proteins of the thin and thick myofilaments or the Z disc have been linked to HCM (Ho, Charron, et al. 2015); (Iacopo Olivotto et al. 2015). HCM-associated mutations fall in genes encoding for: β-MyHC, cardiac myosin binding protein-C (cMyBP-C), regulatory (RLC) and essential (ELC) myosin light chains, cardiac Troponin I (cTnI), cardiac Troponin T (cTnT), cardiac Troponin C (cTnC), α-tropomyosin (α-Tm), actin and titin. Approximately 30-60% of individuals with HCM are considered to have myofilament-positive HCM, while the remaining patients have no distinguishable myofilament mutations and are considered to have myofilament-negative HCM. HCM due to myofilament gene mutations is characterized by more frequent alteration of LV function than myofilament-negative HCM (Iacopo Olivotto et al. 2008) (***Fig. 1.20***).
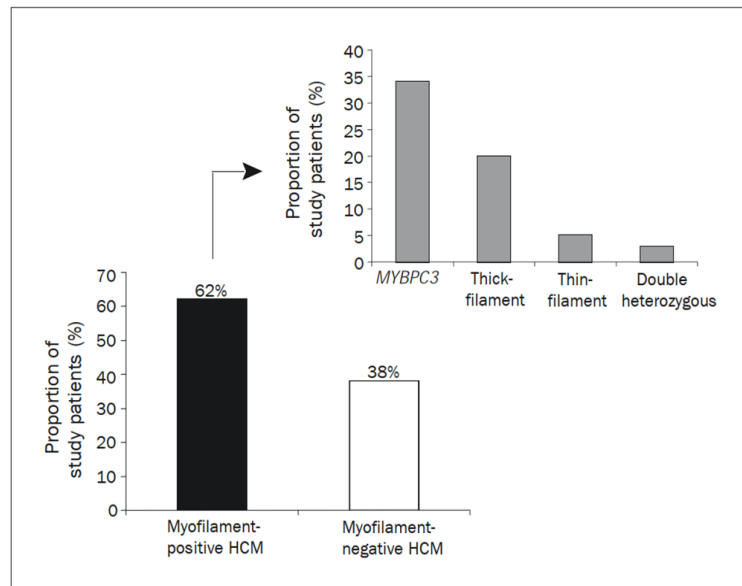
Figure 1.20. Prevalence and distribution of sarcomeric myofilament protein gene mutations among the 203 study patients with hypertrophic cardiomyopathy (HCM) Modified from Olivotto et al, 2008.

In ~70% of HCM subjects, the most commonly affected genes are MYH7 (β-MyHC), MYBPC3 (cMyBP-C). Although some early studies showed that HCM mutations depress cardiac contractility, more recent studies suggest that HCM mutations increase contractility, leading to a "hypercontractile phenotype." The precise impact of HCM mutations on the maximal force-generating capacity of human cardiac sarcomeres still remains controversial, however, several recent works on different HCM mutations affecting both thick filament proteins (MYBPC3, MYH7) and thin filament proteins (TPM1, TNNI3, TNNT2) show increased motor activity rather decreased function (Belus et al. 2008); (Stelzer, Fitzsimons, and Moss 2006). It is known that HCM-associated sarcomeric mutations lead to compromised energetics by altering cross-bridge transition kinetics. It has been observed that for both mutations on the thick (R403Q) (Belus et al. 2008); (Witjas-Paalberends et al. 2014) and thin filament (K280N)(Piroddi et al. 2019), one of the main effects is the acceleration of the cross-bridge turnover rate, causing a higher energy cost of tension generation. Energy deficit may have a significant impact on the electromechanical activity of cardiomyocytes, contributing to their remodeling over the course of the disease. One of the consequences predicted by the energy depletion hypothesis for HCM is the impairment of Ca^{2+} reuptake in the sarcoplasmic reticulum, due to the extreme energy requirements of the cardiac SERCA pump (He et al. 2007; Spindler et al. 1998). Elevated diastolic intracellular $[Ca^{2+}]$ and impaired function of other ion transporters could make the myocardium vulnerable to arrhythmias.
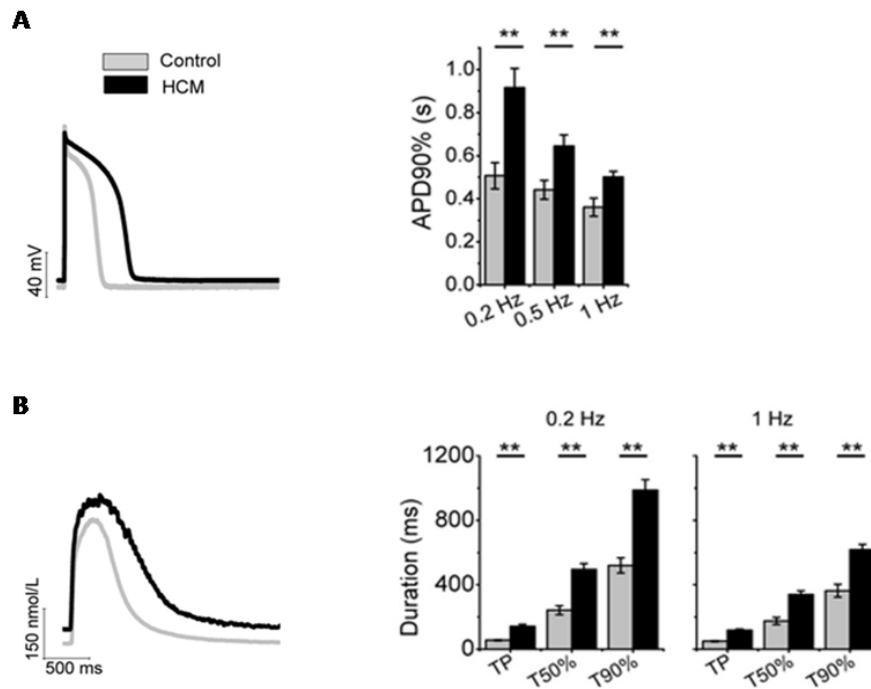
Figure 1.21*. Prolonged action potentials and altered Ca²⁺i handling in HCM cardiomyocytes. **A)** Representative action potentials recorded during stimulation at 0.2 Hz from HCM cardiomyocytes and control cardiomyocytes, on the left, and action potential duration at 90% repolarization (APD90%) at 0.2, 0.5, and 1 Hz, on the right. **B)** Ca²⁺i transients traces and Ca²⁺i transient time from peak (TP), TP to 50% (T50%), and TP to 90% (T90%) decay in HCM and control myocytes stimulated at 0.2 and 1 Hz. Modified from (Coppini et al. 2013)*

Coppini's group (Coppini et al. 2013) analyzed the electromechanical profile of cardiomyocytes from HCM patients undergoing myectomy by patch-clamp and intracellular Ca^{2+} studies, and it was observed that HCM cardiomyocytes were more vulnerable compared with controls and showed prolonged action potential correlated with increased late Na^+ (I_{NaL}) and Ca^{2+} currents and decreased repolarizing K^+ currents **(Fig. 1.21)**. These changes were related to enhanced Ca^{2+}/calmodulin kinase II (CaMKII) activity and increased phosphorylation of its targets. Therefore, such electrophysiological abnormalities present in ventricular myocytes and trabeculae of HCM patients suggest potential therapeutic implications of I_{NaL} and CaMKII inhibition.

1.3.2 Cardiac Myosin Binding Protein C

Muscle contraction and relaxation occur at the sarcomeric level through the sliding movement of thick and thin filaments. This process is driven by the cyclic interaction between myosin heads and actin filaments, coupled with ATP hydrolysis and myosin head conformational changes (Geeves and Holmes 1999). In addition to actin and myosin, the sarcomere contains several additional proteins involved in regulating the force, rate, and timing of contraction. One important protein is myosin-binding protein C (MyBP-C), a thick filament protein crucial for sarcomere organization and maintenance of normal cardiac function. Previous work showed that cMyBP-C knockout in mouse models results in altered sarcomere structure, contractile deficits evident at both the whole heart and single cell levels, cardiac hypertrophy and severe heart failure, indicating the importance of cMyBP-C for baseline cardiac function (Vignier et al. 2009a; Harris et al. 2002).

MyBP-C is a multi-modular protein (~140-150 kDa) arranged transversely in the C-zones of the A-bands of the sarcomere (Luther et al. 2008), and the cardiac isoform, expressed exclusively in the heart, consists of 11 domains termed C0-C11 from the N to the C-terminus. The Ig-like C0 domain is specific for the cardiac isoform, and the proline-alanine-rich region between C0 and C1 has sequences proposed to bind actin (Squire, Luther, and Knupp 2003). The N-terminal binding site, consisting of the C1 and C2 immunoglobulin domains connected by a flexible linker, interacts with the S2 segment of myosin in a phosphorylation-regulated manner, while the C7 and C10 domains anchor MyBP-C to the thick filament through strong binding interactions with the light meromyosin (LMM) and titin backbone (Tonino et al. 2019).
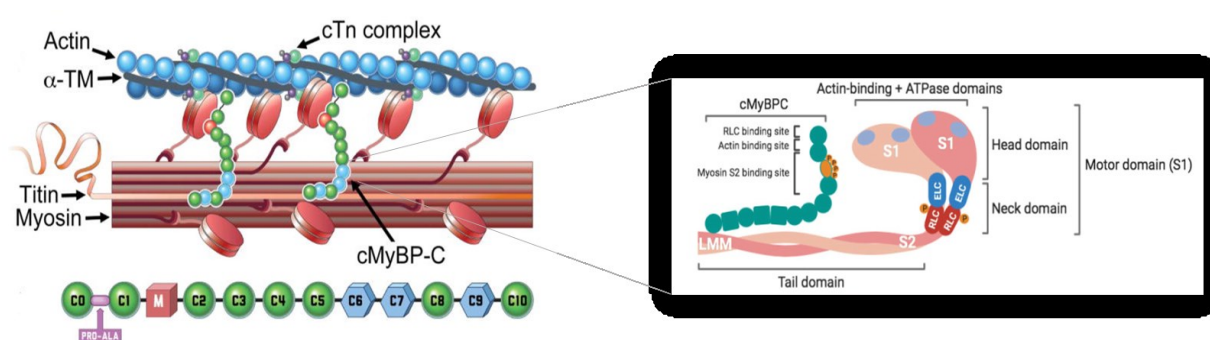

Figure 1.22. Schematic representation of MyBP-C localization. The cMyBP-C protein transversely connects both thick and thin filament proteins; it is composed of 8 immunoglobulin (Ig) domains and 3 type III fibronectin domains (C0-C1) and between the C0 and C1 domains there is a proline-alanine-rich region and a phosphorylation motif (M domain). The C0-C2 domains interact with thin filament proteins such as actin and thick filament proteins such as myosin S2, while the C8-C10 domains interact with titin and the light meromyosin (LMM). On the right, representation of β-cardiac myosin II, formed by the characteristic double-headed structure with motor domains and a coiled-coiled tail domain, and cMyBPC exhibiting binding sites for sarcomeric proteins. Modified from (Sadayappan and de Tombe 2012)(Schmid and Toepfer 2021)

Thus, through its different domains, MyBP-C can interact with various sarcomeric components. The binding of cMyBP-C to its partners is regulated by the phosphorylation status of the M domain, which contains three serine residues (S275, S284, and S304), all of which are targeted by the cAMP-dependent protein kinase (PKA) and individually by a variety of other protein kinases (Bardswell et al. 2010; Sadayappan and de Tombe 2012); (Hartzell and Glass 1984); (Gautel et al. 1995). Phosphorylation of cMyBP-C promotes the cross-bridges formation, as the interaction between cMyBP-C and thick filament heads is reduced. The acute phase of activation is mediated by calcium binding to the thin filament leading to crossbridge attachment. However, in its de-phosphorylated state, cMyBP-C predominantly binds to myosin S2 and restrains crossbridge formation. Therefore, the function of cMyBP-C is to regulate the formation of cross-bridges, promoting normal cardiac function. Based on the function of cMyBP-C, it is not surprising that mutations in this protein can impair heart function.
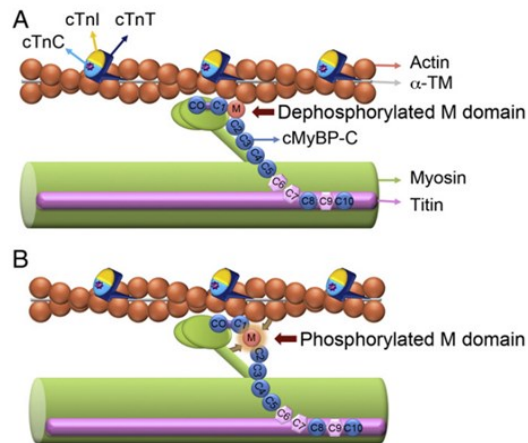
Figure 1.23. *Phosphorylation and dephosphorylation mechanism of cMyBP-C's M domain. The M domain phosphorylation facilitates the cross-bridges formation.* **A)** *In the absence of phosphorylation, the C1-M-C2 domains are bound to myosin S2 region, instead, when the M domain is phosphorylated* **B)**, *the interaction with the myosin S2 region is reduced, inducing changes in the thick filament orientation. From (Barefield and Sadayappan 2010)*

1.3.3 cMyBP-C mutations and human cardiomyopathy

As described before, MyBP-C has defined roles in both structural assembly and sarcomere stability by modulating contraction. Mutations in the gene encoding for MyBP-C are known to underlie the development of cardiomyopathies, such as arrhythmogenic right ventricular cardiomyopathy, DCM, HCM, and restrictive cardiomyopathy (Watkins et al. 1995; Bonne et al. 1995). Studies suggest that mutations in the cMyBP-C gene have been inherited in more than 60 million people worldwide (Dhandapany et al. 2009; Barefield and Sadayappan 2010) and that these mutations are the second most frequent cause of hypertrophic cardiomyopathy, accounting for >30% of all HCM cases (Iacopo Olivotto et al. 2008; Richard et al. 2003); this indicates the importance of understanding the role of this protein in order to develop preventive clinical measures. It has been reported in the literature that in the presence of truncating mutations in cMyBP-C at the C-terminal level (including nonsense mutations, insertions or deletions, splicing or branch point mutations), total cMyBP-C levels are reduced, suggesting that the pathological mechanism could be haploinsufficiency (Marston et al. 2009b; van Dijk et al. 2009). It is possible that truncated proteins are eliminated from cells by nonsense-mediated mRNA decay (NMD) and the Ubiquitin-Proteasome system (UPS) (Vignier et al. 2009b). In addition, an increasing number of pathogenic missense mutations in *MYBPC3* have been identified in HCM, and it has been observed that HCM patients carrying *MYBPC3* missense mutations showed reduced total levels of cMyBP-C, causing haploinsufficiency (Marston et al. 2009b; Page et al. 2012; Iacopo Olivotto et al. 2008). For example, the c.772G>A has been repeatedly reported among *MYBPC3* variants (p. Glu258Lys, E258K); it is considered a rare variant worldwide and is characterized by peculiar clinical features including marked propensity to systolic dysfunction and disease progression (Girolami et al. 2006b; Gajendrarao et al. 2015). This mutation involves a missense substitution of the amino acid lysine for glutamic acid at position 258 and the nucleotide change results in an exon skipping event by altering the last nucleotide of exon 6 and interfering with splicing

(Singer et al. 2019). Functional studies related to this mutation have been performed on engineered murine cardiac tissue, in which incorporation of a missense-mutated (p.Glu258Lys, E258K) or truncated cMyBP-C into cardiac sarcomeres and impaired contractile function were observed (De Lange et al. 2013), while other work shows that expression of a truncated protein has never been detected in the cardiac tissue of HCM patients carrying the E258K mutation (Marston et al. 2009b, 2012).
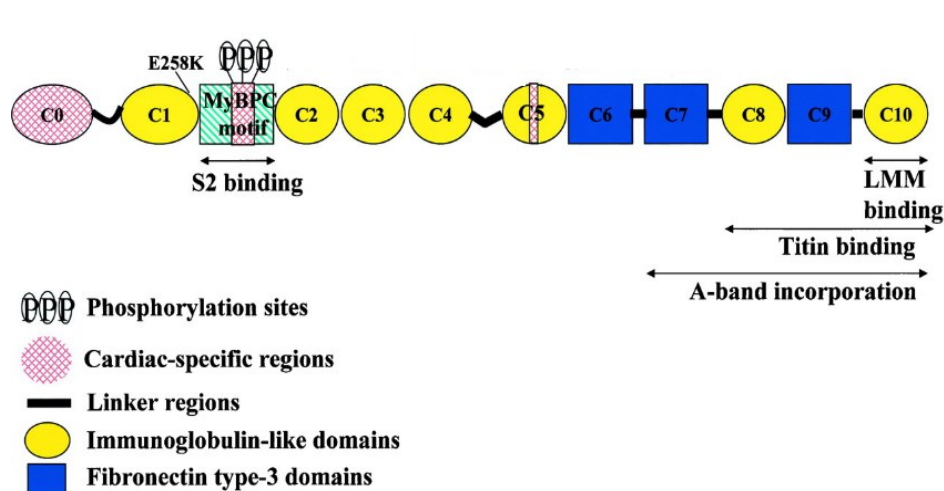
Figure 1.24. *Schematic representation of cardiac myosin-binding protein-C. Domains with known function and the location of the E258K mutation causing HCM are indicated. Modified from (Moolman-Smook et al. 2002)*

The MYBPC3-E258K mutation affects the last residue of the C1 IgC2 domain (L. Carrier et al. 1997; Niimura et al. 1998; Ababou et al. 2008) and replacement of this acidic residue with a basic lysine residue can weaken or abrogate the interaction between the C1 domain of cMyBPC and the S2 segment of myosin (Govada et al. 2008). Furthermore, given the proximity of this mutation to phosphorylation sites in the MyBPC motif, the mutation may alter cMyBP-C phosphorylation, indirectly disrupting the interaction between the N-terminal cMyBP-C and S2 (Niimura et al. 1998). It has therefore been hypothesized that disruption of the cMyBP-C-S2 interaction may cause acceleration of contractile kinetics and an increase in contraction force, resulting from an increased probability of cross-bridge formation (de Lange et al. 2013).

AIMS OF THE THESIS

The development of patient-derived iPSCs differentiated into cardiomyocytes (hiPSC-CMs) may play an important role in the study of pathological mechanisms underlying inherited genetic heart diseases. The overall goal of this work was to use hiPSC-CMs as a platform for the *in vitro* study of genetic cardiomyopathies, particularly dilated cardiomyopathy (DCM), using an iPSC model from patients with Duchenne Muscular Dystrophy (DMD), and hypertrophic cardiomyopathy (HCM), using hiPSC from patients with a mutation in the gene encoding the cardiac myosin binding protein C (*MYBPC3*-p: cMyBP-C). Given the immature characteristics of these cardiomyocytes, we used several approaches to enhance their maturation and perform electrophysiological and mechanical studies.

In **Chapters 3** of this work, the aim was to demonstrate how long-term culture and variation in substrate stiffness affect the maturation and function of hiPSC-CMs; in particular, hiPSC-CMs obtained from DMD patients were used to evaluate the effects of dystrophin deficiency on intracellular Ca^{2+} management. To better define the maturation of calcium handling, APs and Ca-T were measured simultaneously using fluorescent indicators at specific time points of maturation.

In **Chapter 4** we used patient-specific hiPSC-differentiated cardiomyocytes (hiPSC-CMs) to evaluate the molecular and cellular mechanisms leading to the development of HCM. In this study, to investigate the pathogenetic mechanisms driven by the *MYBPC3:c.772G>A* mutation we used human disease models, such as surgical myectomy samples, hiPSC-CMs and engineered cardiac tissues (EHTs) to perform functional and molecular analyses. A point of interest was to compare the results obtained from the native myocardium of HCM patients carrying the c.772G>A variant with those of hiPSC-CMs and hiPSC-EHTs generated from the cell lines of the same patients.

Another goal of our research is to validate the possible antiarrhythmic role of pharmacological compounds in reducing arrhythmic risk in HCM patients. Given the difficulties of using human samples for long-term drug testing, we applied hiPSC-EHTs for long-term drug exposure and evaluation of biophsyical parameters such as action potentials, electrical conduction, Ca^{2+} transients, and mechanics. Therefore, as shown in the last **chapter 5**, our aim was to evaluate the response to acute and long-term exposures of Mavacamten, a novel myosin inhibitor used to manage and treat patients with obstructive HCM (Olivotto et al. al. 2020) using patient and isogenic corrected hiPSC-EHTs. The results of the long-term effect of Mavacamten on hiPSC-EHTs are presented for electrophysiological, contractile and molecular changes.

Chapter 2

MATERIALS AND METHODS

2.1 Stem cell line generation

- Urine-derived cells from a healthy male donor into hiPSC lines (UC3-4 A1) using a lentiviral vector carrying Oct3/4, Sox2, Klf4 and c-Myc. We used cell lines from a DMD patient carrying a deletion of exon 50 in DMD gene (UC72039) and compared to a healthy control (UC3-4) (Guan et al., 2014) and its isogenic cell line (c.263delG, UC1015-6) previously generated from control cell line by CRISPR-Cas9-mediated deletion of a single frame at the 5' of Exon1 in DMD gene (Pioner et al., 2020). Both UC72039 and UC1015-6 were previously characterized for the absence of the full-length dystrophin (Dp427) (Guan et al., 2014; Macadangdang et al., 2015; Pioner et al., 2020; Bremner et al., 2022).

- Peripheral blood mononuclear cells were isolated using a standard isolation method and patient blood samples were collected at Careggi Hospital (Florence, Italy). PBMCs were isolated by density gradient centrifugation Ficoll (sodium diatrizoate, polysaccharides, and water, density of 1.08 g/mL) in equal volume of whole blood diluted in PBS and centrifuged for 40 minutes at 400-500 x g without brake. The "ring" of PBMCs were collected at 2×10^6 cell/ml in 20% dimethyl sulfoxide (DMSO) and 90% Fetal Bovine Serum (FBS) (Life Technologies) and placed inside a freezing container (Nalgene Mr. Frosty) at -80°C overnight to allow gradual cooling and moved to liquid nitrogen the following day. Six cell lines (PBMCs) obtained from patients carrying the c.772G>A mutation were shipped to the University of Washington where they were reprogrammed into iPSCs utilizing the CytoTune®-iPS 2.0 Sendai Reprogramming Kit (Gibco). Two representative clones per patient iPSC line were selected based on flow cytometry of four pluripotency markers (Oct4, Nanog, SSEA-4, and TRA-1-60) **(Fig. 2.1A).** Further quality control of these patient clones was performed including karyotyping (Cytogenetics) **(Fig. 2.1B)**, Sanger sequencing for the missense mutation (GeneWiz) **(Fig. 2.1C)**. A representative patient line (AOUC-HCM4) was genome edited using CRISPR/Cas9 (Clustered Regularly Interspaced Short Palindromic Repeats/Cas9) to create a homozygous isogenic control line. hiPSC lines utilized for this work include, WT-C11 line engineered by Dr. Bruce Conklin (The Gladstone Institute), the ID3 iPSC line (AOUC-HCM4) and the corrected ID3 isogenic control line.

ID Code	Age	Gender	Disease	Mutation	Source
AOUC-HCM1	46	M	HCM	*MYBPC3-c.772G>A*	PBMCs
AOUC-HCM2	70	M	HCM	*MYBPC3-c.772G>A*	PBMCs
AOUC-HCM3	43	M	HCM	*MYBPC3-c.772G>A*	PBMCs
AOUC-HCM4	58	M	HCM	*MYBPC3-c.772G>A*	PBMCs
AOUC-HCM5	46	M	HCM	*MYBPC3-c.772G>A*	PBMCs
AOUC-HCM7	52	F	HCM	*MYBPC3-c.772G>A*	PBMCs

Table 1. *List of six cell lines (PBMCs) isolated from HCM patients carrying the c.772G>A mutation and reprogrammed into hiPSCs*

A

	Pluripotency Markers			
	Oct4	Nanog	SSEA-4	TRA-1-60
Cell Line				
WTC11	98.2%	90.8%	99.9%	97.6%
Clone 1 ID3	99.1%	95.5%	100.0%	91.6%
Corrected ID3	99.6%	97.7%	99.9%	99.8%

B

Clone 1 ID3   Corrected ID3

C

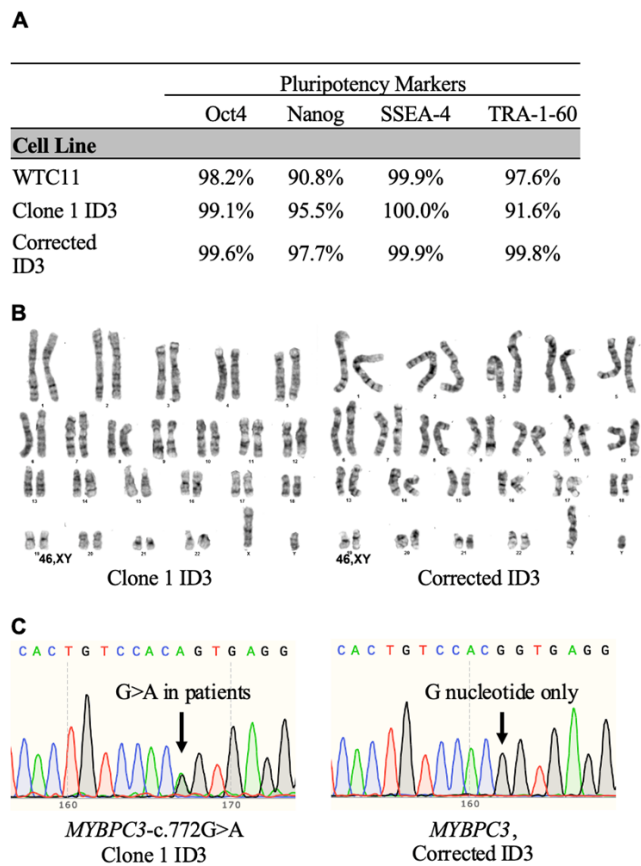*MYBPC3-*c.772G>A Clone 1 ID3   *MYBPC3*, Corrected ID3

Figure 2.1. *Characterization of hiPSC lines.* ***A)*** *Oct4, Nanog, SSEA-4, and TRA-1-60 pluripotency markers quantified by flow cytometry,* ***B)*** *healthy karyotyping, and* ***C)*** *confirmed presence of the MYBPC3-c.772G>A nucleotide switch in the patient ID3 line and restoration of the normal genotype in the corrected ID3 line.*

2.2 Human pluripotent stem cell culture and cardiac differentiation

Undifferentiated hiPSC cell lines were expanded under serum-free conditions in mTeSR medium (StemCell Technologies) on a Corning® Matrigel hESC-Qualified Matrix (StemCell Technologies), at 37°C, 5% CO_2. For cardiac differentiation, a monolayer directed differentiation protocol was applied using the cardiac PSC Cardiomyocyte Differentiation Kit (Life Technologies). Reaching a confluence of 70-80%, hiPSC colonies were chemically dissociated using Tryple 1X (Life Technologies) and incubated at 37°C for approximately 3-5 minutes, until cells rounded up. The cell suspension was centrifuged at 200 x g for 4 minutes at room temperature and the pellet was resuspended in the appropriate volume of mTeSR with 5µM of Y-27632 ROCK inhibitor (StemCell Technologies). The single cells were seeded in each well of a 24-well plate at cell density of 60.000-80.000 cell/well; after 24 hours, the cells reached 5-15% confluence and the mTeSR medium was changed, without the addition of ROCK inhibitor.

- **Note:** It's recommended to determine the optimal cell density for differentiation of each iPSC cell line

At 70% of confluency (~2 days after dissociation) the medium was changed to Cardiomyocyte Differentiation Medium A (referred to as day 0 of the differentiation protocol). Two days later, Medium A was replaced with Cardiomyocyte Differentiation Medium B (day 2) and after a further 2 days with Cardiomyocyte Differentiation Medium C (day 4), which was subsequently changed every 2 days, until spontaneously beating appear (day 8 of differentiation). On day 12, Medium C was replaced with RPMI plus B-27 supplement (Life Technologies). Differentiated cells can be cultured until day 12-15 for dissociation and/or cryopreservation, as beyond this time cells are difficult to harvest and recover. Alternatively, the cardiomyocytes can be maintained for a month or more for long-term studies.
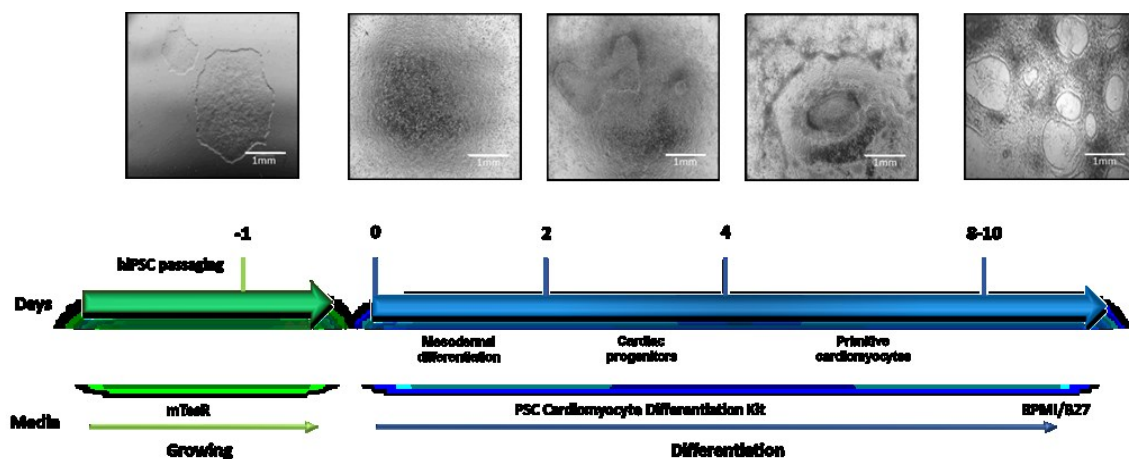
Figure 2.2. *Cardiac differentiation protocol. hiPSC differentiated into cardiomyocytes using PSC Cardiomyocyte Differentiation Kit. Day 0 refers to the addition of culture medium A, which induces embryonic to mesoderm germ layer transition; on day 2, culture medium B induces differentiation into cardiac progenitors, and then, on day 4, the change to culture medium C promotes the formation of primitive cardiomyocytes. Around day 8 spontaneously beating monolayers are visible and from day 12, the medium is replaced with RPMI/B27.*

56

2.3 Single hiPSC-CMs dissociation

Beating monolayers were pre-incubated with RPMI/B27 with Y-27632 ROCK inhibitor (1:1000) 1h before dissociation of single cells. Monolayers were chemically digested at day 15 using Tryple 1X for 10-15 minutes at 37°C. Single cells are harvested and pelleted in RPMI/B27 medium plus 50% fetal bovine serum (FBS). Single hiPSC-CMs are replaced in RPMI/B27 medium plus 10% FBS and Y-27632 ROCK inhibitor.

2.4 Protein analysis

hiPSC-CMs cultured in a monolayer were collected at day 14-, 30-, 45-, and 60-days post initiation of differentiation and spun down at 1000 rpm for 5 min. Supernatant was removed, and cell pellets were immediately frozen in liquid nitrogen. Cell pellets were then stored at -80°C. Protein was isolated from these cell pellets utilizing lab made lysis buffer (150mM NaCl, 0.1% Triton X-100, 50mM Tris-HCl at pH 8.0) with 1:100 protease inhibitor cocktail (Sigma). Protein concentration was quantified utilizing the Bradford Assay (BioRad, 5x stock) and BSA standards (2 mg/ml stock, Thermo) on a plate reader measuring absorbance at 595 nm. Western blot (WB) was performed to probe for proteins of interest. Briefly, 20μg of protein per sample was diluted in 4x Laemmli buffer (BioRad) and denatured at 95°C for 5 mins. Samples were separated using 4-20% gradient Mini-PROTEAN® TGX Stain-Free Protein Gels (BioRad) and then transferred onto Immuno-Blot® LF PVDF Membranes (BioRad). Membranes were blocked in the Blocking Buffer for Fluorescent Western Blotting (Rockland). Primary antibodies incubated overnight: cMyBP-C (1:2000, gift from Dr. Samantha Harris, University of Arizona, Tucson, AZ, USA), α-actinin (1:300, Abcam, ab9465), and GAPDH (1:2000, Invitrogen, AM4300). Secondary antibodies, Alexa Fluor 488 and 647, were diluted 1:2000 in a blocking buffer for 1h at RT (Life Technologies). Antibody stripping was performed to quantify multiple proteins from the same blot. Restore™ western blot stripping buffer (Thermo Scientific) was added to membranes and incubated at RT for 30 mins and then washed off with TBS-T (3x). Membranes were re-blocked prior to subsequent primary antibody incubation. Fluorescent western blots were imaged utilizing a ChemiDoc MP (BioRad) and quantified using FIJI.

2.5 hiPSC-CMs maturation on biomimetic hydrogels

On day 20 post differentiation, single hiPSC-CMs were obtained from beating monolayers. hiPSC-CMs were pre-treated with 5μM Y27632 in the RPMI/B27 medium for 1 hour. For single cell dissociation, after careful medium wash with PBS 1X, monolayers were incubated for enzymatic dissociation with Tryple (Life Technologies, Thermo Fisher scientific, Carlsbad, CA, USA Life Technologies) (10 min at 37 °C). Plating media was composed of RPMI/B27 and 10 μM ROCK inhibitor. Single hiPSC-CMs were spun and sparsely seeded at the density of 20,000 cells/cm^2 (at least 40,000 cell/substrate) onto fibronectin. (Human Fibronectin Native Protein, Life Technologies, 10μg/ml) substrates (25 mm of diameter) (PEG or DEG or commercial Polyurethane Acrylate (PUA)-based nanopatterned substrates purchased from CuriBio, Seattle, WA, USA) in 6-well plate. Single hiPSC-CMs were fed every other day until experimental days. Dual recording experiments of long-term cultured hiPSC-CMs were performed at day 60, 75 and 90 p.d.
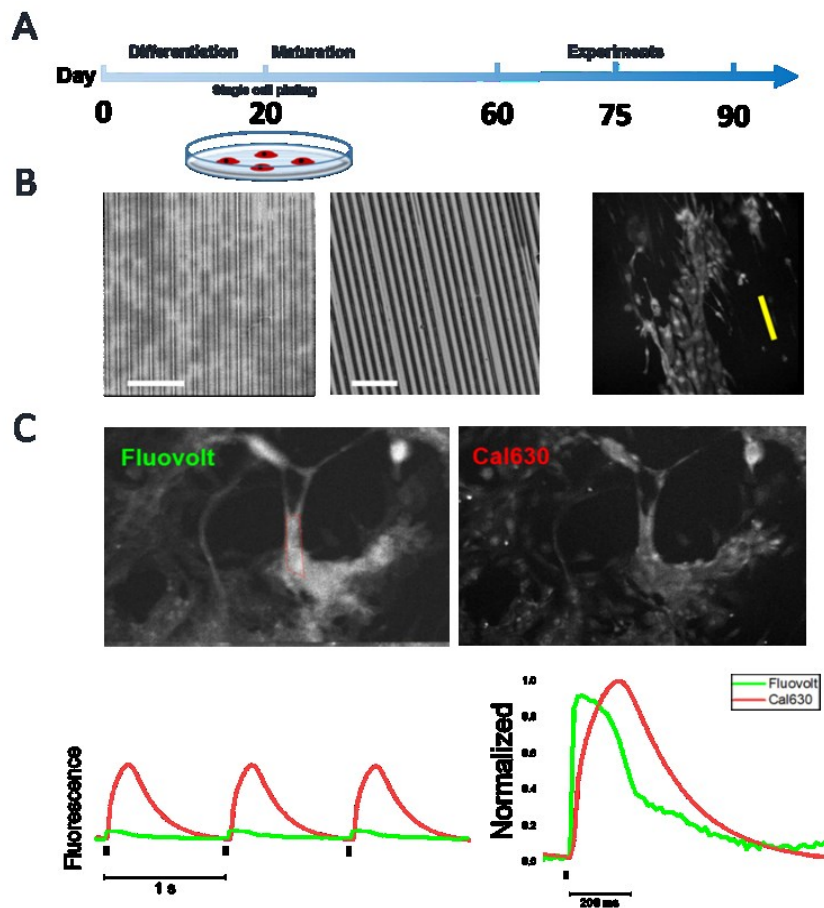
Figure 2.3. *Experimental procedure. Human iPSCs are differentiated into cardiomyocytes (hiPSC-CMs) with monolayer-directed differentiation protocol.* **A)** *At day 20 post differentiation, single hiPSC-CMs are seeded onto hydrogel-based micropatterned surfaces and cultured until experimental day 60, 75 and 90.* **B)** *Left: fabrication of micropatterned hydrogel with PDMS mold and PEG-DA hydrogel synthesis by soft lithography (scale bars equal to 10 and 60 μm respectively). hiPSC-CM preferential spreading along the pattern direction (indicated by yellow line).* **C)** *Simultaneous recording of action potential and calcium transients using Fluovolt (Ex/em 522/535 nm) and Cal630 (Ex/Em 608/626 nm), respectively*

2.6 Fabrication of PEG-DA Hydrogel Substrate with Micropatterned Topography

Micropatterned substrates were prepared by soft lithographic technique. A master sample was replicated by a PDMS (polydimethylsiloxane) mold that is used as template for the pattern replication.

Master fabrication: Master samples were obtained by laser writer lithography (μPG101 laser writer, Heidelberg, city, state abbrev, country, 800 nm resolution). A commercial optical resist (AZ 1505 Merck Performance Materials GmbH, Merck Group, Darmstadt, Germany) was spun over 2 cm × 2 cm Si wafers and exposed to a laser spot (λ = 375 nm) with beam intensity of 16 mW. The length of the linear stripes was set to 1 cm, while their width and spacing were fixed to 0.6 μm and 1.4 μm respectively. After the exposure process, the samples were developed for 30 s in a 1:1 solution of AZ Developer

(Merck Performance Materials GmbH, Merck Group, Darmstadt, Germany) in water, and subsequently rinsed in deionized water for 120 s.

Glass slides treatment: Glasses to support the PEG patterns were silanized to prevent the peeling-off of the hydrogel during the cell culture. First, glasses were washed with an alkaline piranha solution (water, aqueous ammonia and hydrogen peroxide 5:1:1 v/v) at 70° C for 15 min. Then, the glass were rinsed with water and the isopropyl alcohol and, after drying, they were immersed in a solution of 3-(trimethoxysilyl) propyl methacrylate) (MAPTMS, 0.064 mM in ethanol) for 1h. At the end, glasses were washed with isopropanol and dried.

Fabrication of PDMS mold: Monomeric PDMS mixture was prepared by mixing the two components of a commercially available PDMS kit (Sylgard 184, Sigma-Aldrich, Merck Group, St. Louis, MI, USA) in a 10:1 *w/w* ratio (base and curing agent) and then casted on the silicon master. After curing at 100° C for 30 min, the crosslinked PDMS mold was peeled off by the master.

PEG-DA pattern printing: A small amount (~20μL) of a solution of PEG-DA (250 Mn, Sigma-Aldrich, Merck Group, St. Louis, MI, USA) and Irgacure 389 photoinitiator (1% w/w) was dropped on a silanized glass slides and then, the PDMS mold was directly placed onto the surface. Irradiation by UV light (λ = 385nm) (M385CP1-C4, ThorLabs, Newton, NJ, USA) for 10 min allowed the formation of the crosslinked PEG-DA network. PDMS mold was gently peeled off from the substrates and used again after washing in water and methanol. Images of mold and micropatterned PEG-DA hydrogels were obtained by scanning electron microscopy (SEM).

2.7 Dual Recording of Action Potential and Calcium Transient

For dual recordings of APs and CaTs, hiPSC-CMs were loaded with 2 μL/mL Fluovolt (Thermo Fisher, Waltham, MA, USA), 2 μL/ml of Cal630 (AAT Bioquest, Sunnyvale, CA , USA) and 5 μL of Power Load™ concentrate (Thermo Fisher, Waltham, MA, USA) for 30 min at 37 °C and then washed with pre-warmed culture media before placing the cover slide into the experimental chamber. The experimental chamber features platinum electrodes for electrical field stimulation, connected to a stimulator (DigiTimer, Welwyn Garden City, UK) delivering short (3ms) voltage pulses. During measurements, cells were continuously perfused with a heated Tyrode buffer to keep the temperature stable at 37±1°C. For fluorescence studies, cells were simultaneously illuminated by LED light at two different wavelengths, blue (488 nm) for excitation of Fluovolt and yellow (580 nm) for Cal630 dye excitation, using a multi-led system (Lumencor SPECTRA X, Beaverton, OR, USA). A dual-wavelength band-pass filter cube (Semrock, IDEX, Lake Forest, IL, USA) was used to allow fluorescence light from the two dyes to be collected by a single camera (Photometrics Prime sCMOS, Teledyne, Tucson, AZ, USA): in particular, the filter allowed green light (515–545 nm, emission of Fluovolt) and red light (615–655 nm, emission of Cal630) to be collected. To separate the two emission wavelengths, we used an OptoSplit II light splitter (Cairn Research Ltd, Kent, UK) that was able to separate the two spectral components of the fluorescence image and focus them simultaneously on the upper and lower half of the camera chip. MetaMorph software (Molecular Devices, San Jose, CA, USA) was used to collect and analyze fluorescence images. The camera collected images at an average rate of 90 frames per second. In each selected microscope view field, several single hiPSC-CMs were selected

and chosen as regions of interest. The background-corrected average fluorescence values from the pixels in each selected region of interest (myocyte) were recorded at each of the two wavelengths under different stimulation conditions for 5 to 10 s in each condition. For the analysis of action potential or calcium transient kinetics during steady-state stimulation, the average of 5–10 subsequent AP or CaT traces was calculated to reduce noise. Pearson's correlation coefficient (r2) was calculated from the linear fitting of values distribution recorded from individual cells.

2.8 Freezing of hiPSC-CMs

For hiPSC-CM freezing, s single hiPSC-CMs previously exposed to 1h of ROCK inhibitor 10µM were obtained with Tryple-dissociation and resuspended in KO-DMEM (1:1), centrifuged at 1000 rpm for 5 minutes. Cells were rapidly resuspended in CryoStor© CS10 freezing medium (StemCell Technologies) and frozen in cryovials at 1°C/min at -80°C for at least overnight before moving to liquid nitrogen.

2.9 Cell fractional shortening

Single hiPSC-CM fractional shortening was visualized using a Nikon TS100 inverted microscope coupled to a video-based edge detection system at 40x of magnification (Olympus). For measures of single hiPSC-CMs cultured for 60 days, at 20 days post differentiation, single hiPSC-CMs were re-plated onto 10µg/ml human fibronectin-coated surfaces (35mm diameter, Fisher). All cells were perfused at 37°C with a Tyrode solution (in mM: NaCl 138, KCl 3.7, HEPES 20, KH_2PO_4 1.2, $MgSO_4 \cdot 7H_2O$ 1.2, Glucose 5, $CaCl_2 \cdot 2H_2O$ 1.8, pH 7.0) subjected to a sequential pacing train of at least 10 seconds at 1Hz. Traces were analyzed using the IonWizard (IonOptix) software. A minimum of five traces were analyzed and averaged for each cell. Spontaneously beating hiPSC-CMs were excluded from this analysis.

2.10 Generation of Engineered Heart Tissues

For the generation of EHTs tissues were considered wells of hiPSC-CMs at ~90% confluency. On day 15 of differentiation culture, beating cells were washed with 1X PBS and dissociated with 1X Tryple for 10 min at 37°C. Gently, the cell suspension was transferred into a centrifuge tube with RPMI/B27 medium supplemented with 10% FBS. HiPSC-CMs were centrifuged at 1000 rpm for 5 min and resuspended in cardiac medium with 10% FBS and Y-27632 ROCK inhibitor (1:1000). Human EHTs were generated following previously described protocol (Mannhardt I., et al., 2017). Briefly, agarose casting molds were prepared in 24-well tissue culture plates with 2% Agarose (Life Technologies), dissolved in the appropriate volume of PBS; 1,6mL of warm agarose was pipetted into the wells and then Teflon spacers (EHT Technologies GmbH) were inserted. After agarose solidification (~10 min), Teflon spacers were removed and silicone PDMS racks (EHT Technologies GmbH) were positioned upside down in the middle of each agarose well **(Fig.2.4)**. EHTs were generated with 100µl per EHT consisted of 1 x 10^6 cells in RPMI/B27 with 5 mg/ml Fibrinogen from bovine plasma (Sigma-Aldrich) and 3 U/mL Thrombin (Sigma-Aldrich).
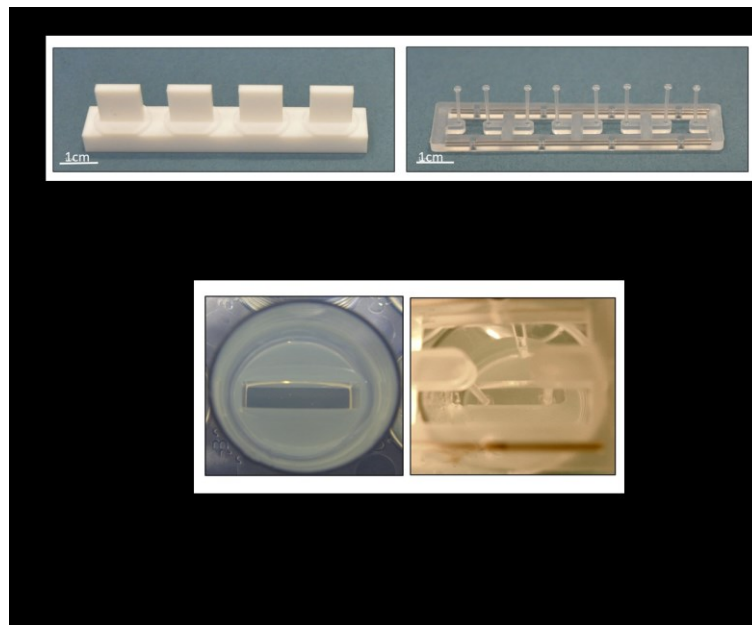
Figure 2.4. Casting mold preparation. *A)* PTFE spacer to create agarose casting molds and a silicone PDMS rack to generate EHTs. *B)* Generation of agarose casting molds and pillar insertion. (Mannhardt et al. 2017)

- **CRITICAL STEP**: Calculate an extra volume for each tissue to compensate for mixture loss during pipetting

The mixture was pipetted into the agarose-slots and incubated for 80 min at 37°C, 5% CO_2.

- **CRITICAL STEP**: It's important to pipette quickly and avoid bubble formation. If bubbles form, gently remove them with a small pipette tip.

After fibrin polymerization, each well was covered with a small amount of RPMI/B27 (300uL) and incubated again for 10 minutes to easily remove the fibrin gels from the agarose molds. Then the PDMS racks were carefully removed from the agarose wells and transferred to the EHT-medium consisting of the RPMI plus B27 with insulin, 10% FBS and 33µg/ml Aprotinin (Sigma-Aldrich) **(Fig. 2.5)**.

Figure 2.5. Generation of EHTs by embedding hiPSC-CMs in a fibrin hydrogel and seeded in the agarose casting molds between the 2 silicone pillars.

- **Note:**

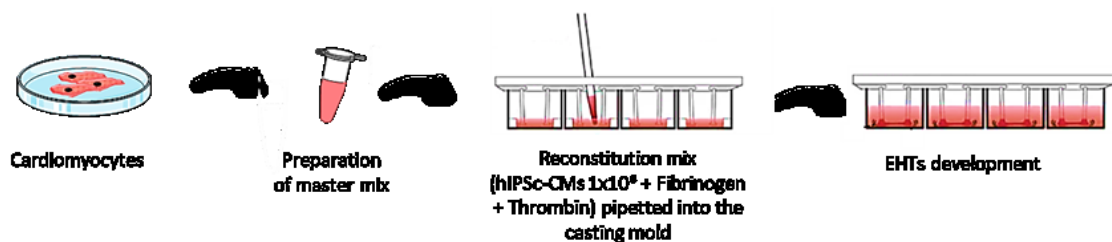   1. If the tissue does not form, the problem could be the fibrinogen or thrombin quality. In this case, fresh fibrinogen or thrombin should be prepared. On the other hand, if tissue forms, but degrades during maintenance in culture, the problem is the aprotinin quality. Again, fresh stock should be prepared.

    2. If after EHTs generation, the tissues do not beat well, the problem may be related to low efficiency of cardiac differentiation or very aggressive cell enzymatic dissociation. For this reason, it is important to use cardiomyocytes at early stages of differentiation, because it is easier to dissociate them to a single cell.

Reagents	Description
hiPSCs culture medium	mTesR1 basal medium is a feeder-free maintenance medium for human iPS cells supplemented with the 5X mTesR1 supplement and 1% penicillin-streptomycin. Aliquots stored at -20°C.
Cardiac PSC Cardiomyocyte Differentiation media	Three serum-free and xenon-free media that do not require thawing or mixing and allow efficient differentiation of hiPSCs into contracting cardiomyocytes in only 8 days. Stored at 4°C.
Cardiac Maintenance medium	RPMI 1640 Medium supplemented with B-27 Supplement and 1% penicillin-streptomycin. Stored at 4°C.
Cryopreservation medium	CryoStor CS10 is recommended for storing cells in ultra low temperature environments; this medium provides greater cellular viability and functionality. Stored at 4°C.
Y-27632 Dihydrochloride	Y-27632 is a Rho-associated kinase (ROCK) inhibitor, which improves survival of human pluripotent stem cells after dissociation into single cells. Dissolved at 1mM in UltraPure DNase/RNase-free distilled water and stored at -20°C.
Tryple express	Recombinant enzyme used for dissociation of attached cells. Compared with trypsin and other dissociation reagents, it is an animal-free enzyme and is gentle on cells.
Corning® Matrigel matrix	Aliquoted considering the Dilution Factor and stored at -20°C
Corning® Fibronectin	Glycoprotein of the extracellular matrix used for well coating. It promotes cell adhesion and growth; is diluted in distilled water and stored at -20°C
Aprotinin	Aprotinin is a non-specific serine protease inhibitor; it is dissolved in deionized water at 33mg/mL and stored at -20°C
Fibrinogen	Fibrinogen is part of the coagulation protein cascade. It is dissoved in 0,9% NaCl at 37°C and filtered. Is stored at -80°C
Thrombin	Serine protease that selectively cleaves Arg-Gly bonds in fibrinogen to form fibrin. Dissoved in three parts sterile PBS and two parts deionized water at 100U/mL and stored at -20°C

Table 2. Reagent list

2.10.1 Contractile force measurements

- **Spontaneous contractions recordings:** spontaneous auxotonic tension and beating frequency were regularly measured from day 20 to 50 of culture by optical tracking of the flexible post deflection at 10x of magnification (Olympus) using an Evos FL2 auto system (20 seconds, 33 frame/sec) (Life Technologies) with an on-stage incubator connected to a BenchPro 2100 Plasmid Purification System (Invitrogen). The recordings were performed at 37°C, 5% CO_2 in the RPMI/B27 culture medium with ~0.4mM of Ca^{2+}. The relationship between the deflection of the individual pillars and force is 0.28 µN/µm. Tension was analyzed using customized Labview analysis program and EHT cross-sectional area was calculated assuming an elliptical cross section (A= $\pi/4$ x width x thickness) for force normalization.
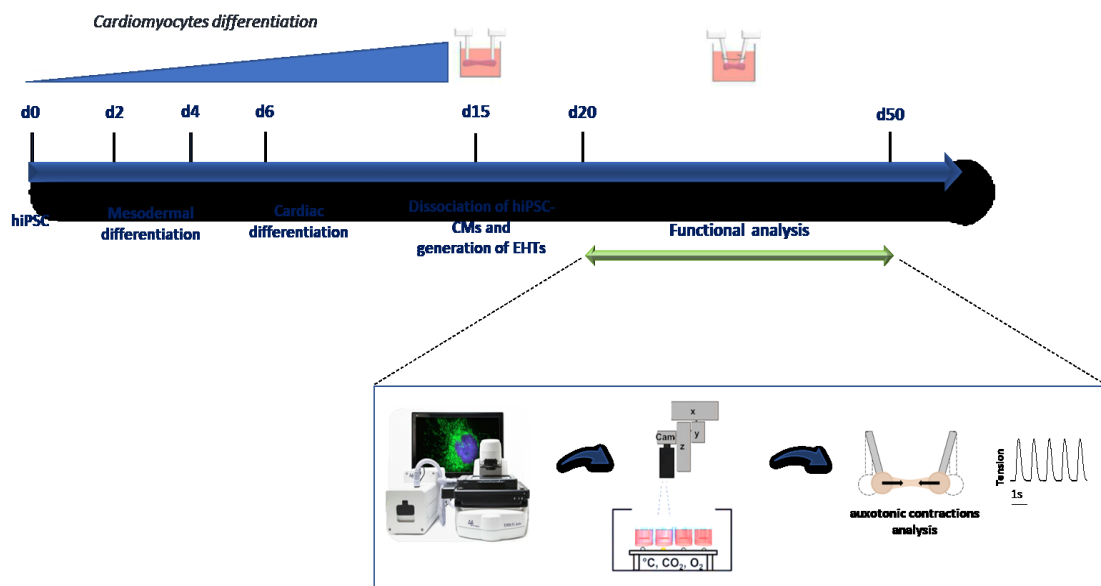

Figure 2.6. *Auxotonic contraction recordings. EHT analysis instrument with computer-controlled camera (Evos FL2 auto system). The 24-well plate is placed in a CO₂ and temperature-controlled incubator (on the left). On the right view of an EHT during spontaneous contraction analysis and an exemplary contraction pattern displaying contraction force measured with 33 FPS.*
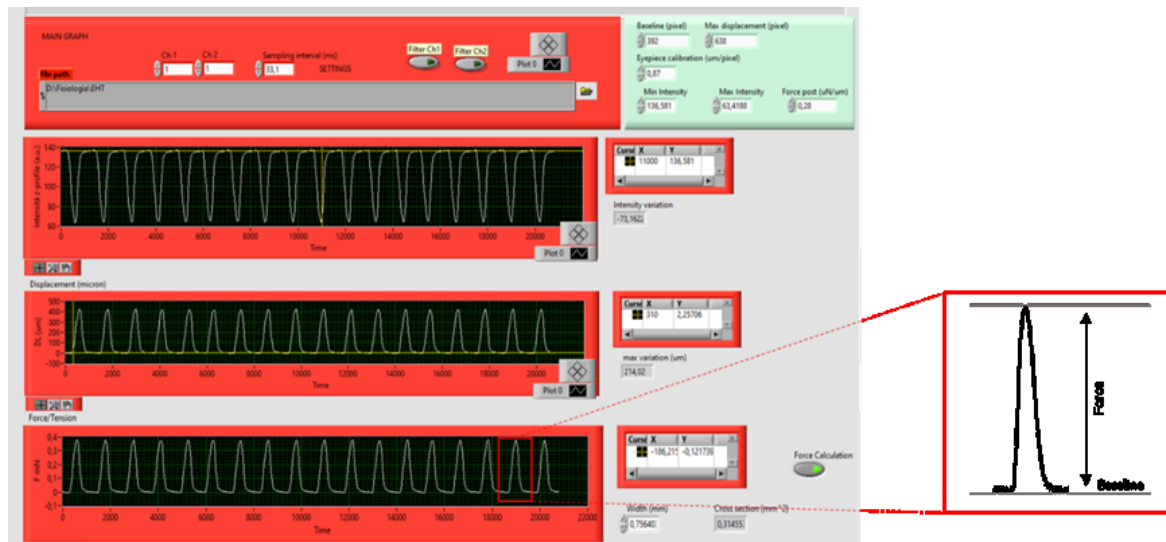
Figure 2.7. *Spontaneous contractions analysis. Example of contractile force analysis of an EHT using LabView software and enlarged schematic peak displaying the force analysis parameter.*

- **Isometric force measurements:** At day 50, EHTs are manually detached from the silicon pillars and immediately transferred into Krebs/Henseleit buffer, containing (in mM) 119 NaCl, 4.7 KCl, 2.5 $CaCl_2$, 1.2 $MgSO_4$, 1.2 KH_2PO_4, 25 $NaHCO_3$ with the addition of BDM (20mM). Then the EHT is mounted between a force transducer (KG7A, Scientific Instruments Heidelberg, Germany) and a motor (Aurora Scientific Inc. Aurora, Canada), perfused with Krebs/Henseleit buffer, without BDM, at pH 7.4 with 95%O_2:5%CO_2 and controlled by a custom Labview (National Instruments, Austin, Texas) program. After EHT fixation, tissue length and width were determined using a stereomicroscope with a reticle in the eyepiece and then tissue length was slowly increased in approximately 3% strain increments, while passive force was continuously recorded. Isometric force was recorded at 35±2°C. The EHTs were stimulated at increasing pacing rates (0.2-2.5 Hz) and recordings were performed at different Ca^{2+} concentration (0.5, 0.8, 1, 1.2, 1.8, 2, 3 and 4mM). Post-rest potentiation was also evaluated at the first stimulated beat after the pause. Isometric force was recorded *via* custom LabView software and was calculated using the same cross-sectional area as for the spontaneous measurements.

64

Cardiomyocytes differentiation

1mm

d0   d2   d4   d6   d15   d50

hiPSC   Mesodermal
differentiation   Cardiac
differentiation   Dissociation of hiPSC-
CMs and
generation of EHTs   Functional analysis
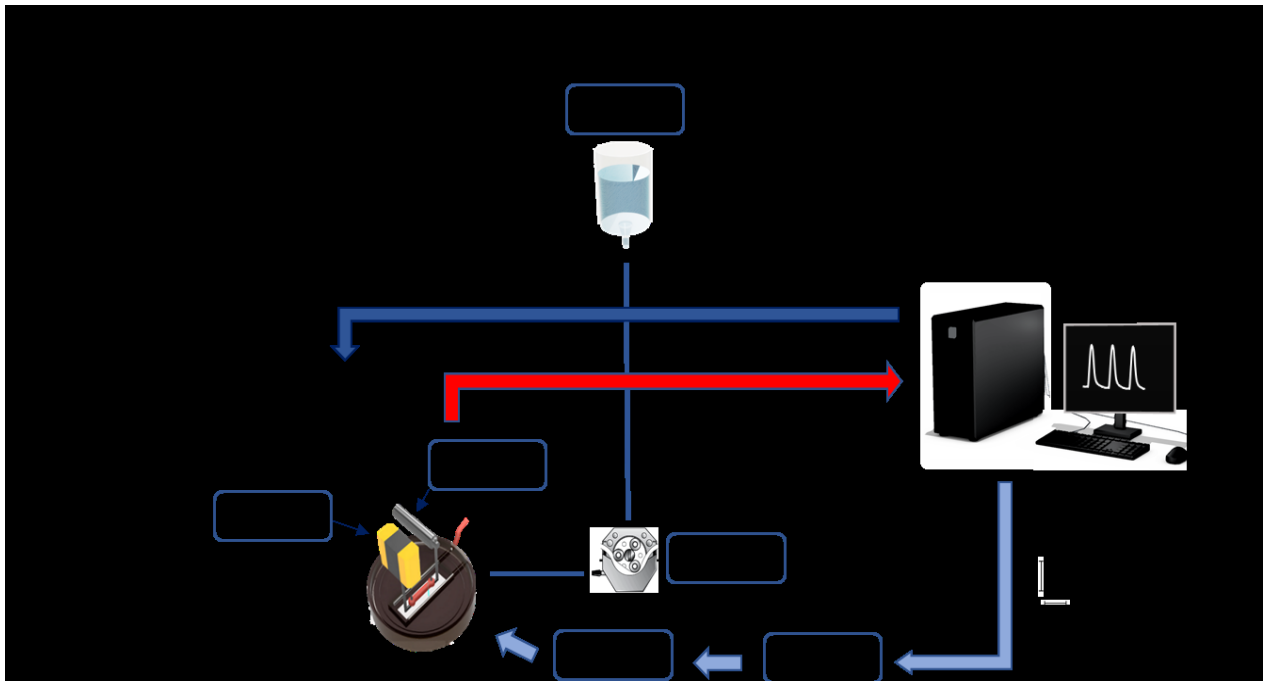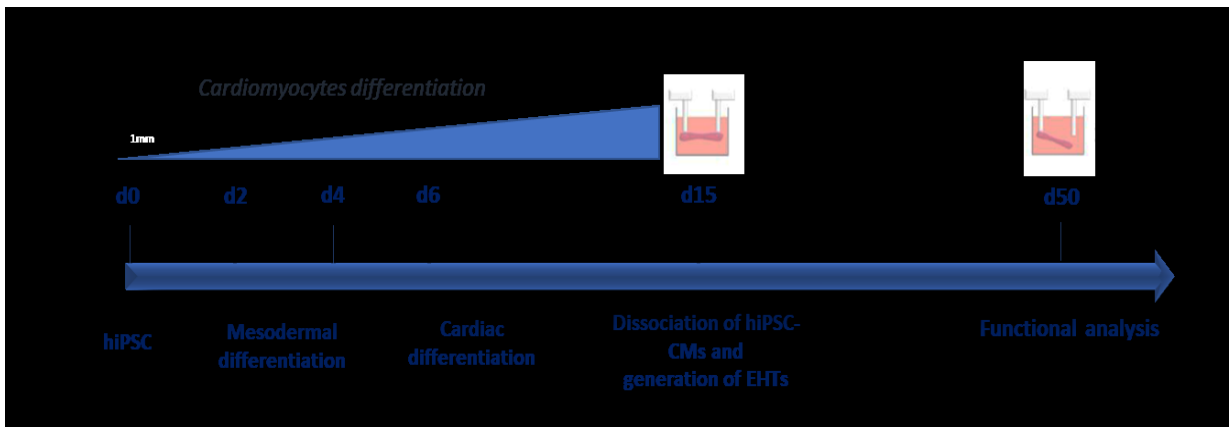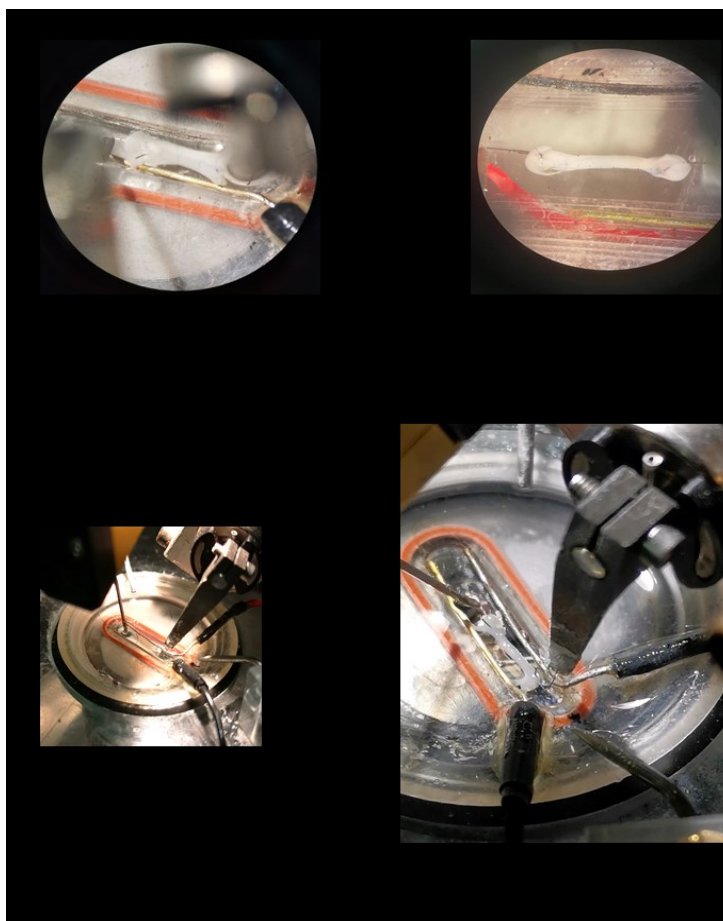
*Figure 2.8. Isometric contraction recordings. **A)** Timeline of cardiomyocyte maturation and EHTs generation. Detachment of EHTs from pillars at d50 p.d. for isometric measurements. **B)** Schematic representation of force recording apparatus to measure twitch contractions in isometric conditions. **C)** Images of mounting the EHT between a force transducer and a motor arm and width and length measurements before recordings.*

2.10.2 Drug screening

For drug screening on EHTs, Mavacamten (MYK-461, MAVA; Axon medchem BV -Groningen, The Netherlands) was dissolved in DMSO to obtain a 10 mM stock solution. To study the acute effect, Mavacamten was diluted to 1µM into Krebs solution. After recordings under basal conditions, the solution with the drug was continuously perfused during the experiment, and the force was recorded under isometric conditions at different pacing frequencies, as previously described. Instead, for chronic treatment, Mavacamten was dissolved in DMSO at the dilution of 1mM and further diluted to 0.33µM or 0.75µM in the culture medium (RPMI/B27). When the EHTs started to beat spontaneously, measurements were performed by optical tracking of the flexible post deflection before drug treatment for about 1 week. Then the EHTs were treated for 20 days with Mavacamten dissolved in RPMI/B27. Spontaneous contractile force was monitored during the treatment. After the 20-day treatment, the EHTs were maintained in culture in the presence of the drug-free medium for 2 days and then tension measurements were performed under isometric conditions.
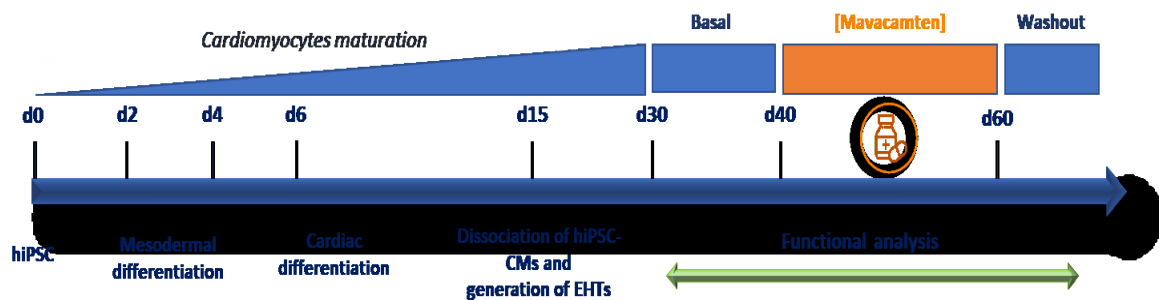
Figure 2.9. Schematic representation of chronic treatment of EHTs from day 40 to d60 p.d. Analysis of spontaneous contractions were performed during culture with and without drugs. EHTs were kept in culture in RPMI/B27 medium, at 37°C, 5% CO$_2$.

2.11 Patients for in vitro studies

In vitro studies were performed at the University of Florence. Protocols were approved by the ethical committee of Careggi University-Hospital (2006/0024713; renewed May 2009). In vitro studies were performed on cardiac samples from three c.772G>A patients consecutively referred to surgical myectomy for relief of drug-refractory symptoms related to LV outflow tract obstruction.

2.12 Tissue processing

Septal samples from HCM and control patients were rapidly washed in ice-cold cardioplegic solution containing (in mmol/L): KH$_2$PO$_4$ 50, MgSO$_4$ 8, HEPES 10, adenosine 5, glucose 140, mannitol 100, taurine 10 (pH 7.4 with KOH). Within 15 minutes from excision, a small portion of the tissue was frozen in liquid nitrogen and used for protein isolation. The remaining fresh tissue is kept in ice-cold cardioplegic solution and used to isolate multicellular preparations, single myofibrils and single cardiomyocytes. Endocardial trabeculae suitable for mechanical measurements (300-800 μm diameter) were dissected, while the remaining tissue was minced to small pieces (~1mm^3) and subjected to enzymatic and mechanical dissociation to obtain viable single myocytes, as described before. In brief, tissue chunks are transferred to to small pieces (~1mm^3) in a scraping device and the bathing solution changed to Ca^{2+}-free dissociation buffer containing (in mM): NaCl 113, KCl 4.7, KH$_2$PO$_4$ 0.6, Na$_2$HPO$_4$ 0.6, MgSO$_4$-7H$_2$O 1.2, NaHCO$_3$ 12, KHCO$_3$ 10, HEPES 10, taurine 20, Na pyruvate 4, glucose 10, BDM 10 (pH 7.3 with NaOH) and heated to 37 ºC. Collagenase Type V and Protease Type XXIV (Sigma) were subsequently added and tissue chunks digested for a total 2 hours' time. During the digestion, the buffer containing dissociated myocytes was collected every 15 minutes from the scraping device and diluted with KB solution at room temperature. KB solution contained (in mM): KCl 20, KH$_2$PO$_4$ 10, glucose 25, mannitol 5, L-glutamic acid monopotassium salt 70, β-hydroxybutyric acid 10, EGTA 10 and 2 mg/mL albumin (pH 7.2 with KOH). The myocytes were left to settle and then resuspended in Ca^{2+}-free Tyrode solution containing (in mM): 132 NaCl, 4 KCl, 1.2 MgCl$_2$ 10 HEPES, and 11 glucose (pH 7.35 NaOH). CaCl$_2$ was added stepwise up to 0.6 mM. Cells were stored in this solution and used within 3 hours.

2.13 Simultaneous energetic and mechanical measurements in skinned ventricular multicellular strips

Ventricular muscle strips were dissected parallel to the long axis of the fibers in a cold relaxing solution under a dissecting microscope. Subsequently, muscle strips were chemically permeabilized by overnight incubation in a relaxing solution with 1% Triton X-100 at 4 °C. Tissues were then extensively washed in a fresh ice-cold relaxing solution, stored at 4 °C, and used within 24 h. Experimental solutions and equipment used were as described previously (Coppini et al. 2014). Briefly, the skinned preparations were mounted horizontally between a force transducer and a length controller via aluminum T-clips. The length of the preparations was adjusted on the basis of the passive tension stretching them about 15% below the slack length, which corresponds to a sarcomere length of about 2.1-2.2 μm. Mean dimensions (± S.E.M.) of HCM and donor ventricular preparations amounted to 1.34±0.06 and 1.53±0.07 mm in length, 0.31±0.01 and 0.27±0.01 μm in width, and 0.28±0.01 and 0.23±0.01 μm in depth, respectively. Isometric force and ATPase activity were simultaneously measured at saturating (pCa 4.5) and sub-saturating Ca^{2+} concentration at 25 °C. The skinned fibers were activated inside a small (30 μl) chamber with quartz windows containing activating solution, and force generated and ATP consumed were measured simultaneously during each contraction (Witjas-Paalberends et al. 2014). Maximal force was determined at steady-state level and normalized to the cross-sectional area (CSA, mm^2) of the muscle strip to calculate tension (force/CSA, mN/mm^2). The CSA of the preparation was estimated based on an elliptical shape, i.e, CSA = (width x depth x π) / 4. The muscle was manually transferred between different baths and exposed to a range of activating calcium so that the pCa-force relationship could be determined. Tension values at different pCa were fitted with a modified Hill equation and the concentration of Ca^{2+} required to reach the half of maximum force (pCa50) was estimated to determine myofibril-Ca^{2+} sensitivity (Wijnker et al. 2014). Solutions with intermediate $[Ca^{2+}]$ were obtained by appropriate mixing of the activating and relaxing solutions.

ATPase activity was measured by an UV-coupled optical absorbance enzyme assay (Narolska et al. 2005). Briefly, ATP hydrolysis, inside the muscle, was coupled to the oxidation of NADH to NAD^+ catalyzed by pyruvate kinase and L-lactic dehydrogenase. NADH oxidation, and thus ATP consumption, was measured photometrically from the absorbance at 340 nm of near-UV light. This absorbance signal was calibrated using multiple injections of 50 nl of 10 mM ADP in the measuring bath. Using this calibration, ATPse activity ($pmol*ul^{-1}*s^{-1}$) in the preparation was derived from the slope of the absorbance signal. Maximal Ca^{2+} activated ATPase activity, at each $[Ca^{2+}]$, was calculated, by subtracting basal rate of ATPase activity in relaxing solution (pCa10) and normalizing to the volume (length x CSA, mm^3) of the muscle strip. Tension cost (isometric ATPase per unit force, $pmol*ul^{-1}*s^{-1}/mN/mm^2$) was calculated from the slope of the linear relationship between mean values of tension and ATPase activity once all the data were pooled in 10% wide normalized steady state force bins or as the ratio between maximal isometric tension and maximal ATPase activity. The comparison of mechanical and energetic measurements between donor and mutant trabeculae is meaningful if cardiomyocyte orientation along the muscle strips and mechanical conditions of contraction are the same for both groups of preparations. Altered cardiomyocyte alignment and myofibril "disarray",

described patchily in HCM myocardium (Poggesi and Ho 2014), may per se reduce isometric tension while increasing the ATP consumption, due to larger 'internal shortening'.

2.14 Mechanical Measurements in Myofibrils

Single myofibrils or small bundles of myofibrils were isolated from LV human samples and used for mechanical experiments as previously described (Piroddi et al. 2007). Thin strips of the ventricular samples were incubated overnight in cold relaxing solution (pCa9) with added 0.5% Triton-X 100 (Belus et al. 2008). After Triton removal, the strips were homogenized in a relaxing solution to obtain a myofibril suspension that was stored at 4°C. Myofibrils were mounted in a custom-built apparatus (pCa9, 15 °C) and mounted between two glass micro-needle, one connected to a high-speed length controller and the other one acting as a calibrated cantilever force probe. The initial sarcomere length was set at 2.2 µm. Activating and relaxing solutions calculated as previously described (Piroddi et al. 2007)(Belus et al. 2008) , were at pH 7.0 and at ionic strength 200 mmol/L. Myofibrils were maximally activated and fully relaxed by rapid switching (<5 ms) between two continuous streams of activating (pCa4.5) and relaxing (pCa9) solutions flowing from a double-barreled glass pipette. Fast solution switching technique allowed for the measurements of steady-state isometric force as well as the rate of force activation and relaxation. Maximal isometric force (mN) was normalized to the cross-sectional area of the myofibril (mm^2). The time required to reach 50% of the maximal force was used to estimate the rate constant of force development, k_{ACT} (s^{-1}), and the rate constant of force redevelopment following release/restretch protocol applied at steady state force, k_{TR} (s^{-1}). The kinetics of the two phases of relaxation were estimated as follows: 1. The rate constant of the slow early phase of relaxation, slow k_{REL} (s^{-1}), was calculated from the slope of the regression line fitted to the tension trace normalized to the entire tension relaxation transient; 2. The rate constant of the final fast phase of relaxation, fast k_{REL} (s^{-1}), was measured from a mono-exponential fit. All solutions contained a cocktail of protease inhibitors: 10 mM leupeptin, 5 mM pepstatin A, 200 mM phenyl-methylsulphonylfluoride, 10 mM E64, 500 mM NaN3 and 2 mM dithiothreitol. The level of contaminant inorganic phosphate in the solutions was kept less than 5 umol/L using a phosphate scavenging system (purine-nucleoside-phosphorylase with substrate 7-methyl-guanosine)(Tesi et al. 2002). The regeneration of MgATP inside the solutions was achieved by adding Creatine phosphate (10mM) and creatine kinase (200unit ml^{-1}).
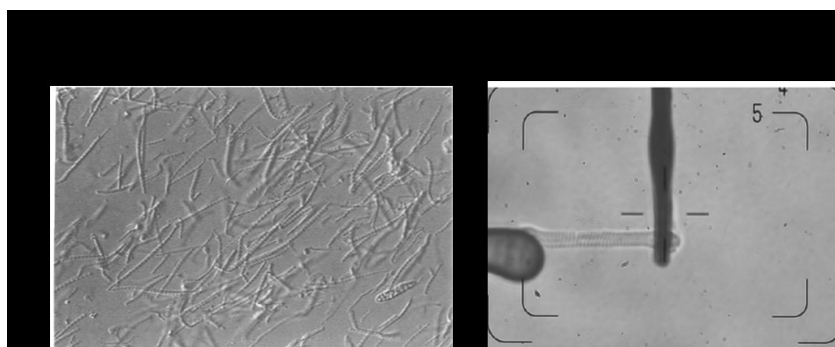

Figure 2.10. A) *Suspension of isolated myofibrils obtained by homogenization. Scale bar 25 µm. B) Phase-contrast images of a single or thin bundle of myofibrils mounted between the rigid motor lever arm and the blackened cantilever force probe. Scale bar 10 µm.*

2.15 Intact trabeculae studies

Intact ventricular trabeculae were mounted between a basket-shaped end of a force transducer (KG7A, Scientific Instruments Heidelberg, Germany) and a motor (Aurora Scientific Inc., Aurora, Canada), controlled by a custom Labview (National Instruments, Austin, Texas) program. Muscles were mounted in cold cardioplegic solution and then perfused with Krebs/Henseleit buffer, containing (in mM) 119 NaCl, 4.7 KCl, 2.5 CaCl$_2$, 1.2 MgSO$_4$, 1.2 KH$_2$PO$_4$, 25 NaHCO$_3$; pH 7.4 with 95%O$_2$:5%CO$_2$. Muscles were allowed to stabilize for at least 30 min before recordings. Diastolic sarcomere length was assessed by calculating the average distance of striations and set at 2.10-2.20 μm. Isometric force was recorded at 35±2°C under various conditions. In brief, inotropic responses to increased pacing frequencies, stimulation pauses, and beta-adrenoceptor agonist isoproterenol (10^{-7}M) were evaluated and kinetics of isometric twitches was assessed under all conditions. The trabecula was stimulated at increasing pacing rates (0.1-2.5 Hz): at each frequency, force reached steady-state before recordings. Stimulation pauses (30s) were inserted after the last contraction of a steady series (at 0.5 Hz) and post-rest potentiation was evaluated at the first stimulated beat after the pause. Finally, the muscle section was measured for force normalization.
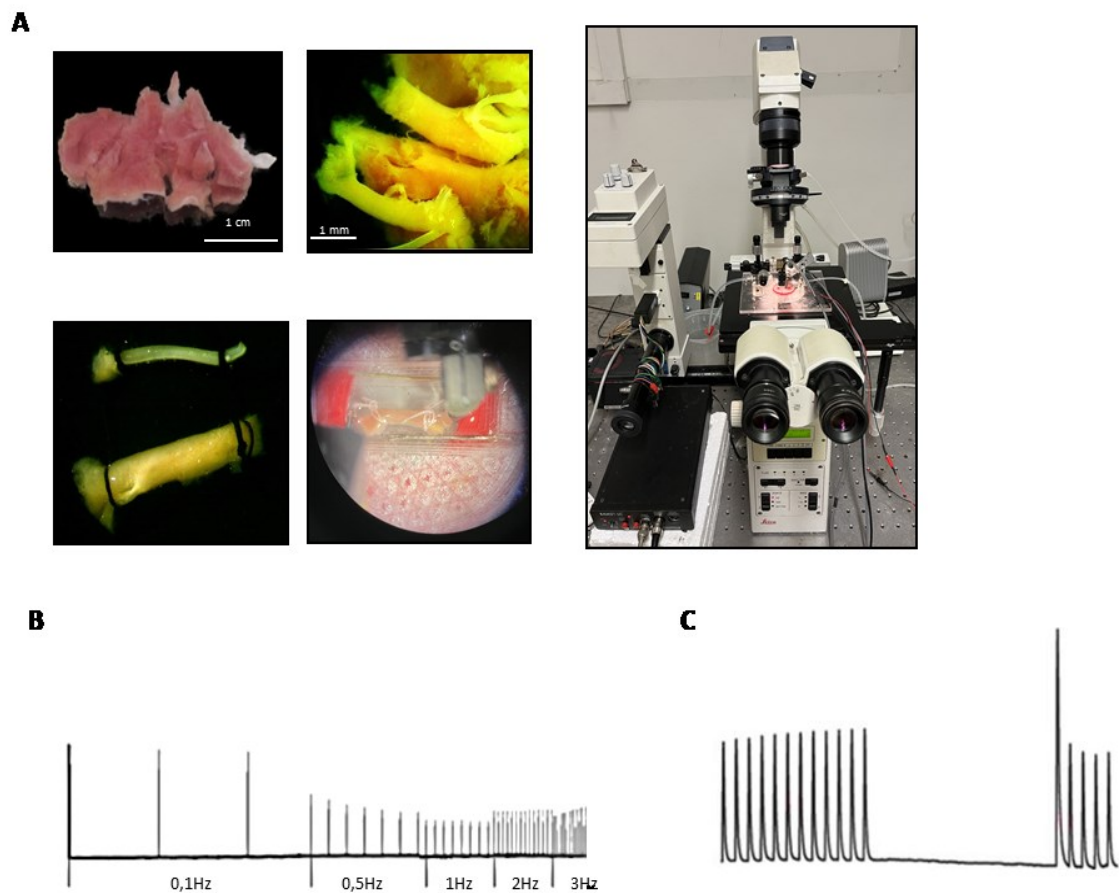

Figure 2.11. A) Images of intact trabeculae isolated from cardiac tissue and setup for steady-state recordings (on the top). Representation of force-frequency relationship **(B)**, post-rest potentiation **(C)**.

2.16 Cardiomyocytes isolation and current clamp/intracellular Ca^{2+} studies

The method described below is used to characterize alterations in myocardial cell function under conditions of cardiac disease. With this technique, cardiomyocytes are isolated from the interventricular septum of patients with hypertrophic cardiomyopathy (HCM) undergoing myectomy surgery and compared with those of non-hypertrophic patients (Coppini et al. 2013).

Surgical samples are highly variable in size and thickness; they are cut into small chunks, which are transferred into the chamber of the digestion device and used for isolation of single cells. For isolation of single cardiomyocytes, cardiac tissue chunks were reduced into small pieces ($\sim$1mm^3) and transferred to a scraping device; the bathing solution was changed to Ca^{2+}-free dissociation buffer containing (in mM): NaCl 113, KCl 4.7, KH_2PO_4 0.6, Na_2HPO_4 0.6, $MgSO_4$-$7H_2O$ 1.2, $NaHCO_3$ 12, $KHCO_3$ 10, HEPES 10, taurine 20, Na pyruvate 4, glucose 10, BDM 10 (pH 7.3 with NaOH) and heated to 37 ºC. Collagenase Type V and Protease Type XXIV (Sigma) were subsequently added, and tissue chunks digested for a total 2 hours' time. During the digestion, the buffer containing dissociated myocytes was collected every 15 minutes from the scraping device and diluted with KB solution at room temperature. The myocytes were left to settle and then resuspended in Ca^{2+}-free Tyrode solution. $CaCl_2$ was added stepwise up to 0.6mM and cells were stored in this solution and used within 3 h. Myocytes were incubated 30' with the Ca^{2+} indicator Fluoforte (Enzo Life Sciences, Farmingdale, New York) at room temperature, washed and transferred to the microscope-mounted recording chamber. Fluoforte fluorescence was detected at 505-520nm (using a high-speed high-sensitivity EMCCD Camera, model Evolve Delta by Photometrics, USA), during bright-field illumination at 492±3 nm (using a dedicated LED light source, model SpectraX by Lumencor). Experimental temperature was 35±5 °C for all protocols. Cardiomyocytes isolated by this method from human ventricle samples are used for voltage-clamp recordings of specific transmembrane currents, recordings of intracellular Ca^{2+} and/or cellular shortening during electric field stimulation, and evaluation of sarcolemma structure by confocal microscopy.

Action potentials (APs) were measured simultaneously using the perforated-patch configuration (amphotericin-B method). APs were activated with short depolarizing stimuli (<3ms) at different pacing frequencies (0.2Hz, 0.5Hz and 1Hz, 1 minute at each frequency). Action potential and current signals were measured with a Multiclamp 700B amplifier, using a standard 10 kHz longpass digital filter. Patch-clamp signals were digitized simultaneously using Digidata 1440A. Acquisition and analysis were controlled by dedicated software (pClamp10.0). Ca^{2+}-fluorescence videos were recorded at > 200 frames per second, and individual cell fluorescence was analyzed using Metafluor software (Molecular Devices).
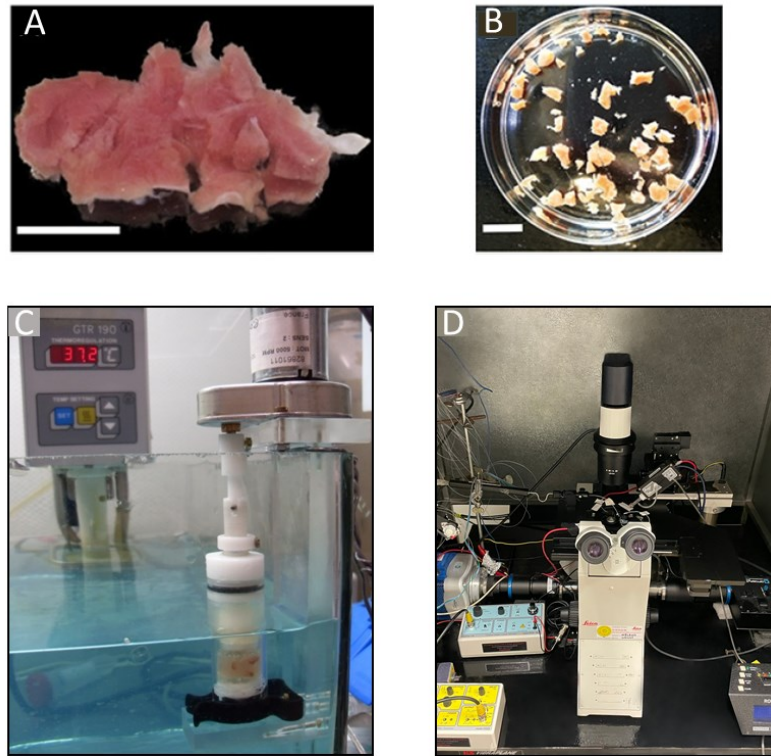
Figure 2.12. A) Representative image showing a sample of ventricular myocardium from a patient with HCM who underwent septal myectomy operation. Calibration bar= 5mm. *B)* Chunks of ventricular tissue cut from a ventricular surgical specimen, to be used for cell isolation. Calibration bar= 5mm. *C)* Image showing the digestion device in the thermostated bath during enzymatic digestion of ventricular tissue. *D)* Representation of action potentials and ion currents recordings by the" perforated patch" technique.
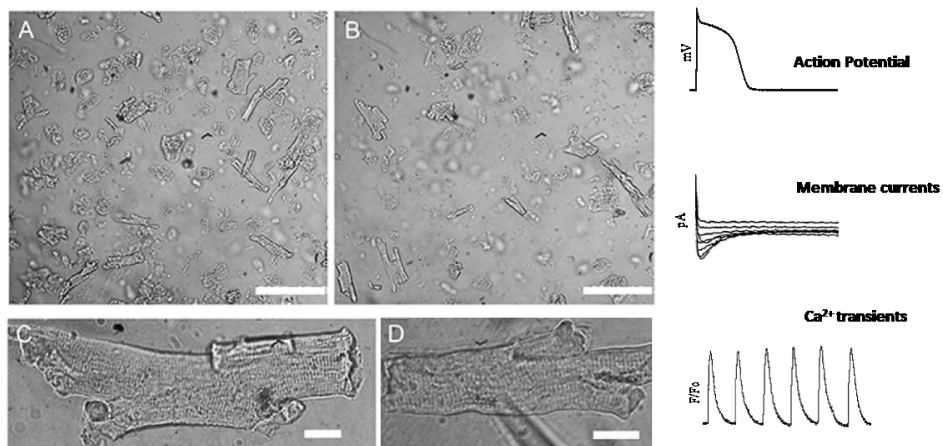
Figure 2.13. Isolated human ventricular cardiomyocytes. *A)* and *B)* photomicrographs of two microscope fields (10x objective) showing representative cardiomyocyte suspensions. Calibration bar= 100µm. *C)* Representative image of human cardiomyocytes isolated from a specimen of an HCM patient (40x objective) and *D)* image showing human ventricular cardiomyocytes touched by the tip of the patch pipette for recordings. Calibration bar= 20µm. On the right, representative trace showing membrane potential, ion currents and intracellular calcium recordings.

2.17 RT-PCR

Total mRNA was isolated from frozen samples using the RNeasy Fibrous Tissue Mini Kit (Qiagen) following manufacturer's instructions. Subsequently, complementary DNA (cDNA) was synthesized from 1μg of total RNA using iScript ™ cDNA Synthesis kit (Bio-Rad Laboratories S.r.l.). All these steps were performed according to the manufacturer's instructions. Real-time quantitative PCR (Q-PCR) was performed using iTaq™ SYBR® Green Universal Supermix and predesigned primers assays for the following genes: KCNQ1, KCNH2, KCND3, KCNIP2, KCNE1 (Bio-Rad Laboratories S.r.l.). All reactions were performed in triplicate and included a negative control. Relative quantification of the mRNA level for the different genes was determined by the Bio-Rad CFX Maestro software (Bio-Rad Laboratories S.r.l.), using the comparative method ($\Delta\Delta Ct$). In brief, the threshold cycle (Ct) difference of the index gene and the reference gene, calculated from each specimen, is subtracted from the average Ct of the control group; this value is used as the exponent of to calculate $\Delta\Delta Ct$ for each specimen. For all mRNA quantification assays, the housekeeping gene 18S ribosomal RNA was used as a reference gene.

2.18 In silico human-based electromechanical simulations

To test some of the hypotheses that arise from the experimental data, we employed a previously described model of HCM human cardiomyocytes (Margara et al. 2021; Brenner 1988).

In brief, mechanistic simulations of human ventricular myocyte electromechanical function were conducted in MatLab (Mathworks Inc. Natick, MA, USA) using the ordinary differential equation solver ode15s. A stimulus current of -53 µA/µF with 1ms duration was applied and steady-state was reached at 1Hz pacing. First, the effect of altered crossbridge cycling on force generation was analyzed. For this, a scaling factor of 2, consistent with experimental evidence, was applied to the model transition rates k_{ws} and k_{su}. In the Land model of human cardiac contraction, these drive the transitions from the pre-powerstroke to the post-powerstroke state and from the post- powerstroke to the detached state, respectively. Then, the effect of altered crossbridge cycling was evaluated in the context of HCM ionic remodeling. Simulated action potential, calcium transient, and active tension waveforms were compared to experimental data. In addition, to understand the mechanisms underlying the prolongation of the AP/calcium transient in the presence of the c.772G>A-MYBPC3 mutation, the excitation-contraction coupling remodeling was mimicked according to the ionic remodeling described in Coppini et al., 2013 for HCM cardiomyocytes with different genetic backgrounds. 2-tailed Student's t test was used to compare normally-distributed data and differences between groups were considered significant when $P \leq 0.05$.

2.19 Validation of the EHTs as an alternative ex-vivo model to study cardiac mechanics: a comparison with adult and fetal human tissue

Engineered heart tissues were generated with hiPSC-CMs isolated during the early stage of maturation (day 15 p.d.). Single hiPSC-CMs were encapsulated in the fibrin hydrogel between the two flexible silicone posts and the generated EHTs started to beat spontaneously and regularly 7-8 days after casting. During maturation, EHTs were used for optical analysis under auxotonic conditions: tension

and spontaneous beat frequency were analyzed from day 20 to day 50 of culture by optical tracking of the flexible posts deflection using an automated Evos system. The force calculated from the posts deflection was normalized by the cross-sectional area of each EHT. Measurements under auxotonic conditions of two control lines show a significant increase in force-generating capacity over time in all EHTs and a reduction in spontaneous beating frequency, as shown in **Figure 2.14**.

At day 50 p.d EHTs were detached from the pillars and fixed on a force recording apparatus to measure twitch contractions under isometric conditions between a force transducer and a motor arm, used to control EHT length. Under these conditions, the mechanical properties of EHTs were analyzed, including the passive tension.
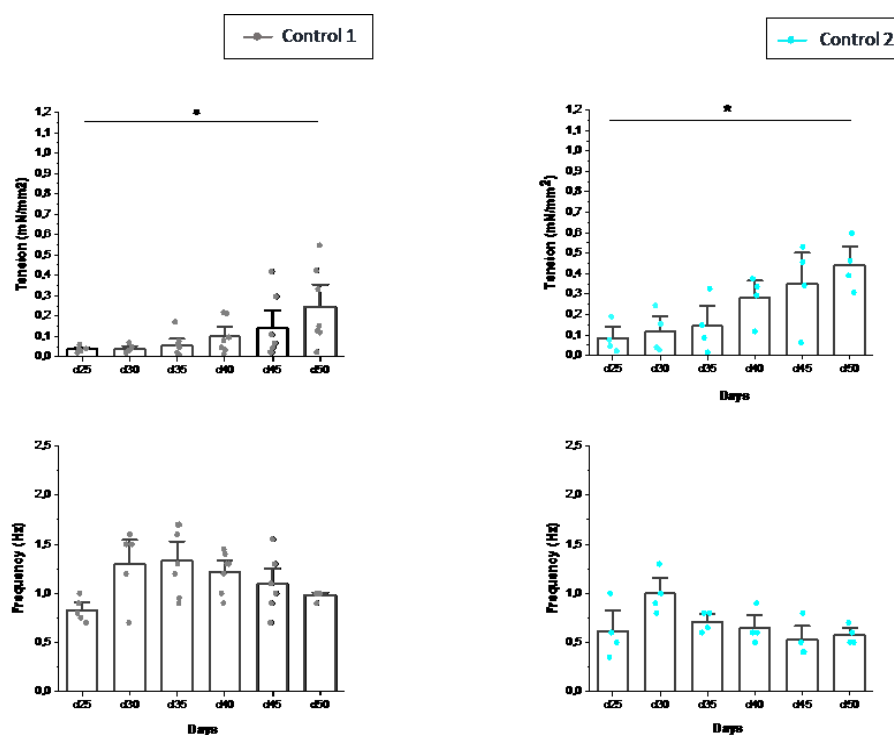
Figure 2.14. Spontaneous auxotonic twitch tension of EHTs from day 25 to 50 of differentiation (on the top), measured at 37°C in RPMI/B27 culture medium with 5% CO_2 (~0.4mM of [Ca^{2+}]) and progression of spontaneous beating frequency of all EHTs from day 20 to 50 (on the bottom). (Control 1, n=8, and Control 2, n=9). One-way analysis of variance (ANOVA) with a Tukey post-hoc test was used to compare the different time points. * $p < 0.05$ and ** $p < 0.01$ versus d25.

The passive mechanical properties of tissues are major determinants of cardiac function and changes in tissue stiffness can alter their active responses to stretch, including changes in contractility. To assess mechanical properties, we generally characterize the relationship between stress (σ= F/CSA), and strain ($\mathcal{E}$= $\Delta L/L_0$) and the slope of the linear stress-strain relationship is defined as the elastic or Young's modulus (E).

The stiffness of the surface to which cells adhere is an important factor as it can influence morphology, protein expression and cell migration and differentiation. Interactions between cells and the extracellular environment can be studied using 3D hydrogels, such as fibrin hydrogels, which are often used to study biophysical cell-ECM interactions. Here we analyzed the mechanical properties of

engineered heart tissues by applying a stress relaxation-recovery protocol to analyze tissue stiffness, by which strain is applied rapidly and then held constant while stress is measured; the stress is maximum when the target strain is reached and decreases during tissue relaxation (**Fig. 2.15A-B**).
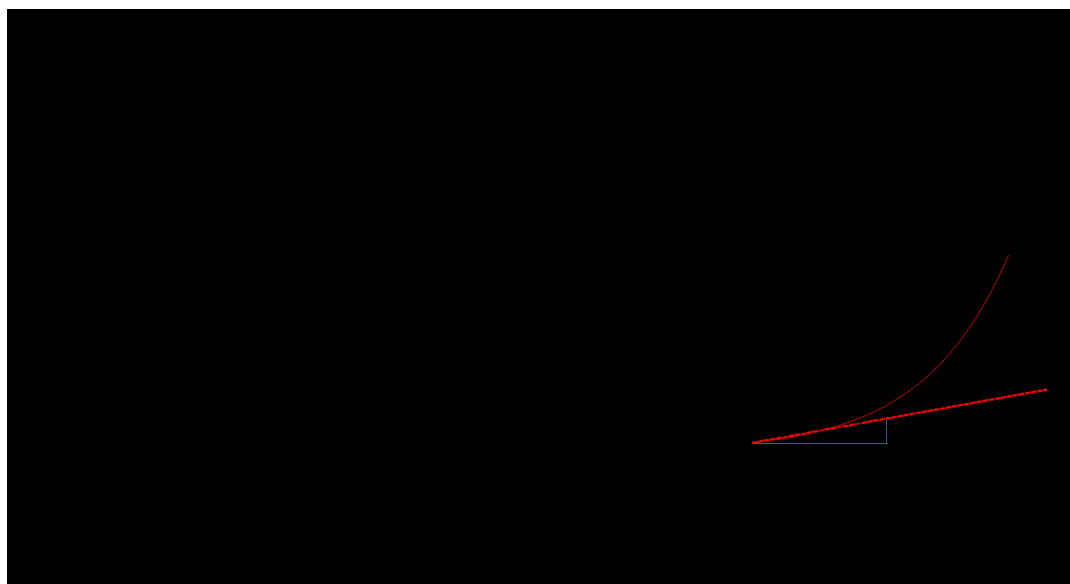
Figure 2.15*. **A)** Schematic diagram of the stress relaxation-recovery protocol applied to each EHT under isometric conditions and in the presence of stimulation at 0.5Hz. **B)** Representative curve of the stress-strain relationship and calculation of Young's modulus as the slope of the linear region of the stress-strain curve.*

The tissue was stretched with strain increments of approximately 3% up to the length at which the maximum contraction force was exerted and stimulated at 0.5Hz and the stiffness was calculated as the slope of the linear region of the stress-strain curve. The bulk stiffness of the EHTs was measured both without cells and in the presence of hiPSC-CMs. The stiffness of the fibrin gel was approximately 0.08KPa, slightly softer than the EHTs with the cells, whose stiffness was ~0.2-0.3KPa in both control lines (**Fig. 2.16B**). The results show that the matrix stiffness of EHTs is softer than that of adult human myocardium (~7-8KPa), as also reported in the literature (Leonard et al. 2018). Also, all EHTs showed a positive Frank-Starling response, with an increase in twitch force when stretched (**Fig. 2.16C**). Of note, length variations imposed to the muscle were in the range of 0-40%: these length steps are unlikely to translate into equal elongations of hiPSC-CMs and consequently sarcomere length. Indeed, direct measurement of sarcomere length variations were not performed.
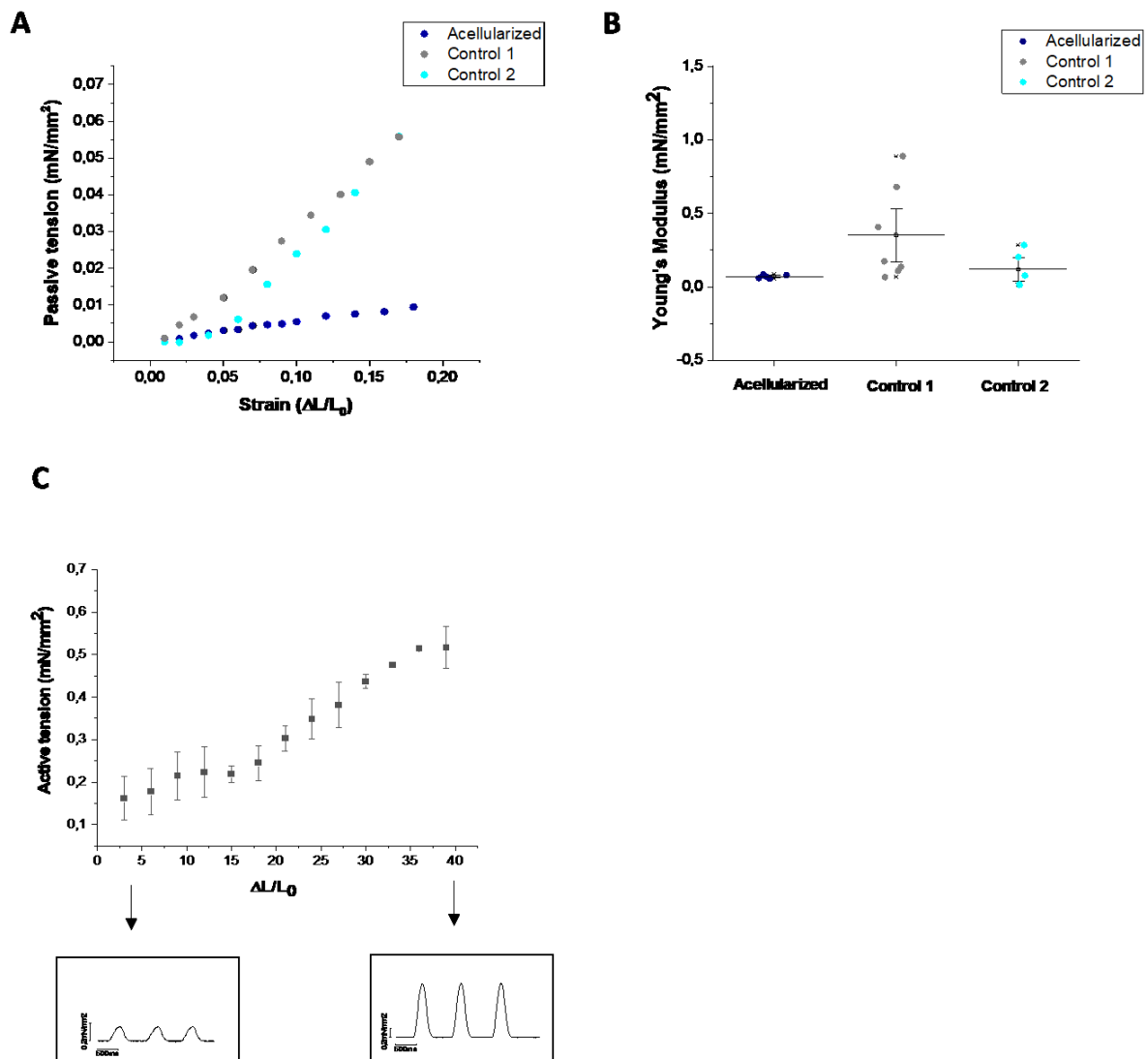
Figure 2.16. A) *Representative graph of passive stress of EHTs stretched up to 20% and **B)** stiffness comparison between control EHTs (Control 1, n=6; Control 2, n= 5) and fibrin gel without cells (n=5). **C)** Frank-Starling curve of EHTs (from 0% to 40% strain) and active tension graphs (0.5Hz pacing) at slack length and Lmax show an increase in isometric twitch force with stepwise increase in EHT length.*

Under the same experimental conditions, the force generated by the EHTs under isometric conditions was analyzed at increasing stimulation frequencies (0.2-2.5Hz), as is done for human trabeculae, and we observed that at the stimulation frequency below 1Hz, the frequency control in all EHTs was incomplete, due to the presence of spontaneous contractions. Unlike healthy human myocardium, in EHTs we observed a less positive FFR and reduced rate adaptation of twitch duration (**Fig. 2.17A**) in comparison with the adult human myocardium (Coppini et al. 2013, 2019; Ferrantini et al. 2017), probably related to an immature SR function (Mannhardt et al. 2016; Shen et al. 2022).
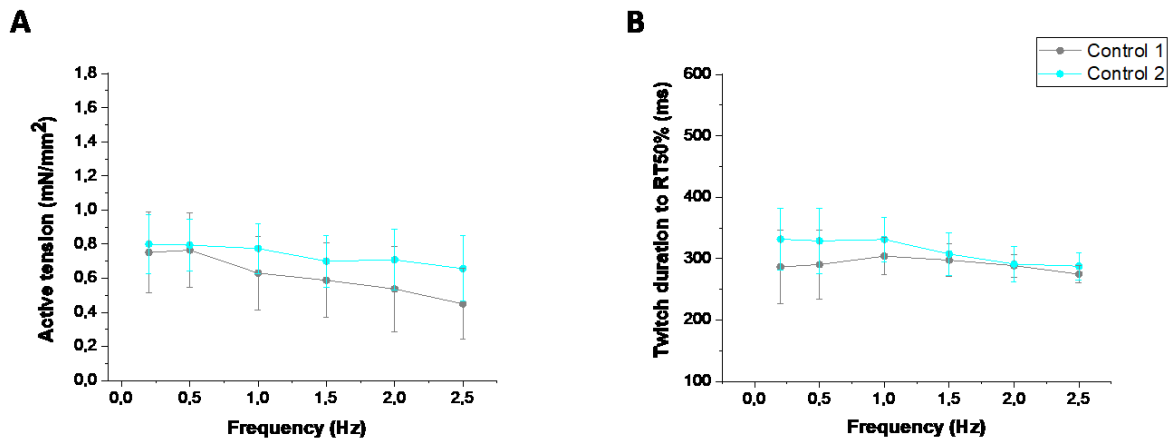
Figure 2.17. A) *Active tension and* **B)** *twitch duration to 50% of relaxation of both control EHTs (Control 1, n=8; Control 2, n=7). EHTs were measured in isometric conditions at 37°C in the Krebs-Henselheit solution with 1.8mM of [Ca²⁺] under imposed pacing.*

By comparison with samples of human fetal ventricles and human adult myocardium, we observed that the tension generated by the control hiPSC-EHTs (~0,5-0,6mN/mm²), under stimulation (0,5Hz) and in the presence of 1.8mM [Ca²⁺], was comparable to the force of the fetal samples (~0,4mN/mm²), but was lower than that generated by the adult myocardium (~5mN/mm²). However, in terms of contraction duration, control EHTs do not differ significantly from fetal ventricles (300-350 ms) **(Fig. 2.18).**
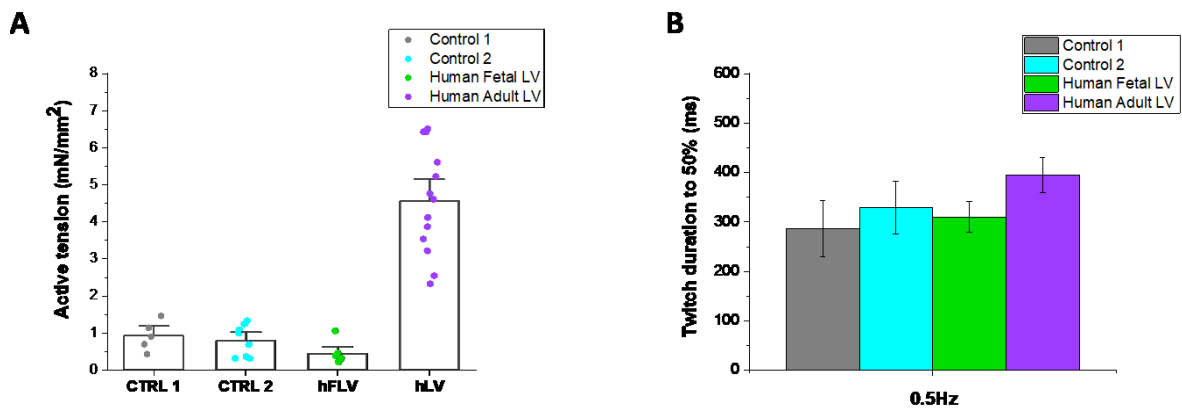
Figure 2.18. A) *Comparison of active tension and* **B)** *twitch duration to 50% of relaxation between control EHT, human fetal left ventricle and human myocardium. (Control 1, n=5; Control 2, n=8; hFLV, n=6; hALV, n=13). EHTs were measured in isometric conditions at 37°C in the Krebs-Henselheit solution with 1.8mM of [Ca²⁺] at 0.5Hz.*

In addition, to investigate the EHT contractile reserve, we analyzed the inotropic response to pacing pauses and high extracellular calcium ([Ca²⁺]$_{out}$ up to 4mM). We observed that all EHTs showed a positive inotropic response by increasing extracellular calcium concentrations from 0.5mM to 4mM. At the maximal calcium concentration (4mM), active tension was found to be increased approximately 2-fold compared with the force recorded at submaximal calcium concentration (0.5mM) **(Fig. 2.19B)**.
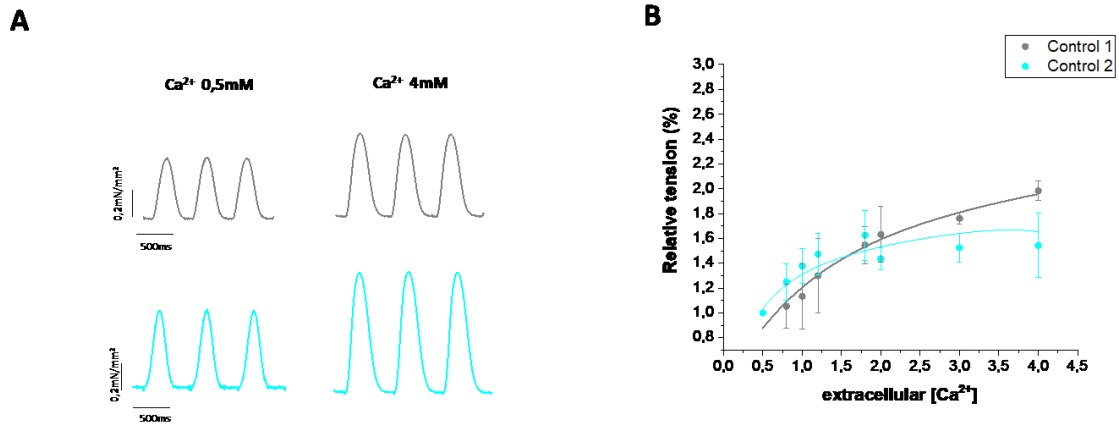
Figure 2.19. A) Representative isometric twitches in the presence of 0.5mM [Ca²⁺] and 4mM [Ca²⁺]. B) Fitting curves of the percentage of variation of EHTs tension amplitude at 1Hz electrical stimulation at increasing calcium concentration (from 0.5mM to 4mM) (Control 1, n=8; Control 2, n=7).

In addition, a post-rest potentiation was assessed by pacing EHTs at 3Hz and after a 2.5s stimulation pause the amplitude of the first peak after resuming stimulation was measured to evaluate the rest-mediated potentiation. The results showed that in both control EHTs, the amplitude after the rest pause exhibits slight potentiation compared with the amplitude before the pause, probably due to incomplete SR development **(Fig. 2.20)**.
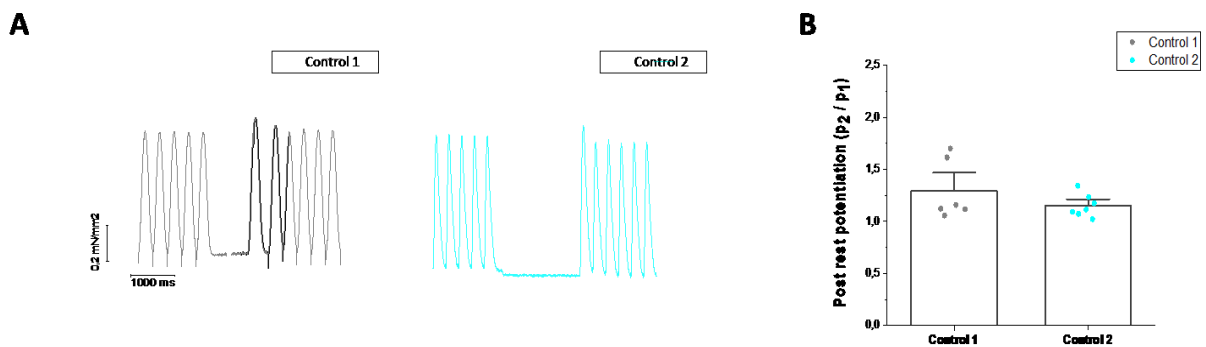
Figure 2.20. A) Representative continuous recording from control hiPSC-EHTs during a post-rest protocol and B) positive inotropic responses to pauses in EHTs from the 2 cell lines. (Control 1, n=8; control 2, n=7). EHTs were measured in isometric conditions at 37°C in the Krebs-Henselheit solution with 1.8mM of [Ca²⁺] under imposed pacing.

Chapter 3

2D-modeling of genetic cardiomyopathies

J. M.l Pioner*, L. Santini, C. Palandri, M. Langione, B. Grandinetti, S. Querceto, D. Martella, C. Mazzantini, B. Scellini, L. Giammarino, F. Lupi, F. Mazzarotto, A. Gowran, D. Rovina, R. Santoro, G. Pompilio, C. Tesi, C. Parmeggiani, M. Regnier, E. Cerbai, D. L. Mack, C. Poggesi, C. Ferrantini and R. Coppini.

ABSTRACT

Cardiomyocytes differentiated from human induced Pluripotent Stem Cells (hiPSC- CMs) are a unique source for modeling inherited cardiomyopathies. In particular, the possibility of observing maturation processes in a simple culture dish opens novel perspectives in the study of early-disease defects caused by genetic mutations before the onset of clinical manifestations. For instance, calcium handling abnormalities are considered as a leading cause of cardiomyocyte dysfunction in several genetic-based dilated cardiomyopathies, including rare types such as Duchenne Muscular Dystrophy (DMD)-associated cardiomyopathy. To better define the maturation of calcium handling we simultaneously measured action potential and calcium transients (Ca-Ts) using fluorescent indicators at specific time points. We combined micropatterned substrates with long-term cultures to improve maturation of hiPSC-CMs (60, 75 or 90 days post-differentiation). Control-(hiPSC)-CMs displayed increased maturation over time (90 vs. 60 days), with longer action potential duration (APD), increased Ca-T amplitude, faster Ca-T rise (time to peak) and Ca-T decay (RT50). The progressively increased contribution of the SR to Ca release (estimated by post-rest potentiation or Caffeine-induced Ca-Ts) appeared as the main determinant of the progressive rise of Ca-T amplitude during maturation. As an example of severe cardiomyopathy with early onset, we compared hiPSC-CMs generated from a DMD patient (DMD-ΔExon50) and a CRISPR-Cas9 genome edited cell line isogenic to the healthy control with deletion of a G base at position 263 of the DMD gene (c.263delG-CMs). In DMD-hiPSC-CMs, changes of Ca-Ts during maturation were less pronounced: indeed, DMD cells at 90 days showed reduced Ca-T amplitude and faster Ca-T rise and RT50, as compared with control hiPSC-CMs. Caffeine-Ca-T was reduced in amplitude and had a slower time course, suggesting lower SR calcium content and NCX function in DMD vs. control cells. Nonetheless, the inotropic and lusitropic responses to forskolin were preserved. CRISPR-induced c.263delG-CM line recapitulated the same developmental calcium handling alterations observed in DMD-CMs. We then tested the effects of micropatterned substrates with higher stiffness. In control hiPSC-CMs, higher stiffness leads to higher amplitude of Ca-T with faster decay kinetics. In hiPSC-CMs lacking full-length dystrophin, however, stiffer substrates did not modify Ca-Ts but only led to higher SR Ca content. These findings highlighted the inability of dystrophin-deficient cardiomyocytes to adjust their calcium homeostasis in response to increases of extracellular matrix stiffness, which suggests a mechanism occurring during the physiological and pathological development (i.e. fibrosis).

INTRODUCTION

Recent evidence suggested that abnormalities of cardiomyocyte maturation and cardiac muscle development contribute to functional and structural cardiac anomalies in genetically-determined cardiomyopathies (Girolami et al. 2022). Cardiomyopathy-related mutations may alter the function of the developing cardiac cells determining pathological changes that may persist in the adult heart (Iacopo Olivotto, Girolami, et al. 2009). The multisystemic and heterogeneous presentation of many types of inherited cardiomyopathies is a challenge for clinicians, and delay in diagnosis is a significant concern (Limongelli et al. 2022). As an example, a number of cardiac abnormalities, including mitral valve leaflet elongation and coronary vessel wall thickening, may be the consequence of developmental abnormalities (Iacopo Olivotto, Cecchi, et al. 2009; Monteiro da Rocha et al. 2016; Krane et al. 2021). However, studying the abnormalities of cardiac development at cell level in transgenic rodent cardiomyopathy models has many limitations and concerns, due to the large differences in cardiac embryonic maturation between mice and humans. Patient-specific induced pluripotent stem-cells differentiated into cardiomyocytes (hiPSC-CMs) are at the frontier for in vitro modeling of genetic cardiac diseases and reproduce several disease-specific pathological changes observed in human hearts (Marchianò et al. 2019). Notably, differentiation from hiPSC and maturation of hiPSC-CMs summarize the changes occurring in the cardiac muscle during the embryonic and fetal period. However, most studies used early stage (30-45 days post-differentiation) hiPSC-CMs and the longer time-point of maturation were not monitored. We previously showed that control hiPSC-CMs grown on surfaces with microgrooved topography for an extended culture time (60-75-90 days) can regularly follow an external pacing frequency and more closely reflect the functional properties of native human cardiomyocytes from healthy hearts (Pioner et al. 2019). The first issue that this work seeks to address are the possible effects of cardiomyopathy-associated mutations on the cardiac differentiation and maturation of hiPSC-CM lines. In particular, calcium handling has a prominent role in cardiomyocyte development. Immature cardiomyocytes lack transverse (T)-tubules and have a poorly organized sarcoplasmic reticulum (SR). For this reason, in the early phases after differentiation, calcium diffusion in the intracellular compartments is slower compared to later-stages of cardiomyocyte development (Lundy et al. 2013). Moreover, calcium fluxes rise before the development of the myofibril contractile apparatus and alterations of calcium handling during the development may strongly influence the mechanical function of mature cardiomyocytes (Josè Manuel Pioner et al. 2020). A second issue that is often overlooked in current hiPSC-CM research are the effects of the different culture substrates on cardiomyocyte structure and function (Querceto et al. 2022). Increased substrate stiffness and anisotropic surface morphology have both shown to be valuable biomimetic tools for advancing the structural and functional maturation of immature cardiomyocytes in culture (Querceto et al. 2022). Specifically, cardiomyocytes increase their contraction force in response to increased stiffness via adaptation of calcium handling and myofibril structural organization (A. J. S. Ribeiro et al. 2015; M. C. Ribeiro et al. 2020; Rodriguez et al. 2011). Morphological anisotropy of culture surfaces leads to a more rapid elongation of cardiomyocytes, improves myofibril alignment and increases sarcomere length (Carson et al. 2016). hiPSC-CMs are immature and beat spontaneously for a long time in culture. In our previous work, we showed that micropatterned surfaces with alternated linear grooves and ridges strongly impacted on

cardiomyocyte regulation of calcium homeostasis and cellular electrophysiology (Pioner et al. 2019). However, effects of substrate stiffness on hiPSC-CM function are rarely assessed. Understanding and translating the impact of substrate features on hiPSC-CM maturation is indeed highly relevant for in vitro cardiomyopathy modeling to avoid under- or over-estimation of mutation-related effects in studies involving patient-specific hiPSC-CMs. Additionally, changes of extracellular stiffness may occur in cardiomyopathies (e.g. due to accumulation of myocardial fibrosis) and severely affect cardiomyocyte function. To highlight the possible implications of developmental anomalies and substrate changes for cardiomyopathy studies with hiPSC-CMs, we compared cardiomyocytes from a Duchenne Muscular Dystrophy (DMD) patient carrying a deletion of exon 50 in the DMD gene (Guan et al. 2014) with control cell lines and with an isogenic control created by CRISPR-Cas9 targeting the DMD gene (c.263delG) (J. Manuel Pioner et al. 2020). DMD-CMs were chosen over other cardiomyopathy models because the lack of full-length dystrophin in diseased cardiomyocytes may directly affect the interaction of cardiac cells with the extracellular environment (Pioner et al. 2020). Therefore, the final aim of the study is to assess: (i) the effects of the lack of dystrophin on the maturation of intracellular Ca^{2+} handling during development and (ii) the effects of substrate stiffness on the function of hiPSC-CMs with and without dystrophin, by growing cells on micropatterned surfaces with different mechanical properties.

RESULTS

3.1. Analysis of Ca^{2+}-transient amplitude during cardiomyocyte maturation

Single control- and DMD-(hiPSC)-CMs were dissociated from beating monolayers after differentiation (day 15) and plated onto custom-made photopolymerized polyethylene glycol-diacrylate (PEG-DA 100%) surfaces with a micro-structured topography. The geometry of this biomimetic substrate featured an array of parallel micro-grooves with 0.6 μm width, 1.5 μm depth and 1.4 μm distance between lines (Pioner et al. 2019). To verify differences in the maturation of calcium handling, we compared control and DMD-CMs at different stages of cardiac differentiation (at day 60, 75 and day 90 from the beginning of cardiac differentiation, (**Fig. 3.1A**). In control iPSC-CMs, calcium transient (Ca-T) amplitude increased significantly during maturation from d60 to d90 (**Fig. 3.1B**). In DMD-CMs vs. controls, however, Ca-T amplitude was smaller at d60 and failed to increase at d90. We then used a post-rest potentiation protocol to assess calcium storage in the sarcoplasmic reticulum (SR) of iPSC-CMs, as previously described (J. Manuel Pioner et al. 2020). Rest periods of 10 s were introduced during 2 Hz stimulation and the amplitude of the post-rest potentiated contraction was plotted against that of the last regular contraction during regular pacing (**Fig. 3.1C**). In control cells, post-rest potentiation was larger at d90 vs. d60, indicating an increase of SR Ca storage. In contrast, the potentiation of Ca-T in DMD-CMs was lower compared to control-CMs and did not significantly change from d60 to d90 (**Fig. 3.1D**). Similarly, these results were recapitulated in age-matched CRISPR-Cas9 edited control cardiomyocytes lacking full-length dystrophin (c.263delG-CMs).
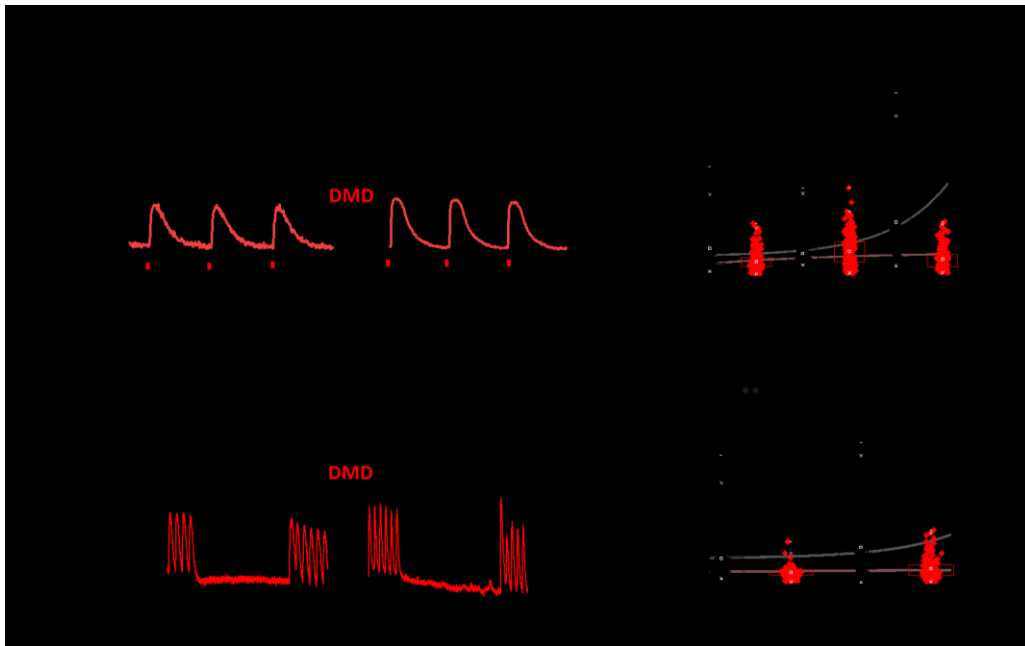
Figure 3.1. *Changes of calcium transient amplitude during hiPSC-CM maturation. Calcium transients were estimated at day 60, 75 and 90 post differentiation at 37°C, 1.8 mM [Ca²⁺]. **A)** Representative CaT profiles at day 60 and 90 and average CaT amplitude (Fluorescence Arbitrary Units, A.U.) of DMD- versus control-CMs at day 60,75 and 90. **B)** Sarcoplasmic reticulum (SR) contribution in calcium handling maturation was tested by a post rest potentiation protocol at multiple maturation time-points. **C)** The post-rest potentiation of CaT amplitude was estimated after a resting pause of 5 s, inserted in a regular train of stimulation at 2 Hz. **D)** The potentiation is expressed as the % of increase of the first post-rest CaT with respect to the CaT pacing train before the pause (%). Post rest potentiation of DMD- versus control-CMs is estimated at day 60 and day 90. Exponential curves with Stirling's approximation were used to show the variation of maturation in both groups. Control d60 N=3, n=336; d75 N=5, n=251; d90 N=3 n=165; DMD d60 N=3, n=193, d75 N=4, n=292; d90 N=4, n=169. One-way analysis of variance (ANOVA) with a Tukey post-hoc test with statistical significance set at †† p <0.01 versus time point; * p < 0.05 and ** p 0.01 versus control-CMs.*

3.2 Changes of action potential and calcium transient kinetics during cardiomyocyte maturation

In addition to amplitude, the kinetics of Ca-T under the influence of the kinetics of action potentials (APs) can greatly influence cardiomyocyte contractile properties. Therefore, we then analyzed the kinetics of both phenomena. APs were measured by acquiring the FluoVolt voltage-sensitive dye fluorescence together with Ca-T (Cal630 fluorescence), during regular pacing with field-stimulation at 1Hz (**Fig. 3.2**). Representative traces simultaneously recorded at day 75 and 90 post cardiac induction are reported in **Fig. 3.2A**. In both control and DMD -CMs, AP duration (APD) increased during maturation (**Fig. 3.2B**). At day 75, APD in DMD -CMs was shorter as compared with controls. At d90, however, no differences in APD50 were observed in DMD vs. control cells. Interestingly, in both control and DMD cells, APD did not show a significant rate adaptation at day 75 (APD50 at 1 and 2 Hz were comparable) but the shortening of APD with increased pacing rate (1 vs 2 Hz) was observed at d90 (**Fig. 3.3**). Ca-T kinetics was also measured at each time point of maturation (**Fig. 3.2C-D**). In control of hiPSC-CMs, the kinetics of Ca-Ts accelerated from d60 to d90. Similarly, in DMD-CMs, the kinetics of calcium rise (time to peak, TTP) and decay (time from peak to 50% of CaT decay, RT50)

became more rapid after 90 days in culture (**Fig. 3.5D**). However, the kinetics of Ca-Ts were consistently faster in DMD vs. controls myocytes (**Fig. 3.2D**).
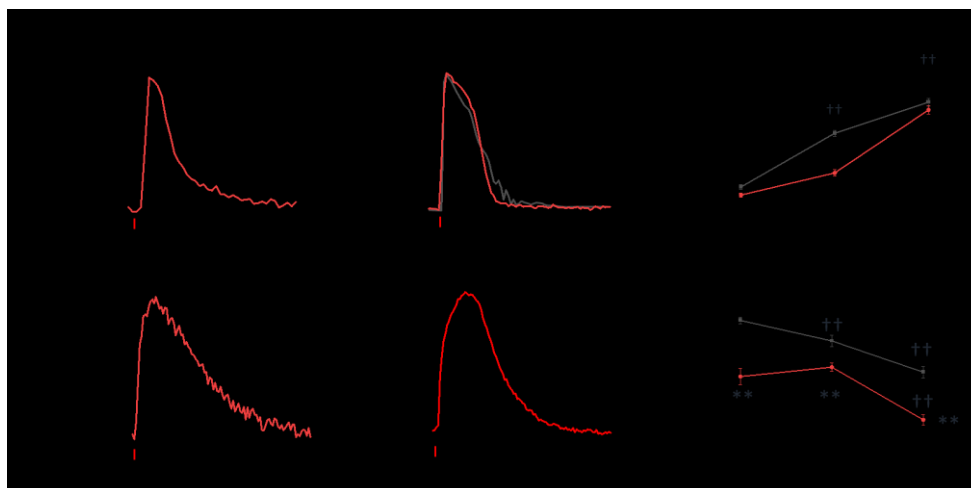
Figure 3.2. *Changes of action potential and calcium transient kinetics during hiPSC-Cm maturation. Dual recording of action potential and calcium transients was performed at day 60, 75 and 90 post differentiation at 37°C at an external [Ca²⁺] = 1.8 mM on the softer substrate (PEG).* ***A)*** *Superimposed action potential (AP) traces of day 75 (Control d75 N = 2; n = 186; DMD d75 N = 2; n = 91) vs day 90 (Control N = 2; n = 119; DMD: d90 N = 2; n = 44) recorded by FluoVolt* ***(B)*** *50% of action potential durations (APD50, ms) at 1 Hz are reported as Mean ± SEM.* ***C)*** *Superimposed traces of calcium transients recorded by Cal630 at day 60, 75 and 90* ***(D)*** *average calcium transient (CaT) (difference of 50% of CaT decay and TTP, RT50, ms) are reported, during pacing at 1 Hz. Control d60 N = 3, n = 336; d75 N = 5, n = 251; d90 N = 3, n = 165; DMD d60 N = 3, n =193, d75 N = 4, n = 292; d90 N = 4, n = 169. Supporting information given in Table S2. One-way analysis of variance (ANOVA) with a Tukey post-hoc test with statistical significance set at ††p < 0.01 versus time point; *p < 0.05 and **p 0.01 versus control-CMs.*

Figure 3.3. *Rate adaptation of action potential duration in late-stage hiPSC-CMs. Superimposed action potential (AP) profile of hiPSC-CMs was recorded both at 1 and 2 Hz to evaluate action potential duration (APD50, ms) and the response to frequency changes at both day 75 (Control N=2, n=186; DMD N=2; n=91) and 90 (Control N=2, n=119; DMD N=2; n=44). Data were represented as box plots. † p < 0.05, †† p < 0.01 or NS for not significant versus 1Hz.*

3.3 Preserved response to forskolin in DMD-CMs

To investigate the response to the β-adrenergic pathway activation, hiPSC-CMs were acutely exposed to forskolin (FSK), a phosphodiesterase inhibitor, to increase cAMP levels and activate PKA. **Fig. 3.4A-B** shows representative traces of Ca-Ts at baseline and with FSK, recorded in control and DMD-CMs respectively. In both DMD- and control-CMs, CaT amplitude increased by around 30% following FSK incubation compared to the basal condition (**Fig. 3.4C-D**), suggesting preserved positive inotropic responses to catecholaminergic stimuli in DMD-CMs. In addition, the acceleration of RT50 with forskolin in both cell lines suggested a positive lusitropic response to beta-adrenergic stimulation.
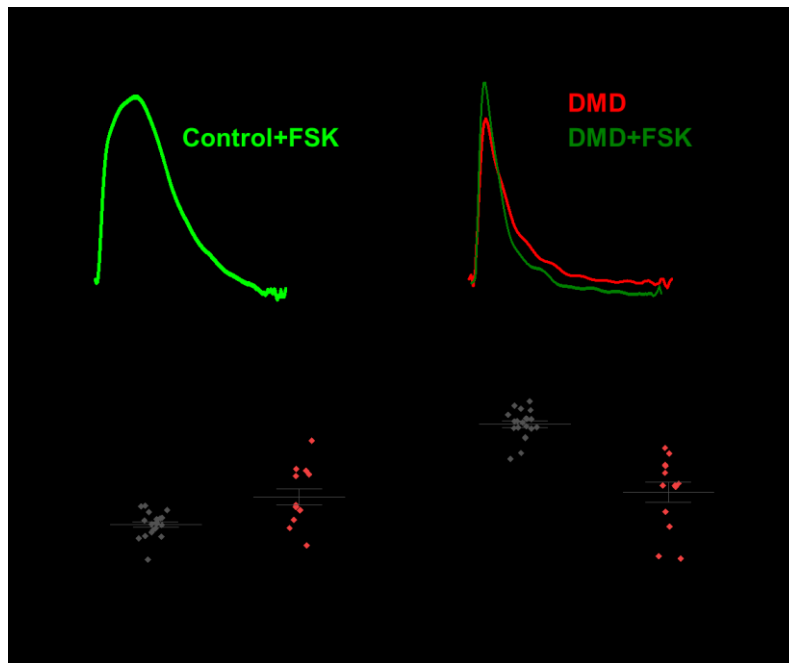
Figure 3.4. Effects of forskolin on calcium transients. Calcium transients of the before and after forskolin addition in day 60 control- and DMD-hiPSC-CMs. **(A, B)** Superimposed normalized traces of calcium transients recorded in the control hiPSC-CMs line, before and after treatment with forskolin (FSK, light green controls, dark green DMD), reported as the variation (%) compared with the basal condition. **C)** Calcium transient amplitude is reported, during pacing at 1 Hz, as the % variation related to the basal condition compared to the treatment with FSK in DMD. **D)** CaT decay (difference of 50% of CaT decay and TTP, RT50, ms) is reported, during pacing at 1 Hz, as the % variation related to the basal condition compared to the treatment with FSK in controls and DMD.

3.4 CaMKII and and RyR2 phosphorylation

At later-stages (d90), DMD-CMs have a higher level of phosphorylated CaMKII compared to controls, indicating increased CaMKII activity (**Fig. 3.5A-B**). We assessed the relative abundance of two phosphorylations (p-) sites of the ryanodine receptors (RyR2) using antibodies against p-RyR S2814 and p-RyR S2808, which are targets of CaMKII and PKA, respectively (**Fig. 3.5C-D**). CaMKII-specific phosphorylation at site S2814 was increased in DMD-CMs compared to controls ($p < 0.01$). Contrarily, RyR2 phosphorylation at the PKA site (S2808) was not affected. Increased phosphorylated RyR2 is associated with increased diastolic open probability, often associated with SR calcium leakage. This finding may partially account for reduced Ca-T amplitude of DMD-CMs.
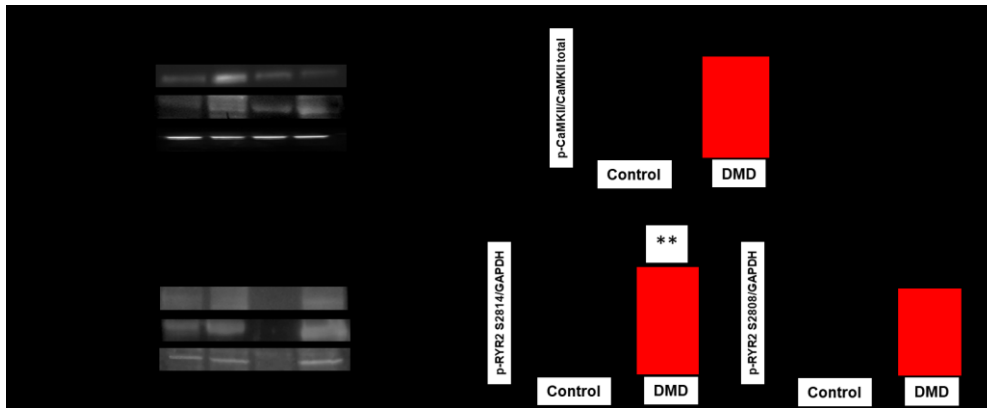
*Figure 3.5. Phosphorylation of RyR2 and CaMKIIδ in hiPSC-CMs. Western blot (WBs) analysis of Ryanodine receptors (RyR2) phosphorylation status and verification of CaMKII activity in day 90 DMD-vs Control-hiPSC monolayers. **A)** Representative WB of CaMKIIδ **(B)** and analysis normalized for total CaMKII. **C)** Representative WB analysis of **(D)** RyR2 sites of phosphorylation (phospho-specific anti Ser 2814 target of CaMKII and Ser 2808 target of PKA) normalized for GAPDH, *p < 0.05 in ANOVA DMD vs Controls N = 3 (differentiation runs) and n = 2–5 (gel repetitions).*

3.5 Stiffer substrates increase calcium transient amplitude in control hiPSC-CMs

We tested a palette of micropatterned substrates with increasing stiffness to assess the impact of substrate stiffness on calcium handling in hiPSC-CM (**Fig. 3.6A**). Mixing PEG with adjustments of the crosslinker diethylene glycol-diacrylate (DEG-DA) concentration (PEG:DEG %: 75:25, 50:50, 25:75 and DEG 100%) resulted in increased substrate stiffness (**Fig. 3.6B-C**). Control hiPSC-CMs (day 60 post-differentiation) showed a gradual increase of Ca-T amplitude with the increase of the substrate stiffness (**Fig. 3.6D-E**, **Fig. 3.7A-B**), obtained by increasing the percentage of DEG-DA in the monomer mixture. The maximal amplitude was obtained using polyurethane (PUA)-based rigid substrates (**Fig. 3.6E**). Moreover, the time to peak (TTP, ms) and the time to the 50% of CaT decay (RT50, ms) were faster in control cells grown on stiffer substrates (DEG 100%) as compared with those grown on softer patterns (PEG 100%, see **Fig. 3.7C-D**). We then tested the effects of substrate stiffness on cell contractility. In line with the effects on Ca-T amplitude, control hiPSC-CMs displayed higher % cell shortening on stiffer PEG substrates, compared to cells grown on DEG patterns. In further analysis, a pacing train protocol of 2Hz followed by a rest pause of 10 seconds was applied to evaluate the post rest potentiation of cell shortening. The amplitude of post-rest potentiated beats was higher in cells grown on stiffer substrates, but the relative increase was similar when compared with cells grown on soft surfaces, suggesting a similar inotropic reserve.

Figure 3.6. Ca-transients in DMD-hiPSC-CMs grown on PEG vs DEG patterned substrates. **A)** Time course of media (mT mTeSR + suppl.; A + B + C cardiac differentiation kit) and substrates (TC tissue plate;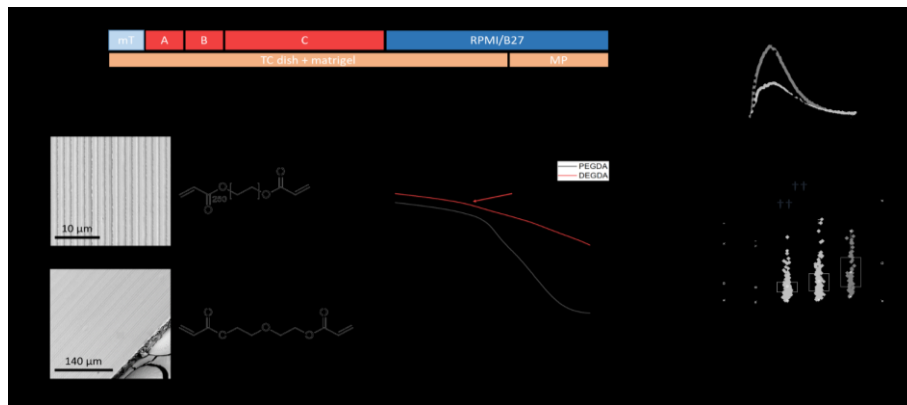 MP micropatterned substrates). **B)** S.E.M. image of Poly (ethylene glycol) diacrylate (PEG-DA)- and Di(ethylene glycol) diacrylate (DEG-DA)-based substrates with micropatterned grooves. Scale bars 10 μm. **C)** Samples of PEGDA and DEGDA for dynamical mechanical analysis (DMA) with 1% wt. The samples were clamped in tension mode in a DMA800 analyzer (Perkin Elmer). Samples were analyzed in strain-control mode, imposing a 0.020 mm strain with 1 Hz frequency, in the -20°C-120°C temperature range. The mechanical characterization was repeated three times for PEGDA100 and DEGDA100 samples. The value of the storage modulus at E' was obtained by calculating the integral mean of the E'-T curve between 36°C and 38°C. Values are expressed as mean ± SEM. **D)** The impact of substrate stiffness in normal control-CMs was tested for CaT amplitude on microgrooved surfaces with increasing ratio of polyethyleneglycole (PEG) and dyethylenglycole (DEG) concentration and polyurethane-based nanopatterned surfaces (PUA) at 37 °C at and external $[Ca^{2+}]$ = 1.8 mM. Representative CaT profiles at day 60 and of CaT amplitude (Fluorescence Arbitrary Units, A.U.) of control-CMs under PEG (N = 3; n = 336), PEG:DEG 75:25 (N = 2; n = 150), 50:50 (N = 2; n = 147), 25:75 (N = 2; n = 150), DEG (N = 2; n = 50) and PUA (N = 2; n = 59). (E) Data were represented as a box (median [interquartile range]) and whisker plots. †p < 0.05, ††p < 0.01 versus control condition (PEG).
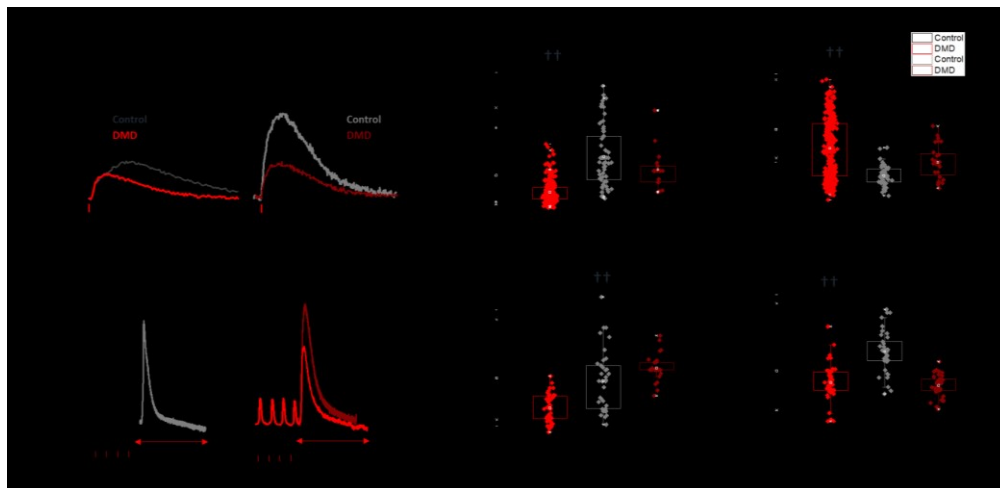
Figure 3.7. Impact of substrate stiffness on calcium transient amplitude and duration. To evaluate the impact of substrate stiffness on loss of full-length dystrophin, DMD- and control-CMs were compared for CaT amplitude and caffeine-evoked CaT on softer (PEG)- versus stiffer (DEG)-microgrooved surfaces (MPs) at 37°C at and external $[Ca^{2+}]$ = 1.8 mM. **A)** Representative CaT profiles at day 60 and of CaT amplitude (Fluorescence Arbitrary Units, A.U.) and RT50 of CaT decay (ms) of DMD-versus control-CMs under softer or stiffer MPs. **B)** Data are reported in box plots report control-versus DMD-CaT amplitude and RT50 (ms) on both softer or stiffer substrates (PEG: Control N = 3, n = 336; DMD N = 5, n = 251; DEG: Control N = 2, n = 50; DMD N = 3, n = 67). **C)** Caffeine-induced CaTs (quick exposure to 10 mM Caffeine) after a series of 2 Hz paced CaTs. (D) Average of caffeine-induced CaT amplitude (Fluorescence Arbitrary Units, A.U.) was measured by localized caffeine exposure after steady-state calcium transients at 2 Hz prior. Caffeine transient CaT amplitude (CaTA CAFF/CaTA 2 Hz ratio) and decay (τ, s^{-1}) of DMD- and control-hiPSC-CMs were compared on both PEG (softer) and DEG (stiffer) substrates. (PEG: Control N = 2, n = 83; DMD N = 2, n = 46; DEG: Control N = 2, n = 23; DMD N = 2, n = 21). Data were represented as a box (median [interquartile range]) and whisker plots. One-way analysis of variance (ANOVA) with a Tukey post-hoc test with statistical significance set at *p <0.05 and **p <0.01 versus control and ††p <0.01 versus internal substrate condition.

3.6 Stiffer substrates do not enhance calcium release in DMD hiPSC-CMs, despite a higher SR Ca²⁺ content.

Figure 3.7 reports the impact of stiffer substrates on age-matched control and DMD hiPSC-CMs. DMD-(hiPSC)-CMs grown on 100% DEG patterns displayed increased Ca-T amplitude when compared with the softer substrate (PEG 100%), (**Fig. 3.5A-B**). However, compared to controls, DMD-hiPSC-CMs had reduced Ca-T amplitude on both soft and stiff substrates. Moreover, in control cells the kinetics of Ca-T decay accelerated significantly in cells grown on 100% DEG substrates as compared with those grown on softer substrates (**Fig. 3.7A-B**). Contrarily, in DMD-CMs the kinetics of Ca-Ts did not change substantially on stiffer vs. softer substrates (**Fig. 3.7A-B**). To gain insights into the role of SR calcium content, we analyzed caffeine-evoked Ca-Ts (**Fig. 3.7C-D**). In control-CMs, caffeine Ca-T amplitude was similar between the softer and stiffer substrate (**Fig. 3.7D**). Additionally, caffeine Ca-T decay kinetics (tau, s⁻¹) became faster in control-CMs grown on the stiffer substrate, suggesting increased capability of intracellular calcium removal by the sodium calcium exchanger (NCX). Conversely, in DMD-CMs caffeine-induced calcium transient amplitude on DEG surfaces was markedly increased when compared to the softer PEG substrates. Indeed, the amplitude of caffeine-induced Ca-Ts from DMD-CMs grown on stiffer substrates became like controls (**Fig. 3.7D**). The decay kinetics (tau, s⁻¹) of Caffeine-induced Ca-Ts was slower compared to controls, regardless of the substrate stiffness. Taken together, these results may indicate a reduced capability of intracellular calcium extrusion in DMD-CMs (**Fig. 3.5D**) and increased diastolic Ca²⁺ levels.

DISCUSSION

In striated muscle the full-length dystrophin (Dp427) network covers almost the entire cytoplasmic surface of the plasma membrane. Within the cytoskeletal lattice complex termed costameres, dystrophin serves as a shock absorber, promoting membrane stability and transduction of mechanical force from the extracellular matrix during muscle contraction or stretch (Rahimov and Kunkel 2013). Calcium handling abnormalities have been described as a major consequence of dystrophin and other dilated cardiomyopathy (DCM)-related mutations, but the mechanisms linking dystrophin deficiency to abnormal calcium cycling remain unclear (Pioner et al. 2020). For Duchenne Muscular Dystrophy (DMD), the two main hypotheses related to calcium handling abnormalities are membrane fragility/damage (Carson et al. 2016), as reported in the human DMD-hiPSC-cardiomyocyte (Guan et al. 2014) (J. Macadangdang et al. 2015) and mdx mouse (Fanchaouy et al. 2009) model, or altered ion channel function with dysregulation of calcium homeostasis as a direct consequence of the altered dystrophin glycogen complex (DGC) (Zhan et al. 2014). In this work, we have studied the Ca-Ts and APs recorded from DMD hiPSC-CMs obtained from a patient with DMD-related cardiomyopathy, carrying a deletion of exon 50 (Δ exon 50) in DMD gene (Pioner et al. 2020). We compared these with the results obtained in control cell lines and a positive isogenic control created by CRISPR-Cas9 targeting the DMD gene (c.263delG), as previously described (Querceto et al. 2022). Previous reports using these DMD hiPSC-CM lines exhibited membrane fragility (Guan et al. 2014) and diminished

structural/functional response to an underlying substrate with nanotopographic grooves compared to normal cardiomyocytes that was associated to a lower level of actin cytoskeleton turnover (Macadangdang et al. 2015). Moreover, we recently reported that absence of full-length dystrophin is sufficient to slow Ca-T kinetics, causing an overall impairment of contractility in single hiPSC-CM (Pioner et al. 2019) (Bremner et al. 2022). This work showed that highly matured DMD-hiPSC-CMs are capable to display mechanisms of contractile dysfunction that are independent of systemic alterations occurring in vivo. A major impact was attributed to cell growth on nanopatterned substrates compared to the commonly used flat glass coverslips. However, these findings suggested either retarded or altered maturation of cardiomyocyte structures associated with these functions. In this work, Ca-Ts were recorded from hiPSC-cardiomyocytes at specific time points of maturation (60, 75, 90 days from cardiac induction) on custom-made soft PEG- based micropatterned surfaces. We performed simultaneous recordings of APs and Ca-Ts with fluorescent indicators at the single cell level, to assess the key regulatory mechanisms of cardiac contraction of mature DMD-hiPSC-CMs (Pioner et al. 2019). At any time point of maturation, DMD-hiPSC-CMs on PEG- substrates showed lower Ca-T amplitude as compared with controls. This is consistent with the reduced post rest potentiation of Ca-Ts, which suggested a reduced amount of calcium stored in the sarcoplasmic reticulum (SR) during the resting pause. This observation is also confirmed by the caffeine-evoked Ca-Ts, which demonstrated a strong reduction of SR-calcium content in DMD-hiPSC-CMs with respect to controls. In agreement, increased CaMKII activity and phosphorylation of RyR2 S2814 may be related to higher RyR open probability and to SR calcium leakage (Meyer et al. 2021) in DMD-hiPSC-CMs. Calcium leakage from the SR during diastole can partially account for the reduced Ca-T amplitude of DMD-hiPSC-CMs, as previously observed in the mdx mouse model (Ather et al. 2013; Ullrich et al. 2009; S. Kyrychenko et al. 2013). Previous studies have shown that the SR Ca^{2+} release mechanism through RyR is impaired in both cardiac and skeletal muscles in DMD (Fauconnier et al. 2010; Bellinger et al. 2009). In cardiac muscle, other studies showed that genetic inhibition of RyR2 phosphorylation at S2808 or S2814 can reduce RyR2 oxidation, suggesting a potential interaction between these post translational pathways (Kyrychenko et al. 2013) (Q. Wang et al. 2015). In addition, other authors identified S-nitrosylation and calstabin 2 as a cause of RyR2 Ca^{2+} leakage leading to sudden cardiac arrhythmias in mdx mice (Fauconnier et al. 2010). In addition, we tested the function of the β-adrenergic pathway in DMD-hiPSC-CMs. Previous observations of the expression profile of β-adrenergic receptors (AR) in hiPSC-CM displayed a time-dependent increase of β2 and particularly β1 ARs (G. Jung et al. 2016). To avoid discrepancy related to different AR expression or reduced level of cAMP due high activity of phosphodiesterases (PDEs) (Giannetti et al. 2021), we used forskolin (FSK, an activator of adenylyl cyclase) to test the activation of the downstream pathway. In the presence of forskolin, Ca-Ts doubled in amplitude in both control and DMD, suggesting preserved positive inotropic responses. This is in keeping with the similar acceleration of Ca-T kinetics in DMD and CTR cells under FSK. Preserved phosphorylated RyR-S2808 level confirmed no alterations of the PKA phosphorylation target. With simultaneous recording of voltage-sensitive and calcium fluorescent dyes, we observed that APs had a similar profile in control- and DMD-hiPSC-CMs and showed a longer plateau phase at later stages of maturation with respect to earlier stages. These results are in line with previous observations (Jelinkova et al. 2020) but do not exclude the presence of minor electrophysiological abnormalities in DMD-hiPSC-CMs, as previously reported (Eisen et al. 2019). On the other hand, Ca-T decay, which reflects the mechanisms of calcium recovery after contraction, was overall significantly faster in DMD

vs. control and became even faster at longer times in culture. While control cells display a gradual increase of Ca-T amplitude with advanced maturation, DMD-hiPSC-CMs do not show any significant enhancement of Ca release at later stages of maturation, suggesting a specific impairment of systolic Ca release. Interestingly, our data support the idea that a lesser maturation or impairment of the SR apparatus, preventing any increase of SR Ca storage with maturation, is responsible for the lack of Ca-T increase with increasing time in culture. Finally, we observed that cardiomyocytes obtained from the CRISPR-Cas9 gene-edited cell line (c.263delG) recapitulated the features of calcium handling observed in the patient-specific cell line (Δ exon 50), as we previously observed (Pioner et al. 2019; Macadangdang et al. 2015). These findings support the idea that smaller Ca-Ts are a stable alteration affecting developing cardiomyocytes lacking full-length dystrophin and this is associated with the reduced force generation reported in other DMD cell lines (Chang et al. 2021). However, shorter calcium transient duration was not expected, according to our previous finding on single cells (Pioner et al. 2019) and other findings obtained in 3D tissues (A. Moretti et al. 2020; V. Kyrychenko et al. 2017)reporting slower calcium transients. However, most of the previous results were obtained with stiff substrates or matrixes (glass or polyurethane-based coverslides), which may change the kinetics of Ca-Ts, as we have clearly observed. Indeed, we tested a palette of substrate materials with increasing stiffness obtained by changing the percentage of polyethylene glycol, (PEG-DA) and diethylene glycol, (DEG-DA). Increasing the amount of DEG led to stiffer substrates, the maximal stiffness was obtained with 100% DEG-DA. In the control cell lines, we observed a clear increase of basal and post rest Ca-T amplitude with the increase of substrate stiffness. In DMD-hiPSC-CMs, however, we observed a much smaller increase of Ca-Ts when cells were grown on DEG substrates. Moreover, on stiffer substrates, Ca-T decay became slower in DMD-hiPSC-CMs compared to control cells grown in the same conditions. In addition, slower caffeine-induced CaT decay suggested that DMD-hiPSC-CMs have reduced ability to extrude calcium suggesting reduced NCX function in DMD-CMs. Together with increased RyR open probability (due to CaMKII phosphorylation), this may increase diastolic Ca^{2+} levels and expose cardiomyocytes to a higher risk of cellular arrhythmias. All together, these results emphasize the idea that calcium transient dysregulation is a major disease mechanism in developing DMD cardiomyocytes. In addition, the reduced ability to extrude intracellular calcium is a possible additional defect reducing the adaptation of DMD-hiPSC-CMs to changes of the substrate stiffness. The mechanical stiffness of the surrounding extracellular matrix (ECM) critically determines normal cell function, stem cell differentiation and tissue homeostasis (Engler et al. 2006). Among these, cardiomyocytes actively probe the rigidity of their extracellular environment by exerting traction forces via transmembrane proteins named integrins (Santoro et al. 2019). However, it is still poorly understood how cardiac cells sense matrix stiffness and how they transduce the mechanical information into specific cellular responses or functional phenotypes (Querceto et al. 2022). Key proteins in this scenario may include dystrophin and the glycoproteic complex (DGC). In dystrophin-associated cardiomyopathies, i.e. Duchenne (DMD) and Becker (BMD) Muscular Dystrophies, caused by the absence or the decreased expression of full-length dystrophin, respectively, the sarcolemma becomes fragile and susceptible to damage. For instance, the lack of dystrophin leads to reduced expression of its binding partner dystroglycan, a key link to laminin. Glycosylation of alpha-dystroglycan is necessary for its binding to laminin (Fallon and McNally 2018). For instance, when the external load varies due to an increase of the extracellular matrix stiffness from

pathological remodeling (e.g. myocardial fibrosis), DMD cells would be less capable of adapting force production to the new environmental features, amplifying their contractile impairment.

Study limitations

In this work, we explored another important feature of hiPSC-CMs, related to the ability of these cells to adapt their function in response to an external cue. These findings highlight that the maturation of cardiomyocytes is strongly influenced by the extracellular microenvironment. Using a time point analysis with different substrate conditions, we identified an important feature of dystrophic cardiomyocytes: e.g. reduced ability to adapt the regulation of calcium handling upon variation of the extracellular matrix load. The underlying substrates can mimic some aspects of cardiac extracellular matrix (cECM), e.g. anisotropy and stiffness. Substrates with low (e.g. PDMS, Matrigel, hydrogels) and high (e.g. glass, polyurethane) stiffness can provide different levels of external load, influencing the force of contraction and protein expression (Querceto et al. 2022). The current work used different substrates that are far from recapitulating the physiological range of extracellular tissue stiffness. For this reason, culture conditions mimicking the physiological stiffness of the cECM are needed to verify the role of cell/cECM. For instance, substrates with 10 vs 35kPa purposed the idea that tissue stiffness may trigger mechanisms related to contractile dysfunction, oxidative stress and telomere shortening in DMD-hiPSC-CMs (including the c.263delG DMD line) (Chang et al. 2021). More physiological conditions should be applied to verify the impact of cardiac cell/extracellular matrix interaction (Querceto et al. 2022; Bremner et al. 2022). However, for 2D cell cultures, stiffer substrates are important to stress additional pathological mechanisms (J. R. Macadangdang et al., n.d.). This is important to discern maturational alterations from maladaptive mechanisms. In addition, this work has evaluated only one of the CaMKII pathway targets (RyR phosphorylation site S2814) but future studies must consider a broader range of E-C coupling proteins. This can be feasible with novel Multi-omics analysis (e.g. transcriptomic, proteomic and/or metabolomic analysis). This work was limited to a previously characterized cell line to study the calcium transient alterations in DMD-null cardiomyocytes (Guan et al. 2014; Pioner et al. 2019; Macadangdang et al. 2015; J. R. Macadangdang et al. 2018) and comparison was made with an unrelated healthy control cell line (Guan et al. 2014; Pioner et al. 2019; Macadangdang et al. 2015) and its isogenic CRISPR-Cas9 edited cell line (c.263delG) (Pioner et al. 2019). Isogenic CRISPR-Cas9 edited cell lines, either induced (DMD-null) in controls or corrected in patient cell lines (Y. Zhang et al. 2022), are the most rigorous model to verify the phenotype caused by gene mutations. Future studies aimed to verify the impact of novel therapies should include multiple isogenic pairs to exclude bias due to interpersonal variability.

Conclusions

Better understanding of the impact of maturation strategies, such as long-term cultures and variation of substrate stiffness on hiPSC-CM function will provide new insights to create microenvironments that may more closely recapitulate the ECM alterations occurring in several pathologies, including DMD. The mechanical properties of ECM induce an adaptive response within the cytoplasm and the nucleus, leading to changes in cell fate specification and function (Nakayama, Hou, and Huang 2014). Downregulation or total absence of proteins involved in the costamere domains cause dramatic

defects in the mechanosensing and mechanotransduction in muscular dystrophies and cardiomyopathies (Querceto et al. 2022)(James M. Ervasti 2003). In this context, hiPSC-CMs obtained from patients are the most suitable platform for the investigation of cell/ECM interaction. To this aim, the possibility of targeting genes of interest by CRISPR-Cas9 gene editing technology allows the validation of the pathogenicity of any cardiomyopathy-associated variant (Pioner et al. 2020) (Bhagwan et al. 2020). Moreover, it may contribute to elucidate the role of specific proteins with debated function and involved in physiological responses during cECM stiffening. In this context, full-length dystrophin plays a crucial role to transmit mechanical signaling throughout extracellular and intracellular compartments. For this reason, the loss of full-length dystrophin and DGC (Duelen et al. 2022) in DMD-hiPSC-CMs can serve as a model to investigate the signaling between the extra- and intracellular cardiac space. The consequences of full-length dystrophin deficiency appear in the very early phases of cardiac cell/tissue development, likely even before cardiac formation (Jelinkova et al. 2019). Ventricular tachyarrhythmias in patients with DMD can be caused by a combination of mechanisms, including conduction abnormalities, fibrosis and fatty replacement of the myocardium (Pioner et al. 2020) (Frankel and Rosser 1976; Fayssoil, Abasse, and Silverston 2017). In addition, enhanced triggered activity due to abnormal myocyte Ca^{2+} homeostasis can promote arrhythmias in patients with DMD. Although DMD patients typically develop cardiac symptoms including arrhythmias in the presence of a structured cardiomyopathy, our strategy used DMD-hiPSC-CMs gain insight into the interplay between causal and adaptive alterations of cardiac cells during the early-stages of disease progression over a longer period. This approach suggested that causal changes can presumably be identified from the beginning of cardiac differentiation, even before the pathology becomes manifest, while adaptive and maladaptive processes can influence the disease progression. For this reason, the natural myocardium stiffness and the increase of fibrosis at later stages of the disease can be major causes of dilated cardiomyopathy and sudden death in DMD patients.

Chapter 4

Novel 3D human induced pluripotent stem cell-derived bioengineered cardiac muscles for genetic cardiomyopathy

ABSTRACT

The pathogenesis of MYBPC3-associated hypertrophic cardiomyopathy (HCM) is still unresolved. We exploited a large and well-characterized patient population carrying the MYBPC3-c.772G>A variant (p. Glu258Lys, E258K) to provide translational insight based on studies on surgical myectomy samples, induced pluripotent stem cell (hiPSC)-cardiomyocytes and engineered heart tissues (EHTs). To gain insights into the pathogenic mechanisms driven by the MYBPC3-c.772G>A mutation using a comprehensive investigation of human disease models. Haplotype analysis revealed MYBPC3-c.772G>A as a founder mutation in Tuscany. The mutation leads to reduced cardiac myosin binding protein-C (cMyBP-C) expression, supporting haploinsufficiency as the main primary disease mechanism. Functional perturbations were studied in left ventricular samples from four patients who underwent myectomy, as well as in human hiPSC-cardiomyocytes and EHTs harboring c.772G>A, compared with samples from non-failing non-hypertrophic surgical patients and hiPSC lines from healthy controls. Mechanical studies in single myofibrils and permeabilized muscle strips highlighted faster cross-bridge cycling, and higher energy cost of tension generation. A novel approach based on tissue clearing and advanced optical microscopy supported the idea that the sarcomere energetics dysfunction is intrinsically related with the reduction in cMyBP-C. Studies in single cardiomyocytes (native and hiPSC-derived), intact trabeculae and hiPSC-EHTs revealed prolonged action potentials, slower Ca^{2+} transients and preserved twitch duration, suggesting that the slower excitation-contraction coupling counterbalanced the faster sarcomere kinetics. This conclusion was strengthened by in silico simulations. Of note, the results from patient tissues and hiPSC-derived models obtained from the same patients were essentially the same, supporting the use of hiPSC-models for HCM studies. HCM-related MYBPC3-c.772G>A mutation invariably impairs sarcomere energetics and cross-bridge cycling. Compensatory electrophysiological changes (e.g. reduced potassium channel expression) appear to preserve twitch contraction parameters but may expose patients to greater arrhythmic propensity and disease progression. Therapeutic approaches correcting the primary sarcomeric defects may prevent secondary cardiomyocyte remodeling.

INTRODUCTION

Hypertrophic cardiomyopathy (HCM) is the most common inherited heart muscle disease, characterized by abnormal and asymmetric thickening of the left ventricle (LV), diastolic dysfunction, and structural remodeling of the myocardium (e.g. myocyte/myofibril disarray). Most genotyped HCM patients harbor a mutation in one of the genes coding for cardiac sarcomeric proteins—hence,HCM is defined primarily as a disease of the sarcomere (Ho, Charron, et al. 2015). A complex and unresolved chain of events leads from sarcomeric protein alterations to mechanical dysfunction and cardiac remodeling. We have previously shown that HCM associated mutations in both thick- and thin-filament proteins (i.e. MYH7:p.R403Q and TNNT3:p.K280N),(Witjas-Paalberends et al. 2014; Piroddi et al. 2019) primarily increase cross-bridge cycling kinetics leading to increased energy consumption during tension generation (tension cost). Inefficient or excessive ATP utilization for tension development may play a central role in the pathogenesis of HCM (Ashrafian et al. 2003). The energy depletion hypothesis is supported by several studies in HCM patients, human heart samples, and animal models (Witjas-Paalberends et al. 2014; Piroddi et al. 2019) (Belus et al. 2008; Cecilia Ferrantini et al. 2017; Luedde et al. 2009). Mutations in MYBPC3, the gene coding for cMyBP-C (cardiac myosin-binding protein-C), represents the most common molecular etiology of HCM (Richard et al. 2003) cMyBP-C is a thick-filament-associated protein that localizes in the cross-bridge bearing C-zone of the A band within the cardiac sarcomere, where it plays important structural and functional roles (Lucie Carrier et al. 2015; Sadayappan and de Tombe 2012). About 70% of known cMyBP-C mutations are either frameshift or nonsense variations, for which a haploinsufficiency mechanism has been postulated (Marston et al. 2009b; van Dijk et al. 2009). Though less common than truncation mutations, a growing number of pathogenic missense mutations in MYBPC3 have been identified in HCM (Page et al. 2012; Iacopo Olivotto et al. 2008) The c.772G>A has been repeatedly reported among MYBPC3 variants, but it's true nature is still debated (De Lange et al. 2013; Krishnamoorthy et al. 2017). Although the c.772G>A transcript change is predicted to result in a missense substitution at position 258 (a lysine residue in place of glutamic acid, p.E258K), several lines of evidence indicate that this nucleotide change results in an exon skipping event—ultimately leading to a frame shift—by altering the last nucleotide of exon 6 and interfering with splicing (Singer et al. 2019; Suay-Corredera et al. 2021). Further understanding of these chains of events may prove instrumental to understanding HCM pathogenesis and identifying novel therapeutic targets. To date, the molecular mechanisms of the MYBPC3-c.772G>A pathogenicity remain controversial. By using different experimental models and approaches, we report that the MYBPC3-c.772G>A is a Tuscany founder mutation causing HCM. Our extensive set of analyses in HCM patient samples and human-induced pluripotent stem cell-derived cardiomyocytes (hiPSC-CMs) show that this founder mutation, most likely at early disease stages, causes (1) cMyBP-C deficiency, (2) impaired sarcomere energetics due to changes in cross-bridge cycling, and remodeling in excitation-contraction (E-C) coupling.

RESULTS

4.1 Characterization of the c.772G>A HCM cohort: demonstration of a founder effect in Tuscany

The heterozygous c.772G>A variant in the MYBPC3 gene was found to be present in 93 (5.8%) of 1198 probands analyzed through November 2016 (Mazzarotto et al. 2019), all of them originating from the north-eastern part of Tuscany (**Fig. 4.1A**). They represented 17% of genotype-positive individuals in the HCM Florence cohort (approximately one-third of all patients with *MYBPC3* mutations) (**Fig. 4.1B**). Haplotype analysis in four selected families revealed the presence of a unique haplotype spanning approximately 2 Megabases shared by all the c.772G>A individuals, confirming that the high prevalence of this otherwise rare variant is indeed due to a founder effect (**Fig. 4.1C-D**). At diagnosis, the mean age of the 93 E258K-HCM patients was 50±15 years; 33% were women. The vast majority of patients had classic localization of LV hypertrophy preferentially to the interventricular septum and anterior wall (94%); maximal LV wall thickness was 20±7 mm and LV ejection fraction (LVEF) at baseline was normal or supernormal except in one patient. During a mean follow-up of 6±4 years, 13 of the 93 patients (14%) died of cardiac causes and 8 (9%) experienced nonfatal cardioembolic strokes; the rate of sudden cardiac death was 0.5%/year and heart failure-related death was 1.8%/year. Importantly, over one-fifth of the c.772G>A patients (n=19, 21%) showed advanced LV dysfunction at final evaluation (defined as LVEF <50% and/or restrictive diastolic pattern), suggesting a considerable propensity to disease progression after age 45.

C

D
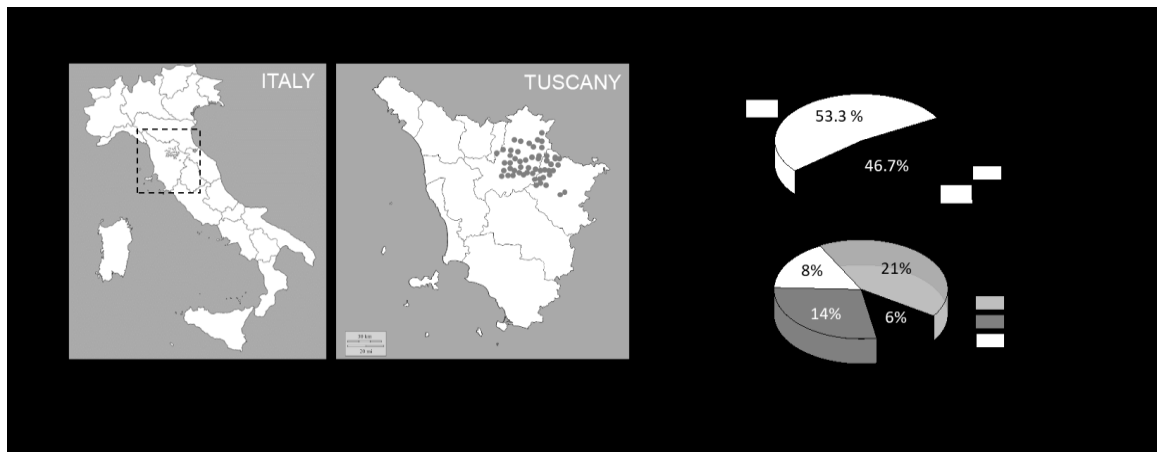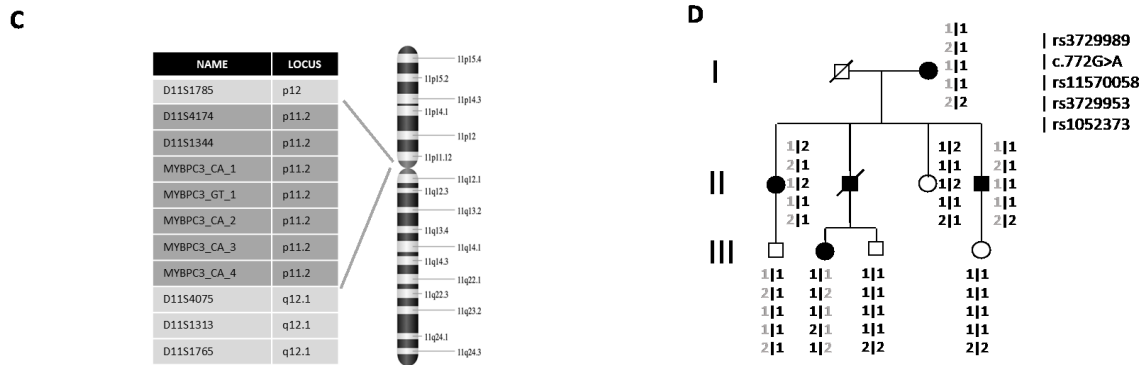
Figure 4.1. *Prevalence of the c.772G>A variant in the Florence HCM cohort. **A)** Geographical origin of HCM patients carrying the MYBPC3-c.772G>A mutation. **B)** Prevalence of genotype positive and genotype negative patients among the overall HCM Florence Cohort. Prevalence and distribution of sarcomeric myofilament protein gene mutations among the 46.7% genotype-positive HCM patients. **C)** and **D)** PCR assays for five intragenic microsatellite markers (CA/GT dinucleotide repeats were designed, and their products sequenced to obtain genotypes for segregation analysis). Numbers were assigned randomly to repeat alleles, and haplotypes were reconstructed with Merlin. The haplotype marked in grey is shown to segregate consistently with HCM in one illustrative large pedigree.*

As shown in **Fig. 4.2A-B**, LVEF tended to decrease with age and the number of patients with LVEF<50% increased progressively after the fifth decade. The four surgical patients who provided samples for in vitro studies were in the fourth (ID4: 33 years) and fifth decade (ID1, ID2 and ID3 45, 47 and 44 years respectively) and had all preserved EF (≥60%; **Fig. 4.2C**).
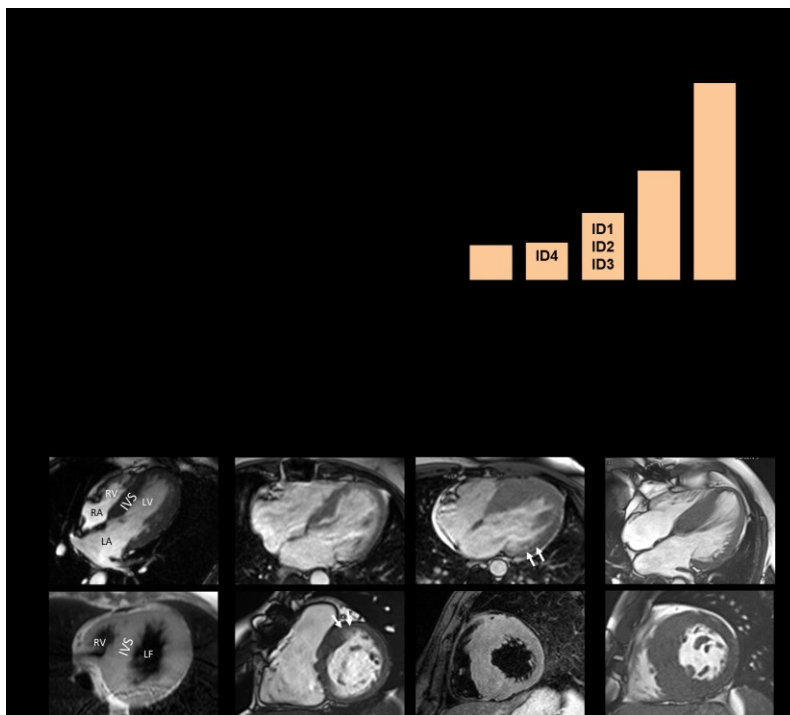
Figure 4.2. *Effect of age on LV function of the c.772G>A population and Cardiac Magnetic Resonance (CMR) imaging of the four patients selected for biophysical phenotyping. **A)** Changes with age in the LV Ejection Fraction (LVEF) of the c.772G>A population and **B)** percentage of c.772G>A patients with LVEF<50% in relation to age. **C)** CMR images from the four subjects who underwent myectomy from whom surgical samples were used for in vitro studies (gender, age and left ventricular ejection fraction on top of each image). Four chamber (Top) and short axis (bottom) views. Arrows show non-homogeneous signals in the hypertrophic IVS. LVEF is ≥ 60% in all four patients. Data collected at the last visit before myectomy. (LVEF, Left Ventricular Ejection Fraction; LA, Left Atrium; LV, Left Ventricle; RA, Right Atrium; RV, Right Ventricle; IVS, InterVentricular Septum.*

4.2 The energy cost of isometric tension is increased in c.772G>A sarcomeres

To investigate the impact of the MYBPC3-c.772G>A mutation on sarcomere energetics, Triton-permeabilized ventricular strips from three patients and two control donors were used to simultaneously measure steady-state Ca^{2+}-activated tension and ATPase activity under isometric conditions at 25 °C. Representative recordings of maximal isometric tension and ATPase activity at saturating Ca^{2+} concentration is shown in **Figure 4.3A**, for both donor and mutant multicellular preparations. The comparison of mechanical and energetic measurements between donor and mutant ventricular strips may suffer from artifacts related to differences in the structural features of the two groups of preparations. Using a combination of advanced tissue clearing, labeling, and optical imaging, we employed a method capable of reconstructing the whole ventricular strip with sufficient contrast and resolution to discriminate sarcomeric Z-lines across the whole length and thickness of the preparations (**Fig. 4.3B**)(Giardini et al. 2021). This imaging analysis allowed us to select strips with an adequate degree (near 100%) of cardiomyocyte alignment and density and a minimal degree (close to zero) of disarray (**Fig. 4.3C**). By comparing structural and functional measurements one-to-one in a direct correlative manner, we found that HCM strips that had the same longitudinal cardiomyocyte alignment as the donor strips showed a significantly increased tension cost measured from the ratio between maximal ATP consumption and isometric tension at saturating $[Ca^{2+}]$ (**Fig. 4.3D**). Impaired energetics of the c.772G>A strips was confirmed when energy cost of isometric tension generation was calculated from the slope of the average relation between isometric steady-state tension and rate of ATP consumption measured at different levels of Ca^{2+}-activation (**Fig. 4.3E**). The slope of the tension-ATPase relation was significantly higher in the c.772G>A strips compared to the donor preparations.
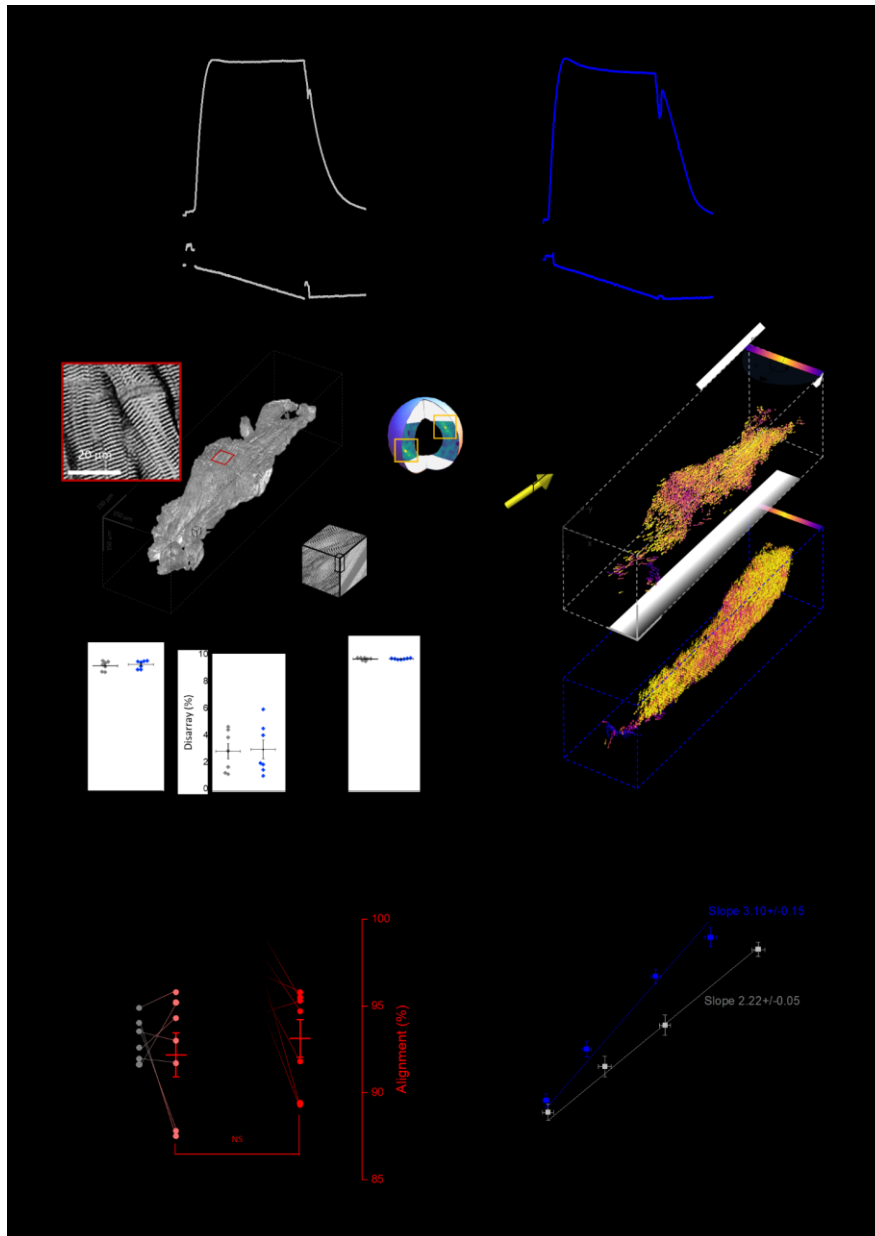
Figure 4.3. *Impact of the c.772G>A mutation on tension cost.* ***A)*** *Representative isometric tension (top) and ATPase activity (bottom) recordings in skinned ventricular strips from donors and c.772G>A samples at saturating [Ca²⁺].* ***B)*** *Reconstruction of a human muscle strip labeled with an anti-α-actinin antibody imaged with two-photon fluorescence microscope. Three representative sagittal planes at different depths show the stitched area after the deconvolution and the contrast equalization. The segmentation result is superimposed as a green border. A magnification showing the sarcomere z-lines at subcellular resolution is displayed in the red square.* ***C)*** *On the left, global alignment of contractile units; the central graph shows disarray, expressed as the measure of the local angular dispersion of nearby cells; on the right, cardiomyocytes density, expressed as the ratio of the volume of contractile tissue vs total muscle volume. Donor N=3, n=7; c.772G>A N=3, n=7; donor and mutant values were compared using linear mixed models; no significant differences were noted.* ***D)*** *One-to-one correlation between tension cost (in black and grey) and alignment (in red and light red) measured on donor and c.772G>A samples (donor N=3, n=7; c.772G>A N=3, n=7). Tension cost is measured as the ratio between maximal ATPase activity and maximal isometric force at saturating [Ca²⁺]. While a significant difference in tension cost was found between donor and HCM strips, no difference was found in cell alignment. P values calculated with linear mixed models; **=P<0.01.* ***E)*** *Average pooled relations between active tension and rate of ATP consumption (tension cost is the slope of the relation) in c.772G>A (blue) and donor (grey) muscle strips (c.772G>A N=3, n=7; donor N=3, n=7) (y = 3.04x and y = 2.08x respectively). Data, expressed as mean ± SEM, were obtained at different activating [Ca²⁺]s, pooled in 10%-wide steady state tension bins and were fit by linear regression as indicated by the solid lines (slope values are shown in the panel). *= The slopes of the two regression curves were compared using Student's T-test and found to be significantly different(P<0.05).*

4.3 The c.772G>A variant accelerates the kinetics of myofibril force generation and relaxation

To understand the mechanism responsible for the increased energy cost of tension generation in the c.772G>A myocardium, ventricular myofibrils from the three c.772G>A patients and five donors were maximally Ca^{2+}-activated (pCa4.5) and fully relaxed (pCa9) by rapid solution switching at 15°C, as previously described3. **Figure 4.4A** shows representative contraction-relaxation traces of both groups of myofibrils. Maximal Ca^{2+}-activated tension was the same in c.772G>A myofibrils compared to donors while resting tension showed a trend to be higher in the mutant group though the difference was not significant (**Fig. 4.4D**). The rate of force activation, k_{ACT}, and the rate of force redevelopment, k_{TR}, were faster in c.772G>A myofibrils **(Fig. 4.4B-D)**, indicating an accelerated apparent cross-bridge turnover in the mutant. Upon sudden Ca^{2+} removal, the time-course of myofibril force relaxation was biphasic, as previously described (Poggesi, Tesi, and Stehle 2005; Piroddi et al. 2007). The early, slow phase of relaxation (rate constant, slow k_{REL}) was markedly faster in the c.772G>A than in the donor myofibrils (**Fig. 4.4C-D**), indicating a faster apparent cross-bridge detachment rate under isometric conditions (Cecilia Ferrantini et al. 2009; Vitale et al. 2021)(Poggesi, Tesi, and Stehle 2005; Piroddi et al. 2007) (Cecilia Ferrantini et al. 2009). The rate of fast relaxation (fast k_{REL}) was also greater in the c.772G>A myofibrils. The results (changes in kinetics with no changes in active tension) suggest that the apparent rates of cross-bridge attachment and detachment are both increased in the c.772G>A myofibrils by 1.5-2 times and that the change in the isometric detachment rate is responsible for the increased tension cost (1.5-2 times) measured in the skinned multicellular preparations (Vitale et al. 2021).

.
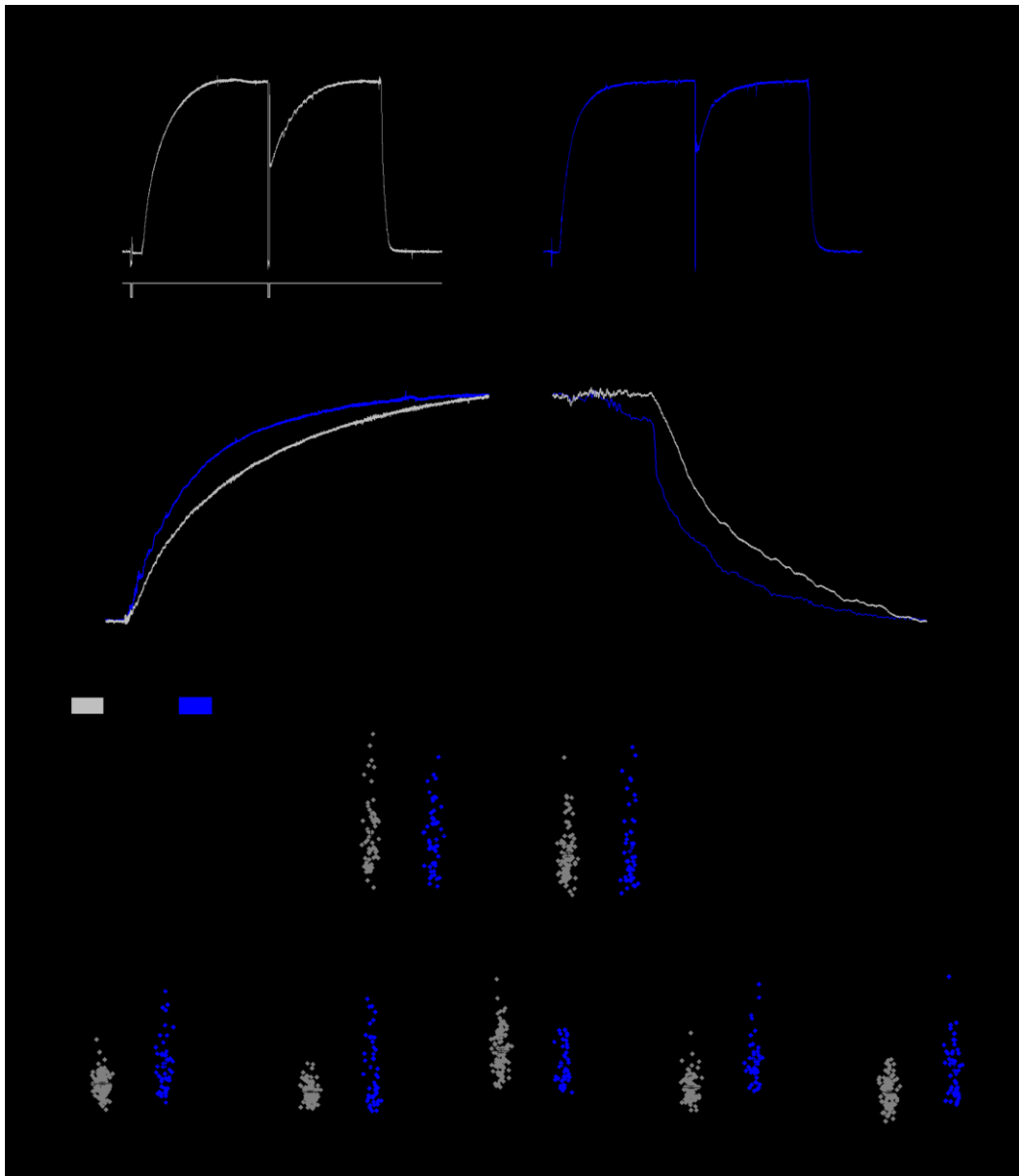
Figure 4.4. *Impact of MYBPC3-c.772G>A mutation on myofibril mechanics and kinetics.* ***A)*** *Representative tension responses (top traces) of donor (grey) and c.772G>A (blue) myofibrils maximally activated (pCa 4.5) and fully relaxed (pCa 9) by fast solution switching; the top and bottom traces are the lengths of the myofibrils that are subjected to release-restretch protocols at rest to measure resting tension and at steady-state contraction to measure k_{TR}.* ***B)*** *and* ***C)*** *The normalized tension curves from the c.772G>A and the donor myofibrils shown in* ***A*** *are superimposed to better compare the kinetics of force activation (**B**) and relaxation (**C**).* ***D)*** *Mechanical and kinetic parameters measured in donor (grey, N=5, n=100) and c.772G>A (blue, N=3, n=50) ventricular myofibrils. Po, maximal Ca^{2+}-activated tension, RT, resting tension, k_{ACT}, rate of tension activation, k_{TR}, rate of tension redevelopment, slow k_{REL}, rate of the initial slow isometric phase of relaxation, Dslow, duration of the slow phase of relaxation, fast k_{REL}, rate of the fast-exponential phase of relaxation. Line and bars indicate means ± SEM. *p<0.05; ** p<0.01. P values were calculated using linear mixed models. N=number of patients, n=number of myofibrils.*

4.4 Analyses of cMyBP-C protein levels in patient myocardium and hiPSC-CMs

The molecular pathomechanism underlying HCM associated with *MYBPC3* mutations has often been identified in cMyBP-C protein deficiency. To test if the same mechanism is associated with the *MYBPC3*-c.772G>A, we analyzed cMyBP-C protein expression in the myectomy samples used for *in vitro* experiments. The results show that the levels of full-length cMyBP-C (relative to α-actinin) were ~30% lower in each of the three c.772G>A samples compared with donor myocardium (**Fig. 4.5A**).

The levels of full-length cMyBP-C protein were also analyzed in cardiomyocytes derived from the patient hiPSC cell line and isogenic control (ID3 and corrected ID3) and from the healthy WT-C11 cell line between day 14 and 60 after initiation of differentiation. The Western immunoblot normalized for sarcomeric α-actinin confirmed that the relative expression of cMyBP-C was reduced in the mutant compared to the healthy cardiomyocytes and partially restored in the isogenic corrected controls from the patient (**Fig. 4.5B**). This result supports the haploinsufficiency hypothesis based on the results obtained from myectomy samples.
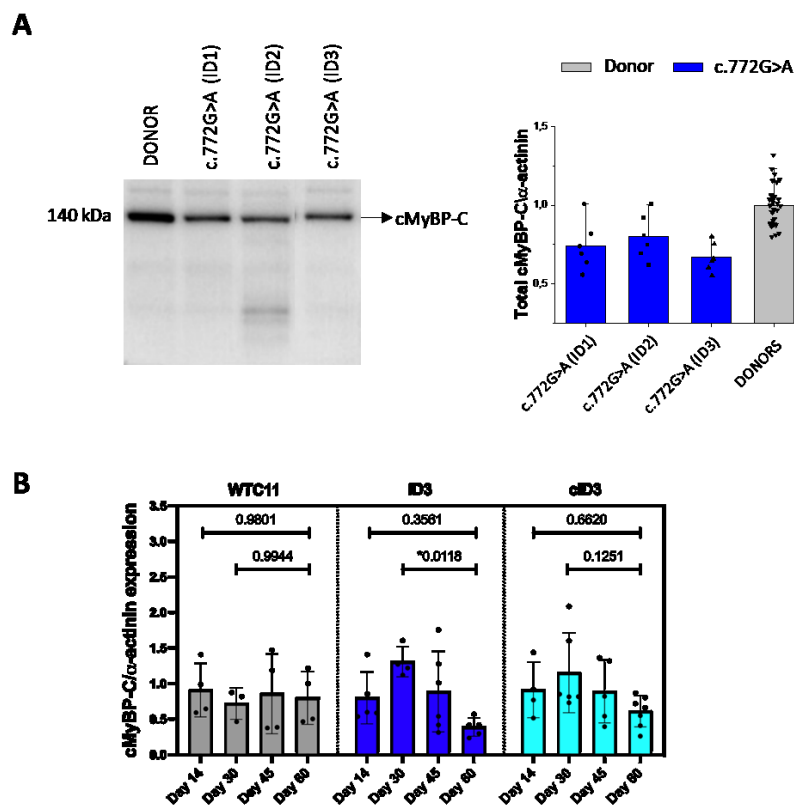
Figure 4.5. A) *Reduced cMyBP-C expression in myectomy samples from MYBPC3-c.772G>A patients. The levels of full-length cMyBP-C were analyzed by Western Immunoblot with the use of the C2-14 antibody and normalized to α-actinin in each of the three c.772G>A myectomy samples (N=4; n=18) compared with donor myocardium (N=5; n=30).* ***B)*** *cMyBP-C expression in hiPSC-CMs from c.772G>A patient and healthy subjects. Protein content was isolated from pellets of mutant (ID3) hiPSC-cardiomyocytes and compared with its isogenic CRISPR-Cas9 corrected control (corrected ID3) and the healthy control cell line (WT-C11) at different maturation time points (day 14, 30, 45 and 60 post initiation of differentiation) (WT-C11 N=7, n=1-5; ID3 N=8, n=1-4; c.ID3 N=7, n=1-4).*

4.5 Action potentials and Ca²⁺ transients in c.772G>A isolated cardiomyocytes

According to what was previously observed in cardiomyocytes isolated from HCM patients with different genetic backgrounds (Coppini et al. 2013), action potential (AP) durations and Ca²⁺ transients were also markedly prolonged in c.772G>A cardiomyocytes compared to controls (**Fig. 4.6A-B**). A reduction in the expression of repolarizing K⁺ channels as observed by reduced mRNA levels of regulatory subunits may at least partially explain the prolongation of the AP (**Fig. 4.6C**). These acquired electrophysiological changes may represent maladaptive mechanisms common to all forms of HCM remodeling, regardless of genotype (Coppini et al. 2013) (Cecilia Ferrantini et al. 2017).
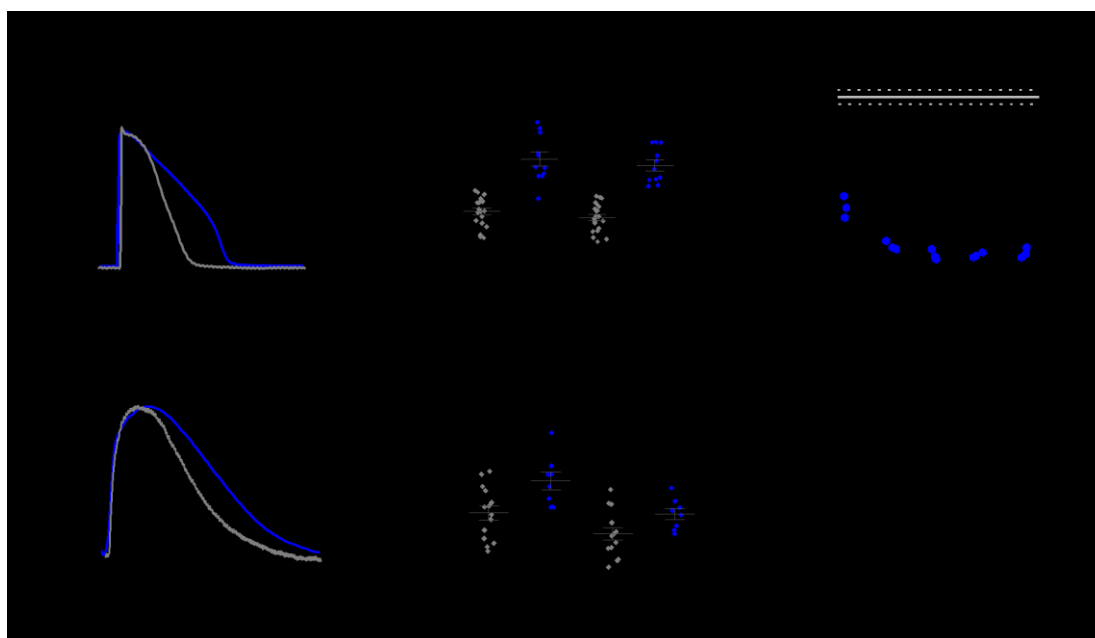
Figure 4.6. *Functional data from isolated cardiomyocytes. **A)** Representative recording of action potential and action potential duration at 90% repolarization (APD90%) from control cardiomyocytes (N=7, n=21) and c.772G>A cardiomyocytes (N=3, n=11), during stimulation at 0.5Hz and 1Hz. **B)** Representative superimposed calcium transient from control and c.772G>A cardiomyocytes during stimulation at 1Hz and Ca²⁺ transient decay duration (time from peak to 50% decay) from control cardiomyocytes (N=6, n=14) and c.772G>A cardiomyocytes (N=2, n=8), during stimulation at 0.5Hz and 1Hz. **C)** RNA expression of potassium current genes relative the 18S ribosomal RNA in control (N=1) and HCM (N=2) samples: secondary I_Kr subunit (KCNE2 or MIRP-1), I_Ks main channel gene (KCNQ1 or KvLQT1) and secondary subunit (KCNE1 or minQ), potassium voltage-gated channel subfamily H member 2 (KCNH2 or hERG1), Kv channel-interacting protein 2 (KCNIP2, KChIP2).*

In addition, contractile function of the c.772G>A ventricular myocardium was also studied, using intact trabeculae dissected from the endocardial layer of myectomy samples and recorded under isometric conditions at different pacing frequencies (procedure described in Methods). As shown in **Fig. 4.7A**, the twitch amplitude appears to be preserved in the c.772G>A trabeculae, as no differences were visible compared with the control tissue; moreover, the c.772G>A samples showed a preserved adaptation of twitch duration to stimulation rate (**Fig. 4.7B**), as observed in other intact trabeculae from patients carrying other HCM-causing mutations (Coppini et al. 2013). Contractile reserve also appears to be preserved in the HCM patient myocardium, as indicated by the positive inotropic response to high pacing frequency (**Fig. 4.7C**), stimulation pauses (**Fig. 4.7D**) and beta-adrenergic stimulation , which are similar to those measured in control cardiomyocytes.
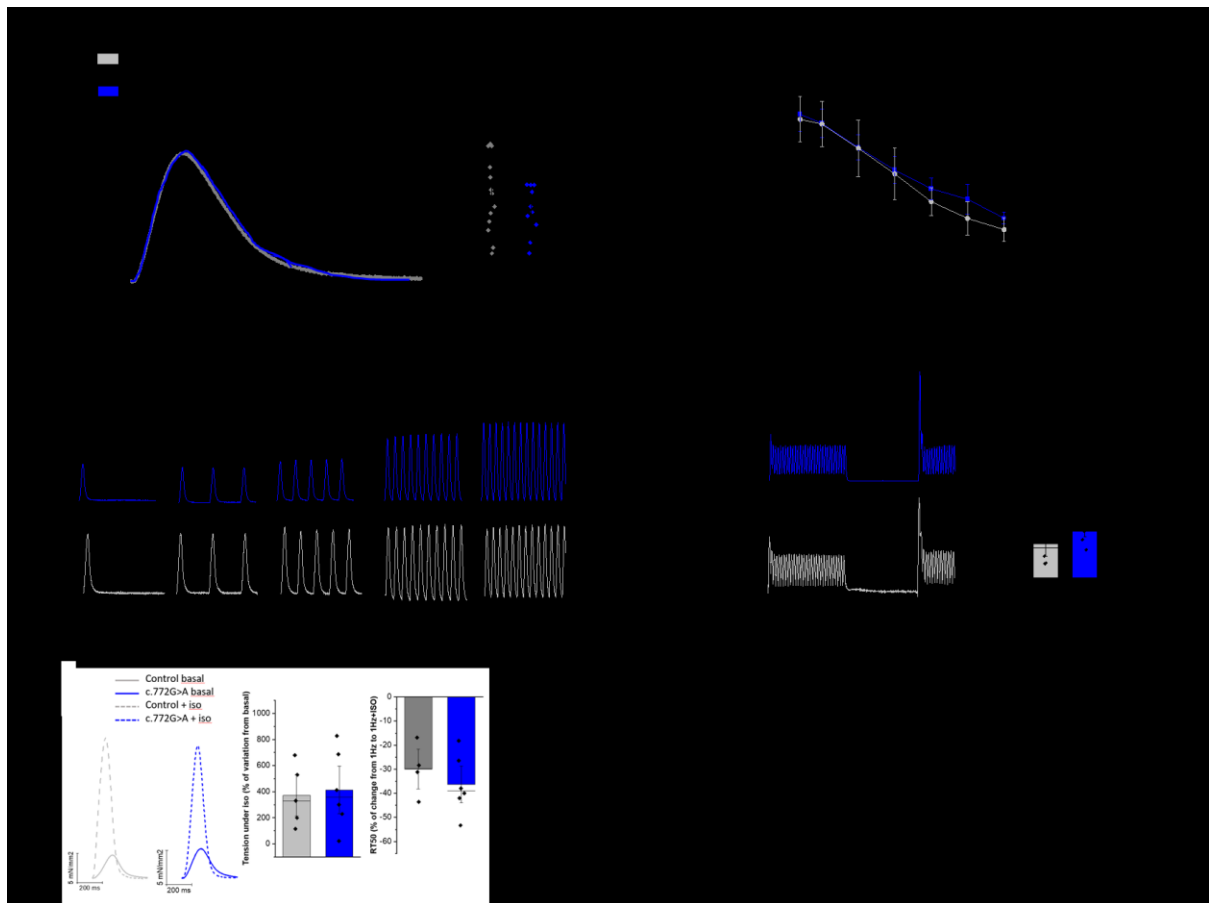
*Figure 4.7. Functional data from intact trabeculae. **A)** Representative superimposed force twitches from control and c.772G>A intact trabeculae during stimulation at 0.5 Hz and 1 Hz (inset: twitch amplitude at 0.5Hz) and **B-C)** twitch duration from stimulus to 50% of relaxation by increasing stimulation frequency (0.2, 0.5, 1, 2 and 2.5 Hz). **D)** Representative continuous recording from an c.772G>A and control trabecula during a post-rest protocol. **E)** Superimposed twitches from an c.772G>A and control trabeculae at baseline and in the presence of 0.1 µmol/L isoproterenol (Iso). Right: average percentage variation of force amplitude and twitch duration to 50% relaxation in control and c.772G>A intact trabeculae upon addition of β-adrenergic stimulation with isoproterenol 10-6M; c.772G>A n=4, N=2; control n=5, N=4. * = p<0.05 and **=p<0.01 by one-way ANOVA with Tukey. N=number of patients; and n=number of cells/trabeculae.*

In addition, the c.772G>A ventricular muscle displayed a preserved adaptation of twitch duration to stimulation rate, as observed previously in surgical samples of intact trabeculae from patients harboring different HCM causing mutations. The mechanism responsible for a preserved twitch duration with the underlying prolonged AP and calcium transients likely arises from the acceleration of cross-bridge cycling described above. To test this hypothesis, we employed a previously described model of HCM human cardiomyocytes (Passini et al. 2016)(Margara et al. 2021). We report above that the c.772G>A mutation accelerates cross-bridge kinetics, as shown by the enhanced k_{ACT} and slow k_{REL}. According to a simple two-state cross-bridge model (Brenner 1988), under the present experimental conditions (nominally zero [P_i]), k_{ACT} reports the sum of the apparent rate constants f_{app} and g_{app} that limits transition of cross-bridges from non-force-generating to force-generating states and from force generating to non-force-generating states, respectively. In terms of cross-bridge turnover kinetics, slow k_{REL} is a measure of g_{app}, which in the model is also equal to the tension cost (isometric ATPase per unit force). Force is proportional to the apparent duty ratio [$f_{app}/(f_{app}+g_{app})$], and an increase in

gapp should lead to a decline in the force generating capacity of the sarcomere unless the increase in gapp is compensated for by an increase in fapp. The myofibril data support the idea that the c.772G>A mutation increases f_{app} and g_{app} to a similar extent, i.e. 1.5-2 folds. A similar increase in g_{app} was estimated from the change in tension cost. **Fig. 4.8A** shows what happens if a 1.5-2-fold change of cross-bridges attachment and detachment rates is imposed in a control cardiomyocyte in the mathematical model (i.e., with preserved AP and calcium transient). The resultant twitch contraction is accelerated (both peak and relaxation times) and slightly increased in amplitude. In **Figure 4.8B** we mimic the prolongation of AP and calcium transient observed in c.772G>A and demonstrate that a 1.5-2-fold increase of cross-bridge attachment and detachment rates would in this case preserve the twitch duration. This provides proof of concept that the impact of increased cross-bridge cycling can be offset by slowing of the calcium transient.
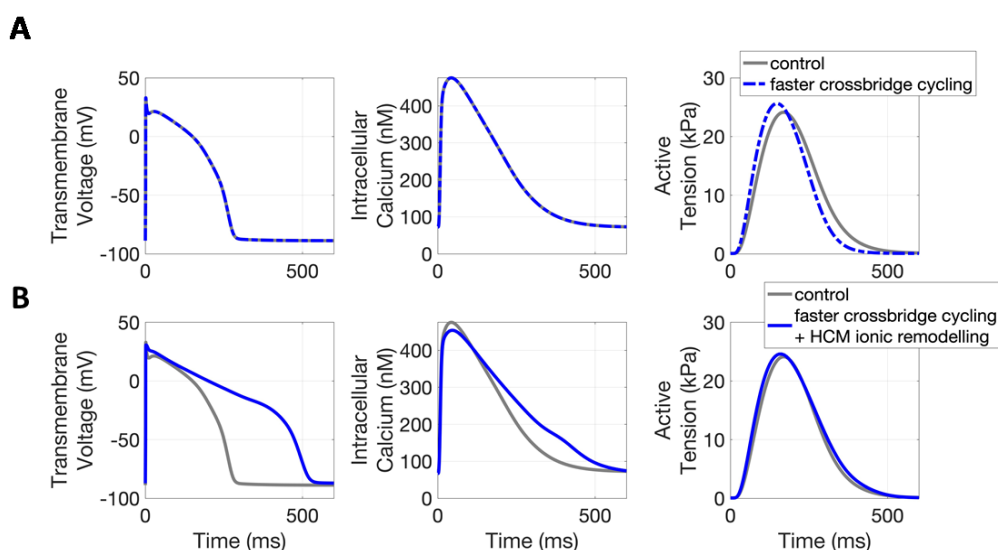
*Figure 4.8. Mechanistic simulations of human ventricular myocyte electromechanical function explain the impact of altered crossbridge cycling on force generation, in the context of HCM ionic remodeling. **A)** (from left to right) Comparison of action potential, calcium transient, and active tension waveforms in control (grey) and under faster crossbridge cycling (blue). **B)** (from left to right) Comparison of action potential, calcium transient, and active tension waveforms in control (grey) and under faster crossbridge cycling and HCM ionic remodeling (blue).*

A prolongation of the AP and Ca^{2+} transient, reducing only repolarizing K$^+$ currents, was simulated under the same conditions, and it was observed that the twitch duration remained unchanged, despite increased cross-bridges attachment and detachment rates (**Fig. 4.8B**). This shows that the impact of increased cross-bridges cycling can be offset by slowing of the calcium transient.

4.6 hiPSC-derived cardiomyocytes and EHTs recapitulate the biophysical phenotype observed in patients' samples.

It is known that prolongation of APs and Ca^{2+}- transients is associated with the development of early and delayed afterdepolarizations (Coppini et al. 2013)(Cecilia Ferrantini et al. 2017), so it is possible that electrophysiological changes appear in the pre-hypertrophic stages of the disease (Coppini et al. 2017). Therefore, to study alterations that occur in the early stage of HCM, we used hiPSC-derived

cardiomyocytes as a model, which can mimic cells in their developmental stage (Marchianò, Bertero, and Murry 2019). Recordings of AP and Ca^{2+} transients in single hiPSC-CMs were performed by an optical method at day 60 post differentiation, using fluorescent indicators. As observed in **Fig. 4.9A-B**, the AP and calcium transients duration was slower in c.772G>A hiPSC-CMs (ID3) than in controls, recapitulating what was observed in cardiomyocytes isolated from patients' surgical samples. Furthermore, consistent with what we saw in cardiomyocytes isolated from native tissue, in hiPSC-CMs carrying the mutation (ID3) we also observed reduced mRNA levels of K$^+$ channel regulatory subunits compared with control cardiomyocytes (Control and ID3 corrected). Compared to controls, ID3 patient hiPSC-CMs had similar fractional shortening, indicating preserved cell contractility (**Fig. 4.9D**). Moreover, the time course of the twitch was comparable to that of the healthy cell line.
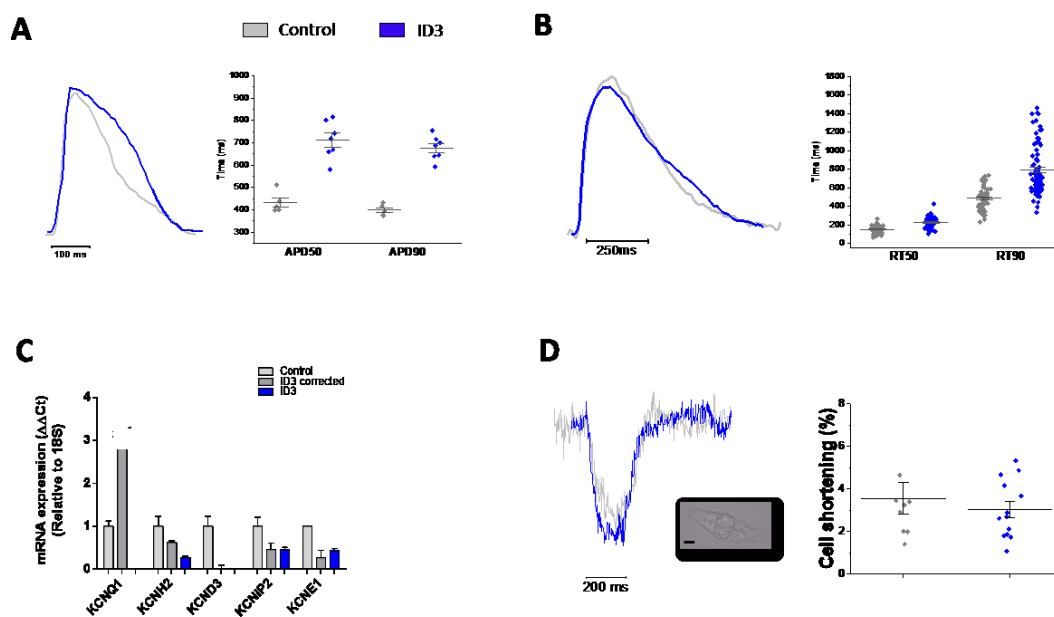
Figure 4.9. The impact of the mutation on the hiPSC-cardiomyocytes function. Simultaneous recording of action potential *A)* and calcium transients *B)* by fluorescent indicators (Cal630 and FluoVolt, respectively). Single mutant hiPSC-cardiomyocytes (ID3 N=4, n=178) were compared with a healthy control cell line (UC3-4, N=3, n=131) for action potential at 50% and 90% of duration (APD50, ms) and the duration from calcium transient peak to 50% and 90% of calcium transient decay (RT50, ms). *C)* RNA expression of potassium current genes relative to the 18S ribosomal RNA in control, isogenic control (ID3 corrected) and c.772G>A hiPSC-CMs (ID3) (N=1). *D)* Analysis of single cardiomyocyte contractility by video-edge detection; percentage of unloaded cell fractional shortening was recorded at 1Hz at 37°C in Tyrode solution with 1.8mM of extracellular calcium. N=3; n=10 for each cell line.

Thus, electrophysiological and E-C coupling remodeling also seems to be present in hiPSC-cardiomyocytes with the c.772G>A mutation, suggesting that this might be an early adaptation mechanism that begins even before the onset of hypertrophy.

Finally, to more closely recapitulate tissue level conditions, engineered heart tissues (EHTs) were fabricated and followed until day 50 while measuring auxotonic spontaneous contraction and frequency. Measurements under auxotonic conditions show a significant increase in force-generating capacity over time in all three cell lines and a reduction in spontaneous beating frequency (**Fig. 4.10**).

106
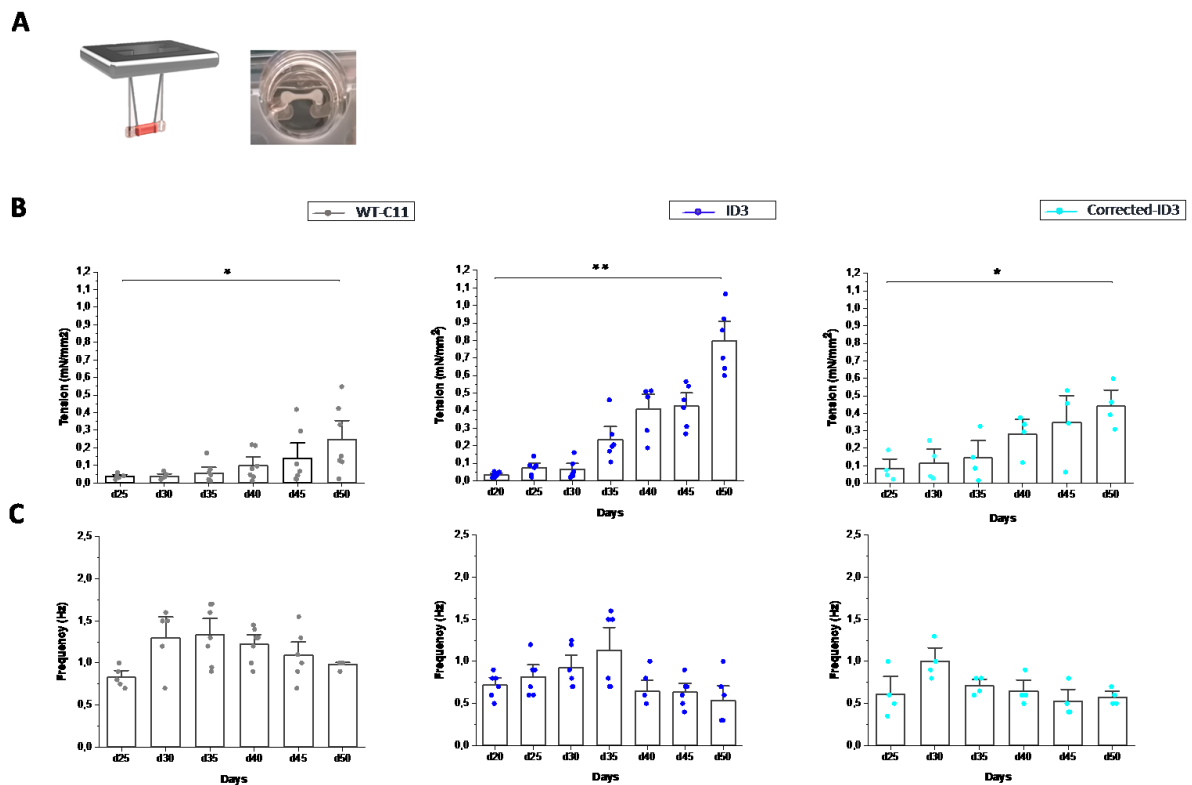
*Figure 4.10. Spontaneous auxotonic contractions of engineered heart tissues (EHTs). **A)** 3D render of silicon posts and EHTs, on the left, and representative image of an engineered heart tissue formed between two calibrated silicone posts. **B)** Spontaneous auxotonic twitch tension of EHTs from day 25 to 50 of differentiation, measured at 37°C in RPMI/B27 culture medium with 5% CO_2 (~0.4mM of [Ca^{2+}]). **C)** Progression of spontaneous beating frequency of all EHTs from day 20 to 50. (WT-C11 n=7, ID3 n=6 and corrected ID3 n=4). One-way analysis of variance (ANOVA) with a Tukey post-hoc test was used to compare the different time points. * p < 0.05 and ** p < 0.01 versus d25.*

At day 50 p.d, EHTs were detached from the pillars and fixed on a force recording apparatus to measure twitch tension and kinetics at day 50 after differentiation, under imposed pacing rates. Compared to the CRISPR-Cas9 corrected ID3- and WT-C11-EHTs, ID3-EHTs showed preserved twitch amplitude together with similar contraction time-course (both force rise and relaxation) and rate adaptation to twitch duration (**Fig. 4.11B**). EHT contractile reserve was also preserved, as indicated by the positive inotropic response to stimulation pauses (**Fig. 4.11D-F**) and high extracellular calcium ($[Ca^{2+}]_{out}$ up to 4mM).
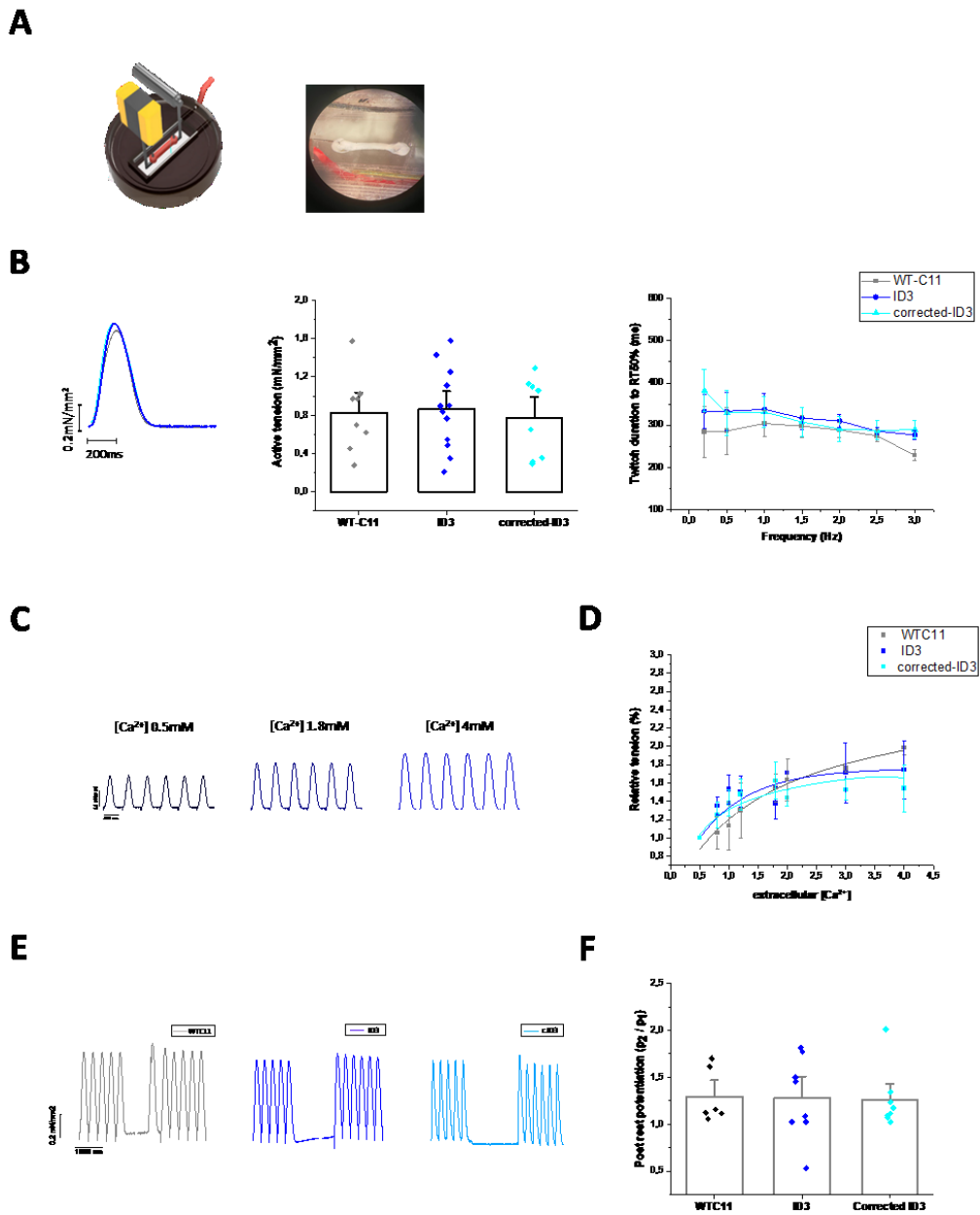
*Figure 4.11. Isometric contractile function of EHTs. **A)** Representative image of an engineered cardiac tissue mounted between a force transducer and a motor arm, which controls the tissue length. **B)** Active tension, under 1Hz pacing, and twitch duration to 50% of relaxation of patient EHTs compared to the corrected isogenic control and the healthy control. EHTs were measured in isometric conditions at 37°C in the Krebs-Henselheit solution with 1.8mM of [Ca²⁺] under imposed pacing. **C)** Superimposed twitches from EHTs at different calcium concentration (0.5 to 4 mM) and **D)** fitting curves of the percentage of variation in force amplitude measured in EHTs upon changes of extracellular calcium concentration from 0.5 to 4mM. **E)** Representative continuous recording from an ID3-(c.772G>A), corrected-ID3 and control WT-C11 hiPSC-EHTs during a post-rest protocol and **F)** positive inotropic responses to pauses in EHTs from the 3 cell lines. ID3 (n=12) were compared with the corrected isogenic control (corrected ID3, n=7) and the healthy control (WT-C11, n=8). Statistical analysis was performed using one-way ANOVA with Tukey post-hoc test. No statistically significant differences emerged.*

DISCUSSION

Since the 1990s the genetic heterogeneity of HCM has been well established (Geisterfer-Lowrance et al. 1990), and a correspondingly large clinical variability has limited the interpretation and clinical actionability of genotype - phenotype correlation studies. The heterozygous variant c.772G>A in the MYBPC3 gene was substantial subset of over 90 individuals (or 17%) of the Florence HCM, all of them originating from the north-eastern part of Tuscany, allowing detailed insight into the pathophysiology of this mutation. Notably, c.772G>A is characterized by peculiar clinical features including marked propensity to systolic dysfunction and disease progression (occurring in 1 patient out of five) (Girolami et al. 2006a; Gajendrarao et al. 2015). The c.772G>A mutation is considered a rare variant worldwide. Haplotype analysis confirmed that the locally high prevalence of this variant is indeed due to a founder effect. We sought to address the molecular mechanism through which the c.772G>A variant is pathogenic. Western blot analysis showed a reduction in full-length cMyBP-C levels (~30%) in all three c.772G>A myectomy samples, compared to donor tissue. In hiPSC-cardiomyocytes from the ID3 patient, the protein expression of cMyBP-C (relative to α-actinin) were decreased in later stages (60 days after initiation of differentiation), but protein levels were preserved in a CRISPR-Cas9-corrected isogenic line. This suggests that the mutation may be the cause of the reduced expression of cMyBP-C in mutant hearts, further supporting the hypothesis of protein haploinsufficiency as the main pathophysiological mechanism. Several studies suggested that truncating mutations in cMyBP-C diminish total protein level and cause HCM through haploinsufficiency (Marston et al. 2009a; van Dijk et al. 2009; Andersen et al. 2004; Marston et al. 2012). The c.772G>A variant affects the splice site consensus sequence at the last nucleotide of exon 6 in the MYBPC3 coding sequence, leading to an out-of-frame skipping of exon 6 in the MYBPC3 gene (Andersen et al. 2004; Helms et al. 2014). In contrast to functional studies on murine engineered cardiac tissue carrying the same mutation, where a missense-mutated (p.Glu258Lys, E258K) or a truncated cMyBP-C was observed to be incorporated into cardiac sarcomeres and directly impaired contractile function (De Lange et al. 2013), the expression of a truncated protein was never detected in affected heart tissue from HCM patients carrying the c.772G>A variant (Marston et al. 2009a, 2012). The c.772G>A is the last base of exon 6 which results in splicing out of exon 6, causing a frameshift and then downstream termination codon. The mRNA is not truncated but contains a premature termination codon which makes it susceptible to nonsense mediated decay. Previous studies indicated the E258K as a splice site mutation and the missense protein has never been shown (Helms et al. 2014). Another possible mechanism associated to haploinsufficiency is supported by other findings using heterozygous MYBPC3-mutant hiPSC-cardiomyocytes, that reported reduced cMyBP-C synthesis rates, partially counteracted by a slower rate of cMyBP-C degradation (Helms et al. 2020). We analyzed the functional consequences of the mutation at the myofilament level and its impact on sarcomere energetics. Isolated myofibrils had markedly enhanced kinetics of force development and crossbridge detachment (k_{ACT} and slow k_{REL}, respectively), but no change of myofibril maximal force. Given that slow $k_{REL} \approx g_{app}$ (Vitale et al. 2021), the observed increase in cross-bridge detachment in c.772G>A myofibrils predicts an increase in the amount of ATP spent to generate a given amount of isometric force (i.e. tension cost). Indeed, we identified higher tension cost in demembranated cardiac muscle strips isolated from c.772G>A myectomy samples compared to donor patients. Faster cross-bridge detachment under isometric conditions and higher energy cost of tension generation are common features of several HCM-

associated mutations (Witjas-Paalberends et al. 2014; Belus et al. 2008; Luedde et al. 2009; Cecilia Ferrantini et al. 2009). Notably, the possibility that lower generated force per unit of ATP spent was caused by fiber misalignment/disarray was excluded, thanks to a newly developed structural correlative approach featuring reconstruction of the whole 3D structure of each ventricular strip (Giardini et al. 2021). Thus, we speculate that the increased tension cost is a direct consequence of the c.772G>A mutation. While a marked impact of many MYH7 or TNNT2 HCM variants on cross-bridge kinetics and sarcomere energetics is expected (Witjas-Paalberends et al. 2014; Belus et al. 2008; Luedde et al. 2009; Cecilia Ferrantini et al. 2009)(Piroddi et al. 2019), the effects of MYBPC3 mutations are less straightforward. Our results support the idea that haploinsufficiency is primarily responsible for sarcomere functional abnormalities due to this MYBPC3 mutation. Normally, the N-terminal C1C2 region of cMyBP-C interacts with myosin heads in the S2 region, inhibiting its binding to actin and thus, reducing cross-bridge formation and cycling (Ababou, Gautel, and Pfuhl 2007; Harris et al. 2004). Reduced cMyBP-C levels likely diminish this inhibitory interaction (Korte et al. 2003; Stelzer, Fitzsimons, and Moss 2006), consistent with the observed acceleration of cross-bridge cycling rates and the increased ATP consumption for tension development.

In line with previous observations in cardiomyocytes isolated from HCM patients with different genetic backgrounds, c.772G>A-cardiomyocytes showed prolonged APs and slower Ca^{2+} transients (Coppini et al. 2013). A reduction of the expression of K^+ repolarizing channels, as observed by reduced mRNA levels of the regulatory subunits, can at least partially account for AP prolongation. These acquired electrophysiological changes may represent universal maladaptive mechanisms that are common to all forms of HCM remodeling, regardless of genotype (Ferrantini et al., 2017; Coppini et al. 2013). In the case of the c.772G>A mutation, we verified by in silico simulations that the prolonged duration of APs is sufficient to prolong calcium transients and counterbalance the faster rate of crossbridge turnover. Changes of the expression and phosphorylation levels of other excitation-contraction coupling proteins in HCM cardiomyocytes (decreased SERCA expression, increased Ca-calmodulin protein kinase II -CaMKII- activity) may also have contributed to the prolongation of Ca^{2+} transients, as previously observed in human HCM samples carrying different mutations (Coppini et al. 2013)(Helms et al. 2016). In the absence of AP and Ca^{2+} transient prolongation, twitch duration would be shortened. Thus, the simulations support the idea that the presence of concurrent prolongation of APs and Ca^{2+} transients is the reason why the time-course and amplitude of contraction in c.772G>A myocardium are similar to those of controls, despite the faster crossbridge turnover. This interpretation suggests that electrophysiological changes are an essential adaptation of c.772G>A myocardium aimed at counteracting the effects of the faster cross-bridge turnover, at the expense of cellular electrical stability. Indeed, prolongation of APs and Ca^{2+} transients is associated with the development of early and delayed afterdepolarizations (Ferrantini et al. 2017; Coppini et al. 2013). In this regard, electrophysiological changes are likely to appear early during disease development (Coppini et al. 2017), in the pre-hypertrophic stages of the disease. The results obtained from hiPSC lines are in support of this hypothesis. It is generally accepted that hiPSC-derived cardiomyocytes mimic cells in their developmental stage (Marchianò et al. 2019) and are therefore representative of the early, pre-hypertrophic stage of HCM typical of young mutation carriers. Electrophysiological and E-C coupling remodeling was present in hiPSC-cardiomyocytes from c.772G>A patients, suggesting that this may be an initial adaptive mechanism that starts even before the onset of overt hypertrophy.

Nonetheless, EP changes at the cardiomyocyte level might expose patients to an increased arrhythmogenic risk even at this early stage of disease. It is important to note that the molecular mechanisms linking impaired sarcomere function to E-C coupling remodeling are still unknown and need to be addressed. This, however, is far beyond the scopes of the present work and would require dedicated molecular approaches.

These results also support the idea that an early treatment of MYBPC3-c.772G>A carrier may prevent or reduce HCM-related pathology, for instance, using the novel myosin inhibitors currently employed in clinical trials on obstructive and non-obstructive HCM patients. cMyBP-C has been suggested to regulate cardiac function by modulating and maintaining the "super-relaxed" (SRX) state of myosin (McNamara et al. 2017, 2016). The decreased SRX fraction results in an increased number of myosin heads capable of interacting with actin, leading to higher sarcomeric energetic requirements, both at rest and during force development. Specifically, mavacamten (Olivotto et al., 2020) may act by stabilizing the SRX in cardiac muscle (Anderson et al. 2018; Toepfer et al. 2020), countering myocardial hyper-contractility, thus normalizing myocardial energetics (Ho et al. 2020). In addition, our study is consistent with the hypothesis that targeting early EP and EC-coupling changes may exert disease modifying effects, as well as reducing the risk of arrhythmias. Indeed, late Na^+ current blockers such as ranolazine or disopyramide acutely reduced cellular arrhythmias in human myocardium and prevented disease progression during long-term treatment in HCM mouse models (Coppini et al. 2013, 2017)(Iacopo Olivotto et al. 2018; Coppini et al. 2019). Similarly, treatment of young pre-hypertrophic mutation-carrier patients with the calcium channel blocker diltiazem slowed the development of HCM (Ho, Lakdawala, et al. 2015). As cardiomyocyte calcium overload and the increased activity of calmodulin kinase (CaMKII) are hallmarks of sarcomeric HCM and drive disease progression (Coppini et al. 2013; Helms et al. 2016)(Lehman et al. 2019), halting the early EC-coupling changes with targeted therapies may be as effective as directly addressing the dysfunctional sarcomeres, with the added benefit of protecting against cellular arrhythmias.

Chapter 5

Cardiac Cell and Tissue Engineering for therapy modeling

Engineered Heart Tissues for studying twitch tension and inotropic pharmacological interventions

M. Langione, S. Steczina, L. Giammarino, I. Della Corte, B. Scellini, R. Coppini, E. Cerbai, C. Tesi, M. Regnier, C. Poggesi, C. Ferrantini, J. M. Pioner

ABSTRACT

Human engineered heart tissues (EHTs) generated from induced pluripotent stem cell-derived cardiomyocytes (hiPSC-CMs) are commonly retained optimal for the description of contraction parameters, but most of the EHTs' mechanical measurements (i) are obtained from the optical detection of pillars' displacement rather than being controlled force-length recordings (ii) are collected during spontaneous beating and (iii) have never been directly compared to myocardial twitches from cardiac patients samples. In this study, we first generated EHTs from different donor/patient hiPSC-CMs and analyzed the rate and characteristics of their spontaneous auxotonic contractions over a period of 50 days using the standard pillar-based optical technique. All EHTs developed greater tension and reduced their spontaneous beating frequency over time. At day 50 p.d., EHTs were detached from pillars and mounted isometrically on a force-length recording apparatus to study twitch contractions at optimal length under different pacing frequency and various inotropic stimuli (e.g. high extracellular calcium, administration of myosin inhibitors). As a paradigm, we analyzed EHTs and corresponding myocardial preparations form a selected HCM myectomy patient carrying the MYBPC3-c.772G>A (p.E258K). E258K EHTs at 50 days p.d. show rate-adaptation of twitch duration and positive inotropic response to high pacing rates and high extracellular calcium (4mM), although less pronounced compared to those of the corresponding native E258K patient myocardium. Next, patient EHTs were compared to isogenic CRISPR/Cas9 corrected control: contraction amplitude and kinetics were similar in both (shown in Chapter 4). Importantly, patient and control EHTs show a negative inotropic response upon acute administration of 1μM Mavacamten, similar in extent to that observed on HCM myectomy samples. In addition, EHTs were used as a model to test the long-term effect of Mavacamten. After chronic treatment for 20 days using Mavacamten 0.3μM and 0.75μM, reduced contractile force development under isometric conditions was observed in drug-treated EHTs compared with untreated EHTs, with mild reduction of the twitch duration. EHTs, widely used for in vitro disease modelling, appear to qualitatively reflect the contraction parameters and the force-interval relationship of the native myocardium, thus representing a useful tool for studying acute and long-term effect of inotropic agents.

INTRODUCTION

Hypertrophic cardiomyopathy (HCM) is the most common mendelian heart disease often referred to as a disease of the sarcomeres (Ho et al. 2018). HCM is commonly associated with myocardial hypercontractility and higher energy cost of contraction that emerged as a suitable target for the development of a novel pharmacological disease-specific approach (Spudich 2019) (Zampieri et al. 2021). Mavacamten, a novel first-in-class allosteric inhibitor of myosin ATPase, demonstrated efficacy and safety in reducing left ventricular outflow tract obstruction and ameliorating exercise capacity, in a phase III clinical trial on patients with obstructive HCM (Iacopo Olivotto et al. 2020) (Zampieri et al. 2021). Furthermore, the phase II MAVERICK-HCM trial conducted in adults with symptomatic nHCM undergoing treatment for 16 weeks, followed by an 8-week washout, showed that Mavacamten was well tolerated in most subjects, but caused a reduction in left ventricular ejection fraction (LVEF) in 10% of patients (Ho et al. 2020).

In HCM, myocardial hypercontractility has been often associated with increased number of myosin heads available (Spudich, 2019). Previous findings proved that Mavacamten may act by stabilizing the SRX in cardiac muscle (Anderson et al. 2018; Toepfer et al. 2020) countering hypercontractility, thus normalizing myocardial energetics in experimental HCM models. In addition, mechanical experiments using single human ventricular myofibril following exposure to Mavacamten showed acceleration of force relaxation and inhibition of the ADP-stimulated force developed in the virtual absence of external Ca^{2+} (Scellini et al. 2021). For this reason, Mavacamten represents one ideal therapeutic intervention for HCM patients, but in selected stages of the disease.

We recently provided new understanding on the pathogenesis of *MYBPC3* variants, the most common cause of familial HCM. In our HCM patient cohort, a large and well-characterized population carry the *MYBPC3*:c.772G>A variant (p.Glu258Lys, E258K), which has a founder effect in the Tuscany region of Italy. This variant provided the unique opportunity to study the basic mechanisms of *MYBPC3*-HCM using patient myocardium and induced pluripotent stem cell-derived models (hiPSCs) of one of the same patients. In the myofibrils of patients carrying the *MYBPC3*:c.772G>A variant, cMyBP-C haploinsufficiency causes acceleration of cross bridge kinetics and increased energetic cost of contraction. Electrophysiological changes (slower action potentials and prolonged calcium transients) appear to counterbalance the faster cross-bridge cycling, ultimately preserving the amplitude and duration of cardiac contraction, at the expense of cardiac electrical stability and diastolic function (Pioner et al., 2023). Prolongation of action potentials and calcium transients is associated with the development of early and delayed afterdepolarizations (Coppini et al., 2013). In HCM, left ventricular (LV) hypertrophy generally becomes evident during puberty or early adult life in patients with HCM. However, little is known about the time of onset of the other features of HCM, although all have been described in very young children, and even in newborn babies (B. J. Maron 2002) (Basso et al. 2000). In this regard, it is generally accepted that hiPSC-derived cardiomyocytes (hiPSC-CMs) mimic cardiac cells in their developmental stage (Marchianò, Bertero, and Murry 2019) and may be representative of the early stage of HCM typical of young mutation carriers. The advantage of using both the HCM patient myocardium and the related patient-derived hiPSC line allowed us to better demonstrate the predictive power of patient-specific hiPSC-CMs for inherited cardiomyopathies. In the

MYBPC3:c.772G>A hiPSC-CMs and engineered heart tissues (EHTs), the same changes found in cardiomyocytes from patient tissue are likely to appear early during disease development, in the pre hypertrophic stages of the disease. These results support the idea that an early treatment *MYBPC3:*c.772G>A carrier with Mavacamten may prevent or reduce HCM-related proarrhythmogenic events.

Therefore, in this study, we generated EHTs from hiPSC-CMs from a patient line carrying the MYBPC3:c.772G>A mutation. As a comparison, its CRISPR-Cas9-corrected isogenic control was used. In view of the results reported in the chapter 4 (Pioner et al., 2023) we used the hiPSC-derived EHTs to validate long-term exposure to Mavacamten and to observe the effects on the contractile function and molecular mechanisms (a transcriptome analysis is ongoing). Mavacamten was tested on c.772G>A hiPSC-EHTs by both acute and long-term treatment (20 days) and in both conditions, tension and contraction kinetics were analyzed under isometric conditions under imposed pacing frequencies and different external calcium concentrations. Preliminary results show that chronic treatment with Macavamten (and after washout) causes force reduction in all EHTs but decreases the time-course of twitch contraction and relaxation only in the HCM-EHTs. Ongoing gene expression profile and structural analysis may provide further understanding on the mechanisms associated with Mavacamten exposure. On a clinical level, this work aims to provide relevant understanding for the prevention and treatment of HCM in the pediatric and pre-hypertrophic stages of the disease.

RESULTS

5.1 Acute Effect of Mavacamten on contractile force and kinetics of hiPSC-EHTs

Mavacamten was tested by acute treatment on mutated and control engineered tissues under isometric conditions and at different pacing frequencies. MAVA showed a dose-dependent effect on isometric force. It was tested at different concentrations in both ID3 and corrected ID3 to calculate EC_{50} (0.1μM, 0.3μM, 0.5μM, 1μM, 3μM). Representative data display the effect at the concentration of 1μM, as in native myocardium. Analysis of contractile force in the presence of high calcium concentration (4mM) and MAVA, shows a reduction in active tension in both mutated EHTs and isogenic control (ID3 = ~-56% and c.ID3= ~-68%) compared with the basal condition (4mM [Ca^{2+}]), but no changes in contractile kinetics are visible.
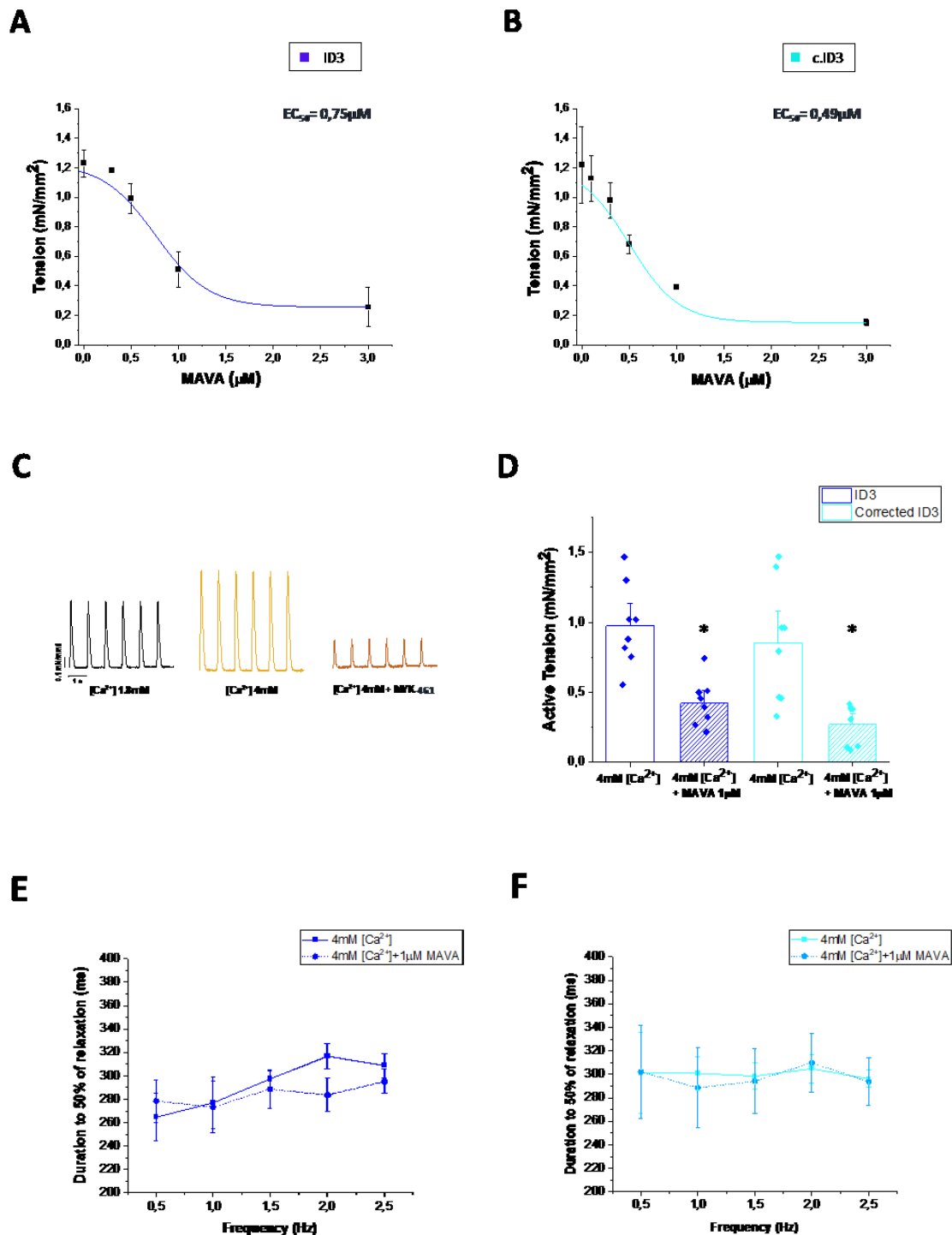
Figure 5.1. *Effect of Mavacamten on contractile force of EHTs.* ***A-B)*** *Representation of the dose-response curves of different concentrations of Mavacamten in ID3 (n=3) and c.ID3 (n=2).* ***C)*** *Representative isometric twitches under 1-Hz in the presence of 1,8mM [Ca²⁺] and 4mM [Ca²⁺] with the addition of Mavacamten (1μM), respectively.* ***D)*** *Active tension and* ***E)*** *twitch duration to 50% of relaxation in the absence and in the presence of 1μM MAVA at 4mM [Ca²⁺] of patient EHTs (ID3, n=8) and* ***F)*** *corrected isogenic control (Corrected ID3, n=8). Measurements are performed in isometric conditions under pacing stimuli at 37°C in the Krebs-Henselheit solution. Data are reported as Mean±SEM. One-way analysis of variance (ANOVA) with a Tukey post-hoc test with statistical significance set at * p < 0.05 and ** p < 0.01.*

Moreover, the effect of the drug was reversible after acute treatment; gradually the contractile force increased following drug removal, and after ~1h the active tension was like that of the basal condition (**Fig. 5.2A-B**).
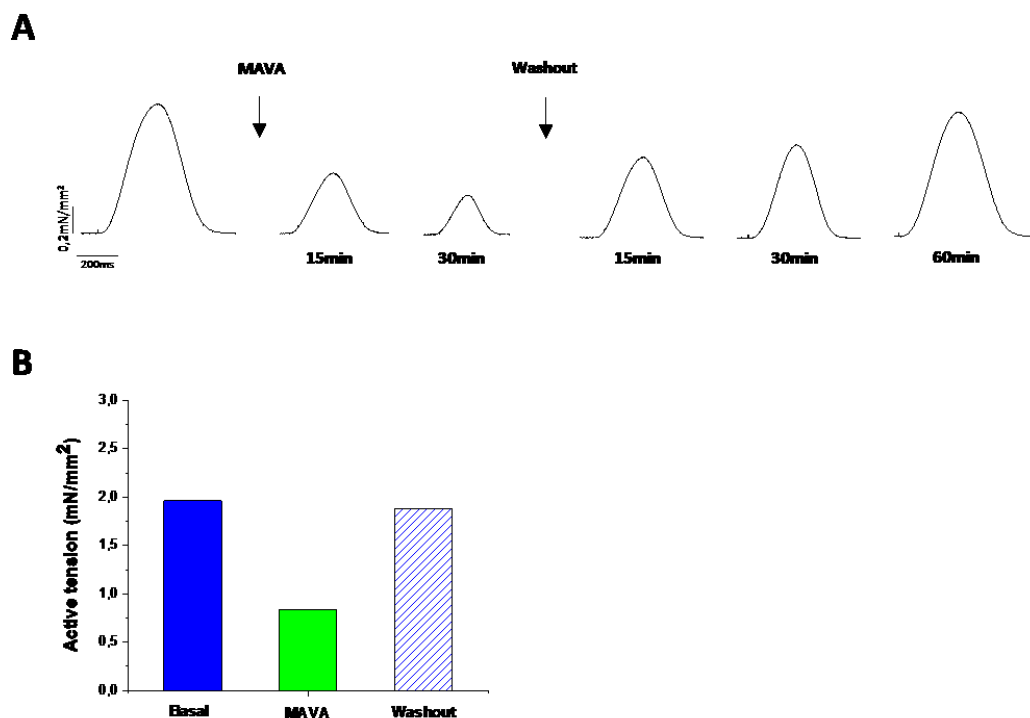
Figure 5.2. A) *Representative twitches traces at 1Hz during and after acute treatment with the MAVA 0.75μM at different time points.* *B)* *Active tension of ID3-EHT at 1Hz before, during, and after acute treatment with Mavacamten 0.75μM. EHTs were measured under isometric conditions at 37°C in Krebs-Henselheit solution with 0.5mM of [Ca^{2+}].*

5.2 Chronic effect of MAVACAMTEN in EHTs

In addition, we tested the long-term exposure of the drug on EHTs to assess any functional changes after prolonged treatment. We then exposed c.772G>A-EHT (ID3) for 20 days to two different concentrations of Mava, at 0.3 μM and 0.75 μM, which were the EC$_{50}$ calculated in the acute contractility experiments. As a sham control group, DMSO was added to the culture medium. Treatment with Mavacamten was started 15 days after the EHTs generation; before and during treatment we monitored and calculated the tension generated by spontaneous auxotonic contractions. As reported in **(Fig. 5.3)**, in untreated EHTs, tension increased gradually over time, while in the treated EHTs, contractile force was reduced (0.3 μM) or absent (0.7μM). After the 20 days of culture, MAVA was removed from the culture medium, and by optical analysis of pillar deflection we observed that in treated c.772G>A-EHTs tension increased again, confirming the reversible effect of the drug.
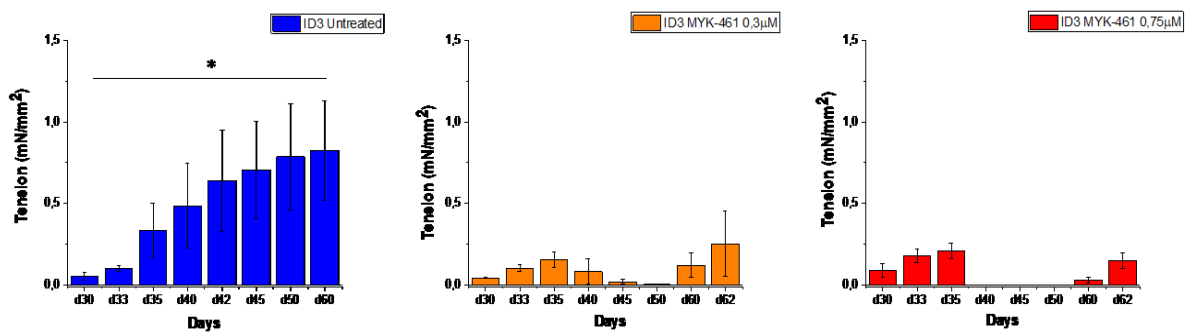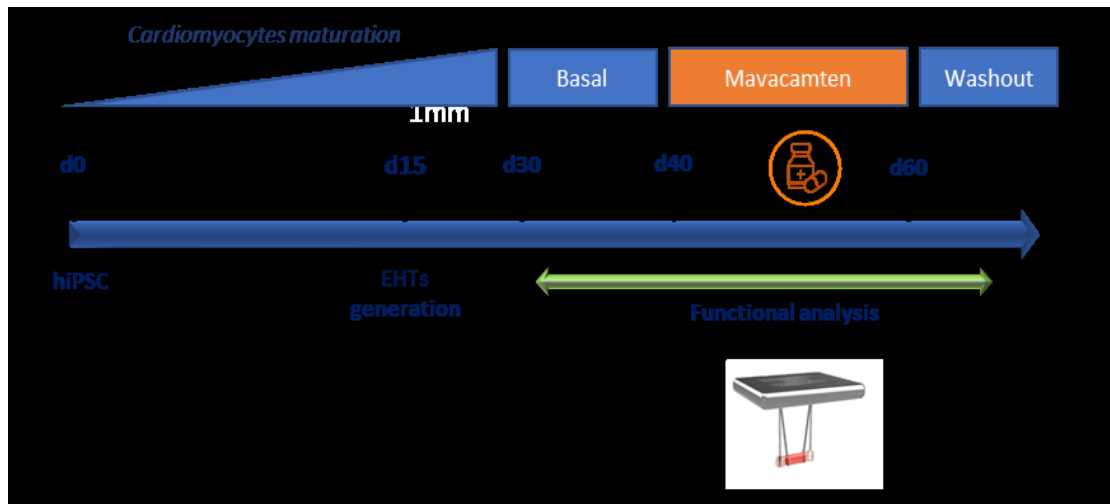
Figure 5.3. *Spontaneous auxotonic contractions of EHTs during chronic treatment with MAVA. Schematic representation of chronic treatment in culture and spontaneous auxotonic tension of c.772G>A-EHTs from day 30 to 60 of differentiation, measured at 37°C in RPMI/B27 culture medium (~0.4mM of [Ca^{2+}]) with and without Mavacamten (n=5). One-way analysis of variance (ANOVA) with a Tukey post-hoc test was used to compare the different time points. * p < 0.05 and ** p < 0.01 versus d30.*

The effect of chronic treatment on EHTs contractility was assessed around day 60 p.d. EHTs were mounted on the force recording apparatus under isometric conditions in response to a pacing frequency and in the absence of MAVA. By analyzing the active tension at 1Hz of stimulation, we observed that c.772G>A-EHTs previously treated chronically show reduced contractile force (ID3 MAVA 0.3µM= 0.52±0.19 mN/mm²; ID3 MAVA 0.75µM= 0.67±0.2 mN/mm²) compared with the respective control with DMSO (ID3 Untreated= 1.4±0.3 mN/mm²) **(Fig. 5.4B)**. In addition, the contraction time in c.772G>A-EHT (TTP and RT50%) seems to be not significantly affected by chronic treatment when compared with the DMSO control **(Fig. 5.4C-D)**.

F — Tension (mN/mm²) vs Extracellular [Ca⁺]

G — Twitch duration to RT50% (ms) vs Extracellular [Ca⁺]

Legend:
- ID3 Untreated
- ID3 MYK-461 0,3 μM
- ID3 MYK-461 0,75 μM
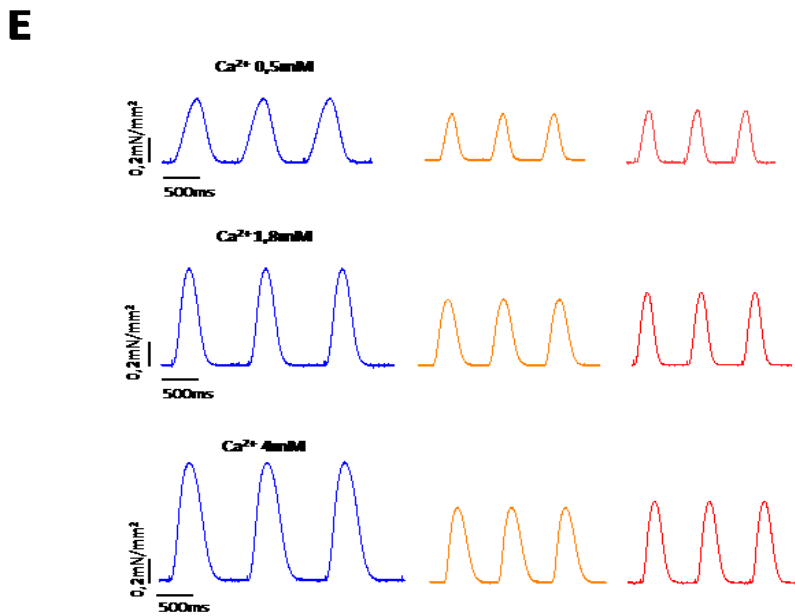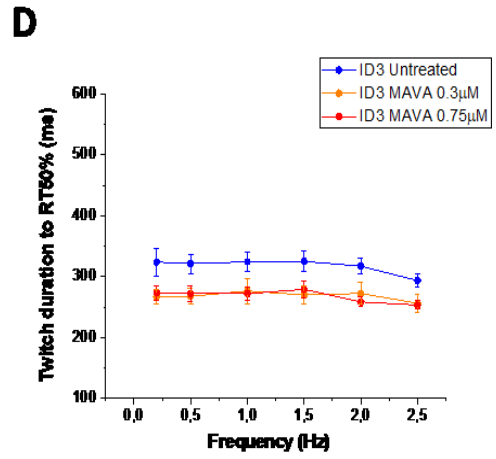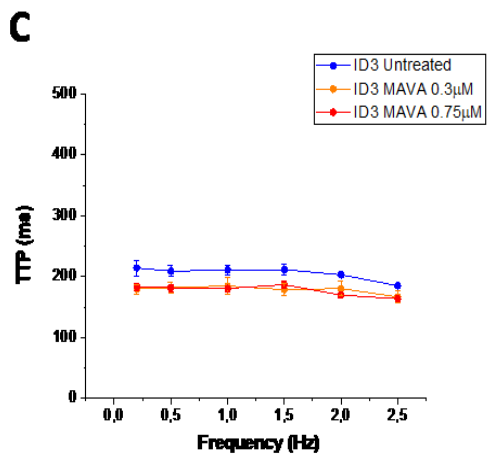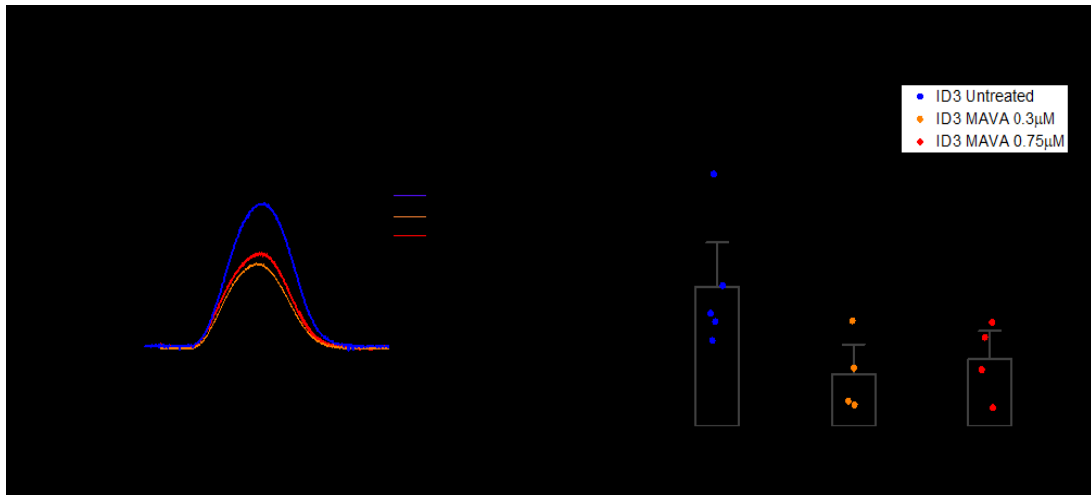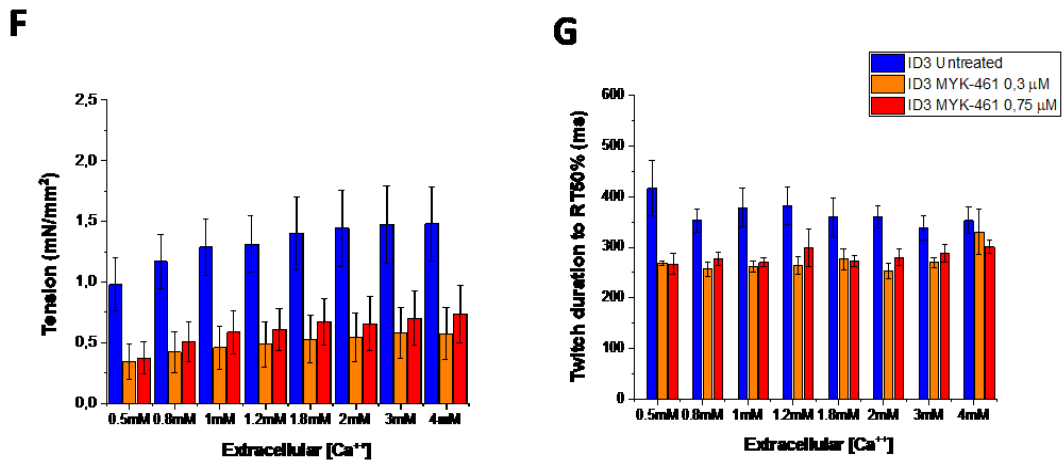
*Figure 5.4. Isometric contractile force in c.772G>A- EHT after chronic treatment. **A)** Representative twitches of untreated and MAVA-treated ID3-EHTs. **B)** Active tension at 1Hz constant pacing of c.772G>A-EHTs treated with Mavacamten 0.3μM and 0.75μM compared with untreated tissues. **C)** Time to peak and **D)** twitch duration at 50% of relaxation at 0.2-2.5Hz of c.772G>A-EHTs treated and untreated with MAVA. EHTs were measured in isometric conditions at 37°C in the Krebs-Henselheit solution with 1.8mM of [Ca²⁺] under imposed pacing (n=4). **E)** Representative twitches of untreated and MAVA-treated ID3-EHTs at 0,5mM, 1,8mM and 4mM of [Ca²⁺]. **F-G)** Force and RT50% measured in all EHTs upon changes of extracellular calcium concentration from 0.5 to 4mM (n=4). Statistical analysis was performed using one-way ANOVA with Tukey post-hoc test. No statistically significant differences emerged.*

The positive inotropic effect given by the gradual increase in extracellular calcium concentrations (from 0.5mM to 4mM) is visible in all ID3-EHTs, but as observed in the graph in **Fig. 5.4F**, the active tension remains lower in EHTs chronically treated with Mavacamten, but there are no statistically significant differences in contraction kinetics **(Fig. 5.4G)**.

For comparison, isogenic control EHTs were exposed to Mavacamten (0.3μM and 0.75μM) for 20 days.

A

Untreated
MYK-461 0,3µM
MYK-461 0,75µM

0,1mN/mm2
100ms

B

- c.ID3 Untreated
- c.ID3 MAVA 0.3µM
- c.ID3 MAVA 0,75µM

Tension (mN/mm²)

3,0
2,5
2,0
1,5
1,0
0,5
0,0

1Hz

C

- c.ID3 Untreated
- c.ID3 MYK-461 0,3uM
- c.ID3 MYK-461 0,75uM

TTP (ms)

500
400
300
200
100
0

0,0 0,5 1,0 1,5 2,0 2,5 3,0
Frequency (Hz)

D

- c.ID3 Untreated
- c.ID3 MYK-461 0,3uM
- c.ID3 MYK-461 0,75uM

Twitch duration to RT50% (ms)

600
500
400
300
200
100

0,0 0,5 1,0 1,5 2,0 2,5 3,0
Frequency (Hz)

E

Ca²⁺ 0,5mM
0,2mN/mm²
500ms

Ca²⁺ 1,8mM
0,2mN/mm²
500ms

Ca²⁺ 4mM
0,2mN/mm²
500ms

Figure 5.5. *Isometric contractile force in c.ID3- EHT after chronic treatment. **A)** Representative twitches of untreated and MAVA-treated c.ID3-EHTs. **B)** Active tension at 1Hz constant pacing of c.ID3-EHTs treated with Mavacamten 0.3μM and 0.75μM compared with untreated tissues. **C)** Time to peak and **D)** twitch duration at 50% of relaxation at 0.2-2.5Hz of c.ID3-EHTs treated and untreated with MAVA. EHTs were measured in isometric conditions at 37°C in the Krebs-Henselheit solution with 1.8mM of [Ca^{2+}] under imposed pacing (n=5). **E)** Representative twitches of untreated and MAVA-treated c.ID3-EHTs at 0,5mM, 1,8mM and 4mM of [Ca^{2+}]. **F-G)** Force and RT50% measured in all EHTs upon changes of extracellular calcium concentration from 0.5 to 4mM (n=6). Statistical analysis was performed using one-way ANOVA with Tukey post-hoc test. No statistically significant differences emerged.*

Also, in control EHTs, as in c.772G>A-EHTs, we observed that the contraction force recorded under isometric conditions after prolonged drug exposure tended to remain lower (c.ID3 MAVA 0.3μM= 0.69±0.35 mN/mm²; ID3 MAVA 0.75μM= 0.42± 0.17 mN/mm² than that generated by untreated EHTs (c.ID3 Untreated= 1.04±0.33 mN/mm²) **(Fig. 5.5B)**. Again, we observed a positive inotropic response by increasing extracellular Ca²⁺ concentrations in all conditions **(Fig. 5.5E)**, but we did not o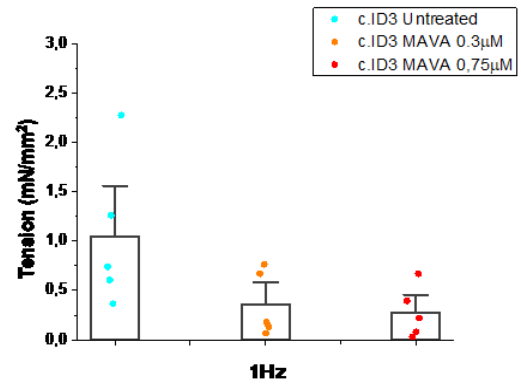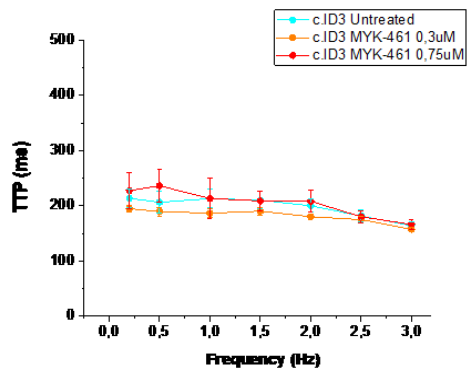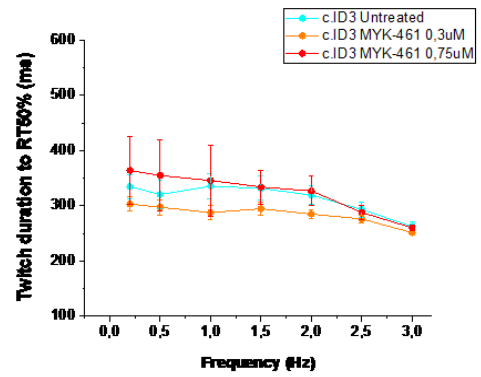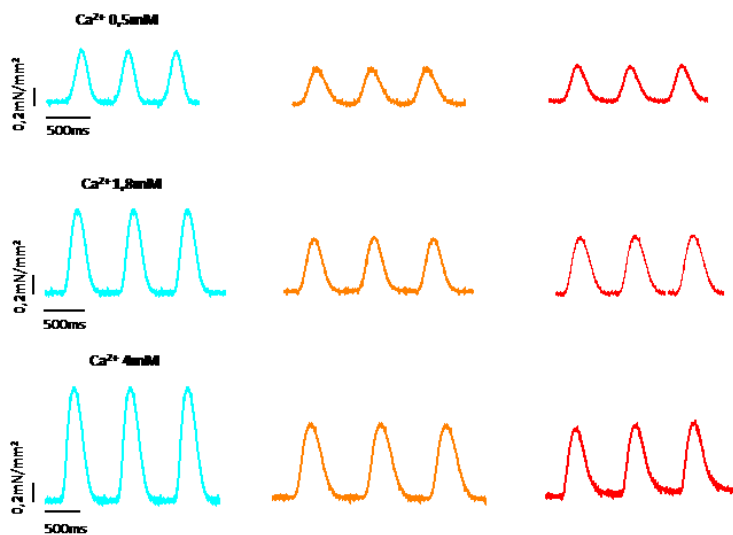bserve differences in contraction kinetics **(Fig. 5.5 C-D-F)**. Further experiments should be performed to confirm these data.

DISCUSSION

Hypertrophic cardiomyopathy (HCM) is a primary myocardial disease with a prevalence of one in 500 in different population cohorts. It is characterized by left ventricular (LV) hypertrophy and hyperdynamic contraction (B. J. Maron 2002, 2004). Many patients develop obstructive cardiomyopathy, with a high risk of heart failure, atrial fibrillation, and death (M. S. Maron et al. 2003; Ho et al. 2019). Some preclinical studies support the idea that the life-threatening ventricular arrhythmias in HCM depend, in part, on functional alterations occurring at the level of individual cardiomyocytes, so identification of specific targets at the cellular level could allow preventive action to slow disease progression. So far, the use of negative inotropic agents, including β-blockers, non-dihydropyridine calcium channel blockers, and disopyramide, has been recommended for pharmacological treatment of HCM to relieve symptoms. Because HCM-related mutations can increase the metabolic cost to maintain cardiac function, leading to a depressed energy state,

normalization of the hypercontractile phenotype can rebalance contractility in HCM. Recently, Mavacamten, an allosteric myosin inhibitor developed to reduce cardiac contractility and improve myocardial energetics, was approved by the FDA (Food and Drug Administration) for oHCM treatment. Mavacamten (Mava) can inhibit myosin heavy chain, thereby reducing the acto-myosin interaction and promoting decreased force generation. In patients with obstructive HCM, the recent randomized, placebo-controlled phase III EXPLORER-HCM clinical trial demonstrated the efficacy and safety of the drug in reducing the left ventricular (LV) outflow tract gradient and improving the health status of patients (Iacopo Olivotto et al. 2020). In addition, previous studies on human iPSC-derived cardiomyocytes (hiPSC-CMs) expressing HCM-related mutations revealed that Mavacamten normalizes pathological changes in intracellular Ca^{2+} handling in diseased cardiomyocytes (Green et al. 2016; Sparrow et al. 2020), and these effects appear to be related to a reduction in Ca^{2+} sensitivity of myofilaments. To understand whether Mavacamten may act in preventing upstream electrophysiological substrates that trigger ventricular arrhythmias, the hiPSC-CM model derived from HCM patients can be used, as they can recapitulate cellular mechanisms of the pre-hypertrophic stages of the disease. In several studies, the hiPSC-CMs model has been used to study the effects of Mava in vitro (Halas et al. 2022; Sewanan, Shen, and Campbell 2021). In this work, we used an hiPSC line derived from an HCM patient carrying the *MYBPC3*:c.772G>A mutation, previously characterized in comparison with patient myectomy samples, compared with its CRISPR-Cas9-corrected isogenic control line (c.ID3) (Josè Manuel Pioner et al. 2023). For this study, engineered heart tissues (EHTs) were generated to perform mechanistic investigations. The aim was to test the long-term effect of Mavacamten and verify the potential ability to prevent the disease progression at the cellular level. After generating the EHTs with hiPSC-CMs in early stages of maturation, the tissues were maintained in culture until day 50 post differentiation and finally recorded on a force-length recording apparatus in isometric conditions under external pacing. Initially, Mavacamten was acutely tested at different concentrations on both c.772G>A-EHT (ID3) and controls (c.ID3) to calculate the EC_{50}. Preliminary results show a different EC_{50} in the tension/mava concentration curve, suggesting different drug sensitivity between the mutated EHTs and the controls. Ongoing experiments will be performed to confirm these data. Furthermore, our results confirm that the effect of the drug is reversible and about an hour after washing, the contractile force rises again as in the baseline condition. For the evaluation of the chronic effect, we analyzed a set of EHTs exposed to two different Mava concentrations (0.3µM and 0.75µM), compared with the respective DMSO exposed control (ID3-Untreated and c.ID3 Untreated). Under Mava exposure in the culture medium, spontaneous contraction of ID3- and c.ID3-EHTs were monitored for 30 days, observing a partial contractile force reduction at 0.3µM and a total reduction at 0.75µM of MAVA. However, at the end of the treatment (MAVA washout) EHT spontaneous force increased again. Analysis of active tension under isometric conditions showed that treated tissues, both mutant (ID3-EHTs) and control (c.ID3-EHTs), had lower active tension than untreated ones. This could be due to a slowdown in the maturation process due to the reduction of contractility in the presence of Mava, but to confirm this, further structural investigations will have to be performed. On the other hand, in the ID3-EHTs it is observed that after prolonged treatment, the contraction kinetics are slightly faster than in the untreated ID3-EHT. Instead, in the control EHTs no difference in contraction kinetics was observed between the treated and untreated. These results could indicate an effect of Mavacamten on cross-bridge kinetics or calcium dynamics in the HCM model. Furthermore, positive inotropic effect related to increased extracellular calcium

concentrations is visible in all EHTs (ID3 and c.ID3), indicating that contractile reserve is preserved. Active tension shows an approximately 1.5-2-fold increase at high calcium concentration (4mM), although it remains lower in drug-treated EHTs. In conclusion, EHTs seem to represent a useful tool to study the acute and long-term effect of drugs, even if further investigations are needed.

For this work, It will be necessary to carry out structural and molecular analyses; It will be interesting to observe the localization and intracellular organization of some target proteins to evaluate the myofilament and membrane organization, the density of the T-tubule, and the SR structure. Furthermore, transcriptome analysis of all drug-exposed EHTs is ongoing, to evaluate any changes in gene expression following chronic treatment. These results suggest that MAVA chronic effect can prevent intracellular pathways that are altered in the early stages after cardiac differentiation. From a biophysical perspective this is also relevant to use MAVA as a tool to investigate the impact of mechanical force production during cardiac cell/tissue development.

Chapter 6

CONCLUSIONS

In this work, we used the hiPSC-CMs model as a tool for modeling genetic cardiomyopathies (HCM and DCM) to understand the alterations underlying these diseases and for drug screening. The undeveloped phenotype of hiPSC-CMs is the limiting aspect that still hinders their potential benefits. In recent years, however, several technologies have been developed that enable the generation of cell and tissue models that more accurately reflect the situation in vivo, providing optimized platforms for drug testing, tissue regenerative approaches, and personalized medicine. These new approaches can promote the development of cultured hiPSC-CMs toward an adult phenotype.

In this thesis work two approaches are described that can improve the hiPSC-CMs maturation, such as biomaterial-based micropatterned substrates (2D system) and engineered cardiac tissues (3D system), which allow us to get closer to the native model and perform functional analysis and drug testing. Engineered cardiac tissues allowed us to perform functional analysis, using techniques that in our laboratory in Florence are normally used to perform studies on myocardial trabeculae, obtained from patients undergoing myectomy. We have demonstrated here the agreement between patient tissues and hiPSC cardiomyocyte models, showing that hiPSC-CMs are indeed a valuable model for electrophysiological and mechanical studies. In summary, therefore, hiPSC-CMs can be used as an alternative tool to model certain diseases *in vitro* and to study known mutations or suspected variants that may contribute to abnormal electrical activity in the heart.

New devices for hiPSC-CMs growth

One of the next goals will be to grow hiPSC-CMs on new materials, namely liquid crystal elastomers (LCEs), which are novel materials that can contract in response to light stimuli and can be used as novel cardiac contractile assist devices. Previous studies have shown that these materials are biocompatible and promote cell alignment and maturation (Martella et al. 2017). Following these results, we want to evaluate the influence of LCEs on cardiomyocyte growth, maturation, and function under long-term contact conditions and the possibility of creating hybrid devices consisting of LCEs coupled to engineered cardiac tissues.
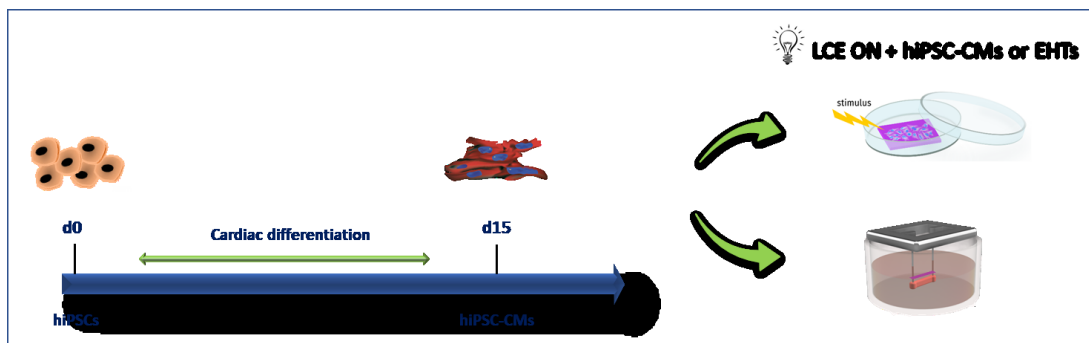
Figure 6.1. Graphical representation of LCEs as a dynamic cell scaffold with hiPSC-CMs

New perspectives for cardiac disease study using hiPSC-CMs

An additional goal will be to perform atrial-like specific differentiation of hiPSC-CMs to further our studies in HCM and also to investigate the mechanisms underlying atrial fibrillation (AF), which is the most common sustained arrhythmia in HCM (Vaidya, Semsarian, and Chan 2017), with a reported prevalence of approximately 20% to 25% (I. Olivotto et al. 2001). It is also known that atrial fibrillation is associated with a hypercoagulation state due to upregulation of FXa, a key component of the coagulation cascade, which can induce PAR receptor activation (Protease-activated receptors). Altered activation of these receptors may contribute to the development of various disorders, such as atherosclerosis and atrial fibrillation (Spronk et al. 2014).

Aberrant activation of the coagulation pathway underlies many fibroproliferative disorders and inflammation. In vitro studies have shown that FXa can induce the expression of pro-inflammatory cytokines. In cardiac fibroblasts, it has been observed that FXa induces upregulation of pro-inflammatory genes and that the use of rivaroxaban can reduce the inflammatory response (D'Alessandro et al. 2021). In collaboration with Maastricht University, I was involved in the study of the possible direct or indirect role of FXa on cardiomyocytes. Our approach was to evaluate the induction of gene expression of hypertrophic markers in the presence of hypertrophic stimuli to study the effects of FXa on cardiomyocytes. We also tested whether in the presence of factorial inhibitors, such as rivaroxaban, there were changes in hypertrophic markers expression and PARs receptors. Mouse and rat cardiomyocyte cell models were used to perform these experiments, and gene expression of brain-type natriuretic peptide (BNP) and atrial natriuretic peptide (ANP) were analyzed as sensitive markers of a hypertrophic response. A good response to stimulation with FXa was obtained only on adult rat cardiomyocytes.
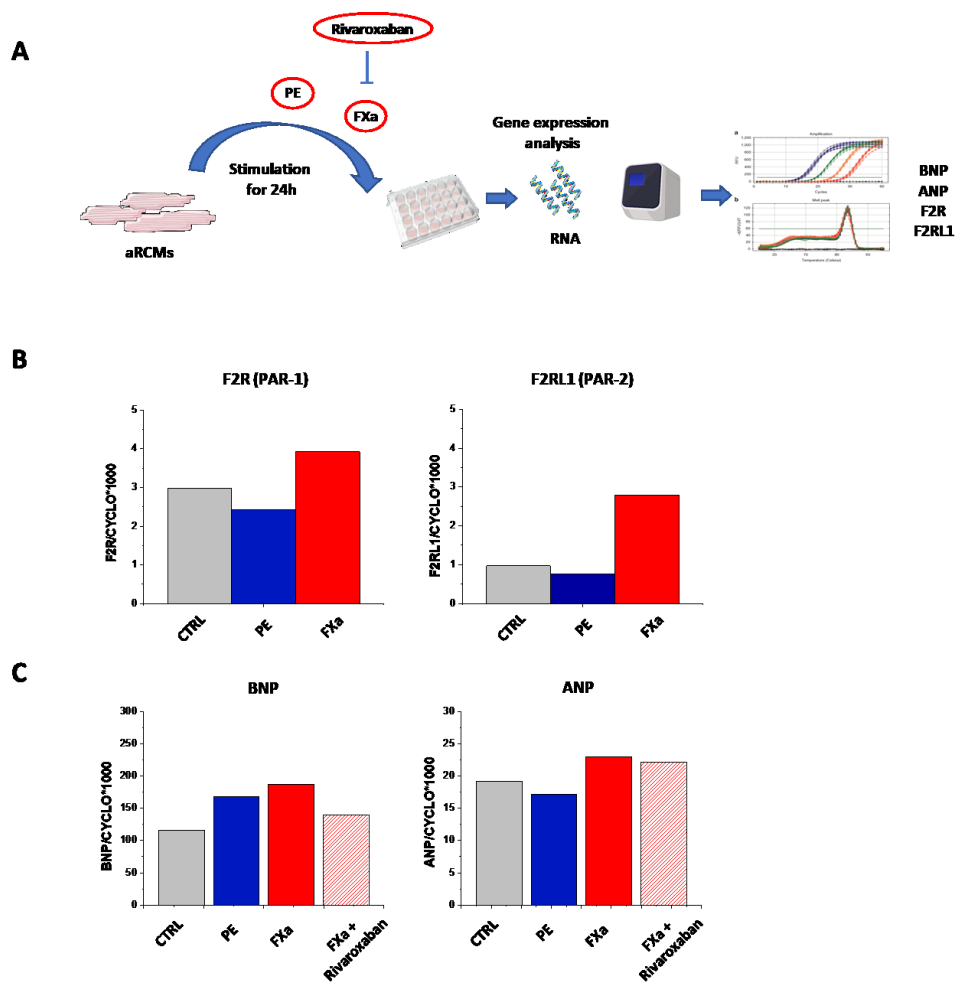
Figure 6.2. *Hypertrophic response in adult rat cardiomyocytes (aRCMs).* ***A)*** *Schematic representation of aRCMs stimulation (24h) with FXa (100nM) and phenylephrine (PE) (100µM) and gene expression analysis of BNP, ANP, F2R and F2RL1.* ***B)*** *Effect of PE and FXa on mRNA expression of F2r (PAR-1 gene) and F2rl1 (PAR-2 gene).* ***C)*** *Effect of PE, FXa and Rivaroxaban on mRNA expression of BNP and ANP. Gene expression was measured by RT-qPCR. Data were normalized to the housekeeping gene Cyclophilin-A.*

Despite the promising results, this cell model has limited availability and it is not possible to keep it in culture for a long time.

Therefore, we thought it would be appropriate to use a different cell model, such as hiPSC-CMs, which could be a good tool to study the hypertrophic effect of FXa, as they are a human model and can be kept in culture for long term. So, the next step will be to evaluate the expression of PAR receptors in hiPSC-CMs to subsequently study the effect of FXa *in vitro* and Rivaroxaban treatment.

References

Ababou, Abdessamad, Mathias Gautel, and Mark Pfuhl. 2007. "Dissecting the N-Terminal Myosin Binding Site of Human Cardiac Myosin-Binding Protein C. Structure and Myosin Binding of Domain C2." *The Journal of Biological Chemistry* 282 (12): 9204–15.

Ababou, Abdessamad, Elena Rostkova, Shreena Mistry, Clare Le Masurier, Mathias Gautel, and Mark Pfuhl. 2008. "Myosin Binding Protein C Positioned to Play a Key Role in Regulation of Muscle Contraction: Structure and Interactions of Domain C1." *Journal of Molecular Biology* 384 (3): 615–30.

Ader, Flavie, Pascal De Groote, Patricia Réant, Caroline Rooryck-Thambo, Delphine Dupin-Deguine, Caroline Rambaud, Diala Khraiche, et al. 2019. "FLNC Pathogenic Variants in Patients with Cardiomyopathies: Prevalence and Genotype-Phenotype Correlations." *Clinical Genetics* 96 (4): 317–29.

Adorisio, Rachele, Erica Mencarelli, Nicoletta Cantarutti, Camilla Calvieri, Liliana Amato, Marianna Cicenia, Massimo Silvetti, et al. 2020. "Duchenne Dilated Cardiomyopathy: Cardiac Management from Prevention to Advanced Cardiovascular Therapies." *Journal of Clinical Medicine Research* 9 (10). https://doi.org/10.3390/jcm9103186.

Amin, Ahmad S., Hanno L. Tan, and Arthur A. M. Wilde. 2010. "Cardiac Ion Channels in Health and Disease." *Heart Rhythm*. https://doi.org/10.1016/j.hrthm.2009.08.005.

Anastasakis, Aris, and Cristina Basso. 2018. "'Primary' Dilated Hearts." *International Journal of Cardiology* 257 (April): 366–70.

Andersen, Paal S., Ole Havndrup, Henning Bundgaard, Lars A. Larsen, Jens Vuust, Anders K. Pedersen, Keld Kjeldsen, and Michael Christiansen. 2004. "Genetic and Phenotypic Characterization of Mutations in Myosin-Binding Protein C (MYBPC3) in 81 Families with Familial Hypertrophic Cardiomyopathy: Total or Partial Haploinsufficiency." *European Journal of Human Genetics: EJHG* 12 (8): 673–77.

Anderson, Robert L., Darshan V. Trivedi, Saswata S. Sarkar, Marcus Henze, Weikang Ma, Henry Gong, Christopher S. Rogers, et al. 2018. "Deciphering the Super Relaxed State of Human β-Cardiac Myosin and the Mode of Action of Mavacamten from Myosin Molecules to Muscle Fibers." *Proceedings of the National Academy of Sciences of the United States of America* 115 (35): E8143–52.

Ashrafian, Houman, Charles Redwood, Edward Blair, and Hugh Watkins. 2003. "Hypertrophic Cardiomyopathy: a Paradigm for Myocardial Energy Depletion." *Trends in Genetics: TIG* 19 (5): 263–68.

Ather, Sameer, Wei Wang, Qiongling Wang, Na Li, Mark E. Anderson, and Xander H. T. Wehrens. 2013. "Inhibition of CaMKII Phosphorylation of RyR2 Prevents Inducible Ventricular Arrhythmias in Mice with Duchenne Muscular Dystrophy." *Heart Rhythm: The Official Journal of the Heart Rhythm Society* 10 (4): 592–99.

Banyasz, Tamas, Ilya Lozinskiy, Charles E. Payne, Stephanie Edelmann, Byron Norton, Biyi Chen, Ye Chen-Izu, Leighton T. Izu, and C. William Balke. 2008. "Transformation of Adult Rat Cardiac Myocytes in Primary Culture." *Experimental Physiology*. https://doi.org/10.1113/expphysiol.2007.040659.

Bardswell, Sonya C., Friederike Cuello, Alexandra J. Rowland, Sakthivel Sadayappan, Jeffrey Robbins, Mathias Gautel, Jeffery W. Walker, Jonathan C. Kentish, and Metin Avkiran. 2010. "Distinct Sarcomeric Substrates Are Responsible for Protein Kinase D-Mediated Regulation of Cardiac Myofilament Ca2+ Sensitivity and Cross-Bridge Cycling." *The Journal of Biological Chemistry* 285 (8): 5674–82.

Barefield, David, and Sakthivel Sadayappan. 2010. "Phosphorylation and Function of Cardiac Myosin Binding Protein-C in Health and Disease." *Journal of Molecular and Cellular Cardiology* 48 (5): 866–75.

Basso, C., G. Thiene, D. Corrado, G. Buja, P. Melacini, and A. Nava. 2000. "Hypertrophic Cardiomyopathy and Sudden Death in the Young: Pathologic Evidence of Myocardial Ischemia." *Human Pathology* 31 (8): 988–98.

Beauchamp, Philippe, Wolfgang Moritz, Jens M. Kelm, Nina D. Ullrich, Irina Agarkova, Blake D. Anson, Thomas M. Suter, and Christian Zuppinger. 2015. "Development and Characterization of a Scaffold-Free 3D Spheroid Model of Induced Pluripotent Stem Cell-Derived Human Cardiomyocytes." *Tissue Engineering. Part C, Methods* 21 (8): 852–61.

Bedada, Fikru B., Sunny S-K Chan, Stefania K. Metzger, Liying Zhang, Jianyi Zhang, Daniel J. Garry, Timothy J. Kamp, Michael Kyba, and Joseph M. Metzger. 2014. "Acquisition of a Quantitative, Stoichiometrically Conserved Ratiometric Marker of Maturation Status in Stem Cell-Derived Cardiac Myocytes." *Stem Cell Reports* 3 (4): 594–605.

Bedada, Fikru B., Matthew Wheelwright, and Joseph M. Metzger. 2016. "Maturation Status of Sarcomere Structure and Function in Human iPSC-Derived Cardiac Myocytes." *Biochimica et Biophysica Acta* 1863 (7 Pt B): 1829–38.

Bellinger, Andrew M., Steven Reiken, Christian Carlson, Marco Mongillo, Xiaoping Liu, Lisa Rothman, Stefan Matecki, Alain Lacampagne, and Andrew R. Marks. 2009. "Hypernitrosylated Ryanodine Receptor Calcium Release Channels Are Leaky in Dystrophic Muscle." *Nature Medicine* 15 (3): 325–30.

Belus, Alexandra, Nicoletta Piroddi, Beatrice Scellini, Chiara Tesi, Giulia D'Amati, Francesca Girolami, Magdi Yacoub, Franco Cecchi, Iacopo Olivotto, and Corrado Poggesi. 2008. "The Familial Hypertrophic Cardiomyopathy-Associated Myosin Mutation R403Q Accelerates Tension Generation and Relaxation of Human Cardiac Myofibrils." *The Journal of Physiology* 586 (15): 3639–44.

Ben Jehuda, Ronen, Yuval Shemer, and Ofer Binah. 2018. "Genome Editing in Induced Pluripotent Stem Cells Using CRISPR/Cas9." *Stem Cell Reviews and Reports* 14 (3): 323–36.

Bers, Donald M. 2002. "Cardiac Excitation-Contraction Coupling." *Nature* 415 (6868): 198–205.

Bertero, Alessandro, Paul A. Fields, Alec S. T. Smith, Andrea Leonard, Kevin Beussman, Nathan J. Sniadecki, Deok-Ho Kim, et al. 2019. "Chromatin Compartment Dynamics in a Haploinsufficient Model of Cardiac Laminopathy." *The Journal of Cell Biology* 218 (9): 2919–44.

Beuckelmann, D. J., M. Näbauer, and E. Erdmann. 1992. "Intracellular Calcium Handling in Isolated Ventricular Myocytes from Patients with Terminal Heart Failure." *Circulation* 85 (3): 1046–55.

Bhagwan, Jamie R., Diogo Mosqueira, Karolina Chairez-Cantu, Ingra Mannhardt, Sara E. Bodbin, Mine Bakar, James G. W. Smith, and Chris Denning. 2020. "Isogenic Models of Hypertrophic Cardiomyopathy Unveil Differential Phenotypes and Mechanism-Driven Therapeutics." *Journal of Molecular and Cellular Cardiology* 145 (August): 43–53.

Bhavsar, P. K., G. K. Dhoot, D. V. Cumming, G. S. Butler-Browne, M. H. Yacoub, and P. J. Barton. 1991. "Developmental Expression of Troponin I Isoforms in Fetal Human Heart." *FEBS Letters* 292 (1-2): 5–8.

Bielawski, Kevin S., Andrea Leonard, Shiv Bhandari, Chuck E. Murry, and Nathan J. Sniadecki. 2016. "Real-Time Force and Frequency Analysis of Engineered Human Heart Tissue Derived from Induced Pluripotent Stem Cells Using Magnetic Sensing." *Tissue Engineering. Part C, Methods* 22 (10): 932–40.

Bird, S. 2003. "The Human Adult Cardiomyocyte Phenotype." *Cardiovascular Research*. https://doi.org/10.1016/s0008-6363(03)00253-0.

Birket, Matthew J., Marcelo C. Ribeiro, Georgios Kosmidis, Dorien Ward, Ana Rita Leitoguinho, Vera van de Pol, Cheryl Dambrot, et al. 2015. "Contractile Defect Caused by Mutation in MYBPC3 Revealed under Conditions Optimized for Human PSC-Cardiomyocyte Function." *Cell Reports* 13 (4): 733–45.

Boateng, Samuel Y., and Paul H. Goldspink. 2008. "Assembly and Maintenance of the Sarcomere Night and Day." *Cardiovascular Research* 77 (4): 667–75.

Bondue, Antoine, Eloisa Arbustini, Anna Bianco, Michele Ciccarelli, Dana Dawson, Matteo De Rosa, Nazha Hamdani, et al. 2018. "Complex Roads from Genotype to Phenotype in Dilated Cardiomyopathy: Scientific Update from the Working Group of Myocardial Function of the European Society of Cardiology." *Cardiovascular Research* 114 (10): 1287–1303.

Bonne, G., L. Carrier, J. Bercovici, C. Cruaud, P. Richard, B. Hainque, M. Gautel, et al. 1995. "Cardiac Myosin Binding Protein-C Gene Splice Acceptor Site Mutation Is Associated with Familial Hypertrophic Cardiomyopathy." *Nature Genetics* 11 (4): 438–40.

Borovjagin, Anton V., Brenda M. Ogle, Joel L. Berry, and Jianyi Zhang. 2017. "From Microscale Devices to 3D Printing: Advances in Fabrication of 3D Cardiovascular Tissues." *Circulation Research* 120 (1): 150–65.

Bosman, Alexis, Laura Sartiani, Valentina Spinelli, Martina Del Lungo, Francesca Stillitano, Daniele Nosi, Alessandro Mugelli, Elisabetta Cerbai, and Marisa Jaconi. 2013. "Molecular and Functional Evidence of HCN4 and Caveolin-3 Interaction during Cardiomyocyte Differentiation from Human Embryonic Stem Cells." *Stem Cells and Development* 22 (11): 1717–27.

Bremner, Samantha B., Christian J. Mandrycky, Andrea Leonard, Ruby M. Padgett, Alan R. Levinson, Ethan S. Rehn, J. Manuel Pioner, Nathan J. Sniadecki, and David L. Mack. 2022. "Full-Length Dystrophin Deficiency Leads to Contractile and Calcium Transient Defects in Human Engineered Heart Tissues." *Journal of Tissue Engineering* 13 (August): 20417314221119628.

Brenner, B. 1988. "Effect of Ca2+ on Cross-Bridge Turnover Kinetics in Skinned Single Rabbit Psoas Fibers: Implications for Regulation of Muscle Contraction." *Proceedings of the National Academy of Sciences of the United States of America* 85 (9): 3265–69.

Brixius, K., R. Lu, B. Boelck, S. Grafweg, F. Hoyer, C. Pott, U. Mehlhorn, W. Bloch, and R. H. G. Schwinger. 2007. "Chronic Treatment with Carvedilol Improves Ca^{2+}-Dependent ATP Consumption in Triton X-Skinned Fiber Preparations of Human Myocardium." *The Journal of Pharmacology and Experimental Therapeutics* 322 (1): 222–27.

Broughton, K. M., J. Li, E. Sarmah, C. M. Warren, Y-H Lin, M. P. Henze, V. Sanchez-Freire, R. J. Solaro, and B. Russell. 2016. "A Myosin Activator Improves Actin Assembly and Sarcomere Function of Human-Induced Pluripotent Stem Cell-Derived Cardiomyocytes with a Troponin T Point Mutation." *American Journal of Physiology. Heart and Circulatory Physiology* 311 (1): H107–17.

Burdick, Jason A., and Gordana Vunjak-Novakovic. 2009. "Engineered Microenvironments for Controlled Stem Cell Differentiation." *Tissue Engineering. Part A* 15 (2): 205–19.

Burridge, Paul W., Sebastian Diecke, Elena Matsa, Arun Sharma, Haodi Wu, and Joseph C. Wu. 2015. "Modeling Cardiovascular Diseases with Patient-Specific Human Pluripotent Stem Cell-Derived Cardiomyocytes." *Methods in Molecular Biology*. https://doi.org/10.1007/7651_2015_196.

Burridge, Paul W., Gordon Keller, Joseph D. Gold, and Joseph C. Wu. 2012. "Production of De Novo Cardiomyocytes: Human Pluripotent Stem Cell Differentiation and Direct Reprogramming." *Cell Stem Cell*. https://doi.org/10.1016/j.stem.2011.12.013.

Cai, Jinglei, Wen Li, Huanxing Su, Dajiang Qin, Jiayin Yang, Fan Zhu, Jianyong Xu, et al. 2010. "Generation of Human Induced Pluripotent Stem Cells from Umbilical Cord Matrix and Amniotic Membrane Mesenchymal Cells." *Journal of Biological Chemistry*. https://doi.org/10.1074/jbc.m109.086389.

Campbell, Matthew D., Marc Witcher, Anoop Gopal, and Daniel E. Michele. 2016. "Dilated Cardiomyopathy Mutations in δ-Sarcoglycan Exert a Dominant-Negative Effect on Cardiac Myocyte Mechanical Stability." *American Journal of Physiology. Heart and Circulatory Physiology* 310 (9): H1140–50.

Campostrini, Giulia, Viviana Meraviglia, Elisa Giacomelli, Ruben W. J. van Helden, Loukia Yiangou, Richard P. Davis, Milena Bellin, Valeria V. Orlova, and Christine L. Mummery. 2021. "Generation, Functional Analysis and Applications of Isogenic Three-Dimensional Self-Aggregating Cardiac Microtissues from Human Pluripotent Stem Cells." *Nature Protocols* 16 (4): 2213–56.

Carrier, L., G. Bonne, E. Bährend, B. Yu, P. Richard, F. Niel, B. Hainque, et al. 1997. "Organization and Sequence of Human Cardiac Myosin Binding Protein C Gene (MYBPC3) and Identification of Mutations Predicted to Produce Truncated Proteins in Familial Hypertrophic Cardiomyopathy." *Circulation Research* 80 (3): 427–34.

Carrier, Lucie, Giulia Mearini, Konstantina Stathopoulou, and Friederike Cuello. 2015. "Cardiac Myosin-Binding Protein C (MYBPC3) in Cardiac Pathophysiology." *Gene* 573 (2): 188–97.

Carson, Daniel, Marketa Hnilova, Xiulan Yang, Cameron L. Nemeth, Jonathan H. Tsui, Alec S. T. Smith, Alex Jiao, et al. 2016. "Nanotopography-Induced Structural Anisotropy and Sarcomere Development in Human Cardiomyocytes Derived from Induced Pluripotent Stem Cells." *ACS Applied Materials & Interfaces* 8 (34): 21923–32.

Ceholski, Delaine K., Irene C. Turnbull, Chi-Wing Kong, Simon Koplev, Joshua Mayourian, Przemek A. Gorski, Francesca Stillitano, et al. 2018. "Functional and Transcriptomic Insights into Pathogenesis of R9C Phospholamban Mutation Using Human Induced Pluripotent Stem Cell-Derived Cardiomyocytes." *Journal of Molecular and Cellular Cardiology* 119 (June): 147–54.

Chang, Alex C. Y., Andrew C. H. Chang, Anna Kirillova, Koki Sasagawa, Willis Su, Gerhard Weber, Jue Lin, et al. 2018. "Telomere Shortening Is a Hallmark of Genetic Cardiomyopathies." *Proceedings of the National Academy of Sciences of the United States of America* 115 (37): 9276–81.

Chang, Alex C. Y., Gaspard Pardon, Andrew C. H. Chang, Haodi Wu, Sang-Ging Ong, Asuka Eguchi, Sara Ancel, et al. 2021. "Increased Tissue Stiffness Triggers Contractile Dysfunction and Telomere Shortening in Dystrophic Cardiomyocytes." *Stem Cell Reports* 16 (9): 2169–81.

Chan, Yau-Chi, Sherwin Ting, Yee-Ki Lee, Kwong-Man Ng, Jiao Zhang, Zi Chen, Chung-Wah Siu, Steve K. W. Oh, and Hung-Fat Tse. 2013. "Electrical Stimulation Promotes Maturation of Cardiomyocytes Derived from Human Embryonic Stem Cells." *Journal of Cardiovascular Translational Research*. https://doi.org/10.1007/s12265-013-9510-z.

Chin, Mark H., Mike J. Mason, Wei Xie, Stefano Volinia, Mike Singer, Cory Peterson, Gayane Ambartsumyan, et al. 2009. "Induced Pluripotent Stem Cells and Embryonic Stem Cells Are Distinguished by Gene Expression Signatures." *Cell Stem Cell*. https://doi.org/10.1016/j.stem.2009.06.008.

Chopra, Anant, Matthew L. Kutys, Kehan Zhang, William J. Polacheck, Calvin C. Sheng, Rebeccah J. Luu, Jeroen Eyckmans, et al. 2018. "Force Generation via β-Cardiac Myosin, Titin, and α-Actinin Drives Cardiac Sarcomere Assembly from Cell-Matrix Adhesions." *Developmental Cell* 44 (1): 87–96.e5.

Clements, Mike, and Nick Thomas. 2014. "High-Throughput Multi-Parameter Profiling of Electrophysiological Drug Effects in Human Embryonic Stem Cell Derived Cardiomyocytes Using Multi-Electrode Arrays." *Toxicological Sciences*. https://doi.org/10.1093/toxsci/kfu084.

Cohn, Rachel, Ketan Thakar, Andre Lowe, Feria A. Ladha, Anthony M. Pettinato, Robert Romano, Emily Meredith, et al. 2019. "A Contraction Stress Model of Hypertrophic Cardiomyopathy due to Sarcomere Mutations." *Stem Cell Reports* 12 (1): 71–83.

Collins, Francis S., and Harold Varmus. 2015. "A New Initiative on Precision Medicine." *New England Journal of Medicine*. https://doi.org/10.1056/nejmp1500523.

Cong, Le, F. Ann Ran, David Cox, Shuailiang Lin, Robert Barretto, Naomi Habib, Patrick D. Hsu, et al. 2013. "Multiplex Genome Engineering Using CRISPR/Cas Systems." *Science* 339 (6121): 819–23.

Coppini, Raffaele, Cecila Ferrantini, Alessandro Aiazzi, Luca Mazzoni, Laura Sartiani, Alessandro Mugelli, Corrado Poggesi, and Elisabetta Cerbai. 2014. "Isolation and Functional Characterization of Human Ventricular Cardiomyocytes from Fresh Surgical Samples." *Journal of Visualized Experiments: JoVE*, no. 86 (April). https://doi.org/10.3791/51116.

Coppini, Raffaele, Cecilia Ferrantini, Josè Manuel Pioner, Lorenzo Santini, Zhinuo J. Wang, Chiara Palandri, Marina Scardigli, et al. 2019. "Electrophysiological and Contractile Effects of Disopyramide in Patients With Obstructive Hypertrophic Cardiomyopathy: A Translational Study." *JACC. Basic to Translational Science* 4 (7): 795–813.

Coppini, Raffaele, Cecilia Ferrantini, Lina Yao, Peidong Fan, Martina Del Lungo, Francesca Stillitano, Laura Sartiani, et al. 2013. "Late Sodium Current Inhibition Reverses Electromechanical Dysfunction in Human Hypertrophic Cardiomyopathy." *Circulation* 127 (5): 575–84.

Coppini, Raffaele, Luca Mazzoni, Cecilia Ferrantini, Francesca Gentile, Josè Manuel Pioner, Annunziatina Laurino, Lorenzo Santini, et al. 2017. "Ranolazine Prevents Phenotype Development in a Mouse Model of Hypertrophic Cardiomyopathy." *Circulation: Heart Failure*. https://doi.org/10.1161/circheartfailure.116.003565.

Crescioli, Clara, Roberta Squecco, Lorenzo Cosmi, Mariangela Sottili, Stefania Gelmini, Elisa Borgogni, Erica Sarchielli, et al. 2008. "Immunosuppression in Cardiac Graft Rejection: A Human in Vitro Model to Study the Potential Use of New Immunomodulatory Drugs." *Experimental Cell Research* 314 (6): 1337–50.

D'Alessandro, Elisa, Billy Scaf, Chantal Munts, Arne van Hunnik, Christopher J. Trevelyan, Sander Verheule, Henri M. H. Spronk, et al. 2021. "Coagulation Factor Xa Induces Proinflammatory Responses in Cardiac Fibroblasts via Activation of Protease-Activated Receptor-1." *Cells* 10 (11). https://doi.org/10.3390/cells10112958.

De Lange, Willem J., Adrian C. Grimes, Laura F. Hegge, Alexander M. Spring, Taylor M. Brost, and J. Carter Ralphe. 2013.

"E258K HCM-Causing Mutation in Cardiac MyBP-C Reduces Contractile Force and Accelerates Twitch Kinetics by Disrupting the cMyBP-C and Myosin S2 Interaction." *The Journal of General Physiology* 142 (3): 241–55.

DeWitt, Megan M., Heather M. MacLeod, Betty Soliven, and Elizabeth M. McNally. 2006. "Phospholamban R14 Deletion Results in Late-Onset, Mild, Hereditary Dilated Cardiomyopathy." *Journal of the American College of Cardiology* 48 (7): 1396–98.

Dhandapany, Perundurai S., Sakthivel Sadayappan, Yali Xue, Gareth T. Powell, Deepa Selvi Rani, Prathiba Nallari, Taranjit Singh Rai, et al. 2009. "A Common MYBPC3 (cardiac Myosin Binding Protein C) Variant Associated with Cardiomyopathies in South Asia." *Nature Genetics* 41 (2): 187–91.

Dijk, Sabine J. van, Dennis Dooijes, Cris dos Remedios, Michelle Michels, Jos M. J. Lamers, Saul Winegrad, Saskia Schlossarek, et al. 2009. "Cardiac Myosin-Binding Protein C Mutations and Hypertrophic Cardiomyopathy: Haploinsufficiency, Deranged Phosphorylation, and Cardiomyocyte Dysfunction." *Circulation* 119 (11): 1473–83.

Di Pasquale, E., F. Lodola, M. Miragoli, M. Denegri, J. E. Avelino-Cruz, M. Buonocore, H. Nakahama, et al. 2013. "CaMKII Inhibition Rectifies Arrhythmic Phenotype in a Patient-Specific Model of Catecholaminergic Polymorphic Ventricular Tachycardia." *Cell Death & Disease* 4 (10): e843.

Dolnikov, Katya, Mark Shilkrut, Naama Zeevi-Levin, Sharon Gerecht-Nir, Michal Amit, Asaf Danon, Joseph Itskovitz-Eldor, and Ofer Binah. 2006. "Functional Properties of Human Embryonic Stem Cell–Derived Cardiomyocytes: Intracellular Ca2 Handling and the Role of Sarcoplasmic Reticulum in the Contraction." *Stem Cells*. https://doi.org/10.1634/stemcells.2005-0036.

Doss, Michael Xavier, José M. Di Diego, Robert J. Goodrow, Yuesheng Wu, Jonathan M. Cordeiro, Vladislav V. Nesterenko, Héctor Barajas-Martínez, et al. 2012. "Maximum Diastolic Potential of Human Induced Pluripotent Stem Cell-Derived Cardiomyocytes Depends Critically on I(Kr)." *PloS One* 7 (7): e40288.

Doudna, Jennifer A., and Emmanuelle Charpentier. 2014. "Genome Editing. The New Frontier of Genome Engineering with CRISPR-Cas9." *Science* 346 (6213): 1258096.

Drouin, Emmanuel, Flavien Charpentier, Chantal Gauthier, Karine Laurent, and Herve Le Marec. 1995. "Electrophysiologic Characteristics of Cells Spanning the Left Ventricular Wall of Human Heart: Evidence for Presence of M Cells." *Journal of the American College of Cardiology*. https://doi.org/10.1016/0735-1097(95)00167-x.

Duelen, Robin, Domiziana Costamagna, Guillaume Gilbert, Liesbeth De Waele, Nathalie Goemans, Kaat Desloovere, Catherine M. Verfaillie, Karin R. Sipido, Gunnar M. Buyse, and Maurilio Sampaolesi. 2022. "Human iPSC Model Reveals a Central Role for NOX4 and Oxidative Stress in Duchenne Cardiomyopathy." *Stem Cell Reports* 17 (2): 352–68.

Dumont, Nicolas A., Yu Xin Wang, Julia von Maltzahn, Alessandra Pasut, C. Florian Bentzinger, Caroline E. Brun, and Michael A. Rudnicki. 2015. "Dystrophin Expression in Muscle Stem Cells Regulates Their Polarity and Asymmetric Division." *Nature Medicine* 21 (12): 1455–63.

Eisen, Binyamin, Ronen Ben Jehuda, Ashley J. Cuttitta, Lucy N. Mekies, Yuval Shemer, Polina Baskin, Irina Reiter, et al. 2019. "Electrophysiological Abnormalities in Induced Pluripotent Stem Cell-Derived Cardiomyocytes Generated from Duchenne Muscular Dystrophy Patients." *Journal of Cellular and Molecular Medicine* 23 (3): 2125–35.

Engler, Adam J., Shamik Sen, H. Lee Sweeney, and Dennis E. Discher. 2006. "Matrix Elasticity Directs Stem Cell Lineage Specification." *Cell* 126 (4): 677–89.

Ervasti, James M. 2003. "Costameres: The Achilles' Heel of Herculean Muscle." *The Journal of Biological Chemistry* 278 (16): 13591–94.

Ervasti, J. M., and K. P. Campbell. 1993. "A Role for the Dystrophin-Glycoprotein Complex as a Transmembrane Linker between Laminin and Actin." *The Journal of Cell Biology* 122 (4): 809–23.

Eschenhagen, T., C. Fink, U. Remmers, H. Scholz, J. Wattchow, J. Weil, W. Zimmermann, et al. 1997. "Three-Dimensional Reconstitution of Embryonic Cardiomyocytes in a Collagen Matrix: A New Heart Muscle Model System." *FASEB Journal: Official Publication of the Federation of American Societies for Experimental Biology* 11 (8): 683–94.

Evans, M. J., and M. H. Kaufman. 1981. "Establishment in Culture of Pluripotential Cells from Mouse Embryos." *Nature*. https://doi.org/10.1038/292154a0.

Fallon, Justin R., and Elizabeth M. McNally. 2018. "Non-Glycanated Biglycan and LTBP4: Leveraging the Extracellular Matrix for Duchenne Muscular Dystrophy Therapeutics." *Matrix Biology: Journal of the International Society for Matrix Biology* 68-69 (August): 616–27.

Fanchaouy, M., E. Polakova, C. Jung, J. Ogrodnik, N. Shirokova, and E. Niggli. 2009. "Pathways of Abnormal Stress-Induced Ca2+ Influx into Dystrophic Mdx Cardiomyocytes." *Cell Calcium* 46 (2): 114–21.

Fatima, Azra, Shao Kaifeng, Sven Dittmann, Guoxing Xu, Manoj K. Gupta, Matthias Linke, Ulrich Zechner, et al. 2013. "The Disease-Specific Phenotype in Cardiomyocytes Derived from Induced Pluripotent Stem Cells of Two Long QT Syndrome Type 3 Patients." *PloS One* 8 (12): e83005.

Fatima, Azra, Guoxing Xu, Kaifeng Shao, Symeon Papadopoulos, Martin Lehmann, Juan J. Arnáiz-Cot, Angelo O. Rosa, et al. 2011. "In Vitro Modeling of Ryanodine Receptor 2 Dysfunction Using Human Induced Pluripotent Stem Cells." *Cellular Physiology and Biochemistry: International Journal of Experimental Cellular Physiology, Biochemistry, and Pharmacology* 28 (4): 579–92.

Fauconnier, Jérémy, Jérôme Thireau, Steven Reiken, Cécile Cassan, Sylvain Richard, Stefan Matecki, Andrew R. Marks, and Alain Lacampagne. 2010. "Leaky RyR2 Trigger Ventricular Arrhythmias in Duchenne Muscular Dystrophy." *Proceedings*

of the National Academy of Sciences of the United States of America 107 (4): 1559–64.

Fayssoil, Abdallah, Soumeth Abasse, and Katy Silverston. 2017. "Cardiac Involvement Classification and Therapeutic Management in Patients with Duchenne Muscular Dystrophy." *Journal of Neuromuscular Diseases* 4 (1): 17–23.

Ferrantini, C., C. Crocini, R. Coppini, F. Vanzi, C. Tesi, E. Cerbai, C. Poggesi, F. S. Pavone, and L. Sacconi. 2013. "The Transverse-Axial Tubular System of Cardiomyocytes." *Cellular and Molecular Life Sciences: CMLS* 70 (24): 4695–4710.

Ferrantini, Cecilia, Alexandra Belus, Nicoletta Piroddi, Beatrice Scellini, Chiara Tesi, and Corrado Poggesi. 2009. "Mechanical and Energetic Consequences of HCM-Causing Mutations." *Journal of Cardiovascular Translational Research* 2 (4): 441–51.

Ferrantini, Cecilia, Raffaele Coppini, Josè Manuel Pioner, Francesca Gentile, Benedetta Tosi, Luca Mazzoni, Beatrice Scellini, et al. 2017. "Pathogenesis of Hypertrophic Cardiomyopathy Is Mutation Rather Than Disease Specific: A Comparison of the Cardiac Troponin T E163R and R92Q Mouse Models." *Journal of the American Heart Association*. https://doi.org/10.1161/jaha.116.005407.

Filipczyk, A. A., R. Passier, A. Rochat, and C. L. Mummery. 2007. "Regulation of Cardiomyocyte Differentiation of Embryonic Stem Cells by Extracellular Signalling." *Cellular and Molecular Life Sciences: CMLS* 64 (6): 704–18.

Frank, Derk, Ashraf Yusuf Rangrez, Corinna Friedrich, Sven Dittmann, Birgit Stallmeyer, Pankaj Yadav, Alexander Bernt, et al. 2019. "Cardiac α-Actin (ACTC1) Gene Mutation Causes Atrial-Septal Defects Associated With Late-Onset Dilated Cardiomyopathy." *Circulation. Genomic and Precision Medicine* 12 (8): e002491.

Frankel, K. A., and R. J. Rosser. 1976. "The Pathology of the Heart in Progressive Muscular Dystrophy: Epimyocardial Fibrosis." *Human Pathology* 7 (4): 375–86.

Fu, Jianping, Yang-Kao Wang, Michael T. Yang, Ravi A. Desai, Xiang Yu, Zhijun Liu, and Christopher S. Chen. 2010. "Mechanical Regulation of Cell Function with Geometrically Modulated Elastomeric Substrates." *Nature Methods*. https://doi.org/10.1038/nmeth.1487.

Gajendrarao, Poornima, Navaneethakrishnan Krishnamoorthy, Senthil Selvaraj, Francesca Girolami, Franco Cecchi, Iacopo Olivotto, and Magdi Yacoub. 2015. "An Investigation of the Molecular Mechanism of Double cMyBP-C Mutation in a Patient with End-Stage Hypertrophic Cardiomyopathy." *Journal of Cardiovascular Translational Research* 8 (4): 232–43.

Gao, Ling, Molly E. Kupfer, Jangwook P. Jung, Libang Yang, Patrick Zhang, Yong Da Sie, Quyen Tran, et al. 2017. "Myocardial Tissue Engineering With Cells Derived From Human-Induced Pluripotent Stem Cells and a Native-Like, High-Resolution, 3-Dimensionally Printed Scaffold." *Circulation Research*. https://doi.org/10.1161/circresaha.116.310277.

Gautel, M., O. Zuffardi, A. Freiburg, and S. Labeit. 1995. "Phosphorylation Switches Specific for the Cardiac Isoform of Myosin Binding Protein-C: A Modulator of Cardiac Contraction?" *The EMBO Journal* 14 (9): 1952–60.

Geeves, M. A., and K. C. Holmes. 1999. "Structural Mechanism of Muscle Contraction." *Annual Review of Biochemistry* 68: 687–728.

Geisterfer-Lowrance, A. A., S. Kass, G. Tanigawa, H. P. Vosberg, W. McKenna, C. E. Seidman, and J. G. Seidman. 1990. "A Molecular Basis for Familial Hypertrophic Cardiomyopathy: A Beta Cardiac Myosin Heavy Chain Gene Missense Mutation." *Cell* 62 (5): 999–1006.

Gherghiceanu, Mihaela, Lili Barad, Atara Novak, Irina Reiter, Joseph Itskovitz-Eldor, Ofer Binah, and L. M. Popescu. 2011. "Cardiomyocytes Derived from Human Embryonic and Induced Pluripotent Stem Cells: Comparative Ultrastructure." *Journal of Cellular and Molecular Medicine*. https://doi.org/10.1111/j.1582-4934.2011.01417.x.

Giannetti, Federica, Patrizia Benzoni, Giulia Campostrini, Raffaella Milanesi, Annalisa Bucchi, Mirko Baruscotti, Patrizia Dell'Era, Alessandra Rossini, and Andrea Barbuti. 2021. "A Detailed Characterization of the Hyperpolarization-Activated 'Funny' Current (I) in Human-Induced Pluripotent Stem Cell (iPSC)-Derived Cardiomyocytes with Pacemaker Activity." *Pflugers Archiv: European Journal of Physiology* 473 (7): 1009–21.

Giardini, Francesco, Erica Lazzeri, Giulia Vitale, Cecilia Ferrantini, Irene Costantini, Francesco S. Pavone, Corrado Poggesi, Leonardo Bocchi, and Leonardo Sacconi. 2021. "Quantification of Myocyte Disarray in Human Cardiac Tissue." *Frontiers in Physiology* 12 (November): 750364.

Gigli, Marta, Marco Merlo, Sharon L. Graw, Giulia Barbati, Teisha J. Rowland, Dobromir B. Slavov, Davide Stolfo, et al. 2019. "Genetic Risk of Arrhythmic Phenotypes in Patients With Dilated Cardiomyopathy." *Journal of the American College of Cardiology* 74 (11): 1480–90.

Girolami, Francesca, Iacopo Olivotto, Ilaria Passerini, Elisabetta Zachara, Stefano Nistri, Federica Re, Silvia Fantini, Katia Baldini, Francesca Torricelli, and Franco Cecchi. 2006a. "A Molecular Screening Strategy Based on β-Myosin Heavy Chain, Cardiac Myosin Binding Protein C and Troponin T Genes in Italian Patients with Hypertrophic Cardiomyopathy." *Journal of Cardiovascular Medicine*. https://doi.org/10.2459/01.jcm.0000237908.26377.d6.

Girolami, Francesca, Silvia Passantino, Federica Verrillo, Eszter Dalma Palinkas, Giuseppe Limongelli, Silvia Favilli, and Iacopo Olivotto. 2022. "The Influence of Genotype on the Phenotype, Clinical Course, and Risk of Adverse Events in Children with Hypertrophic Cardiomyopathy." *Heart Failure Clinics* 18 (1): 1–8.

Goldfracht, Idit, Stephanie Protze, Assad Shiti, Noga Setter, Amit Gruber, Naim Shaheen, Yulia Nartiss, Gordon Keller, and Lior Gepstein. 2020. "Generating Ring-Shaped Engineered Heart Tissues from Ventricular and Atrial Human Pluripotent Stem Cell-Derived Cardiomyocytes." *Nature Communications* 11 (1): 75.

Govada, Lata, Liz Carpenter, Paula C. A. da Fonseca, John R. Helliwell, Pierre Rizkallah, Emily Flashman, Naomi E. Chayen, Charles Redwood, and John M. Squire. 2008. "Crystal Structure of the C1 Domain of Cardiac Myosin Binding Protein-C:

Implications for Hypertrophic Cardiomyopathy." *Journal of Molecular Biology* 378 (2): 387–97.

Green, Eric M., Hiroko Wakimoto, Robert L. Anderson, Marc J. Evanchik, Joshua M. Gorham, Brooke C. Harrison, Marcus Henze, et al. 2016. "A Small-Molecule Inhibitor of Sarcomere Contractility Suppresses Hypertrophic Cardiomyopathy in Mice." *Science*. https://doi.org/10.1126/science.aad3456.

Gregorio, Carol C., and Parker B. Antin. 2000. "To the Heart of Myofibril Assembly." *Trends in Cell Biology*. https://doi.org/10.1016/s0962-8924(00)01793-1.

Guan, Xuan, David L. Mack, Claudia M. Moreno, Jennifer L. Strande, Julie Mathieu, Yingai Shi, Chad D. Markert, et al. 2014. "Dystrophin-Deficient Cardiomyocytes Derived from Human Urine: New Biologic Reagents for Drug Discovery." *Stem Cell Research* 12 (2): 467–80.

Halas, Monika, Paulina Langa, Chad M. Warren, Paul H. Goldspink, Beata M. Wolska, and R. John Solaro. 2022. "Effects of Sarcomere Activators and Inhibitors Targeting Myosin Cross-Bridges on Ca^2-Activation of Mature and Immature Mouse Cardiac Myofilaments." *Molecular Pharmacology*. https://doi.org/10.1124/molpharm.121.000420.

Han, Lu, Yang Li, Jason Tchao, Aaron D. Kaplan, Bo Lin, You Li, Jocelyn Mich-Basso, et al. 2014. "Study Familial Hypertrophic Cardiomyopathy Using Patient-Specific Induced Pluripotent Stem Cells." *Cardiovascular Research*. https://doi.org/10.1093/cvr/cvu205.

Hansen, Arne, Alexandra Eder, Marlene Bönstrup, Marianne Flato, Marco Mewe, Sebastian Schaaf, Bülent Aksehirlioglu, Alexander P. Schwoerer, June Uebeler, and Thomas Eschenhagen. 2010. "Development of a Drug Screening Platform Based on Engineered Heart Tissue." *Circulation Research* 107 (1): 35–44.

Harris, Samantha P., Christopher R. Bartley, Timothy A. Hacker, Kerry S. McDonald, Pamela S. Douglas, Marion L. Greaser, Patricia A. Powers, and Richard L. Moss. 2002. "Hypertrophic Cardiomyopathy in Cardiac Myosin Binding Protein-C Knockout Mice." *Circulation Research*. https://doi.org/10.1161/01.res.0000012222.70819.64.

Harris, Samantha P., Elena Rostkova, Mathias Gautel, and Richard L. Moss. 2004. "Binding of Myosin Binding Protein-C to Myosin Subfragment S2 Affects Contractility Independent of a Tether Mechanism." *Circulation Research* 95 (9): 930–36.

Hartzell, H. C., and D. B. Glass. 1984. "Phosphorylation of Purified Cardiac Muscle C-Protein by Purified cAMP-Dependent and Endogenous Ca2+-Calmodulin-Dependent Protein Kinases." *The Journal of Biological Chemistry* 259 (24): 15587–96.

Hasselberg, Nina Eide, Trine Fink Haland, Jørg Saberniak, Pål Haugar Brekke, Knut Erik Berge, Trond Paul Leren, Thor Edvardsen, and Kristina Hermann Haugaa. 2018. "Lamin A/C Cardiomyopathy: Young Onset, High Penetrance, and Frequent Need for Heart Transplantation." *European Heart Journal* 39 (10): 853–60.

Hazeltine, Laurie B., Chelsey S. Simmons, Max R. Salick, Xiaojun Lian, Mehmet G. Badur, Wenqing Han, Stephanie M. Delgado, et al. 2012. "Effects of Substrate Mechanics on Contractility of Cardiomyocytes Generated from Human Pluripotent Stem Cells." *International Journal of Cell Biology*. https://doi.org/10.1155/2012/508294.

He, Huamei, Maryam M. Javadpour, Farhana Latif, Jil C. Tardiff, and Joanne S. Ingwall. 2007. "R-92L and R-92W Mutations in Cardiac Troponin T Lead to Distinct Energetic Phenotypes in Intact Mouse Hearts." *Biophysical Journal* 93 (5): 1834–44.

Helms, Adam S., Francisco J. Alvarado, Jaime Yob, Vi T. Tang, Francis Pagani, Mark W. Russell, Héctor H. Valdivia, and Sharlene M. Day. 2016. "Genotype-Dependent and -Independent Calcium Signaling Dysregulation in Human Hypertrophic Cardiomyopathy." *Circulation* 134 (22): 1738–48.

Helms, Adam S., Frank M. Davis, David Coleman, Sarah N. Bartolone, Amelia A. Glazier, Francis Pagani, Jaime M. Yob, et al. 2014. "Sarcomere Mutation-Specific Expression Patterns in Human Hypertrophic Cardiomyopathy." *Circulation. Cardiovascular Genetics* 7 (4): 434–43.

Helms, Adam S., Vi T. Tang, Thomas S. O'Leary, Sabrina Friedline, Mick Wauchope, Akul Arora, Aaron H. Wasserman, et al. 2020. "Effects of MYBPC3 Loss-of-Function Mutations Preceding Hypertrophic Cardiomyopathy." *JCI Insight* 5 (2). https://doi.org/10.1172/jci.insight.133782.

Herman, Daniel S., Lien Lam, Matthew R. G. Taylor, Libin Wang, Polakit Teekakirikul, Danos Christodoulou, Lauren Conner, et al. 2012. "Truncations of Titin Causing Dilated Cardiomyopathy." *The New England Journal of Medicine* 366 (7): 619–28.

Heuvel, Nikki H. L. van den, Toon A. B. van Veen, Bing Lim, and Malin K. B. Jonsson. 2014. "Lessons from the Heart: Mirroring Electrophysiological Characteristics during Cardiac Development to in Vitro Differentiation of Stem Cell Derived Cardiomyocytes." *Journal of Molecular and Cellular Cardiology*. https://doi.org/10.1016/j.yjmcc.2013.12.011.

Hinson, John T., Anant Chopra, Navid Nafissi, William J. Polacheck, Craig C. Benson, Sandra Swist, Joshua Gorham, et al. 2015. "HEART DISEASE. Titin Mutations in iPS Cells Define Sarcomere Insufficiency as a Cause of Dilated Cardiomyopathy." *Science* 349 (6251): 982–86.

Hinson, J. Travis, Anant Chopra, Andre Lowe, Calvin C. Sheng, Rajat M. Gupta, Rajarajan Kuppusamy, John O'Sullivan, et al. 2016. "Integrative Analysis of PRKAG2 Cardiomyopathy iPS and Microtissue Models Identifies AMPK as a Regulator of Metabolism, Survival, and Fibrosis." *Cell Reports* 17 (12): 3292–3304.

Ho, Carolyn Y., Philippe Charron, Pascale Richard, Francesca Girolami, Karin Y. Van Spaendonck-Zwarts, and Yigal Pinto. 2015. "Genetic Advances in Sarcomeric Cardiomyopathies: State of the Art." *Cardiovascular Research* 105 (4): 397–408.

Ho, Carolyn Y., Sharlene M. Day, Euan A. Ashley, Michelle Michels, Alexandre C. Pereira, Daniel Jacoby, Allison L. Cirino, et al. 2018. "Genotype and Lifetime Burden of Disease in Hypertrophic Cardiomyopathy: Insights from the Sarcomeric Human Cardiomyopathy Registry (SHaRe)." *Circulation* 138 (14): 1387–98.

Ho, Carolyn Y., Sharlene M. Day, Euan A. Ashley, Michelle Michels, Alexandre C. Pereira, Daniel Jacoby, Neal K. Lakdawala, et

al. 2019. "Response by Ho et Al to Letter Regarding Article, 'Genotype and Lifetime Burden of Disease in Hypertrophic Cardiomyopathy: Insights From the Sarcomeric Human Cardiomyopathy Registry (SHaRe).'" *Circulation*. https://doi.org/10.1161/circulationaha.118.039069.

Ho, Carolyn Y., Neal K. Lakdawala, Allison L. Cirino, Steven E. Lipshultz, Elizabeth Sparks, Siddique A. Abbasi, Raymond Y. Kwong, et al. 2015. "Diltiazem Treatment for Pre-Clinical Hypertrophic Cardiomyopathy Sarcomere Mutation Carriers: A Pilot Randomized Trial to Modify Disease Expression." *JACC. Heart Failure* 3 (2): 180–88.

Ho, Carolyn Y., Matthew E. Mealiffe, Richard G. Bach, Mondira Bhattacharya, Lubna Choudhury, Jay M. Edelberg, Sheila M. Hegde, et al. 2020. "Evaluation of Mavacamten in Symptomatic Patients With Nonobstructive Hypertrophic Cardiomyopathy." *Journal of the American College of Cardiology* 75 (21): 2649–60.

Hoffman, Eric P., Robert H. Brown, and Louis M. Kunkel. 1987. "Dystrophin: The Protein Product of the Duchenne Muscular Dystrophy Locus." *Cell*. https://doi.org/10.1016/0092-8674(87)90579-4.

Hof, I. E., J. F. van der Heijden, E. G. Kranias, D. Sanoudou, R. A. de Boer, J. P. van Tintelen, P. A. van der Zwaag, and P. A. Doevendans. 2019. "Prevalence and Cardiac Phenotype of Patients with a Phospholamban Mutation." *Netherlands Heart Journal: Monthly Journal of the Netherlands Society of Cardiology and the Netherlands Heart Foundation* 27 (2): 64–69.

Holubarsch, C. 1998. "Shortening versus Isometric Contractions in Isolated Human Failing and Non-Failing Left Ventricular Myocardium: Dependency of External Work and Force on Muscle Length, Heart Rate and Inotropic Stimulation." *Cardiovascular Research*. https://doi.org/10.1016/s0008-6363(97)00215-0.

Hoppe, U. C., E. Jansen, M. Südkamp, and D. J. Beuckelmann. 1998. "Hyperpolarization-Activated Inward Current in Ventricular Myocytes from Normal and Failing Human Hearts." *Circulation* 97 (1): 55–65.

Horii, Takuro, Daiki Tamura, Sumiyo Morita, Mika Kimura, and Izuho Hatada. 2013. "Generation of an ICF Syndrome Model by Efficient Genome Editing of Human Induced Pluripotent Stem Cells Using the CRISPR System." *International Journal of Molecular Sciences* 14 (10): 19774–81.

Huh, Dongeun, Geraldine A. Hamilton, and Donald E. Ingber. 2011. "From 3D Cell Culture to Organs-on-Chips." *Trends in Cell Biology*. https://doi.org/10.1016/j.tcb.2011.09.005.

Hunkeler, N. M., J. Kullman, and A. M. Murphy. 1991. "Troponin I Isoform Expression in Human Heart." *Circulation Research* 69 (5): 1409–14.

Iorga, Bogdan, Kristin Schwanke, Natalie Weber, Meike Wendland, Stephan Greten, Birgit Piep, Cristobal G. Dos Remedios, et al. 2017. "Differences in Contractile Function of Myofibrils within Human Embryonic Stem Cell-Derived Cardiomyocytes vs. Adult Ventricular Myofibrils Are Related to Distinct Sarcomeric Protein Isoforms." *Frontiers in Physiology* 8: 1111.

Itzhaki, Ilanit, Leonid Maizels, Irit Huber, Amira Gepstein, Gil Arbel, Oren Caspi, Liron Miller, et al. 2012. "Modeling of Catecholaminergic Polymorphic Ventricular Tachycardia with Patient-Specific Human-Induced Pluripotent Stem Cells." *Journal of the American College of Cardiology* 60 (11): 990–1000.

Itzhaki, Ilanit, Leonid Maizels, Irit Huber, Limor Zwi-Dantsis, Oren Caspi, Aaron Winterstern, Oren Feldman, et al. 2011. "Modelling the Long QT Syndrome with Induced Pluripotent Stem Cells." *Nature* 471 (7337): 225–29.

Itzhaki, Ilanit, Sophia Rapoport, Irit Huber, Itzhak Mizrahi, Limor Zwi-Dantsis, Gil Arbel, Jackie Schiller, and Lior Gepstein. 2011. "Calcium Handling in Human Induced Pluripotent Stem Cell Derived Cardiomyocytes." *PLoS One* 6 (4): e18037.

Ivashchenko, Christine Y., Gordon C. Pipes, Irina M. Lozinskaya, Zuojun Lin, Xu Xiaoping, Saul Needle, Eugene T. Grygielko, et al. 2013. "Human-Induced Pluripotent Stem Cell-Derived Cardiomyocytes Exhibit Temporal Changes in Phenotype." *American Journal of Physiology-Heart and Circulatory Physiology*, September. https://doi.org/10.1152/ajpheart.00819.2012.

Jelinkova, Sarka, Petr Fojtik, Aneta Kohutova, Aleksandra Vilotic, Lenka Marková, Martin Pesl, Tereza Jurakova, et al. 2019. "Dystrophin Deficiency Leads to Genomic Instability in Human Pluripotent Stem Cells via NO Synthase-Induced Oxidative Stress." *Cells* 8 (1). https://doi.org/10.3390/cells8010053.

Jelinkova, Sarka, Aleksandra Vilotic, Jan Pribyl, Franck Aimond, Anton Salykin, Ivana Acimovic, Martin Pesl, et al. 2020. "DMD Pluripotent Stem Cell Derived Cardiac Cells Recapitulate Human Cardiac Pathophysiology." *Frontiers in Bioengineering and Biotechnology* 8 (June): 535.

Jensen, Caleb, and Yong Teng. 2020. "Is It Time to Start Transitioning From 2D to 3D Cell Culture?" *Frontiers in Molecular Biosciences* 7 (March): 33.

Judge, Luke M., Juan A. Perez-Bermejo, Annie Truong, Alexandre Js Ribeiro, Jennie C. Yoo, Christina L. Jensen, Mohammad A. Mandegar, et al. 2017. "A BAG3 Chaperone Complex Maintains Cardiomyocyte Function during Proteotoxic Stress." *JCI Insight* 2 (14). https://doi.org/10.1172/jci.insight.94623.

Jung, Christian B., Alessandra Moretti, Michael Mederos y Schnitzler, Laura Iop, Ursula Storch, Milena Bellin, Tatjana Dorn, et al. 2012. "Dantrolene Rescues Arrhythmogenic RYR2 Defect in a Patient-Specific Stem Cell Model of Catecholaminergic Polymorphic Ventricular Tachycardia." *EMBO Molecular Medicine* 4 (3): 180–91.

Jung, Gwanghyun, Giovanni Fajardo, Alexandre J. S. Ribeiro, Kristina Bezold Kooiker, Michael Coronado, Mingming Zhao, Dong-Qing Hu, et al. 2016. "Time-Dependent Evolution of Functional vs. Remodeling Signaling in Induced Pluripotent Stem Cell-Derived Cardiomyocytes and Induced Maturation with Biomechanical Stimulation." *FASEB Journal: Official Publication of the Federation of American Societies for Experimental Biology* 30 (4): 1464–79.

Kamakura, Tsukasa, Takeru Makiyama, Kenichi Sasaki, Yoshinori Yoshida, Yimin Wuriyanghai, Jiarong Chen, Tetsuhisa Hattori, et al. 2013. "Ultrastructural Maturation of Human-Induced Pluripotent Stem Cell-Derived Cardiomyocytes in a Long-Term Culture." *Circulation Journal*. https://doi.org/10.1253/circj.cj-12-0987.

Kensah, George, Angelica Roa Lara, Julia Dahlmann, Robert Zweigerdt, Kristin Schwanke, Jan Hegermann, David Skvorc, et al. 2013. "Murine and Human Pluripotent Stem Cell-Derived Cardiac Bodies Form Contractile Myocardial Tissue in Vitro." *European Heart Journal* 34 (15): 1134–46.

Keung, Wendy, Patrick K. W. Chan, Peter C. Backeris, Eugene K. Lee, Nicodemus Wong, Andy O. T. Wong, Gabriel K. Y. Wong, et al. 2019. "Human Cardiac Ventricular-Like Organoid Chambers and Tissue Strips From Pluripotent Stem Cells as a Two-Tiered Assay for Inotropic Responses." *Clinical Pharmacology and Therapeutics* 106 (2): 402–14.

Kim, Changsung, Johnson Wong, Jianyan Wen, Shirong Wang, Cheng Wang, Sean Spiering, Natalia G. Kan, et al. 2013. "Studying Arrhythmogenic Right Ventricular Dysplasia with Patient-Specific iPSCs." *Nature*. https://doi.org/10.1038/nature11799.

Kim, Deok-Ho, Elizabeth A. Lipke, Pilnam Kim, Raymond Cheong, Susan Thompson, Michael Delannoy, Kahp-Yang Suh, Leslie Tung, and Andre Levchenko. 2010. "Nanoscale Cues Regulate the Structure and Function of Macroscopic Cardiac Tissue Constructs." *Proceedings of the National Academy of Sciences*. https://doi.org/10.1073/pnas.0906504107.

Kim, H. 1992. "Human Fetal Heart Development after Mid-Term: Morphometry and Ultrastructural Study." *Journal of Molecular and Cellular Cardiology*. https://doi.org/10.1016/0022-2828(92)91862-y.

Koenig, M., and L. M. Kunkel. 1990. "Detailed Analysis of the Repeat Domain of Dystrophin Reveals Four Potential Hinge Segments That May Confer Flexibility." *The Journal of Biological Chemistry* 265 (8): 4560–66.

Kokado, H., M. Shimizu, H. Yoshio, H. Ino, K. Okeie, Y. Emoto, T. Matsuyama, et al. 2000. "Clinical Features of Hypertrophic Cardiomyopathy Caused by a Lys183 Deletion Mutation in the Cardiac Troponin I Gene." *Circulation* 102 (6): 663–69.

Korte, F. Steven, Kerry S. McDonald, Samantha P. Harris, and Richard L. Moss. 2003. "Loaded Shortening, Power Output, and Rate of Force Redevelopment Are Increased with Knockout of Cardiac Myosin Binding Protein-C." *Circulation Research* 93 (8): 752–58.

Krane, Markus, Martina Dreßen, Gianluca Santamaria, Ilaria My, Christine M. Schneider, Tatjana Dorn, Svenja Laue, et al. 2021. "Sequential Defects in Cardiac Lineage Commitment and Maturation Cause Hypoplastic Left Heart Syndrome." *Circulation* 144 (17): 1409–28.

Krishnamoorthy, Navaneethakrishnan, Poornima Gajendrarao, Iacopo Olivotto, and Magdi Yacoub. 2017. "Impact of Disease-Causing Mutations on Inter-Domain Interactions in cMyBP-C: A Steered Molecular Dynamics Study." *Journal of Biomolecular Structure & Dynamics* 35 (9): 1916–22.

Kubalak, S. W., W. C. Miller-Hance, T. X. O'Brien, E. Dyson, and K. R. Chien. 1994. "Chamber Specification of Atrial Myosin Light Chain-2 Expression Precedes Septation during Murine Cardiogenesis." *The Journal of Biological Chemistry* 269 (24): 16961–70.

Kujala, Kirsi, Jere Paavola, Anna Lahti, Kim Larsson, Mari Pekkanen-Mattila, Matti Viitasalo, Annukka M. Lahtinen, et al. 2012. "Cell Model of Catecholaminergic Polymorphic Ventricular Tachycardia Reveals Early and Delayed Afterdepolarizations." *PloS One* 7 (9): e44660.

Kyrychenko, Sergii, Eva Poláková, Chifei Kang, Krisztina Pocsai, Nina D. Ullrich, Ernst Niggli, and Natalia Shirokova. 2013. "Hierarchical Accumulation of RyR Post-Translational Modifications Drives Disease Progression in Dystrophic Cardiomyopathy." *Cardiovascular Research* 97 (4): 666–75.

Kyrychenko, Viktoriia, Sergii Kyrychenko, Malte Tiburcy, John M. Shelton, Chengzu Long, Jay W. Schneider, Wolfram-Hubertus Zimmermann, Rhonda Bassel-Duby, and Eric N. Olson. 2017. "Functional Correction of Dystrophin Actin Binding Domain Mutations by Genome Editing." *JCI Insight* 2 (18). https://doi.org/10.1172/jci.insight.95918.

Laflamme, Michael A., Kent Y. Chen, Anna V. Naumova, Veronica Muskheli, James A. Fugate, Sarah K. Dupras, Hans Reinecke, et al. 2007. "Cardiomyocytes Derived from Human Embryonic Stem Cells in pro-Survival Factors Enhance Function of Infarcted Rat Hearts." *Nature Biotechnology*. https://doi.org/10.1038/nbt1327.

Lahmers, Sunshine, Yiming Wu, Douglas R. Call, Siegfried Labeit, and Henk Granzier. 2004. "Developmental Control of Titin Isoform Expression and Passive Stiffness in Fetal and Neonatal Myocardium." *Circulation Research* 94 (4): 505–13.

Lahti, Anna L., Ville J. Kujala, Hugh Chapman, Ari-Pekka Koivisto, Mari Pekkanen-Mattila, Erja Kerkelä, Jari Hyttinen, et al. 2012. "Model for Long QT Syndrome Type 2 Using Human iPS Cells Demonstrates Arrhythmogenic Characteristics in Cell Culture." *Disease Models & Mechanisms* 5 (2): 220–30.

Lan, Feng, Andrew S. Lee, Ping Liang, Veronica Sanchez-Freire, Patricia K. Nguyen, Li Wang, Leng Han, et al. 2013. "Abnormal Calcium Handling Properties Underlie Familial Hypertrophic Cardiomyopathy Pathology in Patient-Specific Induced Pluripotent Stem Cells." *Cell Stem Cell*. https://doi.org/10.1016/j.stem.2012.10.010.

Lange, Willem J. de, Adrian C. Grimes, Laura F. Hegge, and J. Carter Ralphe. 2013. "Ablation of Cardiac Myosin-Binding Protein-C Accelerates Contractile Kinetics in Engineered Cardiac Tissue." *The Journal of General Physiology* 141 (1): 73–84.

Lavine, Kory J., and David M. Ornitz. 2008. "Fibroblast Growth Factors and Hedgehogs: At the Heart of the Epicardial Signaling Center." *Trends in Genetics: TIG* 24 (1): 33–40.

Lee, Peter, Matt Klos, Christian Bollensdorff, Luqia Hou, Paul Ewart, Timothy J. Kamp, Jianhua Zhang, et al. 2012. "Simultaneous Voltage and Calcium Mapping of Genetically Purified Human Induced Pluripotent Stem Cell–Derived

Cardiac Myocyte Monolayers." *Circulation Research*. https://doi.org/10.1161/circresaha.111.262535.

Lee, Sujeong, Hyang-Ae Lee, Sung Woo Choi, Sung Joon Kim, and Ki-Suk Kim. 2016. "Evaluation of Nefazodone-Induced Cardiotoxicity in Human Induced Pluripotent Stem Cell-Derived Cardiomyocytes." *Toxicology and Applied Pharmacology* 296 (April): 42–53.

Lehman, Sarah J., Lauren Tal-Grinspan, Melissa L. Lynn, Joshua Strom, Grace E. Benitez, Mark E. Anderson, and Jil C. Tardiff. 2019. "Chronic Calmodulin-Kinase II Activation Drives Disease Progression in Mutation-Specific Hypertrophic Cardiomyopathy." *Circulation* 139 (12): 1517–29.

Leitolis, Amanda, Anny W. Robert, Isabela T. Pereira, Alejandro Correa, and Marco A. Stimamiglio. 2019. "Cardiomyogenesis Modeling Using Pluripotent Stem Cells: The Role of Microenvironmental Signaling." *Frontiers in Cell and Developmental Biology* 7 (August): 164.

Leonard, Andrea, Alessandro Bertero, Joseph D. Powers, Kevin M. Beussman, Shiv Bhandari, Michael Regnier, Charles E. Murry, and Nathan J. Sniadecki. 2018. "Afterload Promotes Maturation of Human Induced Pluripotent Stem Cell Derived Cardiomyocytes in Engineered Heart Tissues." *Journal of Molecular and Cellular Cardiology* 118 (May): 147–58.

Lieu, Deborah K., Ji-Dong Fu, Nipavan Chiamvimonvat, Kelvin Chan Tung, Gregory P. McNerney, Thomas Huser, Gordon Keller, Chi-Wing Kong, and Ronald A. Li. 2013. "Mechanism-Based Facilitated Maturation of Human Pluripotent Stem Cell–Derived Cardiomyocytes." *Circulation: Arrhythmia and Electrophysiology*. https://doi.org/10.1161/circep.111.973420.

Li, Jiangtao, Xin Feng, and Xiang Wei. 2022. "Modeling Hypertrophic Cardiomyopathy with Human Cardiomyocytes Derived from Induced Pluripotent Stem Cells." *Stem Cell Research & Therapy* 13 (1): 232.

Limongelli, Giuseppe, Rachele Adorisio, Chiara Baggio, Barbara Bauce, Elena Biagini, Silvia Castelletti, Silvia Favilli, et al. 2022. "Diagnosis and Management of Rare Cardiomyopathies in Adult and Paediatric Patients. A Position Paper of the Italian Society of Cardiology (SIC) and Italian Society of Paediatric Cardiology (SICP)." *International Journal of Cardiology* 357 (June): 55–71.

Lin, Bo, Yang Li, Lu Han, Aaron D. Kaplan, Ying Ao, Spandan Kalra, Glenna C. L. Bett, Randall L. Rasmusson, Chris Denning, and Lei Yang. 2015. "Modeling and Study of the Mechanism of Dilated Cardiomyopathy Using Induced Pluripotent Stem Cells Derived from Individuals with Duchenne Muscular Dystrophy." *Disease Models & Mechanisms*. https://doi.org/10.1242/dmm.019505.

Lipshultz, Steven E., Lynn A. Sleeper, Jeffrey A. Towbin, April M. Lowe, E. John Orav, Gerald F. Cox, Paul R. Lurie, et al. 2003. "The Incidence of Pediatric Cardiomyopathy in Two Regions of the United States." *The New England Journal of Medicine* 348 (17): 1647–55.

Li, R. K., D. A. Mickle, R. D. Weisel, S. Carson, S. A. Omar, L. C. Tumiati, G. J. Wilson, and W. G. Williams. 1996. "Human Pediatric and Adult Ventricular Cardiomyocytes in Culture: Assessment of Phenotypic Changes with Passaging." *Cardiovascular Research* 32 (2): 362–73.

Li, Sen, Gaopeng Chen, and Ronald A. Li. 2013. "Calcium Signalling of Human Pluripotent Stem Cell-Derived Cardiomyocytes." *The Journal of Physiology* 591 (21): 5279–90.

Liu, Jie, Zachary Laksman, and Peter H. Backx. 2016. "The Electrophysiological Development of Cardiomyocytes." *Advanced Drug Delivery Reviews*. https://doi.org/10.1016/j.addr.2015.12.023.

Li, Xiaowei, Wen-Jing Lu, Ya 'nan Li, Fujian Wu, Rui Bai, Shuhong Ma, Tao Dong, et al. 2019. "MLP-Deficient Human Pluripotent Stem Cell Derived Cardiomyocytes Develop Hypertrophic Cardiomyopathy and Heart Failure Phenotypes due to Abnormal Calcium Handling." *Cell Death & Disease* 10 (8): 610.

Loh, Yuin-Han, Suneet Agarwal, In-Hyun Park, Achia Urbach, Hongguang Huo, Garrett C. Heffner, Kitai Kim, Justine D. Miller, Kitwa Ng, and George Q. Daley. 2009. "Generation of Induced Pluripotent Stem Cells from Human Blood." *Blood*. https://doi.org/10.1182/blood-2009-02-204800.

Lopaschuk, Gary D., and Jagdip S. Jaswal. 2010. "Energy Metabolic Phenotype of the Cardiomyocyte During Development, Differentiation, and Postnatal Maturation." *Journal of Cardiovascular Pharmacology*. https://doi.org/10.1097/fjc.0b013e3181e74a14.

Louch, William E., Katherine A. Sheehan, and Beata M. Wolska. 2011. "Methods in Cardiomyocyte Isolation, Culture, and Gene Transfer." *Journal of Molecular and Cellular Cardiology*. https://doi.org/10.1016/j.yjmcc.2011.06.012.

Luedde, Mark, Ulrich Flögel, Maike Knorr, Christina Grundt, Hans-Joerg Hippe, Benedikt Brors, Derk Frank, et al. 2009. "Decreased Contractility due to Energy Deprivation in a Transgenic Rat Model of Hypertrophic Cardiomyopathy." *Journal of Molecular Medicine*. https://doi.org/10.1007/s00109-008-0436-x.

Lundy, Scott D., Wei-Zhong Zhu, Michael Regnier, and Michael A. Laflamme. 2013. "Structural and Functional Maturation of Cardiomyocytes Derived from Human Pluripotent Stem Cells." *Stem Cells and Development*. https://doi.org/10.1089/scd.2012.0490.

Luther, Pradeep K., Pauline M. Bennett, Carlo Knupp, Roger Craig, Raúl Padrón, Samantha P. Harris, Jitendrakumar Patel, and Richard L. Moss. 2008. "Understanding the Organisation and Role of Myosin Binding Protein C in Normal Striated Muscle by Comparison with MyBP-C Knockout Cardiac Muscle." *Journal of Molecular Biology* 384 (1): 60–72.

Macadangdang, Jesse, Xuan Guan, Alec S. T. Smith, Rachel Lucero, Stefan Czerniecki, Martin K. Childers, David L. Mack, and Deok-Ho Kim. 2015. "Nanopatterned Human iPSC-Based Model of a Dystrophin-Null Cardiomyopathic Phenotype." *Cellular and Molecular Bioengineering* 8 (3): 320–32.

Macadangdang, Jesse R., Jason W. Miklas, Alec S. T. Smith, Eunpyo Choi, Winnie Leung, Yuliang Wang, Xuan Guan, et al. 2018 "Engineered Developmental Niche Enables Predictive Phenotypic Screening in Human Dystrophic Cardiomyopathy." https://doi.org/10.1101/456301.

MacQueen, Luke A., Sean P. Sheehy, Christophe O. Chantre, John F. Zimmerman, Francesco S. Pasqualini, Xujie Liu, Josue A. Goss, et al. 2018. "A Tissue-Engineered Scale Model of the Heart Ventricle." *Nature Biomedical Engineering* 2 (12): 930–41.

Madhavan, Raghavan, and Harry W. Jarrett. 1994. "Calmodulin-Activated Phosphorylation of Dystrophin." *Biochemistry*. https://doi.org/10.1021/bi00185a018.

Ma, Dongrui, Heming Wei, Jun Lu, Shuswen Ho, Guangqing Zhang, Xiaoming Sun, Yingzi Oh, et al. 2013. "Generation of Patient-Specific Induced Pluripotent Stem Cell-Derived Cardiomyocytes as a Cellular Model of Arrhythmogenic Right Ventricular Cardiomyopathy." *European Heart Journal* 34 (15): 1122–33.

Ma, Dongrui, Heming Wei, Yongxing Zhao, Jun Lu, Guang Li, Norliza Binte Esmail Sahib, Teng Hong Tan, et al. 2013. "Modeling Type 3 Long QT Syndrome with Cardiomyocytes Derived from Patient-Specific Induced Pluripotent Stem Cells." *International Journal of Cardiology* 168 (6): 5277–86.

Magyar, J., N. Iost, A. Körtvély, T. Bányász, L. Virág, P. Szigligeti, A. Varró, et al. 2000. "Effects of Endothelin-1 on Calcium and Potassium Currents in Undiseased Human Ventricular Myocytes." *Pflugers Archiv: European Journal of Physiology* 441 (1): 144–49.

Ma, Junyi, Liang Guo, Steve J. Fiene, Blake D. Anson, James A. Thomson, Timothy J. Kamp, Kyle L. Kolaja, Bradley J. Swanson, and Craig T. January. 2011. "High Purity Human-Induced Pluripotent Stem Cell-Derived Cardiomyocytes: Electrophysiological Properties of Action Potentials and Ionic Currents." *American Journal of Physiology-Heart and Circulatory Physiology*. https://doi.org/10.1152/ajpheart.00694.2011.

Mandel, J. L. 1989. "Dystrophin. The Gene and Its Product." *Nature* 339 (6226): 584–86.

Ma, Ning, Joe Z. Zhang, Ilanit Itzhaki, Sophia L. Zhang, Haodong Chen, Francois Haddad, Tomoya Kitani, et al. 2018. "Determining the Pathogenicity of a Genomic Variant of Uncertain Significance Using CRISPR/Cas9 and Human-Induced Pluripotent Stem Cells." *Circulation* 138 (23): 2666–81.

Mannhardt, Ingra, Kaja Breckwoldt, David Letuffe-Brenière, Sebastian Schaaf, Herbert Schulz, Christiane Neuber, Anika Benzin, et al. 2016. "Human Engineered Heart Tissue: Analysis of Contractile Force." *Stem Cell Reports* 7 (1): 29–42.

Mannhardt, Ingra, Umber Saleem, Anika Benzin, Thomas Schulze, Birgit Klampe, Thomas Eschenhagen, and Arne Hansen. 2017. "Automated Contraction Analysis of Human Engineered Heart Tissue for Cardiac Drug Safety Screening." *Journal of Visualized Experiments: JoVE*, no. 122 (April). https://doi.org/10.3791/55461.

Marchianò, Silvia, Alessandro Bertero, and Charles E. Murry. 2019. "Learn from Your Elders: Developmental Biology Lessons to Guide Maturation of Stem Cell-Derived Cardiomyocytes." *Pediatric Cardiology* 40 (7): 1367–87.

Margara, Francesca, Zhinuo J. Wang, Francesc Levrero-Florencio, Alfonso Santiago, Mariano Vázquez, Alfonso Bueno-Orovio, and Blanca Rodriguez. 2021. "In-Silico Human Electro-Mechanical Ventricular Modelling and Simulation for Drug-Induced pro-Arrhythmia and Inotropic Risk Assessment." *Progress in Biophysics and Molecular Biology* 159 (January): 58–74.

Markati, Theodora, Maryam Oskoui, Michelle A. Farrar, Tina Duong, Nathalie Goemans, and Laurent Servais. 2022. "Emerging Therapies for Duchenne Muscular Dystrophy." *Lancet Neurology* 21 (9): 814–29.

Maron, Barry J. 1999. "Clinical Course of Hypertrophic Cardiomyopathy in a Regional United States Cohort." *JAMA*. https://doi.org/10.1001/jama.281.7.650.

Maron. 2002. "Hypertrophic Cardiomyopathy: A Systematic Review." *JAMA: The Journal of the American Medical Association* 287 (10): 1308–20.

Maron. 2004. "Hypertrophic Cardiomyopathy: An Important Global Disease." *The American Journal of Medicine*. https://doi.org/10.1016/j.amjmed.2003.10.012.

Maron, Barry J., Martin S. Maron, and Christopher Semsarian. 2012. "Genetics of Hypertrophic Cardiomyopathy After 20 Years." *Journal of the American College of Cardiology*. https://doi.org/10.1016/j.jacc.2012.02.068.

Maron, Barry J., Steve R. Ommen, Christopher Semsarian, Paolo Spirito, Iacopo Olivotto, and Martin S. Maron. 2014. "Hypertrophic Cardiomyopathy: Present and Future, with Translation into Contemporary Cardiovascular Medicine." *Journal of the American College of Cardiology* 64 (1): 83–99.

Maron, Martin S., Iacopo Olivotto, Sandro Betocchi, Susan A. Casey, John R. Lesser, Maria A. Losi, Franco Cecchi, and Barry J. Maron. 2003. "Effect of Left Ventricular Outflow Tract Obstruction on Clinical Outcome in Hypertrophic Cardiomyopathy." *New England Journal of Medicine*. https://doi.org/10.1056/nejmoa021332.

Marston, Steven, O'neal Copeland, Katja Gehmlich, Saskia Schlossarek, and Lucie Carrier. 2012. "How Do MYBPC3 Mutations Cause Hypertrophic Cardiomyopathy?" *Journal of Muscle Research and Cell Motility* 33 (1): 75–80.

Marston, Steven, O'neal Copeland, Adam Jacques, Karen Livesey, Victor Tsang, William J. McKenna, Shapour Jalilzadeh, Sebastian Carballo, Charles Redwood, and Hugh Watkins. 2009a. "Evidence From Human Myectomy Samples That *MYBPC3* Mutations Cause Hypertrophic Cardiomyopathy Through Haploinsufficiency." *Circulation Research*. https://doi.org/10.1161/circresaha.109.202440.

Marston, Steven, O'neal Copeland, Adam Jacques, Karen Livesey, Victor Tsang, William J. McKenna, Shapour Jalilzadeh, Sebastian Carballo, Charles Redwood, and Hugh Watkins. 2009b. "Evidence from Human Myectomy Samples That

MYBPC3 Mutations Cause Hypertrophic Cardiomyopathy through Haploinsufficiency." *Circulation Research* 105 (3): 219–22.

Martella, Daniele, Paolo Paoli, Josè M. Pioner, Leonardo Sacconi, Raffaele Coppini, Lorenzo Santini, Matteo Lulli, et al. 2017. "Liquid Crystalline Networks toward Regenerative Medicine and Tissue Repair." *Small* 13 (46). https://doi.org/10.1002/smll.201702677.

Mathur, Anurag, Peter Loskill, Kaifeng Shao, Nathaniel Huebsch, Soongweon Hong, Sivan G. Marcus, Natalie Marks, et al. 2015. "Human iPSC-Based Cardiac Microphysiological System For Drug Screening Applications." *Scientific Reports*. https://doi.org/10.1038/srep08883.

Matsa, Elena, Divya Rajamohan, Emily Dick, Lorraine Young, Ian Mellor, Andrew Staniforth, and Chris Denning. 2011. "Drug Evaluation in Cardiomyocytes Derived from Human Induced Pluripotent Stem Cells Carrying a Long QT Syndrome Type 2 Mutation." *European Heart Journal* 32 (8): 952–62.

Mazzarotto, Francesco, Francesca Girolami, Beatrice Boschi, Fausto Barlocco, Alessia Tomberli, Katia Baldini, Raffaele Coppini, et al. 2019. "Defining the Diagnostic Effectiveness of Genes for Inclusion in Panels: The Experience of Two Decades of Genetic Testing for Hypertrophic Cardiomyopathy at a Single Center." *Genetics in Medicine: Official Journal of the American College of Medical Genetics* 21 (2): 284–92.

McNally, Elizabeth M. 2007. "New Approaches in the Therapy of Cardiomyopathy in Muscular Dystrophy." *Annual Review of Medicine* 58: 75–88.

McNally, Elizabeth M., and Luisa Mestroni. 2017. "Dilated Cardiomyopathy: Genetic Determinants and Mechanisms." *Circulation Research* 121 (7): 731–48.

McNamara, James W., Amy Li, Sean Lal, J. Martijn Bos, Samantha P. Harris, Jolanda van der Velden, Michael J. Ackerman, Roger Cooke, and Cristobal G. Dos Remedios. 2017. "MYBPC3 Mutations Are Associated with a Reduced Super-Relaxed State in Patients with Hypertrophic Cardiomyopathy." *PloS One* 12 (6): e0180064.

McNamara, James W., Amy Li, Nicola J. Smith, Sean Lal, Robert M. Graham, Kristina Bezold Kooiker, Sabine J. van Dijk, Cristobal G. Dos Remedios, Samantha P. Harris, and Roger Cooke. 2016. "Ablation of Cardiac Myosin Binding Protein-C Disrupts the Super-Relaxed State of Myosin in Murine Cardiomyocytes." *Journal of Molecular and Cellular Cardiology* 94 (May): 65–71.

Mehta, Ashish, Glen Lester Sequiera, Chrishan J. A. Ramachandra, Yuliansa Sudibyo, Yingying Chung, Jingwei Sheng, Keng Yean Wong, et al. 2014. "Re-Trafficking of hERG Reverses Long QT Syndrome 2 Phenotype in Human iPS-Derived Cardiomyocytes." *Cardiovascular Research* 102 (3): 497–506.

Meijer van Putten, Rosalie M. E., Isabella Mengarelli, Kaomei Guan, Jan G. Zegers, Antoni C. G. van Ginneken, Arie O. Verkerk, and Ronald Wilders. 2015. "Ion Channelopathies in Human Induced Pluripotent Stem Cell Derived Cardiomyocytes: A Dynamic Clamp Study with Virtual IK1." *Frontiers in Physiology* 6 (February): 7.

Merkle, Florian T., Werner M. Neuhausser, David Santos, Eivind Valen, James A. Gagnon, Kristi Maas, Jackson Sandoe, Alexander F. Schier, and Kevin Eggan. 2015. "Efficient CRISPR-Cas9-Mediated Generation of Knockin Human Pluripotent Stem Cells Lacking Undesired Mutations at the Targeted Locus." *Cell Reports* 11 (6): 875–83.

Merlo, Marco, Gianfranco Sinagra, Elisa Carniel, Dobromir Slavov, Xiao Zhu, Giulia Barbati, Anita Spezzacatene, et al. 2013. "Poor Prognosis of Rare Sarcomeric Gene Variants in Patients with Dilated Cardiomyopathy." *Clinical and Translational Science* 6 (6): 424–28.

Merrick, Deborah, Lukas Kurt Josef Stadler, Dean Larner, and Janet Smith. 2009. "Muscular Dystrophy Begins Early in Embryonic Development Deriving from Stem Cell Loss and Disrupted Skeletal Muscle Formation." *Disease Models & Mechanisms* 2 (7-8): 374–88.

Mestroni, Luisa, Francesca Brun, Anita Spezzacatene, Gianfranco Sinagra, and Matthew Rg Taylor. 2014. "GENETIC CAUSES OF DILATED CARDIOMYOPATHY." *Progress in Pediatric Cardiology* 37 (1-2): 13–18.

Meyer, Pierre, Cécile Notarnicola, Albano C. Meli, Stefan Matecki, Gérald Hugon, Jérémy Salvador, Mirna Khalil, et al. 2021. "Skeletal Ryanodine Receptors Are Involved in Impaired Myogenic Differentiation in Duchenne Muscular Dystrophy Patients." *International Journal of Molecular Sciences* 22 (23). https://doi.org/10.3390/ijms222312985.

Mitzelfelt, Katie A., Pattraranee Limphong, Melinda J. Choi, Frances D. L. Kondrat, Shuping Lai, Kurt D. Kolander, Wai-Meng Kwok, et al. 2016. "The Human 343delT HSPB5 Chaperone Associated with Early-Onset Skeletal Myopathy Causes Defects in Protein Solubility." *The Journal of Biological Chemistry* 291 (29): 14939–53.

Moloughney, Joseph G., and Noah Weisleder. 2012. "Poloxamer 188 (p188) as a Membrane Resealing Reagent in Biomedical Applications." *Recent Patents on Biotechnology* 6 (3): 200–211.

Monteiro da Rocha, Andre, Guadalupe Guerrero-Serna, Adam Helms, Carly Luzod, Sergey Mironov, Mark Russell, José Jalife, Sharlene M. Day, Gary D. Smith, and Todd J. Herron. 2016. "Deficient cMyBP-C Protein Expression during Cardiomyocyte Differentiation Underlies Human Hypertrophic Cardiomyopathy Cellular Phenotypes in Disease Specific Human ES Cell Derived Cardiomyocytes." *Journal of Molecular and Cellular Cardiology* 99 (October): 197–206.

Moolman-Smook, Johanna, Emily Flashman, Willem de Lange, Zhili Li, Valerie Corfield, Charles Redwood, and Hugh Watkins. 2002. "Identification of Novel Interactions between Domains of Myosin Binding Protein-C That Are Modulated by Hypertrophic Cardiomyopathy Missense Mutations." *Circulation Research* 91 (8): 704–11.

Moreau, Adrien, Pascal Gosselin-Badaroudine, Aurélie Mercier, Bettina Burger, Dagmar I. Keller, and Mohamed Chahine. 2018. "A Leaky Voltage Sensor Domain of Cardiac Sodium Channels Causes Arrhythmias Associated with Dilated

Cardiomyopathy." *Scientific Reports* 8 (1): 13804.

Moretti, A., L. Fonteyne, F. Giesert, P. Hoppmann, A. B. Meier, T. Bozoglu, A. Baehr, et al. 2020. "Somatic Gene Editing Ameliorates Skeletal and Cardiac Muscle Failure in Pig and Human Models of Duchenne Muscular Dystrophy." *Nature Medicine* 26 (2): 207–14.

Moretti, Alessandra, Milena Bellin, Andrea Welling, Christian Billy Jung, Jason T. Lam, Lorenz Bott-Flügel, Tatjana Dorn, et al. 2010. "Patient-Specific Induced Pluripotent Stem-Cell Models for Long-QT Syndrome." *New England Journal of Medicine*. https://doi.org/10.1056/nejmoa0908679.

Mosqueira, Diogo, Ingra Mannhardt, Jamie R. Bhagwan, Katarzyna Lis-Slimak, Puspita Katili, Elizabeth Scott, Mustafa Hassan, et al. 2018. "CRISPR/Cas9 Editing in Human Pluripotent Stem Cell-Cardiomyocytes Highlights Arrhythmias, Hypocontractility, and Energy Depletion as Potential Therapeutic Targets for Hypertrophic Cardiomyopathy." *European Heart Journal* 39 (43): 3879–92.

Mulieri, L. A., G. Hasenfuss, B. Leavitt, P. D. Allen, and N. R. Alpert. 1992. "Altered Myocardial Force-Frequency Relation in Human Heart Failure." *Circulation* 85 (5): 1743–50.

Mummery, Christine, Dorien Ward-van Oostwaard, Pieter Doevendans, Rene Spijker, Stieneke van den Brink, Rutger Hassink, Marcel van der Heyden, et al. 2003. "Differentiation of Human Embryonic Stem Cells to Cardiomyocytes." *Circulation*. https://doi.org/10.1161/01.cir.0000068356.38592.68.

Nakayama, Karina H., Luqia Hou, and Ngan F. Huang. 2014. "Role of Extracellular Matrix Signaling Cues in Modulating Cell Fate Commitment for Cardiovascular Tissue Engineering." *Advanced Healthcare Materials* 3 (5): 628–41.

Narolska, N. A., R. B. van Loon, N. M. Boontje, R. Zaremba, S. Eiras Penas, J. Russell, S. R. Spiegelenberg, et al. 2005. "Myocardial Contraction Is 5-Fold More Economical in Ventricular than in Atrial Human Tissue." *Cardiovascular Research* 65 (1): 221–29.

Navarrete, Enrique G., Ping Liang, Feng Lan, Verónica Sanchez-Freire, Chelsey Simmons, Tingyu Gong, Arun Sharma, et al. 2013. "Screening Drug-Induced Arrhythmia Using Human Induced Pluripotent Stem Cell–Derived Cardiomyocytes and Low-Impedance Microelectrode Arrays." *Circulation*. https://doi.org/10.1161/circulationaha.112.000570.

Neagoe, Ciprian, Michael Kulke, Federica del Monte, Judith K. Gwathmey, Pieter P. de Tombe, Roger J. Hajjar, and Wolfgang A. Linke. 2002. "Titin Isoform Switch in Ischemic Human Heart Disease." *Circulation* 106 (11): 1333–41.

Newman, Aaron M., and James B. Cooper. 2010. "Lab-Specific Gene Expression Signatures in Pluripotent Stem Cells." *Cell Stem Cell*. https://doi.org/10.1016/j.stem.2010.06.016.

Ng, Ronald, Heather Manring, Nikolaos Papoutsidakis, Taylor Albertelli, Nicole Tsai, Claudia J. See, Xia Li, et al. 2019. "Patient Mutations Linked to Arrhythmogenic Cardiomyopathy Enhance Calpain-Mediated Desmoplakin Degradation." *JCI Insight* 5 (14). https://doi.org/10.1172/jci.insight.128643.

Ng, Ronald, Lorenzo R. Sewanan, Paul Stankey, Xia Li, Yibing Qyang, and Stuart Campbell. 2021. "Shortening Velocity Causes Myosin Isoform Shift in Human Engineered Heart Tissues." *Circulation Research* 128 (2): 281–83.

Nigro, G., L. I. Comi, L. Politano, and R. J. I. Bain. 1990. "The Incidence and Evolution of Cardiomyopathy in Duchenne Muscular Dystrophy." *International Journal of Cardiology*. https://doi.org/10.1016/0167-5273(90)90082-g.

Niimura, H., L. L. Bachinski, S. Sangwatanaroj, H. Watkins, A. E. Chudley, W. McKenna, A. Kristinsson, et al. 1998. "Mutations in the Gene for Cardiac Myosin-Binding Protein C and Late-Onset Familial Hypertrophic Cardiomyopathy." *The New England Journal of Medicine* 338 (18): 1248–57.

Nistri, Stefano, Iacopo Olivotto, Sandro Betocchi, Maria Angela Losi, Grazia Valsecchi, Bruno Pinamonti, Maria Rosa Conte, et al. 2006. "Prognostic Significance of Left Atrial Size in Patients with Hypertrophic Cardiomyopathy (from the Italian Registry for Hypertrophic Cardiomyopathy)." *The American Journal of Cardiology* 98 (7): 960–65.

Ojala, Marisa, Chandra Prajapati, Risto-Pekka Pölönen, Kristiina Rajala, Mari Pekkanen-Mattila, Jyrki Rasku, Kim Larsson, and Katriina Aalto-Setälä. 2016. "Mutation-Specific Phenotypes in hiPSC-Derived Cardiomyocytes Carrying Either Myosin-Binding Protein C Or α-Tropomyosin Mutation for Hypertrophic Cardiomyopathy." *Stem Cells International* 2016: 1684792.

Olivetti, G. 1996. "Aging, Cardiac Hypertrophy and Ischemic Cardiomyopathy Do Not Affect the Proportion of Mononucleated and Multinucleated Myocytes in the Human Heart." *Journal of Molecular and Cellular Cardiology*. https://doi.org/10.1006/jmcc.1996.0137.

Olivotto, Iacopo, Giulia d'Amati, Cristina Basso, Albert Van Rossum, Monica Patten, Michele Emdin, Yigal Pinto, Benedetta Tomberli, Paolo G. Camici, and Michelle Michels. 2015. "Defining Phenotypes and Disease Progression in Sarcomeric Cardiomyopathies: Contemporary Role of Clinical Investigations." *Cardiovascular Research* 105 (4): 409–23.

Olivotto, Iacopo, Paolo G. Camici, Piera Angelica Merlini, Claudio Rapezzi, Monica Patten, Vicent Climent, Gianfranco Sinagra, et al. 2018. "Efficacy of Ranolazine in Patients With Symptomatic Hypertrophic Cardiomyopathy: The RESTYLE-HCM Randomized, Double-Blind, Placebo-Controlled Study." *Circulation. Heart Failure* 11 (1): e004124.

Olivotto, Iacopo, Franco Cecchi, Corrado Poggesi, and Magdi H. Yacoub. 2009. "Developmental Origins of Hypertrophic Cardiomyopathy Phenotypes: A Unifying Hypothesis." *Nature Reviews. Cardiology* 6 (4): 317–21.

Olivotto, Iacopo, Francesca Girolami, Michael J. Ackerman, Stefano Nistri, J. Martijn Bos, Elisabetta Zachara, Steve R. Ommen, et al. 2008. "Myofilament Protein Gene Mutation Screening and Outcome of Patients With Hypertrophic Cardiomyopathy." *Mayo Clinic Proceedings*. https://doi.org/10.4065/83.6.630.

Olivotto, Iacopo, Francesca Girolami, Stefano Nistri, Alessandra Rossi, Luigi Rega, Francesca Garbini, Camilla Grifoni, Franco

Cecchi, and Magdi H. Yacoub. 2009. "The Many Faces of Hypertrophic Cardiomyopathy: From Developmental Biology to Clinical Practice." *Journal of Cardiovascular Translational Research* 2 (4): 349–67.

Olivotto, Iacopo, Roberto Gistri, Pasquale Petrone, Elena Pedemonte, Daniela Vargiu, and Franco Cecchi. 2003. "Maximum Left Ventricular Thickness and Risk of Sudden Death in Patients with Hypertrophic Cardiomyopathy." *Journal of the American College of Cardiology* 41 (2): 315–21.

Olivotto, Iacopo, Artur Oreziak, Roberto Barriales-Villa, Theodore P. Abraham, Ahmad Masri, Pablo Garcia-Pavia, Sara Saberi, et al. 2020. "Mavacamten for Treatment of Symptomatic Obstructive Hypertrophic Cardiomyopathy (EXPLORER-HCM): A Randomised, Double-Blind, Placebo-Controlled, Phase 3 Trial." *The Lancet* 396 (10253): 759–69.

Olivotto, I., F. Cecchi, S. A. Casey, A. Dolara, J. H. Traverse, and B. J. Maron. 2001. "Impact of Atrial Fibrillation on the Clinical Course of Hypertrophic Cardiomyopathy." *Circulation* 104 (21): 2517–24.

Page, Stephen P., Stavros Kounas, Petros Syrris, Michael Christiansen, Rune Frank-Hansen, Paal Skytt Andersen, Perry M. Elliott, and William J. McKenna. 2012. "Cardiac Myosin Binding Protein-C Mutations in Families with Hypertrophic Cardiomyopathy: Disease Expression in Relation to Age, Gender, and Long-Term Outcome." *Circulation. Cardiovascular Genetics* 5 (2): 156–66.

Paige, Sharon L., Sean Thomas, Cristi L. Stoick-Cooper, Hao Wang, Lisa Maves, Richard Sandstrom, Lil Pabon, et al. 2012. "A Temporal Chromatin Signature in Human Embryonic Stem Cells Identifies Regulators of Cardiac Development." *Cell*. https://doi.org/10.1016/j.cell.2012.08.027.

Park, Jinseok, Hong-Nam Kim, Deok-Ho Kim, A. Levchenko, and Kahp-Yang Suh. 2012. "Quantitative Analysis of the Combined Effect of Substrate Rigidity and Topographic Guidance on Cell Morphology." *IEEE Transactions on NanoBioscience*. https://doi.org/10.1109/tnb.2011.2165728.

Parks, Sharie B., Jessica D. Kushner, Deirdre Nauman, Donna Burgess, Susan Ludwigsen, Amanda Peterson, Duanxiang Li, et al. 2008. "Lamin A/C Mutation Analysis in a Cohort of 324 Unrelated Patients with Idiopathic or Familial Dilated Cardiomyopathy." *American Heart Journal* 156 (1): 161–69.

Passini, Elisa, Ana Mincholé, Raffaele Coppini, Elisabetta Cerbai, Blanca Rodriguez, Stefano Severi, and Alfonso Bueno-Orovio. 2016. "Mechanisms of pro-Arrhythmic Abnormalities in Ventricular Repolarisation and Anti-Arrhythmic Therapies in Human Hypertrophic Cardiomyopathy." *Journal of Molecular and Cellular Cardiology* 96 (July): 72–81.

Peters, N. S., C. R. Green, P. A. Poole-Wilson, and N. J. Severs. 1993. "Reduced Content of connexin43 Gap Junctions in Ventricular Myocardium from Hypertrophied and Ischemic Human Hearts." *Circulation* 88 (3): 864–75.

Pioner, J. Manuel, Xuan Guan, Jordan M. Klaiman, Alice W. Racca, Lil Pabon, Veronica Muskheli, Jesse Macadangdang, et al. 2020. "Absence of Full-Length Dystrophin Impairs Normal Maturation and Contraction of Cardiomyocytes Derived from Human-Induced Pluripotent Stem Cells." *Cardiovascular Research* 116 (2): 368–82.

Pioner, Josè Manuel, Alessandra Fornaro, Raffaele Coppini, Nicole Ceschia, Leonardo Sacconi, Maria Alice Donati, Silvia Favilli, Corrado Poggesi, Iacopo Olivotto, and Cecilia Ferrantini. 2020. "Advances in Stem Cell Modeling of Dystrophin-Associated Disease: Implications for the Wider World of Dilated Cardiomyopathy." *Frontiers in Physiology* 11 (May): 368.

Pioner, Josè Manuel, Alice W. Racca, Jordan M. Klaiman, Kai-Chun Yang, Xuan Guan, Lil Pabon, Veronica Muskheli, et al. 2016. "Isolation and Mechanical Measurements of Myofibrils from Human Induced Pluripotent Stem Cell-Derived Cardiomyocytes." *Stem Cell Reports* 6 (6): 885–96.

Pioner, Josè Manuel, Lorenzo Santini, Chiara Palandri, Marianna Langione, Bruno Grandinetti, Silvia Querceto, Daniele Martella, et al. 2022. "Calcium Handling Maturation and Adaptation to Increased Substrate Stiffness in Human iPSC-Derived Cardiomyocytes: The Impact of Full-Length Dystrophin Deficiency." *Frontiers in Physiology* 13 (November): 1030920.

Pioner, Josè Manuel, Lorenzo Santini, Chiara Palandri, Daniele Martella, Flavia Lupi, Marianna Langione, Silvia Querceto, et al. 2019. "Optical Investigation of Action Potential and Calcium Handling Maturation of hiPSC-Cardiomyocytes on Biomimetic Substrates." *International Journal of Molecular Sciences* 20 (15). https://doi.org/10.3390/ijms20153799.

Pioner, Josè Manuel, Giulia Vitale, Sonette Steczina, Marianna Langione, Francesca Margara, Lorenzo Santini, Francesco Giardini, et al. 2023. "Slower Calcium Handling Balances Faster Crossbridge Cycling in Human HCM." *Circulation Research*, February. https://doi.org/10.1161/CIRCRESAHA.122.321956.

Piroddi, Nicoletta, Alexandra Belus, Beatrice Scellini, Chiara Tesi, Gabriele Giunti, Elisabetta Cerbai, Alessandro Mugelli, and Corrado Poggesi. 2007. "Tension Generation and Relaxation in Single Myofibrils from Human Atrial and Ventricular Myocardium." *Pflugers Archiv: European Journal of Physiology* 454 (1): 63–73.

Piroddi, Nicoletta, E. Rosalie Witjas-Paalberends, Claudia Ferrara, Cecilia Ferrantini, Giulia Vitale, Beatrice Scellini, Paul J. M. Wijnker, et al. 2019. "The Homozygous K280N Troponin T Mutation Alters Cross-Bridge Kinetics and Energetics in Human HCM." *The Journal of General Physiology* 151 (1): 18–29.

Poggesi, Corrado, and Carolyn Y. Ho. 2014. "Muscle Dysfunction in Hypertrophic Cardiomyopathy: What Is Needed to Move to Translation?" *Journal of Muscle Research and Cell Motility* 35 (1): 37–45.

Poggesi, Corrado, Chiara Tesi, and Robert Stehle. 2005. "Sarcomeric Determinants of Striated Muscle Relaxation Kinetics." *Pflugers Archiv: European Journal of Physiology* 449 (6): 505–17.

Prondzynski, Maksymilian, Elisabeth Krämer, Sandra D. Laufer, Aya Shibamiya, Ole Pless, Frederik Flenner, Oliver J. Müller, et al. 2017. "Evaluation of MYBPC3 Trans-Splicing and Gene Replacement as Therapeutic Options in Human iPSC-Derived

Cardiomyocytes." *Molecular Therapy. Nucleic Acids* 7 (June): 475–86.

Prondzynski, Maksymilian, Marc D. Lemoine, Antonia Tl Zech, András Horváth, Vittoria Di Mauro, Jussi T. Koivumäki, Nico Kresin, et al. 2019. "Disease Modeling of a Mutation in α-Actinin 2 Guides Clinical Therapy in Hypertrophic Cardiomyopathy." *EMBO Molecular Medicine* 11 (12): e11115.

Querceto, Silvia, Rosaria Santoro, Aoife Gowran, Bruno Grandinetti, Giulio Pompilio, Michael Regnier, Chiara Tesi, Corrado Poggesi, Cecilia Ferrantini, and Josè Manuel Pioner. 2022. "The Harder the Climb the Better the View: The Impact of Substrate Stiffness on Cardiomyocyte Fate." *Journal of Molecular and Cellular Cardiology*. https://doi.org/10.1016/j.yjmcc.2022.02.001.

Raab, Stefanie, Moritz Klingenstein, Stefan Liebau, and Leonhard Linta. 2014. "A Comparative View on Human Somatic Cell Sources for iPSC Generation." *Stem Cells International* 2014 (November): 768391.

Racca, Alice W., Jordan M. Klaiman, J. Manuel Pioner, Yuanhua Cheng, Anita E. Beck, Farid Moussavi-Harami, Michael J. Bamshad, and Michael Regnier. 2016. "Contractile Properties of Developing Human Fetal Cardiac Muscle." *The Journal of Physiology* 594 (2): 437–52.

Rahimov, Fedik, and Louis M. Kunkel. 2013. "Cellular and Molecular Mechanisms Underlying Muscular Dystrophy." *Journal of Cell Biology*. https://doi.org/10.1083/jcb.201212142.

Ramachandra, Chrishan J. A., Myu Mai Ja Kp, Jasper Chua, Sauri Hernandez-Resendiz, Elisa A. Liehn, Ralph Knöll, Li-Ming Gan, et al. 2022. "Inhibiting Cardiac Myeloperoxidase Alleviates the Relaxation Defect in Hypertrophic Cardiomyocytes." *Cardiovascular Research* 118 (2): 517–30.

Rana, M. S., V. M. Christoffels, and A. F. M. Moorman. 2013. "A Molecular and Genetic Outline of Cardiac Morphogenesis." *Acta Physiologica*. https://doi.org/10.1111/apha.12061.

Reiser, Peter J., Michael A. Portman, Xue-Han Ning, and Christine Schomisch Moravec. 2001. "Human Cardiac Myosin Heavy Chain Isoforms in Fetal and Failing Adult Atria and Ventricles." *American Journal of Physiology-Heart and Circulatory Physiology*, April. https://doi.org/10.1152/ajpheart.2001.280.4.H1814.

Ribeiro, Alexandre J. S., Yen-Sin Ang, Ji-Dong Fu, Renee N. Rivas, Tamer M. A. Mohamed, Gadryn C. Higgs, Deepak Srivastava, and Beth L. Pruitt. 2015. "Contractility of Single Cardiomyocytes Differentiated from Pluripotent Stem Cells Depends on Physiological Shape and Substrate Stiffness." *Proceedings of the National Academy of Sciences of the United States of America* 112 (41): 12705–10.

Ribeiro, Marcelo C., Rolf H. Slaats, Verena Schwach, José M. Rivera-Arbelaez, Leon G. J. Tertoolen, Berend J. van Meer, Robert Molenaar, Christine L. Mummery, Mireille M. A. E. Claessens, and Robert Passier. 2020. "A Cardiomyocyte Show of Force: A Fluorescent Alpha-Actinin Reporter Line Sheds Light on Human Cardiomyocyte Contractility versus Substrate Stiffness." *Journal of Molecular and Cellular Cardiology* 141 (April): 54–64.

Ribeiro, Marcelo C., Leon G. Tertoolen, Juan A. Guadix, Milena Bellin, Georgios Kosmidis, Cristina D'Aniello, Jantine Monshouwer-Kloots, et al. 2015. "Functional Maturation of Human Pluripotent Stem Cell Derived Cardiomyocytes in Vitro – Correlation between Contraction Force and Electrophysiology." *Biomaterials*. https://doi.org/10.1016/j.biomaterials.2015.01.067.

Richard, Pascale, Philippe Charron, Lucie Carrier, Céline Ledeuil, Theary Cheav, Claire Pichereau, Abdelaziz Benaiche, et al. 2003. "Hypertrophic Cardiomyopathy: Distribution of Disease Genes, Spectrum of Mutations, and Implications for a Molecular Diagnosis Strategy." *Circulation* 107 (17): 2227–32.

Ripoll-Vera, Tomás, José María Gámez, Nancy Govea, Yolanda Gómez, Juana Núñez, Lorenzo Socías, Ángela Escandell, and Jorge Rosell. 2016. "Clinical and Prognostic Profiles of Cardiomyopathies Caused by Mutations in the Troponin T Gene." *Revista Espanola de Cardiologia* 69 (2): 149–58.

Roberts, Angharad M., James S. Ware, Daniel S. Herman, Sebastian Schafer, John Baksi, Alexander G. Bick, Rachel J. Buchan, et al. 2015. "Integrated Allelic, Transcriptional, and Phenomic Dissection of the Cardiac Effects of Titin Truncations in Health and Disease." *Science Translational Medicine* 7 (270): 270ra6.

Rochais, Francesca, Karim Mesbah, and Robert G. Kelly. 2009. "Signaling Pathways Controlling Second Heart Field Development." *Circulation Research*. https://doi.org/10.1161/circresaha.109.194464.

Rodriguez, Anthony G., Sangyoon J. Han, Michael Regnier, and Nathan J. Sniadecki. 2011. "Substrate Stiffness Increases Twitch Power of Neonatal Cardiomyocytes in Correlation with Changes in Myofibril Structure and Intracellular Calcium." *Biophysical Journal* 101 (10): 2455–64.

Ronaldson-Bouchard, Kacey, Stephen P. Ma, Keith Yeager, Timothy Chen, Loujin Song, Dario Sirabella, Kumi Morikawa, Diogo Teles, Masayuki Yazawa, and Gordana Vunjak-Novakovic. 2018. "Advanced Maturation of Human Cardiac Tissue Grown from Pluripotent Stem Cells." *Nature* 556 (7700): 239–43.

Ruan, Jia-Ling, Nathaniel L. Tulloch, Maria V. Razumova, Mark Saiget, Veronica Muskheli, Lil Pabon, Hans Reinecke, Michael Regnier, and Charles E. Murry. 2016. "Mechanical Stress Conditioning and Electrical Stimulation Promote Contractility and Force Maturation of Induced Pluripotent Stem Cell-Derived Human Cardiac Tissue." *Circulation* 134 (20): 1557–67.

Sadayappan, Sakthivel, and Pieter P. de Tombe. 2012. "Cardiac Myosin Binding Protein-C: Redefining Its Structure and Function." *Biophysical Reviews* 4 (2): 93–106.

Santini, et al. 2017. "Ranolazine Prevents Phenotype Development in a Mouse Model of Hypertrophic Cardiomyopathy." Circulation: Heart Failure. https://doi.org/10.1161/circheartfailure.116.003565.

Santoro, Rosaria, Gianluca Lorenzo Perrucci, Aoife Gowran, and Giulio Pompilio. 2019. "Unchain My Heart: Integrins at the

Basis of iPSC Cardiomyocyte Differentiation." *Stem Cells International* 2019 (February): 8203950.

Sartiani, Laura, Esther Bettiol, Francesca Stillitano, Alessandro Mugelli, Elisabetta Cerbai, and Marisa E. Jaconi. 2007. "Developmental Changes in Cardiomyocytes Differentiated from Human Embryonic Stem Cells: A Molecular and Electrophysiological Approach." *Stem Cells*. https://doi.org/10.1634/stemcells.2006-0466.

Scellini, Beatrice, Nicoletta Piroddi, Marica Dente, Giulia Vitale, Josè Manuel Pioner, Raffaele Coppini, Cecilia Ferrantini, Corrado Poggesi, and Chiara Tesi. 2021. "Mavacamten Has a Differential Impact on Force Generation in Myofibrils from Rabbit Psoas and Human Cardiac Muscle." *The Journal of General Physiology* 153 (7). https://doi.org/10.1085/jgp.202012789.

Schaaf, Sebastian, Aya Shibamiya, Marco Mewe, Alexandra Eder, Andrea Stöhr, Marc N. Hirt, Thomas Rau, et al. 2011. "Human Engineered Heart Tissue as a Versatile Tool in Basic Research and Preclinical Toxicology." *PloS One* 6 (10): e26397.

Schaper, J., F. Schwarz, H. Kittstein, E. Kreisel, B. Winkler, and F. Hehrlein. 1980. "Ultrastructural Evaluation of the Effects of Global Ischemia and Reperfusion on Human Myocardium." *The Thoracic and Cardiovascular Surgeon*. https://doi.org/10.1055/s-2007-1022104.

Schmid, Manuel, and Christopher N. Toepfer. 2021. "Cardiac Myosin Super Relaxation (SRX): A Perspective on Fundamental Biology, Human Disease and Therapeutics." *Biology Open* 10 (2). https://doi.org/10.1242/bio.057646.

Scuderi, Gaetano J., and Jonathan Butcher. 2017. "Naturally Engineered Maturation of Cardiomyocytes." *Frontiers in Cell and Developmental Biology* 5 (May): 50.

Seeger, Timon, Rajani Shrestha, Chi Keung Lam, Caressa Chen, Wesley L. McKeithan, Edward Lau, Alexa Wnorowski, et al. 2019. "A Premature Termination Codon Mutation in MYBPC3 Causes Hypertrophic Cardiomyopathy via Chronic Activation of Nonsense-Mediated Decay." *Circulation* 139 (6): 799–811.

Semsarian, Christopher, Jodie Ingles, Martin S. Maron, and Barry J. Maron. 2015. "New Perspectives on the Prevalence of Hypertrophic Cardiomyopathy." *Journal of the American College of Cardiology*. https://doi.org/10.1016/j.jacc.2015.01.019.

Sewanan, Lorenzo R., Shi Shen, and Stuart G. Campbell. 2021. "Mavacamten Preserves Length-Dependent Contractility and Improves Diastolic Function in Human Engineered Heart Tissue." *American Journal of Physiology. Heart and Circulatory Physiology* 320 (3): H1112–23.

Shen, Shi, Lorenzo R. Sewanan, Stephanie Shao, Saiti S. Halder, Paul Stankey, Xia Li, and Stuart G. Campbell. 2022. "Physiological Calcium Combined with Electrical Pacing Accelerates Maturation of Human Engineered Heart Tissue." *Stem Cell Reports* 17 (9): 2037–49.

Shimojima, Masaya, Shinsuke Yuasa, Chikaaki Motoda, Gakuto Yozu, Toshihiro Nagai, Shogo Ito, Mark Lachmann, et al. 2017. "Emerin Plays a Crucial Role in Nuclear Invagination and in the Nuclear Calcium Transient." *Scientific Reports* 7 (March): 44312.

Shirokova, Natalia, and Ernst Niggli. 2013. "Cardiac Phenotype of Duchenne Muscular Dystrophy: Insights from Cellular Studies." *Journal of Molecular and Cellular Cardiology*. https://doi.org/10.1016/j.yjmcc.2012.12.009.

Shum, Angie M. Y., Hui Che, Andy On-Tik Wong, Chenzi Zhang, Hongkai Wu, Camie W. Y. Chan, Kevin Costa, Michelle Khine, Chi-Wing Kong, and Ronald A. Li. 2017. "A Micropatterned Human Pluripotent Stem Cell-Based Ventricular Cardiac Anisotropic Sheet for Visualizing Drug-Induced Arrhythmogenicity." *Advanced Materials* 29 (1). https://doi.org/10.1002/adma.201602448.

Shyu, Kou-Gi. 2009. "Cellular and Molecular Effects of Mechanical Stretch on Vascular Cells and Cardiac Myocytes." *Clinical Science* 116 (5): 377–89.

Singer, Emma S., Jodie Ingles, Christopher Semsarian, and Richard D. Bagnall. 2019. "Key Value of RNA Analysis of MYBPC3 Splice-Site Variants in Hypertrophic Cardiomyopathy." *Circulation. Genomic and Precision Medicine* 12 (1): e002368.

Siu, Chung-Wah, Yee-Ki Lee, Jenny Chung-Yee Ho, Wing-Hon Lai, Yau-Chi Chan, Kwong-Man Ng, Lai-Yung Wong, et al. 2012. "Modeling of Lamin A/C Mutation Premature Cardiac Aging Using Patient-specific Induced Pluripotent Stem Cells." *Aging* 4 (11): 803–22.

Smith, James G. W., Thomas Owen, Jamie R. Bhagwan, Diogo Mosqueira, Elizabeth Scott, Ingra Mannhardt, Asha Patel, et al. 2018. "Isogenic Pairs of hiPSC-CMs with Hypertrophic Cardiomyopathy/LVNC-Associated ACTC1 E99K Mutation Unveil Differential Functional Deficits." *Stem Cell Reports* 11 (5): 1226–43.

Snir, Mirit, Izhak Kehat, Amira Gepstein, Raymond Coleman, Joseph Itskovitz-Eldor, Erella Livne, and Lior Gepstein. 2003. "Assessment of the Ultrastructural and Proliferative Properties of Human Embryonic Stem Cell-Derived Cardiomyocytes." *American Journal of Physiology-Heart and Circulatory Physiology*. https://doi.org/10.1152/ajpheart.00020.2003.

Spach, Madison S., J. Francis Heidlage, Roger C. Barr, and Paul C. Dolber. 2004. "Cell Size and Communication: Role in Structural and Electrical Development and Remodeling of the Heart." *Heart Rhythm*. https://doi.org/10.1016/j.hrthm.2004.06.010.

Sparrow, Alexander J., Hugh Watkins, Matthew J. Daniels, Charles Redwood, and Paul Robinson. 2020. "Mavacamten Rescues Increased Myofilament Calcium Sensitivity and Dysregulation of Ca^2 Flux Caused by Thin Filament Hypertrophic Cardiomyopathy Mutations." *American Journal of Physiology-Heart and Circulatory Physiology*. https://doi.org/10.1152/ajpheart.00023.2020.

Spindler, M., K. W. Saupe, M. E. Christe, H. L. Sweeney, C. E. Seidman, J. G. Seidman, and J. S. Ingwall. 1998. "Diastolic Dysfunction and Altered Energetics in the alphaMHC403/+ Mouse Model of Familial Hypertrophic Cardiomyopathy." *The Journal of Clinical Investigation* 101 (8): 1775–83.

Spronk, Henri M. H., Anne Margreet de Jong, Harry J. Crijns, Ulrich Schotten, Isabelle C. Van Gelder, and Hugo Ten Cate. 2014. "Pleiotropic Effects of Factor Xa and Thrombin: What to Expect from Novel Anticoagulants." *Cardiovascular Research* 101 (3): 344–51.

Spudich, James A. 2019. "Three Perspectives on the Molecular Basis of Hypercontractility Caused by Hypertrophic Cardiomyopathy Mutations." *Pflugers Archiv: European Journal of Physiology* 471 (5): 701–17.

Squire, John M., Pradeep K. Luther, and Carlo Knupp. 2003. "Structural Evidence for the Interaction of C-Protein (MyBP-C) with Actin and Sequence Identification of a Possible Actin-Binding Domain." *Journal of Molecular Biology* 331 (3): 713–24.

Stelzer, Julian E., Daniel P. Fitzsimons, and Richard L. Moss. 2006. "Ablation of Myosin-Binding Protein-C Accelerates Force Development in Mouse Myocardium." *Biophysical Journal* 90 (11): 4119–27.

Streckfuss-Bömeke, Katrin, Malte Tiburcy, Andrey Fomin, Xiaojing Luo, Wener Li, Claudia Fischer, Cemil Özcelik, et al. 2017. "Severe DCM Phenotype of Patient Harboring RBM20 Mutation S635A Can Be Modeled by Patient-Specific Induced Pluripotent Stem Cell-Derived Cardiomyocytes." *Journal of Molecular and Cellular Cardiology* 113 (December): 9–21.

Stroik, Daniel R., Delaine K. Ceholski, Philip A. Bidwell, Justyna Mleczko, Paul F. Thanel, Forum Kamdar, Joseph M. Autry, Razvan L. Cornea, and David D. Thomas. 2020. "Viral Expression of a SERCA2a-Activating PLB Mutant Improves Calcium Cycling and Synchronicity in Dilated Cardiomyopathic hiPSC-CMs." *Journal of Molecular and Cellular Cardiology* 138 (January): 59–65.

Suay-Corredera, Carmen, Maria Rosaria Pricolo, Elías Herrero-Galán, Diana Velázquez-Carreras, David Sánchez-Ortiz, Diego García-Giustiniani, Javier Delgado, et al. 2021. "Protein Haploinsufficiency Drivers Identify MYBPC3 Variants That Cause Hypertrophic Cardiomyopathy." *The Journal of Biological Chemistry* 297 (1): 100854.

Sun, Ning, Masayuki Yazawa, Jianwei Liu, Leng Han, Veronica Sanchez-Freire, Oscar J. Abilez, Enrique G. Navarrete, et al. 2012. "Patient-Specific Induced Pluripotent Stem Cells as a Model for Familial Dilated Cardiomyopathy." *Science Translational Medicine* 4 (130): 130ra47.

Synnergren, Jane, Caroline Améen, Andreas Jansson, and Peter Sartipy. 2012. "Global Transcriptional Profiling Reveals Similarities and Differences between Human Stem Cell-Derived Cardiomyocyte Clusters and Heart Tissue." *Physiological Genomics*. https://doi.org/10.1152/physiolgenomics.00118.2011.

Taggart, Peter, Peter M. I. Sutton, Tobias Opthof, Ruben Coronel, Richard Trimlett, Wilfred Pugsley, and Panny Kallis. 2000. "Inhomogeneous Transmural Conduction During Early Ischaemia in Patients with Coronary Artery Disease." *Journal of Molecular and Cellular Cardiology*. https://doi.org/10.1006/jmcc.2000.1105.

Takahashi, Kazutoshi, Koji Tanabe, Mari Ohnuki, Megumi Narita, Tomoko Ichisaka, Kiichiro Tomoda, and Shinya Yamanaka. 2007. "Induction of Pluripotent Stem Cells from Adult Human Fibroblasts by Defined Factors." *Cell*. https://doi.org/10.1016/j.cell.2007.11.019.

Takahashi, Kazutoshi, and Shinya Yamanaka. 2006. "Induction of Pluripotent Stem Cells from Mouse Embryonic and Adult Fibroblast Cultures by Defined Factors." *Cell*. https://doi.org/10.1016/j.cell.2006.07.024.

Takasaki, Asami, Keiichi Hirono, Yukiko Hata, Ce Wang, Masafumi Takeda, Jun K. Yamashita, Bo Chang, et al. 2018. "Sarcomere Gene Variants Act as a Genetic Trigger Underlying the Development of Left Ventricular Noncompaction." *Pediatric Research* 84 (5): 733–42.

Tanaka, Atsushi, Shinsuke Yuasa, Giulia Mearini, Toru Egashira, Tomohisa Seki, Masaki Kodaira, Dai Kusumoto, et al. 2014. "Endothelin-1 Induces Myofibrillar Disarray and Contractile Vector Variability in Hypertrophic Cardiomyopathy-Induced Pluripotent Stem Cell-Derived Cardiomyocytes." *Journal of the American Heart Association* 3 (6): e001263.

Tani, Hidenori, and Shugo Tohyama. 2022. "Human Engineered Heart Tissue Models for Disease Modeling and Drug Discovery." *Frontiers in Cell and Developmental Biology* 10 (March): 855763.

Taylor, Matthew R. G., Dobromir Slavov, Lisa Ku, Andrea Di Lenarda, Gianfranco Sinagra, Elisa Carniel, Kurt Haubold, et al. 2007. "Prevalence of Desmin Mutations in Dilated Cardiomyopathy." *Circulation* 115 (10): 1244–51.

Terrenoire, Cecile, Kai Wang, Kelvin W. Chan Tung, Wendy K. Chung, Robert H. Pass, Jonathan T. Lu, Jyh-Chang Jean, et al. 2013. "Induced Pluripotent Stem Cells Used to Reveal Drug Actions in a Long QT Syndrome Family with Complex Genetics." *The Journal of General Physiology* 141 (1): 61–72.

Tesi, Chiara, Nicoletta Piroddi, Francesco Colomo, and Corrado Poggesi. 2002. "Relaxation Kinetics Following Sudden Ca2 Reduction in Single Myofibrils from Skeletal Muscle." *Biophysical Journal*. https://doi.org/10.1016/s0006-3495(02)73974-x.

Thavandiran, Nimalan, Nicole Dubois, Alexander Mikryukov, Stéphane Massé, Bogdan Beca, Craig A. Simmons, Vikram S. Deshpande, et al. 2013. "Design and Formulation of Functional Pluripotent Stem Cell-Derived Cardiac Microtissues." *Proceedings of the National Academy of Sciences of the United States of America* 110 (49): E4698–4707.

Thavandiran, Nimalan, Christopher Hale, Patrick Blit, Mark L. Sandberg, Michele E. McElvain, Mark Gagliardi, Bo Sun, et al. 2020. "Functional Arrays of Human Pluripotent Stem Cell-Derived Cardiac Microtissues." *Scientific Reports* 10 (1): 6919.

Thompson, Susan A., Craig R. Copeland, Daniel H. Reich, and Leslie Tung. 2011. "Mechanical Coupling between Myofibroblasts and Cardiomyocytes Slows Electric Conduction in Fibrotic Cell Monolayers." *Circulation* 123 (19): 2083–

93.

Tiburcy, Malte, Tim Meyer, Poh Loong Soong, and Wolfram-Hubertus Zimmermann. 2014. "Collagen-Based Engineered Heart Muscle." *Methods in Molecular Biology* 1181: 167–76.

Toepfer, Christopher N., Amanda C. Garfinkel, Gabriela Venturini, Hiroko Wakimoto, Giuliana Repetti, Lorenzo Alamo, Arun Sharma, et al. 2020. "Myosin Sequestration Regulates Sarcomere Function, Cardiomyocyte Energetics, and Metabolism, Informing the Pathogenesis of Hypertrophic Cardiomyopathy." *Circulation* 141 (10): 828–42.

Tonino, Paola, Balazs Kiss, Jochen Gohlke, John E. Smith 3rd, and Henk Granzier. 2019. "Fine Mapping Titin's C-Zone: Matching Cardiac Myosin-Binding Protein C Stripes with Titin's Super-Repeats." *Journal of Molecular and Cellular Cardiology* 133 (August): 47–56.

Towbin, J. A., J. F. Hejtmancik, P. Brink, B. Gelb, X. M. Zhu, J. S. Chamberlain, E. R. McCabe, and M. Swift. 1993. "X-Linked Dilated Cardiomyopathy. Molecular Genetic Evidence of Linkage to the Duchenne Muscular Dystrophy (dystrophin) Gene at the Xp21 Locus." *Circulation* 87 (6): 1854–65.

Tse, Hung-Fat, Jenny C. Y. Ho, Shing-Wan Choi, Yee-Ki Lee, Amy W. Butler, Kwong-Man Ng, Chung-Wah Siu, et al. 2013. "Patient-Specific Induced-Pluripotent Stem Cells-Derived Cardiomyocytes Recapitulate the Pathogenic Phenotypes of Dilated Cardiomyopathy due to a Novel DES Mutation Identified by Whole Exome Sequencing." *Human Molecular Genetics* 22 (7): 1395–1403.

Tulloch, Nathaniel L., Veronica Muskheli, Maria V. Razumova, F. Steven Korte, Michael Regnier, Kip D. Hauch, Lil Pabon, Hans Reinecke, and Charles E. Murry. 2011. "Growth of Engineered Human Myocardium with Mechanical Loading and Vascular Coculture." *Circulation Research* 109 (1): 47–59.

Ullrich, Nina D., Mohammed Fanchaouy, Konstantin Gusev, Natalia Shirokova, and Ernst Niggli. 2009. "Hypersensitivity of Excitation-Contraction Coupling in Dystrophic Cardiomyocytes." *American Journal of Physiology. Heart and Circulatory Physiology* 297 (6): H1992–2003.

Vaidya, Kaivan, Christopher Semsarian, and Kim H. Chan. 2017. "Atrial Fibrillation in Hypertrophic Cardiomyopathy." *Heart, Lung and Circulation*. https://doi.org/10.1016/j.hlc.2017.05.116.

Vasile, Vlad C., Melissa L. Will, Steve R. Ommen, William D. Edwards, Timothy M. Olson, and Michael J. Ackerman. 2006. "Identification of a Metavinculin Missense Mutation, R975W, Associated with Both Hypertrophic and Dilated Cardiomyopathy." *Molecular Genetics and Metabolism* 87 (2): 169–74.

Veerman, Christiaan C., Georgios Kosmidis, Christine L. Mummery, Simona Casini, Arie O. Verkerk, and Milena Bellin. 2015. "Immaturity of Human Stem-Cell-Derived Cardiomyocytes in Culture: Fatal Flaw or Soluble Problem?" *Stem Cells and Development* 24 (9): 1035–52.

Veerman, Christiaan C., Isabella Mengarelli, Kaomei Guan, Michael Stauske, Julien Barc, Hanno L. Tan, Arthur A. M. Wilde, Arie O. Verkerk, and Connie R. Bezzina. 2016. "hiPSC-Derived Cardiomyocytes from Brugada Syndrome Patients without Identified Mutations Do Not Exhibit Clear Cellular Electrophysiological Abnormalities." *Scientific Reports* 6 (August): 30967.

Verdonschot, Job A. J., Mark R. Hazebroek, Kasper W. J. Derks, Arantxa Barandiarán Aizpurua, Jort J. Merken, Ping Wang, Jörgen Bierau, et al. 2018. "Titin Cardiomyopathy Leads to Altered Mitochondrial Energetics, Increased Fibrosis and Long-Term Life-Threatening Arrhythmias." *European Heart Journal*. https://doi.org/10.1093/eurheartj/ehx808.

Verhaart, Ingrid E. C., and Annemieke Aartsma-Rus. 2019. "Therapeutic Developments for Duchenne Muscular Dystrophy." *Nature Reviews. Neurology* 15 (7): 373–86.

Verkerk, A. O., R. Wilders, M. M. G. J. van Borren, R. J. G. Peters, E. Broekhuis, K. Lam, R. Coronel, J. M. T. de Bakker, and H. L. Tan. 2007. "Pacemaker Current (If) in the Human Sinoatrial Node." *European Heart Journal*. https://doi.org/10.1093/eurheartj/ehm339.

Vidarsson, Hilmar, Johan Hyllner, and Peter Sartipy. 2010. "Differentiation of Human Embryonic Stem Cells to Cardiomyocytes for In Vitro and In Vivo Applications." *Stem Cell Reviews and Reports*. https://doi.org/10.1007/s12015-010-9113-x.

Vignier, Nicolas, Saskia Schlossarek, Bodvael Fraysse, Giulia Mearini, Elisabeth Krämer, Hervé Pointu, Nathalie Mougenot, et al. 2009a. "Nonsense-Mediated mRNA Decay and Ubiquitin–Proteasome System Regulate Cardiac Myosin-Binding Protein C Mutant Levels in Cardiomyopathic Mice." *Circulation Research*. https://doi.org/10.1161/circresaha.109.201251.

Vignier. 2009b. "Nonsense-Mediated mRNA Decay and Ubiquitin-Proteasome System Regulate Cardiac Myosin-Binding Protein C Mutant Levels in Cardiomyopathic Mice." *Circulation Research* 105 (3): 239–48.

Viswanathan, Shiv Kumar, Megan J. Puckelwartz, Ashish Mehta, Chrishan J. A. Ramachandra, Aravindakshan Jagadeesan, Regina Fritsche-Danielson, Ratan V. Bhat, et al. 2018. "Association of Cardiomyopathy with MYBPC3 D389V and MYBPC3Δ25bpIntronic Deletion in South Asian Descendants." *JAMA Cardiology* 3 (6): 481–88.

Vitale, Giulia, Cecilia Ferrantini, Nicoletta Piroddi, Beatrice Scellini, Josè Manuel Pioner, Barbara Colombini, Chiara Tesi, and Corrado Poggesi. 2021. "The Relation between Sarcomere Energetics and the Rate of Isometric Tension Relaxation in Healthy and Diseased Cardiac Muscle." *Journal of Muscle Research and Cell Motility* 42 (1): 47–57.

Vreeker, Arnold, Leonie van Stuijvenberg, Thomas J. Hund, Peter J. Mohler, Peter G. J. Nikkels, and Toon A. B. van Veen. 2014. "Assembly of the Cardiac Intercalated Disk during Pre- and Postnatal Development of the Human Heart." *PloS One* 9 (4): e94722.

Wang, Gang, Megan L. McCain, Luhan Yang, Aibin He, Francesco Silvio Pasqualini, Ashutosh Agarwal, Hongyan Yuan, et al. 2014. "Modeling the Mitochondrial Cardiomyopathy of Barth Syndrome with Induced Pluripotent Stem Cell and Heart-on-Chip Technologies." *Nature Medicine* 20 (6): 616–23.

Wang, Lili, Kyungsoo Kim, Shan Parikh, Adrian Gabriel Cadar, Kevin R. Bersell, Huan He, Jose R. Pinto, Dmytro O. Kryshtal, and Bjorn C. Knollmann. 2018. "Hypertrophic Cardiomyopathy-Linked Mutation in Troponin T Causes Myofibrillar Disarray and pro-Arrhythmic Action Potential Changes in Human iPSC Cardiomyocytes." *Journal of Molecular and Cellular Cardiology* 114 (January): 320–27.

Wang, Lili, Dmytro O. Kryshtal, Kyungsoo Kim, Shan Parikh, Adrian Gabriel Cadar, Kevin Richard Bersell, Huan He, Jose R. Pinto, and Bjorn C. Knollmann. 2017. "Myofilament Calcium-Buffering Dependent Action Potential Triangulation in Human-Induced Pluripotent Stem Cell Model of Hypertrophic Cardiomyopathy." *Journal of the American College of Cardiology* 70 (20): 2600–2602.

Wang, Qiongling, Wei Wang, Guoliang Wang, George G. Rodney, and Xander H. T. Wehrens. 2015. "Crosstalk between RyR2 Oxidation and Phosphorylation Contributes to Cardiac Dysfunction in Mice with Duchenne Muscular Dystrophy." *Journal of Molecular and Cellular Cardiology* 89 (Pt B): 177–84.

Watkins, H. 2000. "Sudden Death in Hypertrophic Cardiomyopathy." *The New England Journal of Medicine*.

Watkins, H., D. Conner, L. Thierfelder, J. A. Jarcho, C. MacRae, W. J. McKenna, B. J. Maron, J. G. Seidman, and C. E. Seidman. 1995. "Mutations in the Cardiac Myosin Binding Protein-C Gene on Chromosome 11 Cause Familial Hypertrophic Cardiomyopathy." *Nature Genetics* 11 (4): 434–37.

Wijnker, Paul J. M., Vasco Sequeira, E. Rosalie Witjas-Paalberends, D. Brian Foster, Cristobal G. dos Remedios, Anne M. Murphy, Ger J. M. Stienen, and Jolanda van der Velden. 2014. "Phosphorylation of Protein Kinase C Sites Ser42/44 Decreases Ca(2+)-Sensitivity and Blunts Enhanced Length-Dependent Activation in Response to Protein Kinase A in Human Cardiomyocytes." *Archives of Biochemistry and Biophysics* 554 (July): 11–21.

Williams, Nisa P., Marcus Rhodehamel, Calysta Yan, Alec S. T. Smith, Alex Jiao, Charles E. Murry, Marta Scatena, and Deok-Ho Kim. 2020. "Engineering Anisotropic 3D Tubular Tissues with Flexible Thermoresponsive Nanofabricated Substrates." *Biomaterials* 240 (May): 119856.

Witjas-Paalberends, E. Rosalie, Claudia Ferrara, Beatrice Scellini, Nicoletta Piroddi, Judith Montag, Chiara Tesi, Ger J. M. Stienen, et al. 2014. "Faster Cross-Bridge Detachment and Increased Tension Cost in Human Hypertrophic Cardiomyopathy with the R403Q MYH7 Mutation." *The Journal of Physiology* 592 (15): 3257–72.

Wu, Haodi, Jaecheol Lee, Ludovic G. Vincent, Qingtong Wang, Mingxia Gu, Feng Lan, Jared M. Churko, et al. 2015. "Epigenetic Regulation of Phosphodiesterases 2A and 3A Underlies Compromised β-Adrenergic Signaling in an iPSC Model of Dilated Cardiomyopathy." *Cell Stem Cell* 17 (1): 89–100.

Wu, Haodi, Huaxiao Yang, June-Wha Rhee, Joe Z. Zhang, Chi Keung Lam, Karim Sallam, Alex C. Y. Chang, et al. 2019. "Modelling Diastolic Dysfunction in Induced Pluripotent Stem Cell-Derived Cardiomyocytes from Hypertrophic Cardiomyopathy Patients." *European Heart Journal* 40 (45): 3685–95.

Wyles, S. P., S. C. Hrstka, S. Reyes, A. Terzic, T. M. Olson, and T. J. Nelson. 2016. "Pharmacological Modulation of Calcium Homeostasis in Familial Dilated Cardiomyopathy: An In Vitro Analysis from an RBM20 Patient-Derived iPSC Model." *Clinical and Translational Science* 9 (3): 158–67.

Xue, Yanting, Xiujuan Cai, Linli Wang, Baojian Liao, Hui Zhang, Yongli Shan, Qianyu Chen, et al. 2013. "Generating a Non-Integrating Human Induced Pluripotent Stem Cell Bank from Urine-Derived Cells." *PLoS ONE*. https://doi.org/10.1371/journal.pone.0070573.

Xu, Xiu Qin, Set Yen Soo, William Sun, and Robert Zweigerdt. 2009. "Global Expression Profile of Highly Enriched Cardiomyocytes Derived from Human Embryonic Stem Cells." *Stem Cells*. https://doi.org/10.1002/stem.166.

Xu, Xun, Weiwei Wang, Karl Kratz, Liang Fang, Zhengdong Li, Andreas Kurtz, Nan Ma, and Andreas Lendlein. 2014. "Stem Cells: Controlling Major Cellular Processes of Human Mesenchymal Stem Cells Using Microwell Structures (Adv. Healthcare Mater. 12/2014)." *Advanced Healthcare Materials*. https://doi.org/10.1002/adhm.201470060.

Yamamoto, Yuta, Takeru Makiyama, Takeshi Harita, Kenichi Sasaki, Yimin Wuriyanghai, Mamoru Hayano, Suguru Nishiuchi, et al. 2017. "Allele-Specific Ablation Rescues Electrophysiological Abnormalities in a Human iPS Cell Model of Long-QT Syndrome with a CALM2 Mutation." *Human Molecular Genetics* 26 (9): 1670–77.

Yang, Kai-Chun, Astrid Breitbart, Willem J. De Lange, Peter Hofsteen, Akiko Futakuchi-Tsuchida, Joy Xu, Cody Schopf, et al. 2018. "Novel Adult-Onset Systolic Cardiomyopathy Due to MYH7 E848G Mutation in Patient-Derived Induced Pluripotent Stem Cells." *JACC. Basic to Translational Science* 3 (6): 728–40.

Yang, Xiulan, Lil Pabon, and Charles E. Murry. 2014. "Engineering Adolescence: Maturation of Human Pluripotent Stem Cell-Derived Cardiomyocytes." *Circulation Research* 114 (3): 511–23.

Yasuda, Soichiro, Dewayne Townsend, Daniel E. Michele, Elizabeth G. Favre, Sharlene M. Day, and Joseph M. Metzger. 2005. "Dystrophic Heart Failure Blocked by Membrane Sealant Poloxamer." *Nature* 436 (7053): 1025–29.

Yazawa, Masayuki, Brian Hsueh, Xiaolin Jia, Anca M. Pasca, Jonathan A. Bernstein, Joachim Hallmayer, and Ricardo E. Dolmetsch. 2011. "Using Induced Pluripotent Stem Cells to Investigate Cardiac Phenotypes in Timothy Syndrome." *Nature* 471 (7337): 230–34.

Yermakovich, Danat, Larysa Sivitskaya, Tatiyana Vaikhanskaya, Nina Danilenko, and Iryna Motuk. 2018. "Novel Desmoplakin Mutations in Familial Carvajal Syndrome." *Acta Myologica: Myopathies and Cardiomyopathies: Official Journal of the*

Mediterranean Society of Myology / Edited by the Gaetano Conte Academy for the Study of Striated Muscle Diseases 37 (4): 263–66.

Yilmaz, Ali, Hans-Jürgen Gdynia, Hannibal Baccouche, Heiko Mahrholdt, Gabriel Meinhardt, Cristina Basso, Gaetano Thiene, Anne-Dorte Sperfeld, Albert C. Ludolph, and Udo Sechtem. 2008. "Cardiac Involvement in Patients with Becker Muscular Dystrophy: New Diagnostic and Pathophysiological Insights by a CMR Approach." *Journal of Cardiovascular Magnetic Resonance: Official Journal of the Society for Cardiovascular Magnetic Resonance* 10 (1): 50.

Zaffran, Stéphane, Robert G. Kelly, Sigolène M. Meilhac, Margaret E. Buckingham, and Nigel A. Brown. 2004. "Right Ventricular Myocardium Derives From the Anterior Heart Field." *Circulation Research*. https://doi.org/10.1161/01.res.0000136815.73623.be.

Zampieri, Mattia, Alessia Argirò, Alberto Marchi, Martina Berteotti, Mattia Targetti, Alessandra Fornaro, Alessia Tomberli, Pierluigi Stefàno, Niccolò Marchionni, and Iacopo Olivotto. 2021. "Mavacamten, a Novel Therapeutic Strategy for Obstructive Hypertrophic Cardiomyopathy." *Current Cardiology Reports* 23 (7): 79.

Zaunbrecher, Rebecca J., Ashley N. Abel, Kevin Beussman, Andrea Leonard, Marion von Frieling-Salewsky, Paul A. Fields, Lil Pabon, et al. 2019. "Cronos Titin Is Expressed in Human Cardiomyocytes and Necessary for Normal Sarcomere Function." *Circulation* 140 (20): 1647–60.

Zhang, Jianhua, Matthew Klos, Gisela F. Wilson, Amanda M. Herman, Xiaojun Lian, Kunil K. Raval, Matthew R. Barron, et al. 2012. "Extracellular Matrix Promotes Highly Efficient Cardiac Differentiation of Human Pluripotent Stem Cells: The Matrix Sandwich Method." *Circulation Research* 111 (9): 1125–36.

Zhang, X-H, S. Haviland, H. Wei, T. Sarić, A. Fatima, J. Hescheler, L. Cleemann, and M. Morad. 2013. "Ca2+ Signaling in Human Induced Pluripotent Stem Cell-Derived Cardiomyocytes (iPS-CM) from Normal and Catecholaminergic Polymorphic Ventricular Tachycardia (CPVT)-Afflicted Subjects." *Cell Calcium* 54 (2): 57–70.

Zhang, Yu, Hui Li, Takahiko Nishiyama, John R. McAnally, Efrain Sanchez-Ortiz, Jian Huang, Pradeep P. A. Mammen, Rhonda Bassel-Duby, and Eric N. Olson. 2022. "A Humanized Knockin Mouse Model of Duchenne Muscular Dystrophy and Its Correction by CRISPR-Cas9 Therapeutic Gene Editing." *Molecular Therapy. Nucleic Acids* 29 (September): 525–37.

Zhan, Hong, Ramunas Stanciauskas, Christian Stigloher, Kevin Keomanee-Dizon, Maelle Jospin, Jean-Louis Bessereau, and Fabien Pinaud. 2014. "In Vivo Single-Molecule Imaging Identifies Altered Dynamics of Calcium Channels in Dystrophin-Mutant C. Elegans." *Nature Communications* 5 (September): 4974.

Zhou, Ting, Christina Benda, Sarah Dunzinger, Yinghua Huang, Jenny Cy Ho, Jiayin Yang, Yu Wang, et al. 2012. "Generation of Human Induced Pluripotent Stem Cells from Urine Samples." *Nature Protocols*. https://doi.org/10.1038/nprot.2012.115.

Zhou, Wei, J. Martijn Bos, Dan Ye, David J. Tester, Sybil Hrstka, Joseph J. Maleszewski, Steve R. Ommen, et al. 2019. "Induced Pluripotent Stem Cell-Derived Cardiomyocytes from a Patient with MYL2-R58Q-Mediated Apical Hypertrophic Cardiomyopathy Show Hypertrophy, Myofibrillar Disarray, and Calcium Perturbations." *Journal of Cardiovascular Translational Research* 12 (5): 394–403.

Zimmermann, W. H., C. Fink, D. Kralisch, U. Remmers, J. Weil, and T. Eschenhagen. 2000. "Three-Dimensional Engineered Heart Tissue from Neonatal Rat Cardiac Myocytes." *Biotechnology and Bioengineering* 68 (1): 106–14.

Zimmermann, W-H, K. Schneiderbanger, P. Schubert, M. Didié, F. Münzel, J. F. Heubach, S. Kostin, W. L. Neuhuber, and T. Eschenhagen. 2002. "Tissue Engineering of a Differentiated Cardiac Muscle Construct." Circulation Research 90 (2): 223–30.

Zwaag, Paul A. van der, Ingrid A. W. van Rijsingen, Angeliki Asimaki, Jan D. H. Jongbloed, Dirk J. van Veldhuisen, Ans C. P. Wiesfeld, Moniek G. P. J. Cox, et al. 2012. "Phospholamban R14del Mutation in Patients Diagnosed with Dilated Cardiomyopathy or Arrhythmogenic Right Ventricular Cardiomyopathy: Evidence Supporting the Concept of Arrhythmogenic Cardiomyopathy." *European Journal of Heart Failure* 14 (11): 1199–1207.